Interference Mitigation and Interference Avoidance for Cellular OFDMA-TDD Networks

Ellina P. Foutekova

A thesis submitted for the degree of Doctor of Philosophy.
The University of Edinburgh.
2009

Abstract

In recent years, cellular systems based on orthogonal frequency division multiple access – time division duplex (OFDMA-TDD) have gained considerable popularity. Two of the major reasons for this are, on the one hand, that OFDMA enables the receiver to effectively cope with multipath propagation while keeping the complexity low. On the other hand, TDD offers efficient support for cell-specific uplink (UL)/downlink (DL) asymmetry demands by allowing each cell to independently set its UL/DL switching point (SP). However, cell-independent SP gives rise to *crossed slots*. In particular, crossed slots arise when neighbouring cells use the same slot in opposing link directions, resulting in base station (BS)-to-BS interference and mobile station (MS)-to-MS interference. BS-to-BS interference, in particular, can be quite detrimental due to the exposed location of BSs, which leads to high probability of line-of-sight (LOS) conditions. The aim of this thesis is to address the BS-to-BS interference problem in OFDMA-TDD cellular networks. A simulation-based approach is used to demonstrate the severity of BS-to-BS interference and a signal-to-interference-plus-noise ratio (SINR) equation for OFDMA is formulated to aid system performance analysis. The detrimental effects of crossed slot interference in OFDMA-TDD cellular networks are highlighted by comparing methods specifically targeting the crossed slots interference problem. In particular, the interference avoidance method fixed slot allocation (FSA) is compared against state of the art interference mitigation approaches, *viz:* random time slot opposing (RTSO) and zone division (ZD). The comparison is done based on Monte Carlo simulations and the main comparison metric is spectral efficiency calculated using the SINR equation formulated in this thesis. The simulation results demonstrate that when LOS conditions among BSs are present, both RTSO and ZD perform worse than FSA for all considered performance metrics. It is concluded from the results that current interference *mitigation* techniques do not offer an effective solution to the BS-to-BS interference problem. Hence, new interference *avoidance* methods, which unlike FSA, do not sacrifice the advantages of TDD are open research issues addressed in this thesis.

The major contribution of this thesis is a novel *cooperative* resource balancing technique that offers a solution to the crossed slot problem. The novel concept, termed *asymmetry balancing*, is targeted towards next-generation cellular systems, envisaged to have *ad hoc* and multi-hop capabilities. Asymmetry balancing completely avoids crossed slots by keeping the TDD SPs synchronised among BSs. At the same time, the advantages of TDD are retained, which is enabled by introducing cooperation among the entities in the network. If a cell faces resource shortage in one link direction, while having free resources in the opposite link direction, the free resources can be used to support the overloaded link direction. In particular, traffic can be offloaded to near-by mobile stations at neighbouring cells that have available resources. To model the gains attained with asymmetry balancing, a mathematical framework is developed which is verified by Monte Carlo simulations. In addition, asymmetry balancing is compared against both ZD and FSA based on simulations and the results demonstrate the superior performance of asymmetry balancing. It can be concluded that the novel interference avoidance approach is a very promising candidate to solve the crossed slot problem in next-generation OFDMA-TDD-based cellular networks.

Declaration of originality

I hereby declare that the research recorded in this thesis and the thesis itself was composed and originated entirely by myself in the School of Engineering and Science at Jacobs University Bremen and in the School of Engineering at The University of Edinburgh.

The software used to perform the simulations was written by myself with the following exceptions:

> The channel model used in the study of the comparison between RTSO (random time slot opposing) and FSA (fixed slot allocation) was written by Van Duc Nguyen and Birendra Ghimire.

Ellina P. Foutekova

Acknowledgements

First of all, I would like to thank my supervisor, Harald Haas. His strive for excellence, as well as his hard work, persistence, and attention to detail have all been inspirational to me. If it weren't for his interesting and enthusiastic lectures during the Wireless Communications course at Jacobs University Bremen and his excellent guidance during my BSc thesis project, I would probably have not pursued a degree in this field. Throughout my studies Harald Haas has offered me continuous support as well as detailed feedback enabling me to significantly improve on my work, for which all I am sincerely thankful.

I would also like to thank Sinan Sinanović for his fruitful discussions and advice on the mathematical challenges I was facing. His friendly attitude and apt help are very much appreciated. In addition, I would like to take the opportunity to thank Patrick Agyapong for his key insights which aided the development of the SINR (signal-to-interference-plus-noise ratio) equation for OFDMA (orthogonal frequency division multiple access) systems as well as Christine Evers for her support during the initial RTSO (random time slot opposing) study.

Moreover, I would like to thank Samsung Advanced Institute of Technology as well as The School of Engineering and Electronics at The University of Edinburgh for their financial support of my PhD studies.

My sincere thanks also go out to my office mates at Jacobs University, Dimitar Popov, Patrick Agyapong, Zubin Bharucha, and Birendra Ghimire who all made the time spent in the office fun, as well as the rest of the CWC (cellular and wireless communications) group members at Jacobs University Bremen for the many stimulating discussions and constructive feedback. I would also like to thank Nicola Ferguson and the people from Room 2.01 in the AGB (Alexander Graham Bell) building at the Kings Buildings campus of The University of Edinburgh for their warm welcome and continuous help.

Furthermore, I would like to extend my deepest gratitude to my parents, Peter and Emma, for their love, encouragement, and unconditional belief in me during all these years.

Last but not least, I would like to express my thanks to Stefan for his deep love and support, which I sincerely cherish. He has been tremendously understanding in times of tight deadlines and long work hours. I am also grateful for his interest in my work and his very constructive feedback which surely helped improve my writing style.

Contents

List of figures

List of tables

Acronyms and abbreviations

1G	First generation
2G	Second generation
3G	Third generation
3GPP	Third generation partnership project
4G	Fourth generation
AWGN	Additive white Gaussian noise
BER	Bit-error ratio
BS	Base station
CCI	Co-channel interference
cdf	Cumulative distribution function
CDMA	Code division multiple access
CFR	Common free resources
CoI	Cell of interest
DAB	Digital audio broadcast
DL	Downlink
DVB	Digital video broadcast
FDD	Frequency division duplex
FDM	Frequency division mutliplex
FDMA	Frequency division multiple access
FFR	Fractional frequency reuse
FFT	Fast Fourrier transform
FSA	Fixed slot allocation
GPS	Global positioning system
GRP	Greedy rate packing
GSM	Groupe Speciale Mobile
IFFT	Inverse FFT
IMT	International mobile technology
ISI	Inter-symbol interference
IST-WINNER	Information society technologies - wireless world initiative radio

ITU	International telecommunication union
LAN	Local area network
LOS	Line of sight
LTE	Long term evolution
MAI	Multiple access interference
MC	Multi-carrier
MCN	Multi-hop cellular network
MS	Mobile station
NAMTS	Nippon advanced mobile telephone system
NLOS	Non-line of sight
OFDM	Orthogonal frequency division multiplexing
OFDMA	Orthogonal frequency division multiple access
OTA-SRR	Optimum target assignment - stepwise rate removals
PAPR	Peak-to-average power ratio
pdf	Probability distribution function
PN	Pseudo-noise
PSK	Phase shift keying
QAM	Quadrature amplitude modulation
QoS	Quality of service
RRM	Radio resource management
RS	Relay station
RTG	Receive/transmit transition gap
RTSO	Random time slot opposing
SINR	Signal-to-interference-plus-noise ratio
SC	Single-carrier
SCN	Single-hop cellular network
SNR	Signal-to-noise ratio
SP	Switching point
SSP	Synchronised switching point
TDD	Time division duplex
TDMA	Time division multiple access
TTG	Transmit/receive transition gap
UMB	Ultra mobile broadband

UMTS	Universal mobile telecommunications system
UL	Uplink
VoIP	Voice over internet protocol
WiMAX	Worldwide interoperability for microwave access
WLAN	Wireless local area network
ZD	Zone division

Nomenclature

a	antenna-dependent constant used in the calculation of path loss
$\alpha_{\mathrm{u}}^{\mathrm{UL}}$	user demand in UL
B_{k}	number of BSs per cluster
B_{t}	number of cooperating cells
β_i	set of own-cell links from the perspective of link i such that $i \notin \mathbf{b}_i$
b	path loss exponent dependant constant used in the calculation of path loss
$C_{k,k'}$	modified Dirichlet function
C_{tot}	number of OFDMA chunks per frame
C_{o}	total number of chunks allocated to the off-loading link direction
$\overline{C}_{\mathrm{s}}$	average spectral efficiency per chunk (bps/Hz)
$\overline{C}_k^i$	spectral efficiency (in bps/Hz) on subcarrier k for link i
$\overline{C}_{\mathrm{b}}$	average spectral efficiency per chunk (bps/Hz), including off-loading
$\overline{C}_{\mathrm{r}}$	data rate obtained using Shannon's capacity equation (in bps)
$\tilde{C}_k^i$	data rate attained on subcarrier k for link i using adaptive modulation
c_{c}	number of reusable channels in the system
c_{t}	total number of channels in the system that can be utilised (including reused)
σ	standard deviation of the log-normal distribution of the transmitter-receiver path loss
D	path loss distribution variable depending on the path loss model
Δ_1	path loss margin (in dB)
Δ_2	path loss margin (in dB)
Δf	subcarrier distance between interferer and victim
δ_{f}	carrier spacing (in Hz)
E_{b}	energy per bit (in W·s)
$\boldsymbol{\eta}$	normalised noise vector
η_k	element of the normalised noise vector
ϵ_c	a threshold value for ζ; determines modulation level
ε_{D}	normalised Doppler shift
f_{C}	carrier frequency
F_q	cdf corresponding to f_q

F_y	cdf corresponding to f_y
f_{c}	frequency offset (in Hz) due to synchronisation errors
$f_{\mathrm{D,max}}$	maximum Doppler frequency (in Hz)
f_N	probability distribution of the number of common free resources
$f_q(q)$	MS–BS path loss distribution
f_{r}	frequency reuse factor
$f_x(x)$	MS–RS distance distribution
$f_x(x\|z)$	MS–RS distances distribution for a given distance from the centre (MS–BS), z
$f_y(y)$	MS–RS path loss distribution
$f_y(y\|z)$	MS–RS path loss distribution for a given distance from the centre (MS–BS), z
$f_z(z)$	MS–BS distance distribution
$\mathbf{\Phi}$	normalised link gain matrix
$\Phi_{k,k'}$	element of the normalised link gain matrix
ϕ	phase
G	link gain (general)
G_i	link gain of link i
$G_{i,l}$	link gain between the transmitter on link l and the receiver on link i
$\tilde{G}_k$	weighted link gain for subcarrier k
$\tilde{G}_{k,k'}$	weighted interfering link gain between k and k'
$\mathbf{\Gamma}$	set of SINR targets
γ_j^{mh}	SINR of chunk j for two-hop links
γ_k^i	achieved SINR on subcarrier k for link i
γ_k	SINR on subcarrier k
$\overline{\gamma}_k$	SINR target assigned to subcarrier k
$\tilde{\gamma}_i$	SINR attained at link i
$\|H_k^i\|^2$	channel transfer function of link i at subcarrier k
$\|H_{k'}^{i,l}\|^2$	interference channel transfer function at subcarrier k'
$\mathbf{H}(f)$	FFT pair of $\mathbf{h}(t)$
$\mathbf{h}(t)$	channel impulse response vector
$\mathbf{I}$	identity matrix
$\iota_{\mathrm{b},i}(l)$	buffer length of user i at time instant l
j	imaginary unit
K_{s}	number of clusters in the system

K_{t}	number of first-tier cells which share a common free resource with the CoI
k	Boltzmann's constant
L_{c}	probability that a resource is occupied at the cell of interest
L_{p}	path loss (in dB)
$L_{\mathrm{p}}^{\mathrm{mb}}$	path loss between $\mathrm{BS}_{\mathrm{CoI}}$ and $\mathrm{MS}_{\mathrm{OL}}$ (in dB)
$L_{\mathrm{p}}^{\mathrm{mr}}$	path loss between $\mathrm{MS}_{\mathrm{OL}}$ and RS_{c} (in dB)
$L_{\mathrm{p}}^{\mathrm{br}}$	path loss between BS_{c} and RS_{c} (in dB)
$L_{\mathrm{t},i}$	probability that a resource is occupied at a first-tier cell i
λ_1	dominant eigenvalue of $\mathbf{\Phi}$
$M_{c,k}^i$	number of bits per symbol when modulation level $m_{c,k}^i$ is used
M_{OL}	is the number of chunks actually utilised for off-loading
M_u	total number of chunks allocated to UL by the network-wide switching point
$\overline{M}_{\mathrm{OL}}$	number of DL chunks available for off-loading
m_c	modulation level (constellation size)
$m_{c,k}^i$	modulation level on subcarrier k for link i
μ	path loss exponent
N	number of common free resources (chunks)
N_{c}	OFDM FFT size
N_{o}	thermal noise power density (in W/Hz)
N_{s}	number of parallel streams for MC
$\mathbf{N}_{\mathrm{th}}(f)$	FFT pair of $\mathbf{n}_{\mathrm{th}}$
N_{tot}	total number of subcarriers in the system
n_{DL}	number of DL slots in a TDD frame
n_{TOT}	total number of time slots in a TDD frame
n_{th}	thermal noise power (in Watts) per subcarrier
$\mathbf{n}_{\mathrm{th}}$	thermal noise power in vector notation
n_{UL}	number of UL slots in a TDD frame
ω	the normalised frequency offset due to synchronisation errors
$\mathbf{P}$	vector of transmit power per subcarrier
$\mathbf{P_1}$	eigenvector corresponding to $(1-\lambda_1)$
P_{b}	probability for error per bit
$\mathbf{P}_{\max}$	vector of maximum transmit powers
P_k^i	transmit power of subcarrier k (in Watts)

$P^i_{\mathrm{CCI},k}$	received CCI power on subcarrier k for link i (in Watts)
$P^i_{\mathrm{MAI},k}$	received MAI power on subcarrier k for link i (in Watts)
P_{UL}	probability of an UL time slot
$P_{\mathrm{opp}}(n)$	probability for at least one crossed slot per frame among n cells
p	probability that a chunk is a common free resource
$p_{\mathrm{o}}^{\mathrm{UL}}$	probability that an UL resource is occupied
p_{ucfr}	probability that the CFR is utilised
$\overline{p}$	maximum transmit power per subcarrier
$\varpi_{i,l}$	determines whether link i will experience MAI from link l
$\varpi_{k,k'}$	determines whether subcarrier k will experience MAI from k'
Q	random variable, describing the MS–BS path loss distribution
R	cell radius
R_{asym}	ratio of the number of UL slots and DL slots
R_{b}	bit rate (in bps)
R_{c}	code rate
$\mathbf{R}(f)$	FFT pair of $\mathbf{r}(t)$
R^i_k	received signal power on subcarrier k for link i (in Watts)
R_{ul}	fraction of resources which can be used for UL incl. off-loading
$\mathcal{R}_k$	received modulation symbol on subcarrier k
r_{i}	information rate
r_c	raw channel rate
$\mathbf{r}(t)$	received signal in vector notation
S_k	transmit symbol on subcarrier k
$\mathbf{S}(f)$	FFT of $s_{\mathrm{m}}(n)$
s_i	set of subcarriers belonging to link i
$\tilde{s}_k$	set of subcarriers belonging to the same link as k
$s_{\mathrm{m}}(n)$	modulated signal
T	room temperature (in Kelvin)
T_{G}	cyclic prefix duration
T_{mc}	MC symbol duration
T_{s}	OFDM symbol duration
T_{sc}	SC symbol duration
U_{c}	number of users per cell

$u(r,t)$	user allocated resource r at time instant t
v_{l}	speed of light
v_{m}	speed of mobile
W_{b}	channel bandwidth (in Hz)
W_{mc}	MC channel bandwidth (in Hz)
W_{sc}	SC channel bandwidth (in Hz)
X	random variable, describing the MS–RS separation distances
X_{g}	zero mean Gaussian distributed random variable
$\mathbf{x}$	eigenvector corresponding to λ_1
$x(t)$	OFDM transmitted signal
$\mathbf{x}(t)$	OFDM transmitted signal in vector notation
Y	random variable, describing the MS–RS path loss distribution
ζ	general measure of channel quality (SINR, SNR, etc)

Chapter 1
Introduction

About this work

The work in this thesis targets next-generation wireless communications. In particular, the focus is on interference mitigation techniques, which are key to improved spectrum utilisation in interference limited, full frequency reuse networks. The interest in the topic is governed by the need for enhanced wireless services. The user demands ubiquitous wireless connectivity capable of high data rates and multimedia services. At the same time, for the service provider it is important that the deployed network utilises the spectrum and energy resources efficiently as a maximisation of both metrics ultimately increases revenue and decreases costs.

Motivation

It is recognised that severe interference is one of the major limiting factors for the performance of wireless cellular networks [1, 2]. In light of the high data rates (up to 1 Gbps) to be offered by 4^{th} generation (4G) wireless systems such as LTE (long term evolution) Advanced [3–5], combatting interference is key.

An effective strategy envisioned to ameliorate a network's performance without increasing hardware cost is to make use of existing infrastructure and to introduce cooperation among the network entities. Naturally, such cooperation leads to multi-hop cellular networks (MCN) [6], i.e. cellular networks that have relaying capabilities. A relay station (RS) is an intermediate node between a mobile station (MS) and the servicing base station (BS) and the relay can be either a dedicated transceiver or an MS. Multi-hop cellular networks exploit the flexibility of *ad hoc* communication while making use of the existing infrastructure of the cellular network [7].

In order to enable efficient multi-hop/*ad hoc* communication in the network, deploying time division duplex (TDD) is recommended [1]. TDD is also beneficial due to its efficient support

for asymmetric uplink (UL)/ downlink (DL) traffic [1, 8]. The efficient support for asymmetric traffic is of paramount importance because demand in wireless cellular networks is not limited to voice anymore. On the contrary, multimedia and Internet packet data services are dominant in current and future networks and these services usually exhibit high peak-to-average asymmetry demand ratio [1]. In addition, networks based on a combination of TDD and orthogonal frequency division multiple access (OFDMA) have been acknowledged as advantageous due to the beneficial properties of OFDMA [9, 10]. The main advantages of OFDMA are the ease of implementation, robustness to multi-path effects and inter-symbol interference [9, 10], multi-user diversity, and flexibility of deployment [11] which are all discussed in Chapter 2.

In the context of OFDMA-TDD-based networks, an important question currently open to research is how to resolve the same-entity interference problem that TDD poses. Same-entity interference is a TDD-specific issue that arises when neighbouring cells have dissimilar traffic asymmetry demands. As a result, while a cell is in UL, a neighbouring cell may be in DL and vice versa, resulting in crossed slots. During crossed slots transmitting MSs interfere with receiving MSs (MS→MS interference) and transmitting BSs interfere with receiving BSs (BS→BS interference). Same-entity interference can be quite detrimental especially in the case of BS→BS interference due to the locations of BSs (typically above rooftops) [2] which results in high probability of line of sight (LOS) conditions among BSs.

Contributions

The main focus of this work is to tackle the same-entity interference problem in OFDMA-TDD-based cellular networks. The problem is approached by analysing the severity of the major interference problem, i.e. BS→BS interference, when LOS conditions among BSs are in place. Such an analysis for OFDMA-TDD-based systems has not been reported in literature yet, to the best of the author's knowledge. The detrimental effects of BS→BS interference in OFDMA-TDD cellular networks are highlighted by comparing the interference avoidance method fixed slot allocation (FSA) against state of the art interference mitigation approaches considered by IST-WINNER (Information society technologies - wireless world initiative radio) [12], *viz:* random time slot opposing (RTSO) and zone division (ZD). The principle of FSA is that the UL-DL time slot assignment ratio is kept fixed and constant across the cells in a network (and usually allocates half of the resources to UL and DL each) [13]. While FSA is the most straightforward way to avoid crossed slots, this method compromises the support

for cell-independent traffic asymmetry that TDD otherwise offers. In contrast, both RTSO and ZD allow each cell to independently set its TDD switching point (SP). RTSO [14] is a method which relies on randomisation. In particular, in order to mitigate the same-entity interference problem, RTSO randomly permutes the time slots within a frame. In this way persistent severe interference is avoided, and in effect interference diversity is achieved. In order to investigate the effect of RTSO on crossed slots, this thesis formulates the probability for crossed slots when RTSO is employed. In contrast to RTSO, ZD [15] aims to mitigate same-entity interference by reducing the transmission range during crossed slots. In particular, during crossed slots resources are allocated only to MSs which are located in the inner region of the cell. The reduced transmission range in effect increases the separation distance between transmitters and vulnerable receivers and hence lowers interference as well. The comparison between RTSO and FSA and between ZD and FSA is done based on Monte Carlo simulations and the main comparison metric is spectral efficiency that is calculated using a signal-to-interference-plus-noise ratio (SINR) equation developed in this thesis. Furthermore, the comparison between FSA and RTSO is done utilising the known OTA-SRR (optimum target assignment - stepwise rate removals) resource allocation algorithm which is formulated for OFDMA in this thesis. The simulation results demonstrate that in the presence of crossed slots when LOS conditions among BSs are accounted for, both RTSO and ZD perform worse than FSA for all considered performance metrics. The results suggest that current interference *mitigation* techniques do not offer an effective solution to the BS→BS interference problem. Hence, a new interference *avoidance* method is needed, which unlike FSA, does not sacrifice the advantages of TDD.

In light of the above, the major contribution of this thesis is a novel *cooperative* resource balancing technique that resolves the crossed slot problem. The novel concept, termed *asymmetry balancing*, is targeted towards next-generation cellular systems, envisaged to have *ad hoc* and multi-hop capabilities. Asymmetry balancing completely avoids crossed slots by keeping the TDD SPs synchronised among BSs. At the same time, the advantages of TDD are retained, which is enabled by introducing cooperation among the entities in the network. If a cell faces resource shortage in one link direction, while having free resources in the opposite link direction, the free resources can be used to support the overloaded link direction. In particular, traffic can be offloaded to near-by mobile stations at neighbouring cells that have available resources. This novel concept of supporting cell-specific traffic asymmetries while the network-wide TDD is synchronised among cells is termed *virtual SP*. Asymmetry balancing works both when the UL is overloaded (referred to as *UL* asymmetry balancing) and when the *DL* is overloaded

(referred to as DL asymmetry balancing). This thesis focuses on the case of UL asymmetry balancing. UL asymmetry balancing is deemed more interesting than DL asymmetry balancing in light of the incorporation of multimedia and Internet packet services in cellular networks. In particular, as traffic is envisaged to be generally DL-favoured, the network-wide TDD SP will also be primarily DL-favoured (or occasionally symmetric). This means that there may be cells that require UL-favoured SP and these cells will not be able to support the UL demand. In such cases UL asymmetry balancing can be very beneficial. To model the envisaged gains in employing asymmetry balancing, a mathematical framework is developed which is verified by Monte Carlo simulations. In addition, UL asymmetry balancing is compared against both ZD and FSA based on simulations and the results demonstrate the superior performance of asymmetry balancing. It is concluded that the novel interference avoidance approach is a very promising candidate to resolve the crossed slot problem in future cellular networks based on OFDMA-TDD such as WiMAX (Worldwide interoperability for microwave access) [8] and LTE [4].

Thesis layout

This final section of the first chapter presents the layout of the rest of the thesis, organised into five further chapters as follows:

Chapter 2 starts with a brief discussion of the history of cellular networks to put into perspective current developments and future outlook. The cellular concept is also introduced, as well as the concept of frequency reuse. In addition, an overview of duplex techniques and multiple access techniques is given. Furthermore, the notion of multi-hop networks is presented and a comparison is drawn between multi-hop cellular networks and single-hop cellular networks.

Chapter 3 treats the topic of capacity of OFDMA-TDD cellular networks. The general notion of capacity is defined in the context of cellular networks. Furthermore, the first contribution of this thesis is presented, which is a detailed SINR derivation for OFDMA-TDD cellular networks. The SINR formulation considers a cross-layer approach whereby fast fading effects as well as slow fading effects are accounted for. In addition, the distance (in terms of number of subcarriers) between an interfering subcarrier and the victim subcarrier is taken into account when calculating interference. Shannon's capacity equation and adaptive modulation are also discussed. In addition, limitations to the capacity of OFDMA-TDD-based cellular networks are

reviewed.

Chapter 4 discusses interference mitigation techniques for cellular OFDMA-TDD networks. First, an introduction to interference mitigation is presented. Afterwards, an overview is given to fractional/soft frequency reuse techniques for OFDMA-based cellular networks which are techniques aiming to reduce inter-cell interference. TDD-specific interference mitigation methods are discussed next. In particular, RTSO and ZD are considered in detail and each is compared to the FSA technique via Monte Carlo simulations. The comparative analysis of FSA with RTSO and ZD is the second contribution of this thesis and the analysis aims to expose the adverse effects of BS→BS interference. Two further contributions of this thesis are presented in this chapter. The first one is the analysis of the probability of crossed slots when RTSO is employed. The second contribution is the formulation of the OTA-SRR resource allocation algorithm for OFDMA and this new formulation is used in the comparison between RTSO and FSA.

Chapter 5 discusses interference avoidance for multi-hop cellular OFDMA-TDD networks and presents the fifth and main contribution of this thesis which is the novel asymmetry balancing method that completely resolves the BS→BS interference problem. Asymmetry balancing supports cell-independent traffic asymmetry via a novel concept termed virtual SP, which is the final, sixth contribution of this thesis. Two components of the asymmetry balancing are identified, *viz*: resource availability and availability of relay stations. The impact of these two components on the functioning of asymmetry balancing is formally modelled by a mathematical framework. The mathematical framework is verified by Monte Carlo simulations. In addition, the performance of asymmetry balancing is compared against the performance of ZD and FSA.

Chapter 6 presents the summary and conclusions of the thesis, where limitations of the presented work are discussed and topics for further research are suggested.

Chapter 2
Background to cellular networks

2.1 Introduction

With the rapid headway of technology *ubiquitous wireless connectivity* is already within reach. *Ubiquitous wireless connectivity* means *convergence* of the Internet to "*anytime, anywhere, anything"*. Here "anything" refers to the multitude of devices that are envisioned to be interconnected. For example, according to the concept of smart homes almost any electrical device in a house can be networked in one system to operate in awareness of each other and of the environment [16]. In the particular context of mobile cellular networks, the convergence of the Internet puts ever more zealous demands on the network capabilities. The *anytime* connectivity translates into the network being available at all times, including busy periods. This calls for smart ways of load distribution. Load distribution is an issue of paramount importance especially due to the envisaged high data rate multimedia applications for mobile devices. Furthermore, *anywhere* connectivity means that the network should be capable of delivering the requested services independently of whether terminals are indoors, outdoors, or moving (including movement at high speeds). Such ubiquitous mobile services are envisioned for the next generation of mobile networks by the ITU (international telecommunication union), the body which defines the requirements for each generation of mobile communications systems.

However, a wireless cellular system which can efficiently handle all of the above-mentioned requirements does not exist as yet. This is why improving the capabilities of next-generation wireless cellular networks is of special interest in the current thesis. This chapter first introduces the basics of cellular networks. In particular, an overview of the cellular concept and the frequency reuse concept is given. Next, duplex techniques and multiple access techniques are reviewed. The chapter ends with a discussion on multi-hop cellular networks and their key differences from the traditional single-hop cellular network.

2.2 Cellular networks

2.2.1 History and outlook

The history of cellular networks can be traced back to the year of 1946, when the first commercial mobile network was launched in St. Louis, USA by AT&T [17, 18]. AT&T did not build a cellular network per se, rather, there was a single high-power transmitter with a coverage radius of more than 80 km. The system had only three channels and required operators to manually connect radio calls to the land-line telephone network. Two years later, in 1948, the first fully automatic network was launched in Richmond, Indiana [17]. The popularity of radio communications grew quickly and soon demand could not be met. The probability of an unsuccessful attempt to connect to the network rose to 65% [17] and it was clear that power and bandwidth resources could be utilised more effectively. To this end, the cellular concept was developed at Bell Labs in the 1940s [17]. According to the cellular concept, the coverage area is divided into cells where each cell has its own low-powered transmitter. It took more than 30 years to implement this idea and the first generation (1G) of cellular networks was launched in 1978 in Japan by NTT DoCoMo using the NAMTS (Nippon advanced telephone service) standard [17]. At about the same time, 1G networks were deployed also in the UK, Scandinavia, and Germany. They were all analog-based (raising privacy issues) and also lacked interoperability among them [17]. Four years later, in 1982, Europe responded by forming the GSM (Groupe Speciale Mobile), which aimed to develop a pan-European standard for cellular networks, as well as to digitise the wireless cellular communications [19, 20]. By the year 1987 there were already 13 countries which had committed to employ GSM. In 1991, the first GSM call was made by Radiolinja in Finland which landmarked the first deployment of a second generation (2G) network [19]. One of the appealing features of GSM was the ability to roam, i.e. to use GSM services seamlessly across countries. However, as GSM services were limited to voice and sending short messages, the next goal ahead was to implement a wireless network capable of delivering multimedia services, such as video calls, and mobile Internet access. As this meant that more bandwidth and higher data rates were necessary, multimedia was targeted to be a feature of the next, 3^{rd}, generation (3G) networks. The first network to commercially provide 3G services was launched in South Korea by SK Telecom and LG Telecom in 2000 and was based on CDMA2000 (code division multiple access) technology [21]. The historical time-line of mobile networks is presented in Fig. 2.1.

Now that a review of the history of mobile networks has been presented, it is interesting to

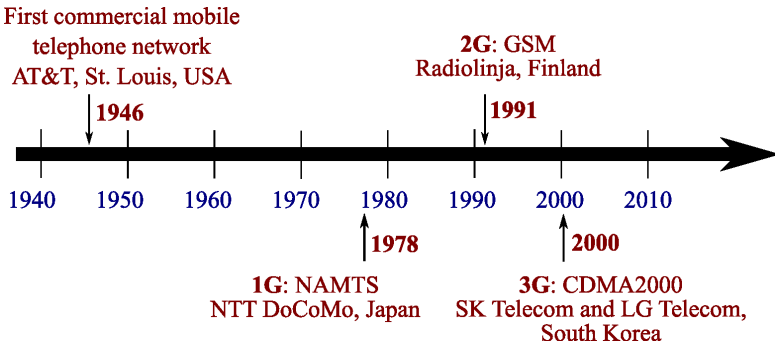

Figure 2.1: *History of the deployment of mobile networks [17, 19, 21].*

discuss future developments. So far mobile networks have been designed for voice services mainly with addons which allow for multimedia services. Next generation systems, however, will be optimised to carry packet-based data and voice traffic will be transported as VoIP (voice over internet protocol) [3, 22]. In addition, the ITU has specified the following requirements for the 4G mobile networks:

- Ubiquitous mobile access [3].
- Worldwide functionality and roaming [23].
- Data rates of 100 mbps for high mobility and 1 Gbps for low mobility users [3].
- *Heterogeneous* and *integrated* services such that subscribers can use any system, any time, anywhere to access a wide range of applications (based on voice, multimedia (including television), and internet [24]). For example, depending on the required services, the same device can access the local area network (LAN), the global positioning system (GPS), and the UMTS network seamlessly and transparently for the user [3, 22].
- *Personalised* services for people of different locations, occupations, and economic standing [22].

It should be noted that the 4G standard, termed IMT-Advanced (international mobile technology) by the ITU, is still to be finalised. Currently there are two technologies which are being developed to meet the requirements for a 4G system. The first one is LTE and specifically, its enhanced version LTE Advanced. LTE is an evolution of the GSM/UMTS family of standards and will be backward-compatible with them [4, 24]. The other technology is WiMAX [8], which offers fixed "last mile" broadband access and is also envisaged to offer portable Internet as a complement to the other mobile networks [25]. Fixed WiMAX (supporting static

subscribers) is already commercially available, however, this technology is 3G-certified by the ITU [26]. Mobile WiMAX solutions conforming to the 4G requirements are currently under development. It is interesting to note here that there is an evolution technology, particularly aimed for CDMA markets, called UMB (Ultra mobile broadband), which is developed by Qualcomm as the alternative to LTE. Just like LTE and WiMAX, UMB is based on OFDM and its network architecture is IP-based [27]. However, in 2008 the project was halted, leaving WiMAX and LTE the two major 4G technologies.

In the context of next generation technologies there is an interesting development called "green radio". "Green radio" is an initiative to make mobile networks more environmentally friendly by minimising power usage and making power consumption more efficient. To this end, according to [28] excess bandwidth needs to be exploited whenever possible. As per Shannon's equation which will be discussed later in this work, an increase in bandwidth results in linear increase in capacity, while an increase in power only results in a logarithmic increase in capacity. Therefore, exploiting underutilised bandwidth is not only a more effective way to increase capacity, but also the "green" way. The novel asymmetry balancing method presented in this work fits perfectly in the vision of "green" communications by utilising underused resources. Asymmetry balancing is discussed in detail in Chapter 5.

2.2.2 The cellular concept & frequency reuse

Cellular networks are a manifestation of the attempt to have large service area coverage in an interference-tolerable manner, as was briefly mentioned in the previous section. According to the *cellular concept* the intended coverage area is divided into cells, each having a relatively low-powered BS. In addition, the concept allows for the system bandwidth to be *reused* in different parts of the network. The cells are grouped together in clusters such that a cluster shares the system bandwidth, part of which is assigned to each cell in the cluster. Such frequency planning is particularly important as it controls the amount of interference that cells using the same frequency band cause each other (termed inter-cell interference or co-channel interference (CCI)). The tolerable inter-cell interference determines the cluster size and typical cluster sizes include four, seven, and twelve [18]. The cellular concept together with the frequency reuse mechanism for a cluster size of seven is illustrated in Fig. 2.2. Note that cell coverage is illustrated as hexagonal-shaped, while in reality coverage depends on propagation conditions. However, hexagonal representation is usually used for drafting convenience to illustrate full

area coverage [17]. A group of cells marked A through G form one cluster and the cells marked by the same letter use the same frequency bands (and are sources of CCI). Intuitively, the larger the cluster size, the fewer times a given band is reused within the system and hence the smaller the interference that each cell experiences from co-channel cells. In contrast, smaller cluster size causes a given band to be reused more often within the network, which in turn means better bandwidth utilisation but also higher interference. Hence, there is a trade-off between bandwidth utilisation and interference, which requires careful frequency planning. This notion is illustrated mathematically in the following [18].

Assume that there are c_{c} reusable channels available in a given system, which are shared by the cells in a cluster. The cluster is replicated K_{s} times in the system, meaning that the total system capacity, i.e. total number of channels that can be utilised, c_{t}, is given as:

$$c_{\mathrm{t}} = c_{\mathrm{c}} \cdot K_{\mathrm{s}}. \tag{2.1}$$

The number of channels per cluster depends on the number of allocated channels per BS, c_{b}, and on the number of BSs per cluster, B_{k}, as shown in:

$$c_{\mathrm{c}} = c_{\mathrm{b}} \cdot B_{\mathrm{k}}. \tag{2.2}$$

Therefore, it can be easily seen that the total number of channels that can be utilised in the system actually can be represented as:

$$c_{\mathrm{t}} = c_{\mathrm{b}} \cdot B_{\mathrm{k}} \cdot K_{\mathrm{s}}. \tag{2.3}$$

The mechanism of the trade-off between bandwidth utilisation and interference that was discussed above can be observed from (2.3). The capacity can be increased if the number of channels per BS is increased, while decreasing the number of BSs per cluster (and keeping the total number of BSs in the system fixed). This, however, will lead to more clusters in the system and higher co-channel interference. The opposite also holds true. Increasing the number of BSs per cluster means fewer clusters in the system, decreased co-channel interference, and decreased bandwidth utilisation. It should be noted that an important metric in this context is the *frequency reuse factor*, f_{r}, which is defined as:

$$f_{\mathrm{r}} = \frac{1}{B_{\mathrm{k}}}. \tag{2.4}$$

The frequency reuse factor essentially shows what fraction of the channels per cluster are used by a single BS.

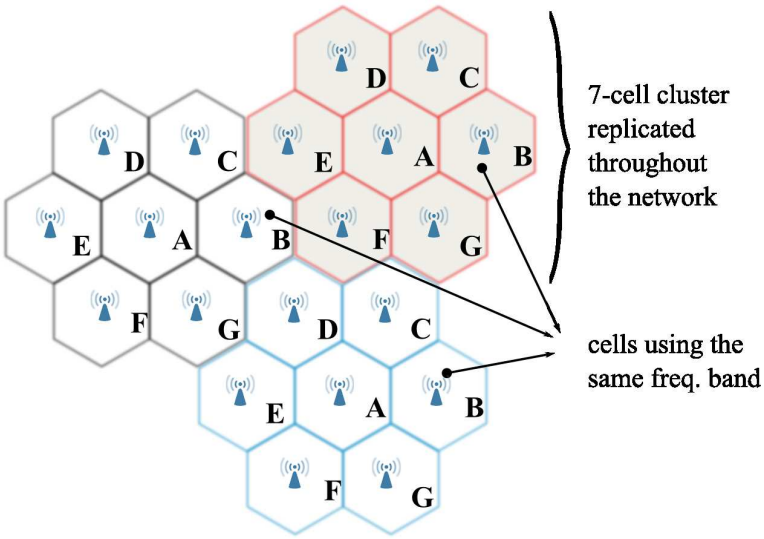

Figure 2.2: *The concept of frequency reuse: frequency bands are reused by spatially separated cells to reduce interference. A group of cells marked A through G form one cluster and the cells marked by the same letter are co-channel cells.*

Due to the high demand on bandwidth today and the envisioned increase in resource demand, next-generation networks will employ a cluster size one, i.e. frequency reuse of one [1], allowing each cell to use the whole available bandwidth. This is why it is very important to have efficient mechanisms to tackle the inter-cell interference problem, as is discussed later in this thesis.

2.3 Duplex techniques

As mentioned in the previous section, in a typical wireless cellular network each cell has a BS and each BS serves the subscribers (also referred to as MSs or users) which are in its respective cell area. In this context, service means providing connectivity in UL or DL or both. As shown in Fig. 2.3, in the case of UL, traffic is directed from the MS to the BS, whereas in the case of DL, traffic is directed from the BS to the MS. There are two duplex techniques, which administer how UL and DL are coordinated: frequency division duplex (FDD) and TDD. These are explained in the next two sections, concentrating on the following specific points of interest:

- Way of UL/DL coordination

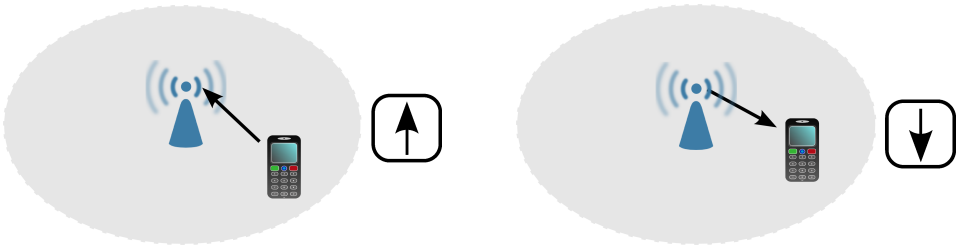

(a) UL: MS→BS (b) DL: BS→MS

Figure 2.3: *As shown in (a), during UL the MS communicates to the BS and UL is denoted by an arrow pointed up, while as shown in (b), during DL the BS communicates to the MS and DL is denoted by an arrow pointing down.*

- Type of inter-cell interference experienced
- Main advantages and drawbacks

2.3.1 Frequency division duplex

Introduction

In FDD, UL and DL are allocated separate non-overlapping frequency bands as shown in Fig. 2.4. These bands are usually equal in bandwidth and are separated by a guard frequency band. Having a dedicated UL frequency band and a dedicated DL frequency band means that

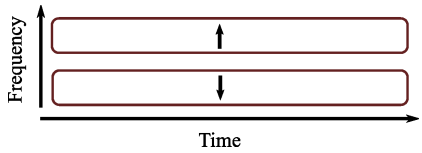

Figure 2.4: *FDD: a frequency band is allocated to UL and DL each.*

the UL communication only interferes with concurrent UL communication and, analogously, the DL communication only interferes with concurrent DL communication. As a consequence, there are two types of interference present in FDD, *viz*: (1) from MS to BS (MS→BS) which occurs during UL and (2) from BS to MS (BS→MS) which occurs during DL. These two types of interference are commonly referred to as *other-entity* interference.

Advantages

The major advantages of FDD are outlined below:

- FDD facilitates continuous and simultaneous transmission in UL and DL by dedicating a frequency band to UL and DL each. This makes FDD particularly suitable for voice traffic.
- Due to the fact that UL and DL take place on separate frequency bands, BSs do not interfere with each other and MSs also do not interfere with each other. This is a particularly important advantage, because as will be subsequently seen, in TDD there is interference among BSs and among MSs in addition to the FDD-specific interference. The lack of interference among the BSs makes cell site planning easier as compared to TDD.

Disadvantages

The major disadvantages of FDD are outlined below:

- The fixed channel allocation in FDD, which is advantageous for voice (symmetric) traffic, is a disadvantage when considering packet-based services such as data traffic and the Internet. These services can be largely asymmetric in nature, hence, cannot be efficiently supported by FDD.
- In order to minimise interference between UL and DL transmissions, FDD utilises a guard band, which is typically two times either the UL or DL band [8]. While the guard band spectrum can indeed be used for other applications, careful frequency planning is necessary to avoid interference.
- The deployment of FDD requires higher hardware costs as compared to TDD. This is because due to the concurrent operation of UL and DL, at each transceiving unit a separate receiver, a separate transmitter, and a duplexer are required, in addition to RF filters needed to isolate the UL and the DL signals.
- Future systems require large bandwidth (greater than 20 MHz [29] and up to 100 MHz [30]) and it might be difficult to find unoccupied paired spectrum necessary for FDD due to the fact that the frequency bands below 10 GHz are heavily utilised worldwide by co-existing systems. In some countries, however, spectrum is being freed up. For example, in the UK spectrum will be released for auction due to switching TV broadcast signals to a more bandwidth efficient digital format - the so-called digital dividend. Nevertheless, this is still an issue worth pointing out.

2.3.2 Time division duplex

Introduction

In contrast to FDD, TDD can adaptively allocate resources by toggling UL and DL in time, while both UL and DL are allocated the whole bandwidth (refer to Fig. 2.5). As a result, only one frequency band is required. Hence, in comparison with FDD, clearly TDD does not require a guard frequency band. However, whenever there is a switch in link direction (i.e. SP), a guard time interval is needed because MSs cannot transmit and receive on the same frequency at the same time [31]. In particular, there are two types of guard-time intervals. The first type is referred to as transmit/receive transition gap (TTG) and is necessary whenever there is a switch from DL to UL [32]. The second type accommodates the reverse switch, from UL to DL, and is referred to as receive/transmit transition gap (RTG) [32]. The TTG needs to accommodate the round-trip delay, i.e. the time needed for the signal to travel from the BS to the MS and back [32]. As all MSs at a given cell synchronously transmit and synchronously receive, the TTG needs to accommodate the round trip delay associated with the MS that is farthest from the BS. Hence, the TTG actually accounts for the round trip delay of the signal travelling to the cell edge and back [31]. In contrast, the RTG is the time needed for the hardware to switch from UL mode to DL mode, and is hence much shorter than the TTG [32]. Note that the TDD frame may require one or more TDD SPs that switch between UL and DL transmission (and vice versa) depending on the UL-DL time slots allocation. Fig. 2.5(a) displays a single TDD frame, where the UL and the DL are allocated two separate contiguous blocks. In this case only one TDD SP per frame is needed (and one at the end or beginning of each frame, which is not shown in the figure). It is also possible to have the UL and DL time slots permuted in a frame, resulting in the need for multiple TDD SPs. This case is shown in Fig. 2.5(b).

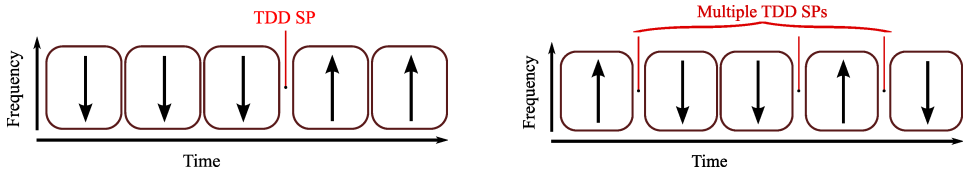

(a) Single SP per frame (b) Multiple SPs per frame

Figure 2.5: *TDD: UL and DL are both allocated the whole bandwidth and are dynamically toggled in time. The TDD frame may require one or more TDD SPs depending on the UL-DL time slots allocation.*

In comparison to FDD, TDD suffers from two types of additional interference, referred to

as *same-entity* interference, namely: (1) MS→MS interference and (2) BS→BS interference. Note that the latter is particularly detrimental due to the exposed location of BSs which causes high probability of LOS. As mentioned in Chapter 1, same-entity interference occurs during *crossed slots*, i.e. whenever two neighbouring cells use the same time slot in opposing link directions, as illustrated in Fig. 2.6. In the case when the UL part of the frame and the DL part of the frame are allocated as two contiguous blocks (Fig. 2.5(a)), crossed slots can arise in two situations [33]. The first situation is when the TDD frames among BSs are synchronised. Then, crossed slots occur if neighbouring cells have allocated a dissimilar number of resources to UL and DL which means that the TDD SPs vary in time across cells. The second situation is when the TDD frames among BSs are not synchronised and BSs start each frame independently of each other. In this case even all of the slots in a frame can be crossed slots. However, if the UL and DL time slots in a frame are not allocated as two contiguous blocks but are randomly permuted instead (Fig. 2.5(b)), crossed slots are bound to occur among cells. In this situation, the number of crossed slots varies depending on the ratio of UL-to-DL slots per frame. Ultimately it does not matter whether or not the BSs begin each time frame in a synchronous manner. A further discussion of this scenario is provided in Section 4.4.1.

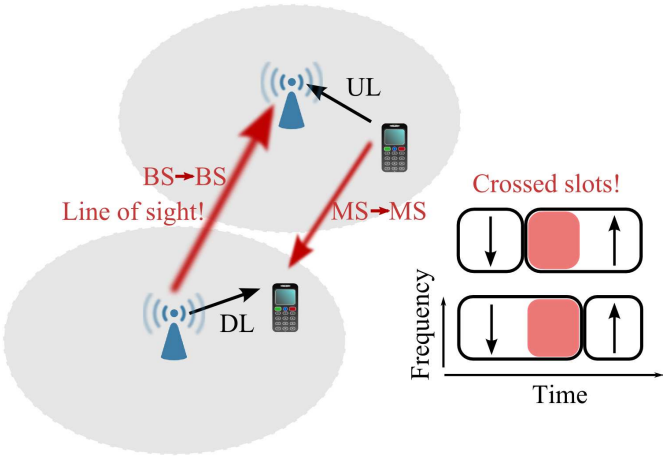

Figure 2.6: *Whenever a cell is in UL while a neighbouring cell is in DL, crossed slots occur, causing same-entity interference.*

Advantages

The major advantages of TDD are outlined below:

- TDD can adapt to cell-specific asymmetry demands, which means that each cell can

allocate UL/DL resources independently. It is of paramount importance to be able to dynamically adapt to the traffic demand in the network because current and future wireless communications are packet-based and characterised by high peak-to-average traffic ratio [1, 2, 34].

- TDD obviates the need to feedback channel information (needed for power control, etc) because UL and DL share the same channel. This property of TDD is usually referred to as channel reciprocity [34].
- The hardware costs needed for TDD implementation can be comparatively lower than the hardware costs needed for FDD implementation, because the UL and the DL can share the same oscillator and filters and, in addition, the need for a duplexer is obviated [32].
- TDD supports multi-hop relaying capabilities within the network at low cost, due to the fact that each relay station (RS) needs only a simple transceiver with an UL/DL switch [35]. Multi-hop networks are discussed in Section 2.5.

Disadvantages

The major disadvantages of TDD are outlined below :

- The major drawback of TDD-based systems is BS→BS interference due to the high probability of LOS among BSs [1, 2, 31, 34].
- Inter-operator interference is another major issue in TDD. Operators which are allocated adjacent channels may experience severe interference due to the fact that adjacent channel rejection is only limited (which is why in FDD guard frequency bands are used). Inter-operator interference is difficult to avoid because operators need to synchronise their networks to a common reference and also to adopt the same asymmetry [36]. Both of these requirements limit the flexibility that operators otherwise have with respect to TDD. This is a major reason as to why FDD is preferred to TDD.
- Even though TDD does not require a guard frequency band, it requires a guard time interval. As was discussed in Section 2.3.2, the TTG should be larger than the round-trip delay in the system. Hence, for large cell sizes, this can lead to significant efficiency losses [32]. This is why usually TDD is considered for small cell sizes [2].

Until now FDD has been primarily used in 2G standards (e.g. GSM [18]) because the major mobile telephone service has been voice. However, due to its numerous advantages in the context of future wireless systems, TDD is of particular interest. This is why research is targeted towards resolving TDD's disadvantages, and in particular, the BS→BS interference problem.

2.4 Multiple access techniques

So far the discussion concentrated on the way BSs and MSs coordinate MS↔BS communication. Another important point to review is how multiple MSs are coordinated in accessing the joint network resources. This is referred to as *multiple access*. The most important multiple access techniques are: frequency division multiple access (FDMA), time division multiple access (TDMA), CDMA, and hybrids thereof. While the first three (most basic) methods are briefly introduced, the focus in this section is on the hybrid OFDMA technique. As already mentioned in Chapter 1, OFDMA is of particular interest for future systems such as LTE and WiMAX and is therefore treated in detail.

2.4.1 Frequency division multiple access and time division multiple access

In FDMA users who require radio resources are served at the same time on different (non-overlapping) frequency bands, as illustrated in Fig. 2.7. FDMA can be combined with both

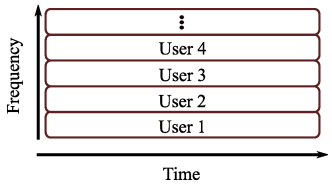

Figure 2.7: *FDMA: users are served at the same time on different frequency bands.*

TDD and FDD. In the case of FDMA-TDD, users who request service use the UL and DL resources at different time instances [18]. This is in contrast to the case of FDMA-FDD where users need to be allocated a pair of frequency bands, one for UL and DL each, and UL and DL communication is concurrent [18].

In TDMA users who demand access to the network are multiplexed in time, as shown in Fig. 2.8, which means that users are allocated the whole bandwidth at different (non-overlapping) time instants. Similarly to FDMA, TDMA can be combined with both TDD and FDD. In the

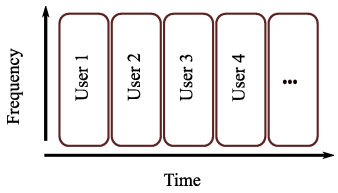

Figure 2.8: *TDMA: users are served using the whole bandwidth at different times.*

case of TDMA-TDD a user who requests service is allocated the whole bandwidth for a given time duration in the UL part of the transmission frame and again in the DL part of the transmission frame. In contrast, in TDMA-FDD users share both the UL and the DL frequency bands in a TDMA fashion, i.e. a user is allocated a TDMA time slot in the UL frequency band and in the DL frequency band. It should be noted that most 2G standards employ FDD with a hybrid form of TDMA and FDMA (e.g. GSM) [20]. An FDMA/TDMA architecture combined with TDD has been employed by cordless systems across Europe and Asia [20]. In addition, a hybrid form of FDMA and TDMA is considered for all new technologies envisioned to be deployed as next generation systems, such as WiMAX [9], LTE (including LTE Advanced) [4, 5], and the IST-WINNER [30].

2.4.2 Code division multiple access

CDMA is fundamentally different from both TDMA and FDMA in that CDMA is a spread spectrum technology. This means that the message signal is multiplied by a spreading signal, having a relatively large bandwidth. The spreading signal is a pseudo noise (PN) code and the PN codes of different users are approximately orthogonal. As a result, the transmitting entities make use of the whole bandwidth at the same time. The basic principle of CDMA is illustrated in Fig. 2.9. Each additional user increases the overall noise level seen by other users, which

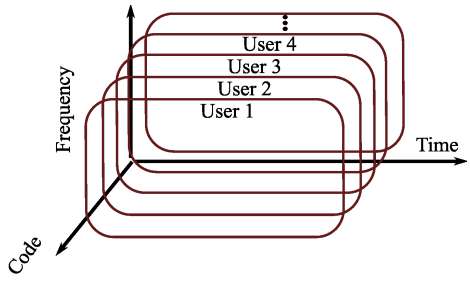

Figure 2.9: *CDMA: users are served at the same time using the whole bandwidth on different PN codes.*

makes CDMA an interference-limited system [37]. Thus, for optimum user experience, perfect power control should be in place, i.e. the received power level needs to be constant over the users. A problem, which arises from lack of power control, is the near-far effect. This problem occurs when the received power from an interfering user is higher than the received power of the desired user. As a result, users close to the BS overpower users that are further away and prevent their signal from being properly received. Notwithstanding, CDMA allows for a frequency reuse of one (due to the fact that interference can be treated as noise [38]) and is the main multiple access technique used in 3G technologies such as UMTS (universal mobile telecommunications system) [39].

2.4.3 Orthogonal frequency division multiple access

Introduction

OFDMA is based on orthogonal frequency division multiplex (OFDM) which is a special case of frequency division multiplex (FDM) [40]. In this section FDM and OFDM are introduced first, and then OFDMA is discussed.

In FDM data is multiplexed onto equally spaced frequencies (no relation between the centre frequencies is implied), separated by a guard band. FDM is a technique for multi-carrier (MC) transmission, as opposed to single-carrier (SC) transmission. The difference between MC transmission and SC transmission is that when the former is employed, a fast serial data stream is transformed into a number of slower parallel data streams. MC is particularly advantageous in light of the demand for higher data rates and, hence, larger bandwidths which makes SC transmission vulnerable to channel effects. There are two main reasons why in comparison to SC transmission MC transmission is considered more robust to the dispersive nature of the channel, both in time domain and in frequency domain. First, the transmission bandwidth per channel in the case of MC is decreased as compared to SC, and second, the duration of the transmit symbol in the case of MC is increased as compared to SC. This can be expressed mathematically as follows: given that the data is transformed into N_{s} parallel streams and that the SC signal bandwidth is W_{sc}, then the MC signal bandwidth is $W_{\mathrm{mc}} = \frac{W_{\mathrm{sc}}}{N_{\mathrm{s}}}$. Furthermore, given that the symbol duration in the case of SC transmission is T_{sc}, the symbol duration when MC transmission is employed can be expressed as $T_{\mathrm{mc}} = T_{\mathrm{sc}} \cdot N_{\mathrm{s}}$. The longer symbol duration means that there is little or no inter-symbol interference resulting from consecutive symbols [18]. In addition, having multiple carriers instead of a single one means that by design the channel

bandwidth can be made smaller than the coherence bandwidth [18]. Note that the coherence bandwidth identifies the range of frequencies within which the channel can be assumed "flat". (A flat channel affects all spectral components in the same way.) Having flat-fading channels within a larger frequency selective bandwidth (where frequency selectivity means that different frequencies fade differently) are beneficial in resource allocation in that different channels can be assigned different data rates based on their individual fading conditions. This topic is further discussed in Chapter 3. The comparison of MC transmission to SC transmission is summarised in Fig. 2.10.

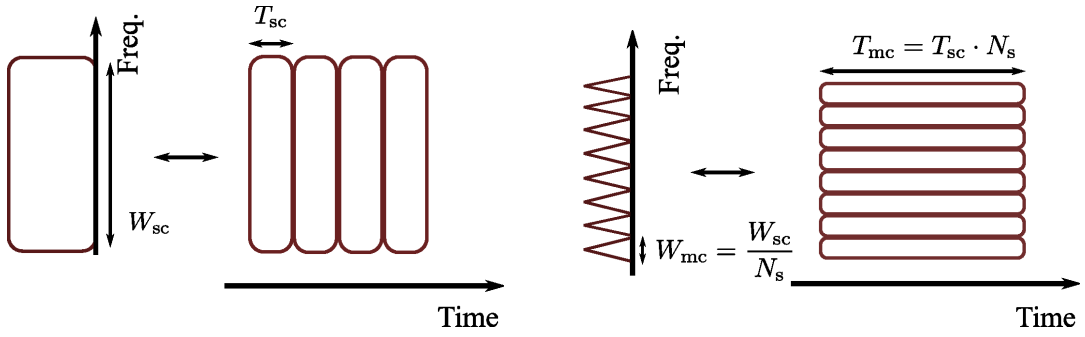

(a) Single carrier transmission (b) Multi-carrier transmission

Figure 2.10: *Large transmission bandwidth results in short symbol duration as shown in (a), while narrow transmission bandwidth results in long symbol duration as shown in (b).*

OFDM, as its name suggests, is not simply an FDM technique. OFDM can be considered a method which is a hybrid of MC transmission and modulation [41]. In particular, in OFDM the serial data stream is divided into a number of parallel bit streams, each of which is then modulated onto individual orthogonal frequency carriers. Orthogonality among subcarriers means that subcarriers do not interfere with each other, even though their spectra overlap. This is attained by setting the subcarrier frequencies to be integer multiples of each other, as demonstrated in Fig. 2.12. As a result, in comparison to FDM, OFDM saves spectrum, as shown on Fig. 2.11, and also power. Power is saved by reducing interference among subcarriers, which is discussed later on in this chapter.

Modulation in OFDM is achieved through the inverse fast Fourier transform (IFFT). In particular, in OFDM after the serial data stream is converted into parallel data streams, the IFFT is performed. The IFFT operation is very computationally inexpensive and significantly decreases the receiver/transmitter complexity. An elegant way in which OFDM maintains orthogonality is by appending a cyclic prefix to each symbol. A cyclic prefix is added by copying the last

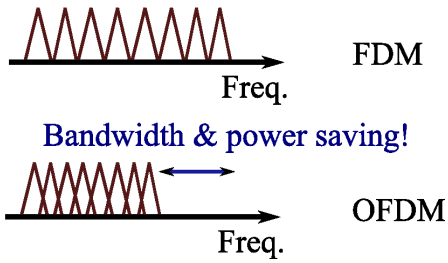

Figure 2.11: *OFDM saves bandwidth and power by making use of orthogonality among sub-carriers.*

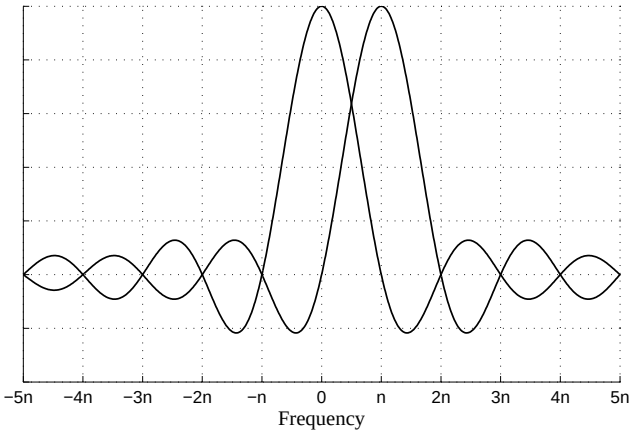

Figure 2.12: *OFDM uses frequency carriers which are integer multiples of the centre frequency.*

χ number of bits of a symbol to the front part of the symbol. In this way, an otherwise linear convolution is "turned" into a circular one, which is of paramount importance in order to be able to restore the transmitted signal properly at the receiver. This concept can be expressed mathematically as follows [41]:

$$x(t) = \frac{1}{\sqrt{T_{\rm s}}} \sum_{m=0}^{N_{\rm tot}-1} s_{\rm m}(n) \exp(j2\pi \frac{m}{T_{\rm s}} t), \;\; nT_{\rm s} - T_{\rm G} \leq t \leq (n+1)T_{\rm s}, \tag{2.5}$$

where $x(t)$ is the transmitted signal; $T_{\rm s}$ is the symbol duration; $N_{\rm tot}$ is the number of sub-carriers; $s_{\rm m}(n)$ is the modulated signal; $T_{\rm G}$ is the duration of the cyclic prefix; and j is the imaginary unit. Due to the cyclic prefix, $x(t)$ is actually partially periodic with period $T_{\rm G}$, i.e.

$$x(t - t_1) = x(T_{\rm s} + t - t_1), \;\; t - t_1 \leq T_{\rm G}.$$

In particular, without the cyclic prefix, performing FFT (fast Fourier transform) at the receiver

means performing FFT on the *linear* convolution of the channel response and the transmitted signal. However, the FFT of this linear convolution does not allow for the transmitted signal to be properly extracted. This is only possible if the FFT is performed on a circular convolution. Appending a cyclic prefix to each symbol serves exactly the purpose of turning a linear convolution to a circular one. The received signal can be expressed mathematically using vector notation as:

$$\mathbf{r}(t) = \mathbf{x}(t) \odot \mathbf{h}(t) + \mathbf{n}_{\mathrm{th}}(t), \tag{2.6}$$

where $\mathbf{r}(t)$ is the received signal vector; $\mathbf{h}(t)$ is the channel impulse response vector; $\mathbf{n}_{\mathrm{th}}(t)$ is the additive noise vector; and $\odot$ denotes circular convolution. Because the FFT transforms circular convolution into multiplication, the received signal at the receiver can be expressed as:

$$\mathbf{R}(f) = \mathbf{S}(f)\mathbf{H}(f) + \mathbf{N}_{\mathrm{th}}(f),$$

where $\mathbf{R}(f)$, $\mathbf{S}(f)$, $\mathbf{H}(f)$, and $\mathbf{N}_{\mathrm{th}}(f)$ are the respective FFT pairs of $\mathbf{r}(t)$, $\mathbf{s}(t)$, $\mathbf{h}(t)$, and $\mathbf{n}_{\mathrm{th}}(t)$.

However, even though it is a strict necessity, the cyclic prefix presents an overhead to the system and also adds redundancy, which directly translates into loss of throughput. To justify these drawbacks and to maximise the benefits of using a cyclic prefix, the cyclic prefix is also exploited to facilitate error correction and synchronisation. For more information on the use of FFT and the cyclic prefix in OFDM, the interested reader may refer to [42].

OFDM, similarly to FDM, has been used as a basis for a multiple access technique and the technique is termed OFDMA. In OFDMA each user is assigned a group of frequency carriers, depending on the channel conditions. Such a technique is efficient, because it can exploit the frequency selectivity of the channel. In particular, as the channel characteristics are generally dissimilar among users, the same frequencies fade differently for different users (which is known as multiuser diversity). Hence, in OFDMA each subcarrier can be allocated to user who experiences the best fading conditions for that subcarrier. Fig. 2.13 illustrates an example, where the channel transfer functions of three users are shown. It can be seen that if the whole bandwidth were assigned to a single user, the spectrum would generally be underutilised, due to the multiple fades a single user would experience. Additionally, the flat fading of the OFDMA channels is beneficial as discussed previously, as well as the scalability of the OFDMA system combined with its low complexity. These advantages and the disadvantages

of OFDMA are reviewed below.

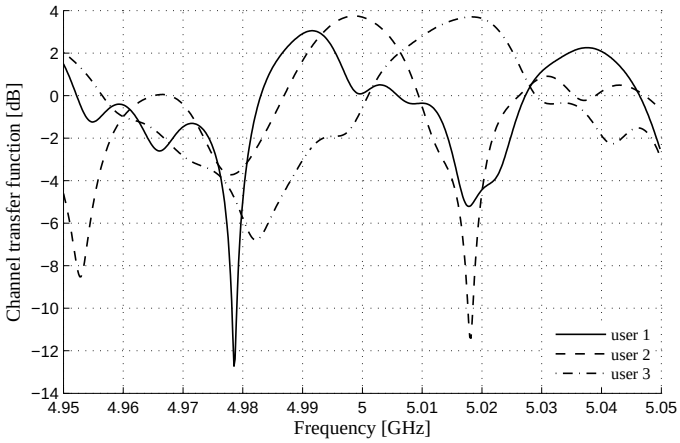

Figure 2.13: *Frequency selectivity and multi-user diversity: different frequencies fade differently and the channel transfer function has dissimilar characteristics among users.*

Advantages

- One of the most important advantages of OFDMA is *scalability* [11]. Scalability means that an OFDMA system can be deployed using a range of bandwidths. This is achieved by keeping fixed the frequency separation between subcarriers as well the symbol duration. As a result, the dimension of the basic resource (in time and frequency) is fixed. In order to support deployments with different bandwidth, the FTT size is adjusted accordingly. This means that the air interface stays practically the same for different deployment scenarios.

- OFDM provides a *low-complexity* solution to one of the most detrimental problems which exist in wireless communications, namely multi-path. The multi-path effect is a manifestation of the surroundings. The transmitted signal bounces off objects, buildings, trees, etc, thus multiple copies of the transmitted signal arrive at the receiver at different times and with different power. This causes the received signal to be distorted and "spread out" in time and the time duration of the spread is termed *delay spread*. The multi-path effect also results in *inter-symbol interference* (ISI), which is the interference between consecutive transmitted symbols, which "leak" into each other. OFDM overcomes the above-mentioned challenges, due to the longer OFDM symbol duration and the cyclic prefix.

Disadvantages

synchronisation In order to maintain the orthogonality among subcarriers and to avoid ISI, OFDM requires frequency and phase synchronisation. As a result, OFDM is prone to synchronisation problems occurring due to synchronisation errors and movement, i.e. Doppler shift.

PAPR High peak-to-average power ratios (PAPR) can occur because the OFDM signal is an addition of many sinusoid waves. When sinusoid waves add constructively, high peak powers are observed. In contrast, when sinusoid waves add destructively, very low powers can result.

There are ways to address the above issues. For example, pilot carriers can be used to facilitate synchronisation, while a way to address the PAPR problem would be via clipping the power to the desired level. Clipping is advantageous because of its simplicity, however, it has a major disadvantage. In particular, clipping introduces distortions and results in loss of orthogonality. (For a detailed treatment of OFDM, the interested reader may refer to [40, 42, 43].) In general, it can be stated that the advantages of OFDM have the potential to offset the disadvantages in light of the requirements of future wireless networks. This is demonstrated by the fact that OFDM is already widely used for technologies such as digital video broadcast (DVB) and digital audio broadcast (DAB) [44] as well as for WLAN (wireless local area network) [41]. Furthermore, OFDM and OFDMA in particular, have great potential for next-generation mobile communication systems [45]. For example, technologies such as mobile WiMAX [9] and LTE Advanced [5] are based on OFDMA.

OFDMA-TDD

As previously mentioned, this thesis concentrates on networks based on OFDMA-TDD. This is particularly because according to the ITU, systems conforming to IMT Advanced need to support both TDD and FDD [3] and TDD still poses open research issues, as already discussed.

A practical example from the LTE technology is used [29], shown on Fig. 2.14, in order to illustrate how resources in OFDMA-TDD are organised. A frame is displayed, made up of eight time slots such that four slots are allocated to UL and DL each. Consider an UL time slot as an example. The slot is divided into chunks (resource blocks [29]), where the duration of the chunk is a number of OFDM symbols such that the chunk duration equals the duration of the time

slot. Note that the chunk is the smallest resource unit which can be allocated for transmission. Furthermore, along the frequency axis, each time slot occupies the whole bandwidth, which is subdivided into a number of chunks. Each chunk is further subdivided into a number of subcarriers. According to the LTE specifications, for the case of UL a suitable number of chunks per time slot is 12, the subcarrier spacing is 15 kHz with a total of 2048 subcarriers (making the system bandwidth 30.72 MHz), and the number of OFDM symbols/chunk is six or seven, depending on the choice of cyclic prefix [29]. Furthermore, note that according to the LTE specifications, there are a number of ways to arrange the UL and DL time slots in the frame. Generally, the UL and the DL slots are spread out in the sense that they are not necessarily arranged in an UL block and a DL block, respectively. However, it is possible to have an UL subframe and a DL subframe as two contiguous blocks as is the case in IST-WINNER [13] and WiMAX [9]. It is also worth to note that while IST-WINNER follows an analogous resource organisation as LTE, the case of resource organisation considered in WiMAX [9] is significantly different. In particular, there are two ways in which subcarriers are grouped together to form a sub-channel. The first way is analogous to what has been defined here as a chunk, i.e. a contiguous group of subcarriers. The second way is to randomly choose subcarriers from across the available spectrum which is analogous to the concept of frequency hopping. For more details, the interested reader may refer to [9].

2.5 Single-hop vs multi-hop cellular networks

The 2G and 3G wireless cellular networks currently deployed are an example of the so-called single-hop cellular networks (SCN). The number of hops reflects the number of intermediate nodes between a transmitter and a destination receiver. Single-hop transmission means that the link between the transmitter and the destination receiver is direct, without any intermediate nodes. SCNs are limited by the coverage of the BS, which means that if an MS is outside the area in which any BS is capable of providing service, the MS will not be served. In addition, a further limitation to SCNs is that a frequency band can be used only once within a given cell area and if the demand for resources is high, congestion may occur.

Upgrading cellular networks to MCNs is an effective way to resolve congestion and improve service coverage without significantly increasing infrastructure cost. In MCNs there can be intermediate nodes serving as RSs between the transmitter and the destination receiver. The RSs can be either an MS or a stationary dedicated transceiver, which is usually replaced based

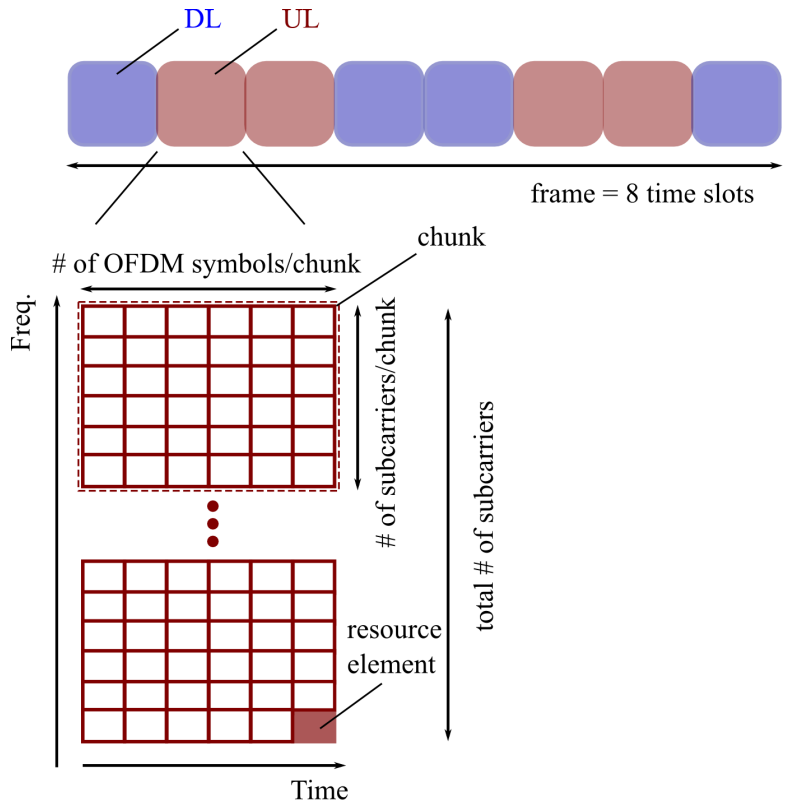

Figure 2.14: *Example for resource organisation of OFDMA-TDD as per the LTE technology [29].*

on traffic demand. Fig. 2.15 displays the main working principles of MCNs and SCNs. The advantages of both types of MCN are discussed below.

Advantages of MCNs with fixed relays

- The position of RSs is carefully planned such that connectivity with the BS is ensured.
- The power budget of an RS is higher than that of an MS.
- As opposed to an MS, a dedicated RS does not have own data to transmit, which potentially means faster relaying.

Advantages of MCNs with mobile relays

- No infrastructure is required. As a result, coverage and potentially data rate, can be

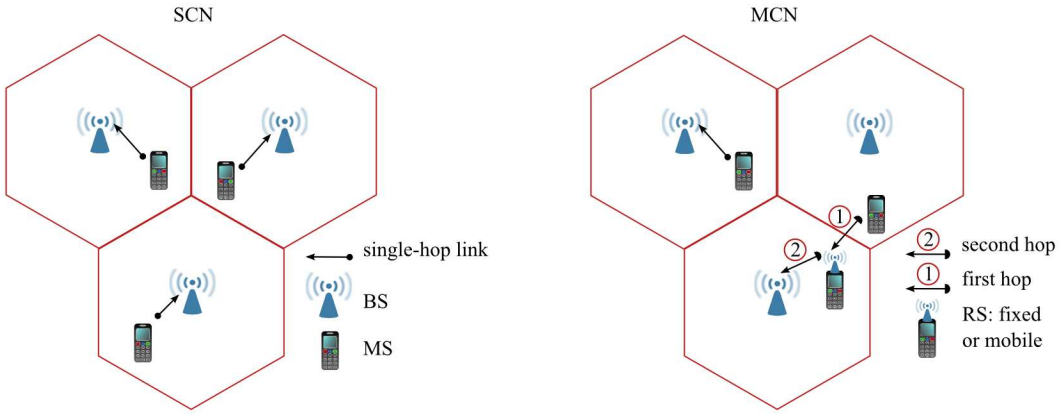

(a) SCN principle (b) MCN principle

Figure 2.15: *The principles of SCNs and MCNs are shown in (a) and (b), respectively. SCNs use a single transmission path from the transmitter to the destination receiver (i.e. one hop), whereas in MCNs it is possible to have multiple sequential transmission paths, such that the data reaches the destination receiver in a number of consecutive hops.*

improved at virtually no cost.

- The network becomes partially self-organising, which is an important feature, as future wireless networks are envisaged to be of a decentralised nature.
- With the increase in popularity of mobile wireless services, the number of idle MSs also increases. This provides a tremendous relaying resource which cannot be matched by deploying fixed RSs.

Currently, the deployment of fixed RSs is easier for providers. This is because even though there is the need for investment, fixed RSs are easier to make use of by applying current know-how gained from BS operation. After all, a fixed RS can be considered as a mini-BS. This is in contrast to implementing RS functionality in MSs, which requires not only new firmware for the mobile phones to enable RS functionality, but also adequate financial rewards for the users who agree to serve as RSs as well as security assurance for the RSs. Regarding the latter, new security protocols will be necessary to ensure that the information of the RSs is protected. In addition, the incoming data to be relayed by RS should also be safeguarded. To date, fixed RSs are considered as extensions to the standard cellular deployment, e.g. WLAN and WiMAX [46]. For next-generation networks, however, integration of fixed RSs in the cellular network is indispensable (e.g. IST-WINNER [7] and LTE [35]). This is why a major focus in this work

is utilising the RS capabilities in MCNs. In particular, this thesis concentrates on MCNs where MSs serve as RSs because no investment in extra infrastructure is needed and, in addition, there is relatively little research on the subject [6]. MCNs with mobile RSs are a promising way to improve system performance in future networks, as is discussed in Chapter 5.

2.6 Summary

The fundamentals of cellular networks were provided in this chapter. The cellular concept, as well as the frequency reuse concept and their importance to cellular networks were introduced. Duplex technologies were also reviewed. It was pointed out that even though TDD suffers from additional interference as compared to FDD, TDD has major advantages. For example, TDD can efficiently support cell-specific traffic asymmetries and in addition, TDD is an enabler for multi-hop communication. Furthermore, multiple access techniques were also discussed. It was pointed out that OFDMA is a suitable candidate for next-generation systems due to its robustness to multi-path fading effects, inter-symbol interference and delay, as well as because OFDMA obviates the need for complex equalisers. Finally, it was emphasised that MCNs are of particular importance for next-generation networks because with the help of RSs both the network coverage can be improved and congestion can be efficiently alleviated.

This chapter identified the promising technologies for next-generation networks, namely MCNs based on OFDMA-TDD. In the subsequent chapters, the thesis concentrates on OFDMA-TDD-based cellular networks, focusing on MCNs, however, SCNs are also considered.

Chapter 3
Capacity of OFDMA-TDD cellular networks

3.1 Introduction

This chapter focuses on the important concept of capacity in the particular case of OFDMA-TDD cellular networks. Capacity is relevant as it facilitates the evaluation of system performance. In the context of capacity, three major topics are addressed. First, the meaning of capacity in the framework of cellular networks is discussed. In particular, different definitions for capacity are presented applicable to the various generations of cellular networks. Next, the chapter discusses how capacity is calculated in the case of OFDMA-based cellular networks. In this context, an SINR equation for OFDMA-based networks is formulated, which is the first contribution of this thesis. A detailed derivation of the SINR equation is presented. The equation accounts for the effects of both small scale fading and large scale fading. Furthermore, in the SINR model a cyclic sinc function is used to account for the subcarrier spacing in terms of number of subcarriers when calculating interference. Next, adaptive modulation is discussed. Both adaptive modulation and Shannon's capacity equation are of interest to this work as they contribute two alternative methods to calculate system capacity. Finally, the physical limitations to capacity are addressed. In particular, bandwidth, transmit power, and fading are discussed.

3.2 What is capacity?

Generally, one of the dictionary meanings of *capacity* is *capability to perform*. Indeed, when talking about cellular networks, capacity is one of the metrics that are used to judge system performance. However, the term capacity can be expressed by different means, depending on the particular system under study.

When a mobile cellular network is exclusively offering voice services (2G networks), capacity is measured as the number of duplex voice channels that can be simultaneously occupied in the

system [18]. As each user requires one duplex voice channel only, the number of supported channels is equivalent to the number of users that can be concurrently served. This equivalence holds true because only one type of service is offered, i.e. voice, which means that the demanded data rate per user is the same across all users. As discussed in the previous chapter, the majority of 2G networks are based on either TDMA/FDMA techniques or CDMA techniques. TDMA/FDMA and CDMA differ in the way capacity is estimated, as in the first case capacity is primarily bandwidth-limited (i.e. depends on the number of channels available), while in the latter case capacity is primarily interference-limited as frequency reuse of one is to be employed. The differences between bandwidth-limited and interference-limited capacity are discussed below.

When capacity is *bandwidth-limited* this means that the maximum number of users that can be simultaneously served by the network is fixed and is determined by the system bandwidth and the cluster size. If the cluster size is small (e.g. three), the bandwidth is reused more often within the system, however, the number of served users per cell is not likely to reach its maximum. As discussed in Section 2.2.2, this is due to the fact that small cluster sizes can give raise to significant co-channel interference. Users demanding service might not be served (i.e. are blocked) in order to ensure that the quality of ongoing calls is not reduced. This means that the capacity of the system depends on the generated interference (and cluster size) and is called *soft capacity* [47]. In contrast, if the network deployment uses large cluster sizes (e.g. 12), the number of available channels per cell is lower in comparison to when the cluster size is small. This means that interference from co-channel cells is small enough such that users are generally guaranteed to meet the demanded data rates. As a result, users are more likely to be denied service due to channel unavailability, rather than due to interference issues. This type of capacity is referred to as *hard capacity* [47].

The *interference-limited* capacity characteristic of CDMA systems can be considered to some extent analogous to the case of soft-capacity discussed above. Because in CDMA each user is assigned a PN code, the transmission of interfering users appears as noise. As a result, the number of instantaneous calls the system can support is purely determined by the tolerated interference level. A key property of CDMA systems is that the cluster size is one and this property is enabled by the employment of PN codes. Some form of interference mitigation mechanisms are still necessary in order to combat the CCI generated among neighbouring cells [18]. This is because CCI is the most dominant factor that limits user capacity in CDMA

systems [48].

So far the discussion was focused on 2G networks, where all users have the same data rate requirement and the number of allocated channels in the system can be equated to the number of users served. However, the situation changes with the introduction of multi-media services (3G and beyond), where users are likely to have dissimilar requirements on data rate depending on the utilised services. Furthermore, in OFDMA systems, for example, each subcarrier can be allocated different data rate depending on the propagation conditions. As a result, a metric, such as the number of served users or the total number of occupied channels, on its own does not provide a full system performance picture. Hence, usually total data rate, i.e. system throughput, is reported as well. However, due to the fact that the total system throughput depends on the system bandwidth, spectral efficiency is sometimes reported instead of throughput to facilitate performance comparison among systems of different bandwidth. Spectral efficiency is defined as the ratio of data rate (total system throughput) to bandwidth. From now on, capacity is used interchangeably to mean spectral efficiency or data rate, and a rigorous definition for spectral efficiency in particular is presented in the next sections.

3.3 Calculating the capacity of an OFDMA-TDD cellular network

3.3.1 SINR for OFDMA

Both the data rate and spectral efficiency achieved on a given link are directly dependent on the SINR that is achieved on that link. The next section treats the formal mathematical relation between SINR and spectral efficiency while this section concentrates on modelling the SINR [49].

As the term suggests, SINR is the ratio of the useful signal power to the received interference power and the thermal noise. In conventional OFDMA systems, the SINR of link i (which can be either in UL or DL) can be expressed as given in:

$$\tilde{\gamma}_i = \frac{1}{||s_i||} \sum_{k \in s_i} \frac{P_k^i |H_k^i|^2 G_i}{\sum_l P_k^l |H_k^{i,l}|^2 G_{i,l} + n_{\text{th}}}, \tag{3.1}$$

where $\tilde{\gamma}_i$ is the SINR achieved by link i; s_i is the set of subcarriers belonging to link i, and the cardinality of $s_i, ||s_i||$, is the number of subcarriers used by link i, which can vary from zero

to $N_{\rm c}$ (total number of subcarriers per BS); P_k^i is the transmit power of subcarrier k (in Watts); $|H_k^i|^2$ is the channel transfer function of link i at subcarrier k; G_i is the link gain of link i; $|H_{k'}^{i,l}|^2$ is the channel transfer function between the receiver on link i and the transmitter on link l at subcarrier k; $G_{i,l}$ is the link gain between the transmitter on link l and the receiver on link i; and $n_{\rm th}$ is the additive white Gaussian noise power (in Watts) per subcarrier. It should be pointed out that the summation in the denominator is over all active links which use subcarrier k, i.e. for which $k \in s_l$. Equation (3.1) in effect averages over the SINR per subcarrier in order to obtain the SINR per link.

Note that the link gain is distance-dependent and reflects the fact that the larger the separation distance between the transmitter and the receiver, the larger the attenuation of the transmitted power will be. The link gain, G, is the inverse of the path loss, $L_{\rm p}$, and the relationship between G and $L_{\rm p}$ is mathematically expressed as:

$$G = 10^{\frac{-L_{\rm p}}{10}}, \tag{3.2}$$

where $L_{\rm p}$ is defined as:

$$L_{\rm p} = a + b\log_{10}(d) + X_{\rm g} \ \ {\rm dB}, \tag{3.3}$$

and where a is an antenna-dependent constant; $b = 10\,\mu$ with μ being the path loss exponent; d is the transmitter-receiver separation distance in metres; and $X_{\rm g}$ is zero mean Gaussian distributed random variable with standard deviation σ in dB to account for log-normal shadowing.

In order to gain insight into the factors that influence the SINR, Fig. 3.1 displays a simple example. There are two simultaneous links, Link1 and Link2, with respective link gains G_1 and G_2 and the SINR of Link1 is of interest in this example. Assume that the set $s_1 = 128, 129, 130, 131$ and $s_2 = 130, 131, 132, 133, 134$, which means that subcarriers 130 and 131 are used by both links. Then, SINR_1 can be expressed as:

$$\text{SINR}_1 = \frac{1}{4}\sum_{k=128}^{131}\frac{P_k^1|H_k^1|^2G_1}{\sum_l P_k^l|H_k^{1,2}|^2G_{1,2} + n_{\rm th}}.$$

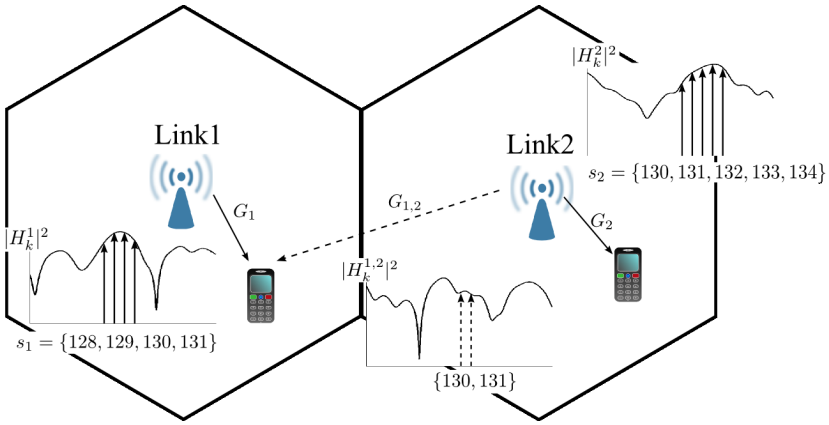

Figure 3.1: *Link2 interferes with Link1 because the sets s_1 and s_2 overlap, i.e. subcarriers 130 and 131 are used by both links simultaneously.*

This expression can be simplified to yield:

$$\mathrm{SINR}_1 = \frac{1}{4}\left(\sum_{k=128}^{129}\frac{P_k^1|H_k^1|^2G_1}{n_{\mathrm{th}}} + \sum_{k=130}^{131}\frac{P_k^1|H_k^1|^2G_1}{\sum_l P_k^l|H_k^{1,2}|^2G_{1,2}+n_{\mathrm{th}}}\right).$$

In a perfectly synchronised system, Link1 receives interference from Link2 only on those subcarriers, which are used concurrently by both links, i.e. subcarriers 130 and 131.

Note that in (3.1) the transmitted power is affected both by the transmitter-receiver separation distance (i.e. path loss) and by the frequency-selectivity of the channel. In previous research, usually only one of the above mentioned channel impairments is considered [44, 50, 51]. In particular, in previous works the transmitted power is assumed to experience either only frequency-selective fading [44, 50], or only distance-dependent fading [51]. However, when evaluating future OFDMA-based systems such as LTE Advanced and IST-WINNER, it is important to apply the above-mentioned cross layer approach. This is because due to the envisaged large bandwidth (e.g. 100 MHz [52]), frequency-selectivity can be rather pronounced, resulting in deep fades (refer to Fig. 2.13) and signal loss. Hence, in order to obtain a holistic SINR model, frequency-selectivity should be accounted for together with the distance-dependent fading. However, the effect of path loss on the transmitted signal is the predominant signal-degrading factor [18]. As an illustration, consider a system with 100 MHz bandwidth and carrier frequency of 5 GHz [52]. According to the WINNER C1 NLOS path loss model [52] applicable in urban areas, the path loss parameters (referring to (3.3)) are $a = 39.61$ and $b = 35.74$, while according to the free space path loss model [18] applicable in LOS conditions, $a = 46.42$

and $b = 20$. In addition, consider a link with sixteen subcarriers. The experienced thermal noise for this link can be calculated as $10\log_{10}(16kT\delta_{\mathrm{f}}) = -144.96$ dBW [52], where k is Boltzmann's constant, T is room temperature (300 K), and δ_{f} is the subcarrier spacing, which is 48.83 kHz according to IST-WINNER [52]. For illustration purposes, log-normal shadowing is not accounted for. As an example, consider that the transmitter is fixed and the destination receiver gradually moves away until the transmitter-receiver separation distance reaches 500 m. Fig. 3.2 demonstrates how the received signal varies with the separation distance and how the received signal compares to the thermal noise level (indicated by the SNR (signal-to-noise ratio) value). Furthermore, Fig. 3.2 also shows how the path loss decreases with distance for the two different path loss models mentioned above. Note the impact of LOS conditions: when comparing Fig. 3.2(a) and Fig. 3.2(b) it can be observed that, for example, at separation distance of 300 metres the SNR attained when using the free space path loss model is more than 25 dB larger in comparison to the SNR attained when using the NLOS path loss model. The impact of LOS interference among BSs on system performance is discussed in detail in Chapter 4.

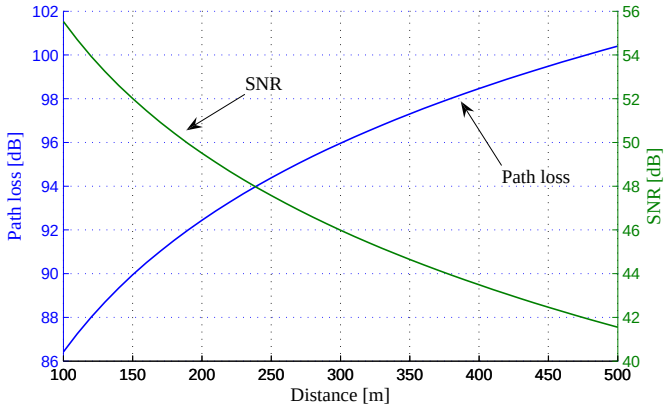

(a) Free space path loss model

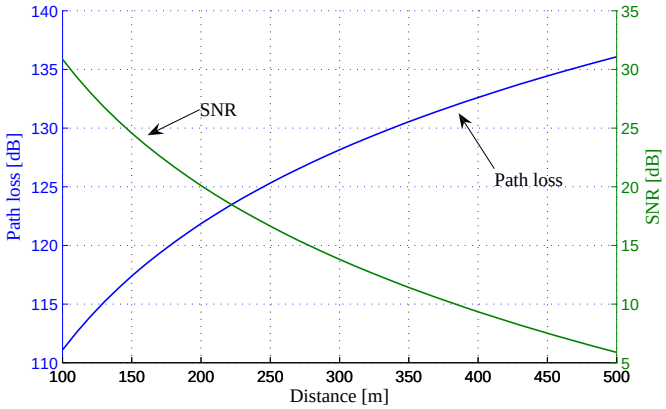

(b) WINNER C1 path loss model

Figure 3.2: *Plots of distance vs. path loss and distance vs. SNR for two different path loss models: the free space path loss model (top plot) and WINNER C1 path loss model (bottom plot).*

When considering SINR, however, there are further important effects to take into account besides path loss and frequency selectivity. In fact, (3.1) is not an entirely accurate model of SINR in OFDMA systems. The summation in the denominator represents the interference term, assuming a perfectly synchronised system. However, as described in Chapter 2, OFDMA systems are prone to frequency offsets due to synchronisation errors and due to Doppler. As a result, interference could result not only from the reused subcarrier, but also from subcarriers neighbouring the reused one. Furthermore, when frequency offset errors are considered, it is important to account not only for CCI but also for multiple-access interference (MAI), which is the interference generated within the cell [53]. The reason is that the transmission on a subcar-

rier used by one user might "leak" onto neighbouring subcarriers used by another user. In the case of point-to-multipoint communication (DL), transmission is easily synchronised, that is why usually in DL MAI can be considered negligible. However, in UL, which is multipoint-to-point communication, synchronisation among the different users transmitting to a BS is difficult to attain. This is why when modelling non-ideal conditions, especially when users are mobile, both MAI and CCI should be accounted for.

In the following, a detailed model of the SINR per subcarrier is presented, taking into account all of the signal-degrading effects mentioned above, namely MAI and CCI, considering offset errors due to both Doppler shifts and lack of synchronisation. The SINR is considered per subcarrier due to the fact that the subcarrier is the most basic time-frequency unit and the equation can be straightforwardly extended to SINR per chunk or SINR per user. First, expressions for the desired signal power per subcarrier, the received MAI power, and the received CCI power are presented, which are then combined to formulate an SINR expression.

The received signal power on subcarrier k for link i, R_k^i, is given by:

$$R_k^i = P_k^i |H_k^i|^2 G_i \ \ [\mathrm{W}]. \tag{3.4}$$

The received MAI power on subcarrier k for link i, $P_{\mathrm{MAI},k}^i$, is given by:

$$P_{\mathrm{MAI},k}^i = \sum_{l \in \beta_i} \varpi_{i,l} \sum_{k' \in s_l} P_{k'}^i |H_{k'}^{i,l}|^2 |C_{k,k'}(\Delta f + \varepsilon_{\mathrm{D}} + \omega)|^2 G_{i,l} \ \ [\mathrm{W}], \tag{3.5}$$

where

$$C_{k,k'}(x) = \left(\frac{1}{N_{\mathrm{c}}}\right) \frac{\sin(\pi x)}{\sin(\pi x / N_{\mathrm{c}})} \exp \frac{j\pi x (N_{\mathrm{c}} - 1)}{N_{\mathrm{c}}}, \tag{3.6}$$

and β_i is the set of links belonging to the same cell as link i and $i \notin \beta_i$; $\varpi_{i,l}$ is defined as:

$$\varpi_{i,l} = \begin{cases} 0, & \text{if } l \in \beta_i \text{ and link } i \text{ is in DL} \\ 1, & \text{otherwise}, \end{cases}$$

and $C_{k,k'}(\Delta f + \varepsilon_{\mathrm{D}} + \omega)$, given in (3.6), is a modified Dirichlet function to account for the amount of interference subcarrier k experiences from subcarrier k'; j is the imaginary unit; $\Delta f = k' - k$; $\varepsilon_{\mathrm{D}} = \frac{f_{\mathrm{D,max}}}{\delta_{\mathrm{f}}}$ accounts for the normalised Doppler shift; $f_{\mathrm{D,max}}$ is the maximum Doppler frequency and δ_{f} is the carrier spacing (in Hz); $\omega = \frac{f_{\mathrm{c}}}{\delta_{\mathrm{f}}}$ is the frequency offset due

to synchronisation errors between subcarriers k and k', with f_{c} is the offset in Hz. The maximum Doppler frequency is defined as: $f_{\mathrm{D,max}} = \frac{v_{\mathrm{m}}}{v_{\mathrm{l}}} f_{\mathrm{C}}$, where v_{m} is the speed of the mobile (in m/s), v_{l} is the speed of light (in m/s), f_{C} is the carrier frequency (in Hz). Given the same transmit power, link gain, and channel, with an increase in $|k' - k + \varepsilon_{\mathrm{D}} + \omega|$, the interference contribution decreases. This behaviour is expected, as synchronisation errors and Doppler effects are significant to neighbouring subcarriers and become negligible when the subcarriers are spaced relatively far apart. A derivation of the modified Dirichlet function is presented in Appendix A, while Fig. 3.3 illustrates how $|C_{k,k'}|$ varies with Δf assuming frequency offset due to synchronisation errors. Note that in the case of perfect synchronisation, $|C_{k,k'}| = 1$ if $k = k'$ and $|C_{k,k'}| = 0$ otherwise. Fig. 3.3 also shows the effect of synchronisation errors due to Doppler on $|C_{k,k'}|$. It can be seen that the effects are rather minor and the shape of $|C_{k,k'}|$ is preserved when ε_{D} is increased from 0 to 0.0039, where 0.0039 corresponds to $f_{\mathrm{D,max}}$=190 Hz, i.e. v_{m}=8.3 m/s. It should to be pointed out that if ω is chosen differently, $|C_{k,k'}|$ need not be symmetric. For example, if $\omega = 0.6$ instead of 0.5, the function $|C_{k,k'}|$ is not symmetric, as expected (ref. to Fig. 3.3.1).

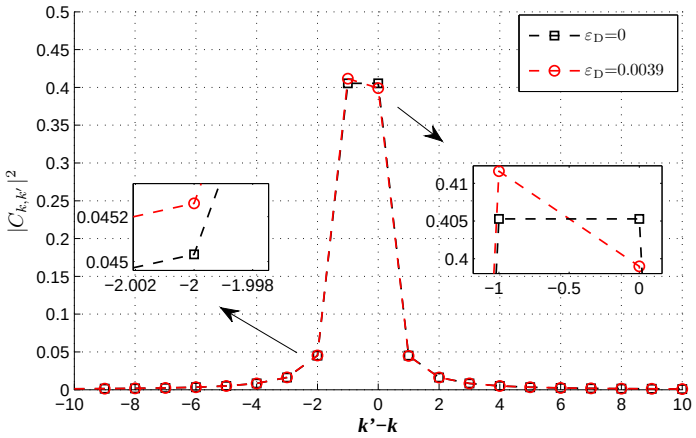

(a) $\omega = 0.5$

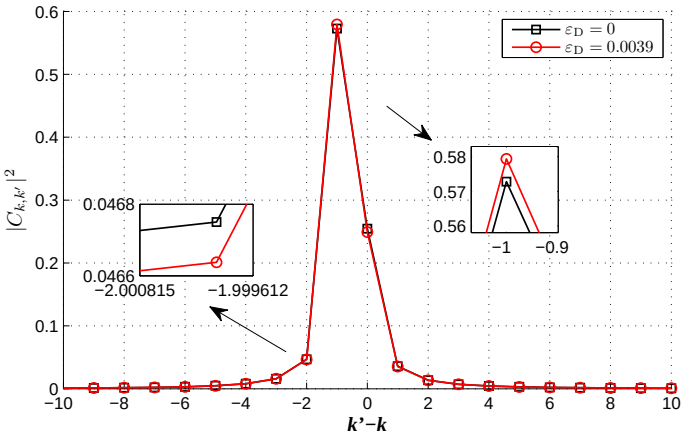

(b) $\omega = 0.6$

Figure 3.3: *The modified Dirichlet function vs. the separation between the interfering subcarrier and the victim subcarrier. For the calculations, it is assumed that* $N_c = 2^{11}$ *[52],* $k = 1000$*,* $k' \in [1, N_c]$*, and* ε_D *is 0 in a) and 0.0039 in b). The plots are zoomed around zero to demonstrate that above* $|k' - k| = 10$ $|C_{k,k'}|$ *is 0.*

There are a couple of important points to discuss at this stage. First, in calculating MAI, subcarrier k from link i does not experience interference from $k' \in s_i$. This is because subcarriers that belong to the same user can be assumed synchronised regardless of whether used as UL or DL. Second, it is assumed that a BS always allocates a given subcarrier to only one link.

The received CCI power on subcarrier k for link i, $P^i_{\mathrm{CCI},k}$, is modelled similarly to the received MAI power and is given by (3.7), where it should be noted that CCI contributions are expected

not only from the reused subcarrier, but also from neighbouring subcarriers, when ε_{D} and/or ω are non-zero:

$$P^{i}_{\mathrm{CCI},k} = \sum_{l \notin \beta_i} \varpi_{i,l} \sum_{k' \in s_l} P^{i}_{k'} |H^{i,l}_{k'}|^2 |C_{k,k'}(\Delta f + \varepsilon_{\mathrm{D}} + \omega)|^2 G_{i,l} \ \ [\mathrm{W}]. \tag{3.7}$$

Note that in (3.7) $\varpi_{i,l}$ is always 1 (because $l \notin \beta_i$) and does not change the result of the expression, however, it is used to show that the (3.7) and (3.5) differ only in the number of subcarriers that contribute interference. When CCI is calculated, l spans all links in the system, that contribute significant interference (usually assumed to be all the links served by the first two tiers of cells surrounding the cell serving link i).

Now (3.4) through (3.7) are combined to formulate the achieved SINR on subcarrier k for link i, γ^{i}_{k}, written as:

$$\gamma^{i}_{k} = \frac{P^{i}_{k} |H^{i}_{k}|^2 G_i}{\sum_{l} \varpi_{i,l} \sum_{k' \in s_l} P^{i}_{k'} |H^{i,l}_{k'}|^2 |C_{k,k'}(\Delta f + \varepsilon_{\mathrm{D}} + \omega)|^2 G_{i,l} + n_{\mathrm{th}}}. \tag{3.8}$$

The next section uses the formulated SINR equation to determine the transmission rate (per link and for the total system).

3.3.2 Shannon capacity

When evaluating the spectral efficiency performance of OFDMA-based cellular systems, two approaches are used in this thesis, *viz*: Shannon's capacity and adaptive modulation. The first approach is a purely theoretical method that provides an upper bound on capacity performance. Shannon's capacity equation assumes infinite code length and uniquely maps each SINR value to a respective data rate value. In contrast, adaptive modulation maps quantised SINR values to data rate values which have been predetermined using finite code lengths for various BER requirements. Both of these approaches are discussed, beginning with Shannon's capacity introduced in this section.

Given the SNR obtained on a channel, the maximum data rate that can be achieved while guaranteeing almost error-free transmission is calculated using Shannon's capacity equation [54], given in:

$$\overline{C}_{\mathrm{r}} = W_{\mathrm{b}} \log_2(1 + \mathrm{SNR}) \ \ [\mathrm{bps}], \tag{3.9}$$

where $\overline{C}_{\mathrm{r}}$ is the data rate and W_{b} is the channel bandwidth in Hz. Note that (3.9) depends on the channel SNR and furthermore, (3.9) is applicable to the case of AWGN (additive white gaussian noise) [18]. In wireless networks, however, accounting for interference is of paramount importance when evaluating system performance. As an approximation, Shannon's equation has been applied using the attained SINR (instead of SNR) [55], assuming perfect error-correction codes [18] to account for a best-case scenario and interference to be white Gaussian, independent and identically distributed (i.i.d.). Equation (3.10) shows a modification of (3.9), using (3.8) to obtain the spectral efficiency of subcarrier k in link i, $\overline{C}_k^i$:

$$\overline{C}_k^i = \log_2(1+\gamma_k^i) \ \ [\mathrm{bps/Hz}]. \tag{3.10}$$

Equation (3.10) can now offer insight into ways to improve the spectral efficiency attained by a given network. It can be seen that, in fact, the spectral efficiency can be improved by improving γ_k^i, i.e. the SINR. As a result, there are two ways to improve spectral efficiency – 1) to increase the numerator of the SINR, which means to use more power; and 2) to decrease the denominator of the SINR, which means to reduce interference. Both of these measures result in an SINR increase.

An example is used to illustrate the effect of interference and transmit power on SINR and capacity. Fig. 3.4(a) displays a scenario where the link gain is -90 dB (corresponding to a transmitter-receiver separation distance of about 150 m if the free space path loss model is considered, referring to Fig. 3.2), the interference is fixed to -150 dBW and the transmit power is varied from 0 to 30 dBm (equivalent to 1 mW and 1 W respectively). Fig. 3.4(b) shows the same example, however, the interference is significantly higher and is fixed to -100 dBW.

There are a few important points that these two figures make: First, it can be observed that, for both the cases of high interference and of low interference, as the transmit power is increased, the SINR increases and capacity also increases, as expected. Second, when comparing the case of low interference and the case of high interference, it can be seen that in the former, the relative increase in capacity achieved by increasing transmit power from 0 to 30 dBm is 4.76-fold. In comparison, in the latter case the capacity increase resulting from the same increase in transmit power is significantly larger – 346-fold. However, the absolute capacity increase is about 12 bps/Hz and about 3.4 bps/Hz for the cases of low interference and high interference, respectively. This means that when interference is high, a 30 dBm (1 W) increase in power achieves a small absolute gain in capacity. In contrast, when interference is low, the same gain

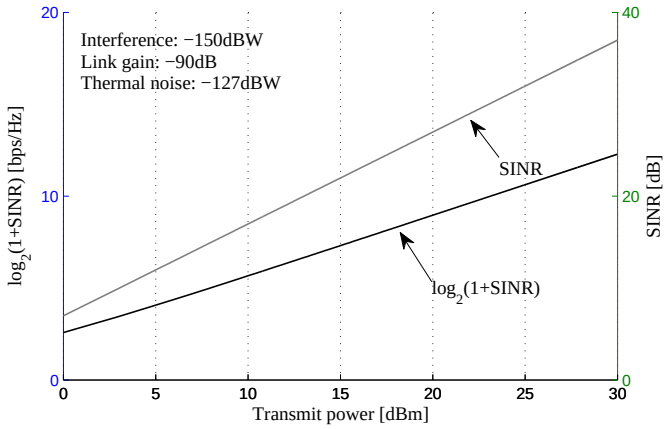

(a) Low interference

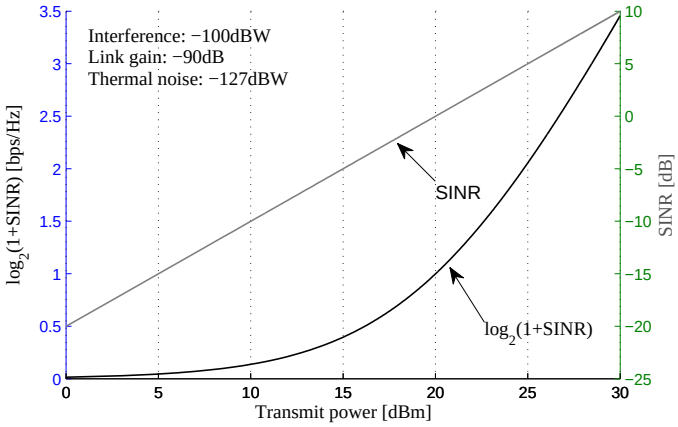

(b) High interference

Figure 3.4: *Effect of transmit power on SINR and capacity: as transmit power is increased, both capacity and SINR increase.*

in capacity can be achieved with significantly less power. With respect to power efficiency, this means that if the interference is high, the improvement in spectral efficiency when increasing transmit power is severely limited. In light of *green radio* one could argue that the best strategy in such cases is to transmit with the minimum power that would just enable data transmission (using the lowest possible modulation scheme).

Considering the same example, Fig. 3.5 displays the effect of interference on SINR and capacity. In this case the transmit power is fixed to 10 dBm (10 mW), while interference is varied between -150 dBW and -100 dBW. It can be observed that when interference is basically zero (-150 dBW to -140 dBW), capacity and SINR are almost constant, as expected. However, when interference is increased such that the SINR drops below about 15 dB, there is a sharp drop in

both SINR and capacity. This is an important observation, because it demonstrates that when

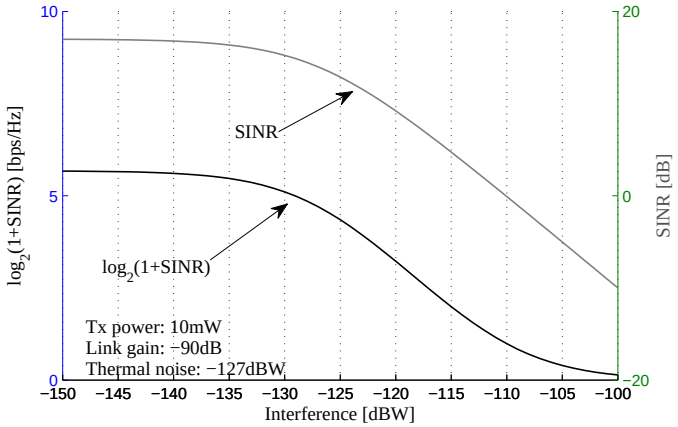

Figure 3.5: *Effect of interference on SINR and capacity: as interference is increased, both capacity and SINR decrease.*

interference is relatively low, even a large increase in interference does not have an effect on capacity. However, when the interference is high, a small increase causes the capacity to decline rapidly. For example, increasing interference by 10 dB, from -120 dBW to -110 dBW, results in more than 2 bps/Hz decrease in capacity.

3.3.3 Adaptive modulation

While the previous section discussed how to theoretically obtain an upper bound on the achievable capacity of a channel based on the attained SINR, this section focuses on a concept actually deployed in cellular networks, i.e. adaptive modulation. OFDMA systems are considered, for which adaptive modulation has been demonstrated to have considerable benefits [56]. Before discussing adaptive modulation, the basic principles of digital modulation are briefly reviewed.

In digital communications the process of modulation is converting a digital bit stream, i.e. the message source, to an analog signal. There are a number of modulation methods, however, quadrature amplitude modulation (QAM) is most widely used in wireless communications today [18]. In QAM, the bit sequence is encoded into symbols and the number of bits per symbol is determined by the set of available modulation symbols, called modulation alphabet. Fig. 3.6 shows the respective constellation diagram for 4QAM as an example. Note that the diagram is a 2-dimensional scatter plot and each symbol is represented as a point in the complex plane (the real and the imaginary part are plotted on the I axis and Q axis, respectively). In encod-

ing, the real and imaginary parts modulate a cosine and a sine wave, respectively, allowing the whole symbol to be transmitted on the same frequency resulting in efficient use of bandwidth. The used modulation alphabet depends on the channel quality. Using fewer number of bits per

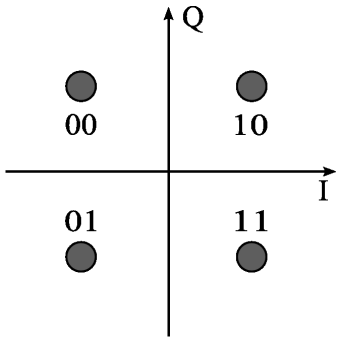

Figure 3.6: *The constellation diagram of 4-QAM, where each symbol is composed of 2 bits.*

symbol results in smaller constellation sizes, whereas increasing the number of bits per symbol results in larger constellation sizes. Intuitively, an increase in constellation size means that the distance between neighbouring constellation points decreases and this results in more error-prone decoding. When considering an AWGN channel, the average probability of error per bit for M-ary QAM, P_{b}, can be mathematically expressed as [57]:

$$P_{\mathrm{b}} \approx \frac{4}{\log_2(M)}\left(1-\frac{1}{\sqrt{M}}\right) Q\left(\sqrt{\frac{3E_{\mathrm{b}}\log_2(M)}{(M-1)N_{\mathrm{o}}}}\right), \tag{3.11}$$

where Q denotes the Q-function; E_{b} is the energy per bit in W·s; and N_{o} is the thermal noise power density in W/Hz. This implies that if the channel quality is good, higher order modulation (i.e. larger constellation size) can be employed, while unfavourable channel conditions call for lower order modulation.

The error probability per bit is referred to as bit error ratio (BER). Different network services have different BER requirements that influence the choice of modulation scheme. For example, for real-time multimedia services, such as video conferencing, the necessary BER is about 10^{-7} [10], while if voice service the required BER is about 10^{-3} [10, 58]. Fig. 3.7 is generated using the Matlab function `berawgn` which produces BER curves for uncoded AWGN channels. The figure shows a plot of BER vs. $E_{\mathrm{b}}/N_{\mathrm{o}}$, where $E_{\mathrm{b}}/N_{\mathrm{o}}$ (also referred to as the SNR per bit) and the SNR are related as shown in (3.12):

$$\mathrm{SNR} = \frac{E_{\mathrm{b}}}{N_{\mathrm{o}}}\frac{R_{\mathrm{b}}}{W_{\mathrm{b}}}, \tag{3.12}$$

where R_{b} is the bit rate in bps [18]. From Fig. 3.7 it can be observed that, as the $E_{\mathrm{b}}/N_{\mathrm{o}}$

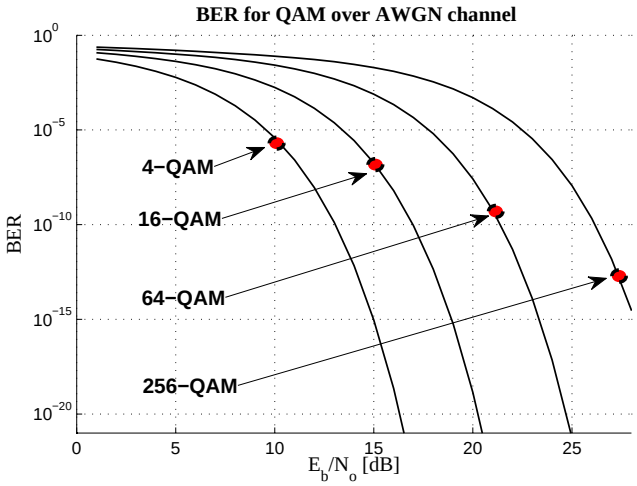

Figure 3.7: *A plot of BER vs $E_{\mathrm{b}}/N_{\mathrm{o}}$ for different QAM constellation sizes.*

increases for a given BER, the modulation order that can be supported also increases. This is a very important property, as it means that if channel conditions improve, the data rate can be increased by switching to a higher modulation order without increasing transmit power.

The method of adjusting the modulation scheme based on the perceived channel quality in order to maintain the required BER is called *adaptive modulation*. The channel quality measure can, in fact, be SINR, SNR, or other quality indicators, hence it is generally denoted here by ζ. Given an adaptive modulation scheme of K levels, an m_c-ary modulation is employed, where $c \in [0, K-1]$ and the c^{th} modulation level is chosen based on the following rule:

$$\text{Choose } m_c \text{ when } \epsilon_c \leq \zeta \leq \epsilon_{c+1},$$

where ϵ_c is a threshold value, belonging to the set $\epsilon_{\mathrm{s}} = \{\epsilon_c | c = [0, K-1]\}$. After the modulation level is determined, data is encoded prior to transmission, whereby redundancy is added in order to correct the effects of the channel upon reception (referred to as channel coding) [59]. Some of the main types of channel codes include block codes, convolutional codes, and turbo codes and the interested reader may refer to [18] for a detailed treatment of channel coding. For demonstration purposes, here the focus is on the first type of codes, block codes, where information is encoded into blocks such that each block contains data bits and code bits. In this context, an important metric is the code rate, R_c, defined as $R_c = r_{\mathrm{i}}/r_c$, where r_{i} is the information (data) rate and r_c is the raw channel rate [18]. For example, if the code rate is 2/3, for every 2 data bits, there is 3-2=1 code bit.

Note that in OFDMA systems, each subcarrier (or chunk of subcarriers) can be assigned a modulation level individually based on propagation conditions. A demonstration is shown on Fig. 3.8, where $K = 9$ and the channel quality metric of a single link is displayed. To account

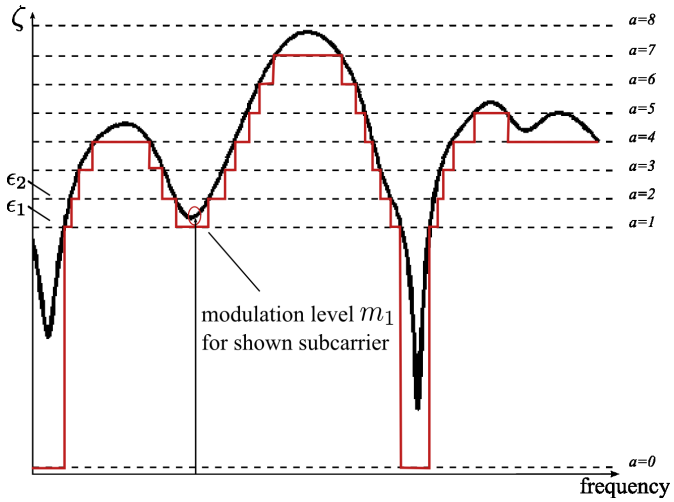

Figure 3.8: *Demonstration of the rule for modulation level assignment: the channel quality metric experienced by a link is quantised and modulation level per subcarrier is assigned accordingly.*

for this degree of freedom, let the modulation level of subcarrier k for link i be set to $m^i_{c,k}$, where $m^i_{c,k}$ is the equivalent of m_c as described above, then the data rate achieved can be calculated as shown in (3.13) [18, 60]:

$$\tilde{C}^i_k = \frac{M^i_{c,k} R_\mathrm{c}}{T_\mathrm{s}} \ [\mathrm{bps}], \tag{3.13}$$

where $M^i_{c,k} = \log_2(m^i_{c,k})$ is the number of bits per symbol; T_s is the OFDM symbol duration (including cyclic prefix).

An example is shown in Table 3.1, where adaptive modulation is achieved with seven different modulation schemes and a set of 2L-D trellis codes, assuming a BER of 10^{-7} [61]. Note that the *cross* and *star* constellations are QAM-variations in order to ensure robustness to interference, as described in [62] and [63], respectively. To obtain the data rate, (3.13) is used and the following parameters are assumed: a code rate of 2/3, bandwidth of 100 MHz, 2048 subcarriers, and cyclic prefix of 20%. Furthermore, the data rate achieved using Shannon's equation (refer to (3.10), multiplied by $\frac{1}{T_\mathrm{s}}$ to obtain data rate from spectral efficiency) is also shown for comparison. As expected, Shannon's capacity is significantly higher than what is achieved using adaptive modulation.

Modulation scheme	4 QAM	8 star	16 QAM	32 cross	64 QAM	128 cross	256 QAM	
SINR	9	14	16	19	22.2	25	28.5	dB
Data rate (AM)	54.24	81.37	108.49	135.61	162.73	189.86	216.98	kbps
Data rate (Shannon)	128.61	191.53	217.73	257.56	300.43	338.11	385.32	kbps

Table 3.1: *Adaptive modulation (AM) example for BER of 10^{-7} [61]*

3.4 Physical limitations to capacity in cellular OFDMA networks

The previous two sections discussed two methods to evaluate the capacity of a system and this section reviews the limitations to capacity and possible methods for capacity increase.

The above discussions revealed that capacity (both in terms of spectral efficiency and data rate) depend on three main factors:

1. bandwidth
2. transmit power
3. interference

Of these factors, the first two (bandwidth and transmit power) are scarce resources, in that in a system they are limited and fixed. The only way in which these two factors can be manipulated to influence capacity is by choosing how to distribute these resources among the users which demand them. The methods of distributing scarce resources among users are collectively referred to as radio resource management (RRM) [64]. Clearly, RRM techniques can also address the issue of how to minimise interference. However, usually the focus is on throughput maximisation or power optimisation *for* throughput maximisation and only recently minimising power consumption has been of interest in light of *green radio* initiatives. This is why while there has been a lot of research on RRM algorithms, e.g. [51, 65–68], there is still research required. This holds true especially considering the unresolved same-entity interference problem in TDD networks.

In light of the above, the focus of this research work is on interference. Questions such as how to mitigate interference, and if possible, how to avoid interference are relevant. These questions are particularly important because of two reasons: 1) decreasing the overall interference in the system improves data rates and reduces the probability of dropped calls, and 2) decreasing the

overall interference in the system allows for less energy consumptions. The second reason is of particular significance, considering recent research initiatives such as *green radio* that aim to minimise the energy consumption of cellular networks.

3.5 Summary

This chapter discussed capacity in OFDMA cellular networks. In particular, capacity was defined as the data rate (or spectral efficiency) that a system can achieve. In a step towards calculating capacity, the SINR equation for OFDMA was rigorously defined. Then, two ways for capacity calculation were discussed, *viz*: Shannon's capacity equation, which is a theoretical approach that provides an upper bound for the attainable capacity, and adaptive modulation that is a practical method which when simulated can provide expected system performance results. Adaptive modulation is of particular importance to OFDMA systems, as frequency selectivity can be exploited. Finally, interference has been identified as the capacity limiting factor of interest and is considered in this work.

In the next two chapters interference mitigation and interference avoidance techniques are discussed and the SINR equation derived in this chapter is used to model the systems under consideration. Furthermore, both adaptive modulation and Shannon's capacity equation are employed to evaluate system performance.

Chapter 4
Interference mitigation for cellular OFDMA-TDD networks

4.1 Introduction

The focus of this chapter is on interference mitigation techniques for OFDMA-TDD cellular networks. First, an overview of the general concept of interference mitigation in cellular networks is given. The particular cases of interference mitigation for OFDMA systems and TDD systems are also discussed. Second, the fractional/soft reuse concept is introduced as a means to mitigate co-channel interference in OFDMA networks and four different variations of the concept are discussed.

Next, this chapter presents the second contribution of this thesis [49, 69, 70], which is a demonstration of the severity of BS→BS interference for networks based on OFDMA-TDD. The demonstration is done by comparing two alternative TDD-specific interference mitigation concepts, *viz* RTSO and ZD, to the classical solution to same-entity interference, namely FSA. The comparison is based on computer simulations and the main comparison metric is spectral efficiency. The study of RTSO and FSA investigates the effect of BS→BS interference on the whole system, whereas the study of ZD and FSA focuses on one "victim" cell of interest. To the best of the author's knowledge such studies have not been presented in literature before.

Two further contributions of the thesis are presented in this chapter. The first one is the analysis of the probability of crossed slots when RTSO is employed [71], while the second one is the OFDMA formulation of the known OTA-SRR [72, 73] resource allocation algorithm. The new formulation [49, 69] is used in the comparison between RTSO and FSA.

4.2 Definition and importance of interference mitigation

Generally speaking, interference is an indispensable part of typical wireless communications where frequencies are spatially reused. Consider, for example, cellular networks, which are

of interest in this work. As was discussed in Chapter 2, the distance between two sites that reuse the same frequencies is dependent on the cluster size. The larger the cluster size, the larger the distance between co-channel cells and hence, the smaller the interference. However, with today's ever increasing demands on data rate, ideally the whole system bandwidth should be reused in each cell. Such a reuse means that a given cell experiences interference from all of its immediate neighbouring cells (which are six, if hexagonal cell structure is assumed). Referring to the previous chapter, this increase in interference (as compared to the clustered design) ultimately results in capacity decrease. To recap, according to Shannon's equation, capacity is defined as $\log_2(1 + \mathrm{SINR})$. Hence, capacity decreases as the SINR decreases and further, SINR decreases as interference is increased (given the same received power and noise). Fig. 3.5 (refer to Chapter 3) demonstrates the effect of interference on SINR and capacity. It is fair to conclude that in order to meet the zealous demands on data rate of next-generation systems such as LTE Advanced, striving to minimise interference is imperative.

Because OFDMA, and in particular OFDMA-TDD is considered for next-generation systems such as LTE [74] and WiMAX [75], research is targeted towards tackling the interference problems that exist in these networks. The next two sections discuss interference mitigation techniques which address the problem of CCI in OFDMA networks and techniques that particularly target the issue of same-entity interference in TDD.

4.3 Fractional/soft frequency reuse

The concept of fractional/soft frequency reuse (FFR) is to improve the capacity of users at the cell edges in OFDMA systems with full frequency reuse. Cell-edge users suffer most severely from CCI because they are closest to interferers from neighbouring cells. The essence of FFR is that the cell is partitioned into regions which have dissimilar reuse factors. In particular, cell-edge regions have larger reuse factors than cell-centre regions as the areas at the cell edges are generally exposed to stronger CCI than the centre of the cell. Variations of this interference mitigation method have been considered by LTE [76, 77] and WiMAX [9]. In this section these variations are presented and in addition, other proposed versions of the method are discussed [78–81].

The FFR method proposed by [78] and [79] suggests that the system bandwidth is split into two parts – one part serves the cell-centre users, while the other part serves the cell-edge users.

Furthermore, the cell-edge bandwidth is split into three bands and the cell-edge region is split into three sectors, such that the three sectors are allocated orthogonal frequency bands. In this way, the cell-edge region is served under frequency reuse of three, while the cell-centre region is served under frequency reuse of one. The method is graphically presented in Fig. 4.1. Note that here the notion of frequency reuse is more extended than what was discussed in Chapter 2. In particular, clusters sharing the available bandwidth can be formed not only by cells, but also by own-cell sectors. For example, in this specific variation of the FFR method, the whole bandwidth is reused in each cell. The cells are sectorised, such that in effect the sectors of each cell form clusters, analogous to the cell clusters discussed in Chapter 2. Because the cell-edge region of each cell is divided into three clusters that are assigned orthogonal frequency bands, it is said that the cell-edge region is operated under frequency reuse of three.

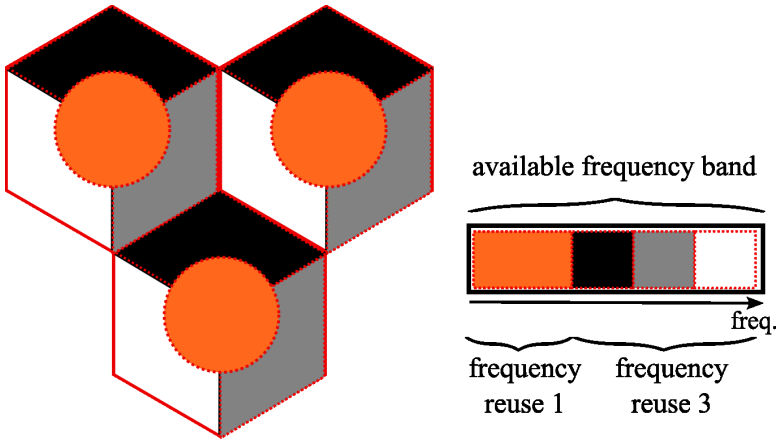

Figure 4.1: *The available bandwidth is divided between the cell-centre users and the cell-edge users. The cell-edge region is further split into sectors, served by orthogonal frequency bands.*

A similar FFR scheme which, in contrast to the previous one, avoids sectoring is proposed by [76, 77, 80]. In effect, the system bandwidth is split into two bands, *viz* a *major band* and a *minor band*. The major band serves the whole cell area under frequency reuse three, while the minor band serves only the cell-centre region under frequency reuse one. This variation of the frequency reuse concept is shown in Fig. 4.2.

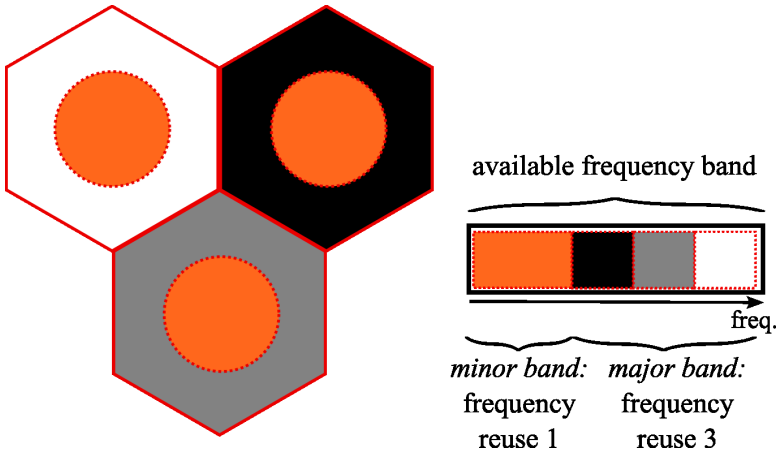

Figure 4.2: *The minor band serves inner-cell users under frequency reuse one, while the major band serves the whole cell area under frequency reuse three.*

Fig. 4.3 displays the FFR method considered by WiMAX [9]. It is almost the same as the previously described variation of the FFR concept, however, the cell-centre region is served by the whole system bandwidth.

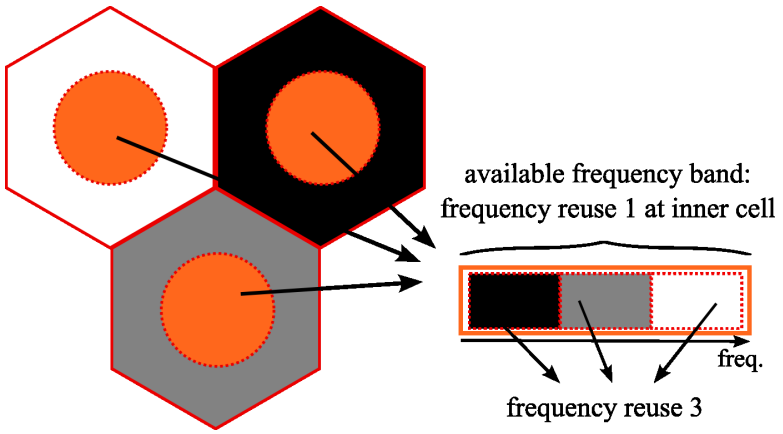

Figure 4.3: *The whole bandwidth serves the cell-centre region under frequency reuse one, while the cell-edge region is served under frequency reuse three.*

It is also possible to mix the two methods shown in Fig. 4.1 and Fig. 4.3, and to allocate the whole bandwidth to the cell-centre users, while the cell-edge region is split into sectors, served by orthogonal frequency bands. This version of the FFR concept has been proposed in [81] and is graphically presented in Fig. 4.4.

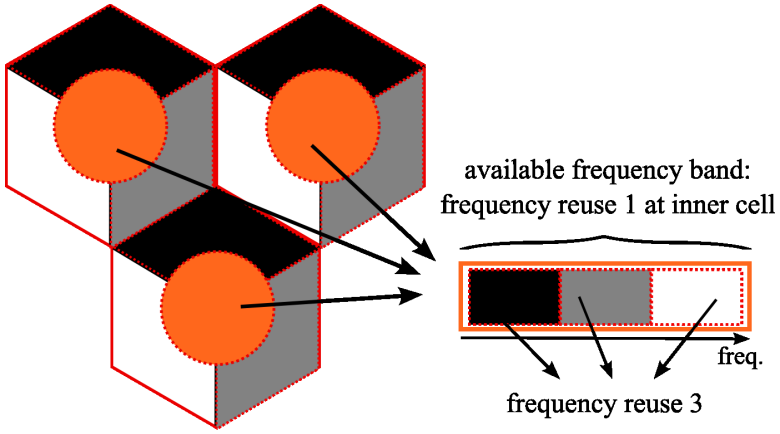

Figure 4.4: *The cell-edge region is sectored and sectors are served by orthogonal frequency bands under frequency reuse three, while the inner-cell region is allocated the whole bandwidth in each cell.*

The FFR concept variations overviewed above target the CCI problem in OFDMA networks. However, FFR does not address the particular issue of crossed slots in TDD systems, i.e. how to handle UL/DL allocation in order to avoid or reduce same-entity interference. The next section addresses the specifics of interference mitigation for TDD-based networks.

4.4 TDD-specific interference mitigation techniques

The most straightforward approach currently considered to resolve the crossed-slot problem in TDD is FSA [13]. The principle of FSA is that all BSs are frame-synchronised and the UL-DL time slot assignment ratio is kept fixed and the same across the cells in a network (and usually allocates half of the resources to UL and DL each) [13]. FSA is convenient because, most importantly, same-entity interference is completely avoided and in addition, the scheme is simple to implement and there is no signalling overhead. The major disadvantage, however, is the lack of flexibility. In other words, one of the main advantages of TDD, namely the support for cell-specific asymmetry demands, is not made use of.

In contrast, the TDD interference mitigation techniques usually allow each cell to set its own SP based on the instantaneous asymmetry demand. Interference mitigation techniques either work in a centralised or a decentralised fashion [13]. In [13] the centralised ZD and the decentralised RTSO are discussed as a flexible alternative to symmetric FSA and are also reviewed here. Both

RTSO and ZD are compared against symmetric FSA.

4.4.1 RTSO

The work presented in this section is based on the work published in [71].

RTSO [14] is a method which relies on randomisation. In order to mitigate the same-entity interference problem, RTSO randomly permutes the time slots within a frame once every time interval Δt (where Δt is a network parameter) as illustrated in Fig. 4.5. The actual timeslot permutation sequence follows a pseudo random pattern. This pattern can be independently generated at both ends (MS and BS). As a consequence, the signalling effort is almost negligible since only a random code at link setup needs to be conveyed. RTSO avoids persistent severe interference, and in effect achieves interference diversity. Note that an analogy can be made between RTSO and frequency hopping. In the latter interference diversity is achieved by hopping through different frequency carriers. RTSO has been previously applied to CDMA systems [14].

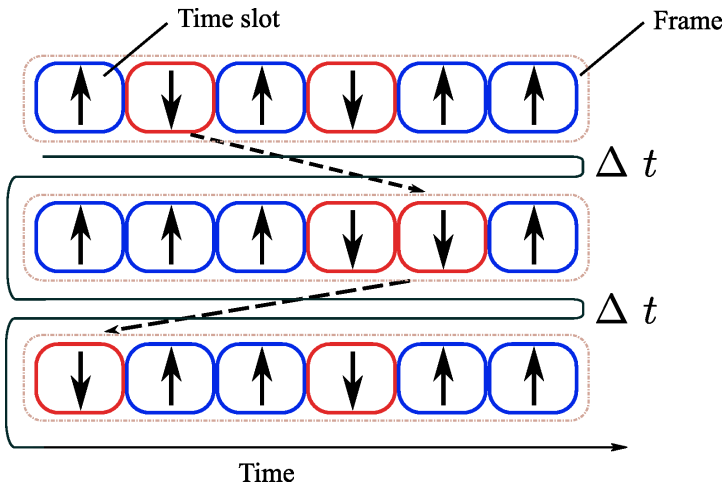

Figure 4.5: *For a given ratio of UL/DL resources, RTSO permutes the UL and DL time slots once every time interval Δt (greater than the frame duration) [14], keeping the UL/DL ratio fixed. Upward-pointing arrow denotes UL, while DL is denoted by a downward-pointing arrow.*

As RTSO avoids persistent severe interference by randomising the sequence of UL/DL time slots per frame, it is interesting to see how the UL/DL asymmetry influences the number of crossed slots. The probability of opposite link assignment for a given slot is dependent on

the asymmetry rate per frame, R_{asym}, defined as $R_{\text{asym}} = \frac{n_{\text{UL}}}{n_{\text{DL}}}$, where n_{UL} and n_{DL} are the number of UL slots and DL slots, respectively. If the probability of a cell being in an UL time slot is $\frac{n_{\text{UL}}}{n_{\text{TOT}}} = P_{\text{UL}}$, where n_{TOT} is the total number of slots per frame, then the probability of two cells being in UL at the same time is $(P_{\text{UL}})^2$. By the same token, the probability of a cell being in a DL time slot is $\frac{n_{\text{DL}}}{n_{\text{TOT}}} = 1 - P_{\text{UL}}$, and that of two cells being in DL at the same time is $(1 - P_{\text{UL}})^2$. Thus, the probability of two cells experiencing at least one crossed slot per frame, $P_{\text{opp}}(2)$, is given by:

$$\begin{aligned} P_{\text{opp}}(2) &= 1 - (P_{\text{UL}}^2 + (1 - P_{\text{UL}})^2) \\ &\equiv 2\frac{n_{\text{UL}} n_{\text{DL}}}{(n_{\text{TOT}})^2}. \end{aligned} \tag{4.1}$$

Now consider a system of n cells, such that there is a centre cell and $n - 1$ surrounding cells. The probability of crossed slots from the view point of the centre cell is derived by expanding (4.1) and is given by:

$$\begin{aligned} P_{\text{opp}}(n) &= 1 - (P_{\text{UL}}^n + (1 - P_{\text{UL}})^n) \\ &\equiv 1 - \frac{(n_{\text{UL}})^n + (n_{\text{DL}})^n}{(n_{\text{TOT}})^n}. \end{aligned} \tag{4.2}$$

A 16-slot frame (i.e. $n_{\text{TOT}} = 16$) and asymmetry rates (UL:DL) of 2:14, 4:12, 6:10, 8:8, 10:6, and 12:4 are considered as an example. A system of up to thirty-six neighbouring cells surrounding the centre cell is considered (i.e. up to three tiers), because it has been demonstrated that the significant portion of interference comes from the first three tiers of cells [82]. Note that when a given asymmetry ratio is considered, all cells have the same asymmetry. Although this is not entirely realistic, such a scenario allows for the systematic analysis of the influence of the number of UL and DL slots per frame on the probability for crossed slots. Results, displaying the probability of crossed slots as a function of the number of surrounding cells, are shown in Fig. 4.6. It can be observed that the results are symmetric with respect to R_{asym} = 8:8. Moreover, the symmetric case exhibits the highest probability of crossed slots and as the asymmetry is shifted to favour either UL or DL, the probability of crossed slots decreases.

Now the discussion focuses on a scenario which better models reality. In particular, the number of UL time slots per frame is considered to be a random variable that is uniformly distributed between 2 and 14 and the distribution among cells is identical and independent. The uniform distribution is chosen as a general case, to account for the fact that each cell can have any

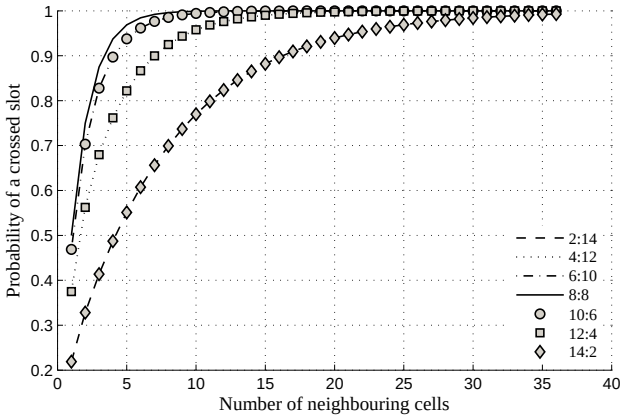

Figure 4.6: *Probability of crossed slots as a function of the number of neighbouring cells surrounding a centre cell for various UL/DL ratios.*

number of UL time slots with the same probability. This situation is simulated using the above parameters. As shown in Fig. 4.7, the results are identical with the symmetric case in Fig. 4.6, which is as expected because the average number of UL time slots per frame in both cases is 8 and because of probability distribution function (pdf) symmetry. However, clearly, in the case when the number of UL time slots is a random variable, the probability of crossed slots is also a random variable. The distribution is not derived analytically, but simulation results are presented in Fig. 4.7 showing the cumulative distribution function (cdf) of the probability for crossed slots. As examples, the cases of $n = 2$, $n = 5$, and $n = 10$ are considered. It can be observed that as the number of cells under consideration increases, the cdf of the probability of crossed slots gets steeper. This effect is expected because increasing the number of cells under consideration means that there is less variation in the probability of at least one crossed slot. This probability tends to 1 as the number of cells increases.

4.4.2 ZD

Unlike RTSO, ZD is a centralised scheme analogous to the fractional frequency reuse concept introduced in Section 4.3 and heavily relies on coordination among BSs. The principle is proposed in [15] as a time slot allocation based on region division for CDMA networks. ZD aims to mitigate same-entity interference by reducing the transmission range during crossed slots. The reduced transmission range in effect increases the separation distance between transmitters and vulnerable receivers and hence reduces interference. BSs share information about their TDD SP and thereby have knowledge of which time slots are crossed slots. Each BS divides its cov-

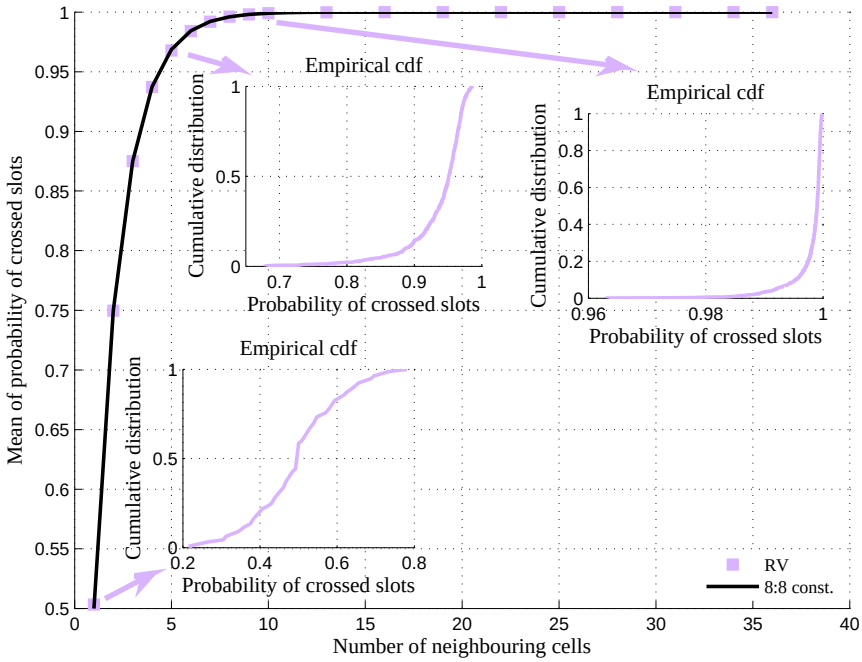

Figure 4.7: *Probability of crossed slots as a function of the number of neighbouring cells surrounding a centre cell in the case of UL:DL=8:8. The cases when the asymmetry is constant and when the number of UL slots is a random variable are both considered. The cdf of the probability of crossed slots for the scenario when the number of UL time slots per frame is a random variable, uniformly distributed betwen 2 and 14 is also displayed for three scenarios depending on the number of cells surrounding the centre cell.*

erage area to an inner region and an outer region. During crossed slots, resources are allocated only to MSs which are located in the inner region (refer to Fig. 4.8). The authors of [15] found the radius of the inner region to be 52% of the cell radius. Assuming a uniform user distribution and a cell radius R, it can be calculated that only $\frac{\pi(0.52R)^2}{\pi R^2} \approx \frac{1}{4}$ of the users are in the inner region. This means that whenever a large number of crossed slots is present in comparison to non-crossed slots, the resources cannot be efficiently utilised. Note that in practice ZD requires significant overhead. The division of a cell to regions needs MSs to report to their respective BSs the received power of a reference signal (for example, the pilot signal BSs usually send). Based on the reported values, BSs tag MSs as being in the inner/outer region. In addition, ZD does not work unless tight DL power control is in place. Tight power control, however, is not desirable in OFDMA systems, because it limits the use of higher order modulation, which is especially important for users experiencing good channel conditions (such as the users close to the BS).

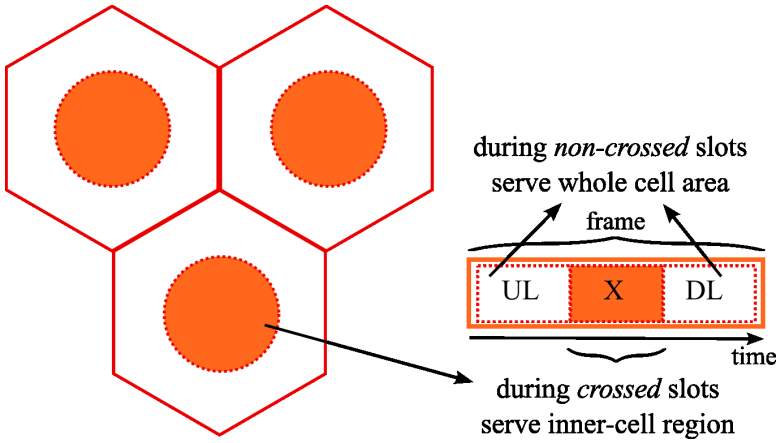

Figure 4.8: *During non-crossed slots users across the whole cell area can be served, while during crossed slots, users in the inner-cell region only can be served.*

The next two sections present simulation results comparing the TDD-specific interference mitigation techniques, RTSO and ZD, to FSA.

4.5 A comparison between RTSO and FSA

This section presents a comparison between RTSO and FSA [49, 69].

4.5.1 Simulation model

The simulation model considers an OFDMA-TDD network with a total of 200 uniformly distributed users in a 19-cell region, where each cell has a centrally-located BS. A best effort full buffer system is in place, which means that all users demand service at all times and the quality of service (QoS) desired by a user corresponds to the maximum data rate it can support. TDD is modelled by assuming a single time slot, where each BS is assigned to either UL or DL, and UL:DL ratios of 1:1, 1:6, and 6:1 are explored. In the case of RTSO, the UL/DL time slot assignment is asynchronous among cells and the assignment of each cell is random with probability depending on the asymmetry ratio studied. When FSA is in place, all cells are synchronously assigned UL or DL with probability depending on the asymmetry ratio studied. Here it should be noted that UL/DL channel allocation and resource allocation are two disjoint processes, so that after each BS has been assigned to either UL or DL, resource allocation takes place. The employed resource allocation algorithm is the OTA-SRR, which jointly allocates rate and power [72, 73]. The OTA-SRR aims to maximise the sum of SINR values of the

users in a cellular system and does so in a fair manner in that there is no power minimisation constraint. As a consequence, all users are initially assigned maximum rate. Rates are then iteratively reduced based on achieved SINR until the system is in a feasible steady state. Refer to Section 4.5.2 for the details of the OFDMA algorithm formulation. The simulated system further employs a quasi-static model where the link gains between transmitters and receivers remain unchanged for a time slot duration. An BS-MS pair (i.e. a link) is formed based on minimum path loss.

The simulation employs adaptive modulation as follows: For each γ_k^i, $\overline{\gamma}_k$ is assigned, where $\overline{\gamma}_k$ is the target SINR of subcarrier k, such that $\overline{\gamma}_k \leq \gamma_k^i$ and $\overline{\gamma}_k \in \mathbf{\Gamma} = \{\tilde{\gamma}_1 < \tilde{\gamma}_2 < \cdots < \tilde{\gamma}_{|\mathbf{\Gamma}|}\}$. Furthermore, it is assumed that there is a number of $K = |\mathbf{\Gamma}|$ discrete transmission rates available depending on the modulation alphabet, such that $r_k \in \{r_1 < r_2 < \cdots < r_K\}$, where each SINR target element corresponds to each rate respectively.

The system parameters used for the simulation platform are shown in Table 4.1. Note that because of the snap-shot nature of the simulation, MSs appear static. However, Doppler frequency offset errors and offset errors due to synchronisation are accounted for by using constant offset values. In particular, a Doppler frequency offset corresponding to a speed of 30 km/h and 50% synchronisation offset are used. The latter value is chosen to reflect a severe interference scenario (e.g. [44] report about 30% offset). Furthermore, in calculating the SINR per subcarrier, in the case of UL both CCI and MAI are considered, while in the case of DL perfect synchronisation is assumed and only CCI is considered.

Number of BSs	19		Number of MSs	200
Cell radius	500 m		Bandwidth	100 MHz
Number of subcarriers	2048		Root mean sq. delay spread	0.27 μs
Carrier frequency	1.9 GHz		Maximum Doppler frequency	190 Hz
Maximum power per link	2 W		Freq. offset due to synchronisation	0.5

Table 4.1: *Fixed simulation parameters*

The small-scale fading effects are simulated via a Monte Carlo method [83], which takes into consideration the effects of Doppler shift and time delay. A power delay profile is used corresponding to the specified delay spread in Table 4.1 [84]. It is assumed that a proper cyclic prefix is in place such that ISI is avoided. The path loss model to account for large-scale fading is of the form presented in Chapter 3 and is modelled according to Terrain Category A [85] (suburban), assuming uncorrelated log-normal shadowing of 10 dB. The path loss is lower-bounded by the free space path loss [18]. The employed system exhibits LOS conditions among BSs

and worst case scenario in terms of interference is assumed with 100% probability of LOS. The path loss in the case of LOS is calculated using the free space path loss model [18]. Non-LOS (NLOS) conditions are assumed for the rest of the TDD interference scenarios (i.e. MS→BS, BS→MS, and MS→MS). Adaptive modulation is achieved with seven different modulation schemes [61] given in Table 3.1, and repeated in Table 4.2 for convenience. The SINR per subcarrier needed to determine the modulation level is calculated using (3.8).

Modulation scheme	4 QAM	8 star	16 QAM	32 cross	64 QAM	128 cross	256 QAM	
Data rate	54.24	81.37	108.49	135.61	162.73	189.86	216.98	kbps
SINR	9	14	16	19	22.2	25	28.5	dB

Table 4.2: *Adaptive modulation parameters for BER of 10^{-7}*

4.5.2 The OTA-SRR algorithm

In this section, the OTA-SRR, previously considered for non-OFDMA systems [72, 73] is formulated as a subcarrier, rate and power allocation algorithm for OFDMA systems. OTA-SRR, first introduced by [72], is particularly chosen to be used in this thesis as it is a fundamental rate and power allocation algorithm which has not been applied to OFDMA yet. An essential part of the new OTA-SRR formulation is the SINR equation presented in Section 3.3.1. The equation enabled the direct application of the existing algorithm constraints and derivations. The modified OTA-SRR is summarised as follows: Initially each user gets a number of subcarriers (depending on the number of users in the cell) with maximum SINR targets, out of a predefined set, assigned to all subcarriers. Under the assumption of a moderately loaded or overloaded system, not all users can support the assigned SINR targets. Iteratively the subcarriers, which experience maximum interference, are identified and their SINR target is decreased in a stepwise manner, in effect adapting the modulation scheme. If the SINR target of a subcarrier is downrated below the minimum value from the target set, the subcarrier is given to a different user from the same BS, such that interference on the subcarrier is minimised. If no such user is found, the subchannel is not used. OTA-SRR is executed until the system reaches feasibility according to the constraints presented in this section.

The algorithm takes into account the interference effects among all subcarriers, thus each subcarrier is given a unique identification (ID). The total number of subcarriers considered in the

algorithm is $BN_{\mathrm{c}} = N_{\mathrm{tot}}$, where B is the total number of BSs considered to contribute significant interference and N_{c} is the number of subcarriers per BS. Hence, the subcarrier IDs are in the range $[1, 2, \ldots, N_{\mathrm{tot}}]$, i.e. subcarrier one used in cell one has ID 1, subcarrier one in cell two has ID $N_{\mathrm{c}} + 1$, subcarrier two used in cell two has ID $N_{\mathrm{c}} + 2$, etc. Based on this, the SINR equation given in (3.8) (and repeated below for completeness) needs to be reformulated slightly, defining new variables, as discussed below.

$$\gamma_k^i = \frac{P_k^i |H_k^i|^2 G_i}{\sum_l \varpi_{i,l} \sum_{k' \in s_l} P_{k'}^i |H_{k'}^{i,l}|^2 |C_{k,k'}(\Delta f + \varepsilon_{\mathrm{D}} + \omega)|^2 G_{i,l} + n_{\mathrm{th}}},$$

where P_k^i is the transmit power of subcarrier k (in Watts); $|H_k^i|^2$ is the channel transfer function of link i at subcarrier k; G_i is the link gain of link i; $\varpi_{i,l}$ is one only when there is MAI between subcarriers k and k' and zero otherwise; s_l is the set of subcarriers belonging to link i, and the cardinality of $s_i, |s_i|$, is the number of subcarriers used by link i, which can vary from zero to N_{c}; $|H_{k'}^{i,l}|^2$ is the channel transfer function between the receiver on link i and the transmitter on link l at subcarrier k'; $|C_{k,k'}(\Delta f + \varepsilon_{\mathrm{D}} + \omega)|^2$ is the cyclic sinc function which determines the amount of interference between subcarriers k and k' based on the subcarrier distance; $G_{i,l}$ is the link gain between the transmitter on link l and the receiver on link i; and n_{th} is the thermal noise power (in Watts) per subcarrier.

Due to the fact that k now is defined to have a unique ID across the BSs, the need to identify to which link a subcarrier belongs is obviated, hence some of the variables used in (3.8) are redefined. Let s_k be the set of subcarriers belonging to the same link as k, excluding k. Furthermore, let $\varpi_{k,k'}$ be defined as:

$$\varpi_{k,k'} = \begin{cases} 0, & k' \in \left[(\lceil \frac{k}{N_{\mathrm{c}}} \rceil + 1) N_{\mathrm{c}} + 1, \lceil \frac{k}{N_{\mathrm{c}}} \rceil N_{\mathrm{c}} + 1 \right] \text{ and } k \text{ is in DL} \\ 1, & \text{otherwise.} \end{cases}$$

The above definition of $\varpi_{k,k'}$ is analogous to the definition of ϖ_l (refer to Section 3.3). In essence, $\varpi_{k,k'}$ determines whether subcarrier k' causes MAI to subcarrier k. MAI is not considered when subcarrier k is in DL and at the same time subcarrier k and k' belong to the same cell. Furthermore, let $\tilde{G}_k = |H_k^i|^2 G_i$ and $\tilde{G}_{k,k'} = \varpi_{k,k'} |H_k^{i,l}|^2 |C_{k,k'}(\Delta f + \varepsilon_{\mathrm{D}} + \omega)|^2 G_{i,l}$.

Based on the above definitions and assumptions, (3.8) can be rewritten as:

$$\gamma_k = \frac{P_k \tilde{G}_k}{\sum\limits_{k' \notin \boldsymbol{s}_k} P_{k'} \tilde{G}_{k,k'} + n_{\mathrm{th}}}. \tag{4.3}$$

Note that (4.3) and (3.8) differ in their representation only. By dividing the numerator and denominator of the right hand side of (4.3) by $\tilde{G}_k$ and transforming it into matrix notation, (4.3) can be further rewritten as:

$$(\mathbf{I} - \mathbf{\Phi})\mathbf{P} \geq \boldsymbol{\eta}, \tag{4.4}$$

where $\mathbf{I}$ is the identity matrix, $\mathbf{\Phi}$ is the normalised link gain matrix (with dimensions $N_{\mathrm{tot}} \times N_{\mathrm{tot}}$) defined as:

$$\Phi_{k,k'} = \frac{\overline{\gamma}_k \tilde{G}_{k,k'}}{\tilde{G}_k}, \tag{4.5}$$

and $\boldsymbol{\eta}$ is the normalised noise vector, given as:

$$\eta_k = \frac{\overline{\gamma}_k n_{\mathrm{th}}}{\tilde{G}_k}, \tag{4.6}$$

with $\overline{\gamma}_k \in \mathbf{\Gamma}$, $\forall k \in N_{\mathrm{tot}}$. The inequality in (4.4) holds as each subcarrier strives to achieve SINR greater or equal to the target. The OTA constraints on the algorithm are defined based on the properties of $\mathbf{\Phi}$ and its dominant eigenvalue λ_1 (real, positive, and unique, according to the Perron-Frobenius theorem [86]). For $\mathbf{\Phi}$ it holds that it is real, nonnegative and irreducible, i.e. the path gains and the SINR targets are real and nonnegative, and the path gains are assumed to be uncorrelated. A solution for the system inequality given in (4.4) exists, only if the right hand side of $\mathbf{P} \geq (\mathbf{I} - \mathbf{\Phi})^{-1}\boldsymbol{\eta}$ converges. The conditions for convergence of the modified OTA-SRR algorithm are presented in Appendix B and the algorithm is shown on Fig. 4.9.

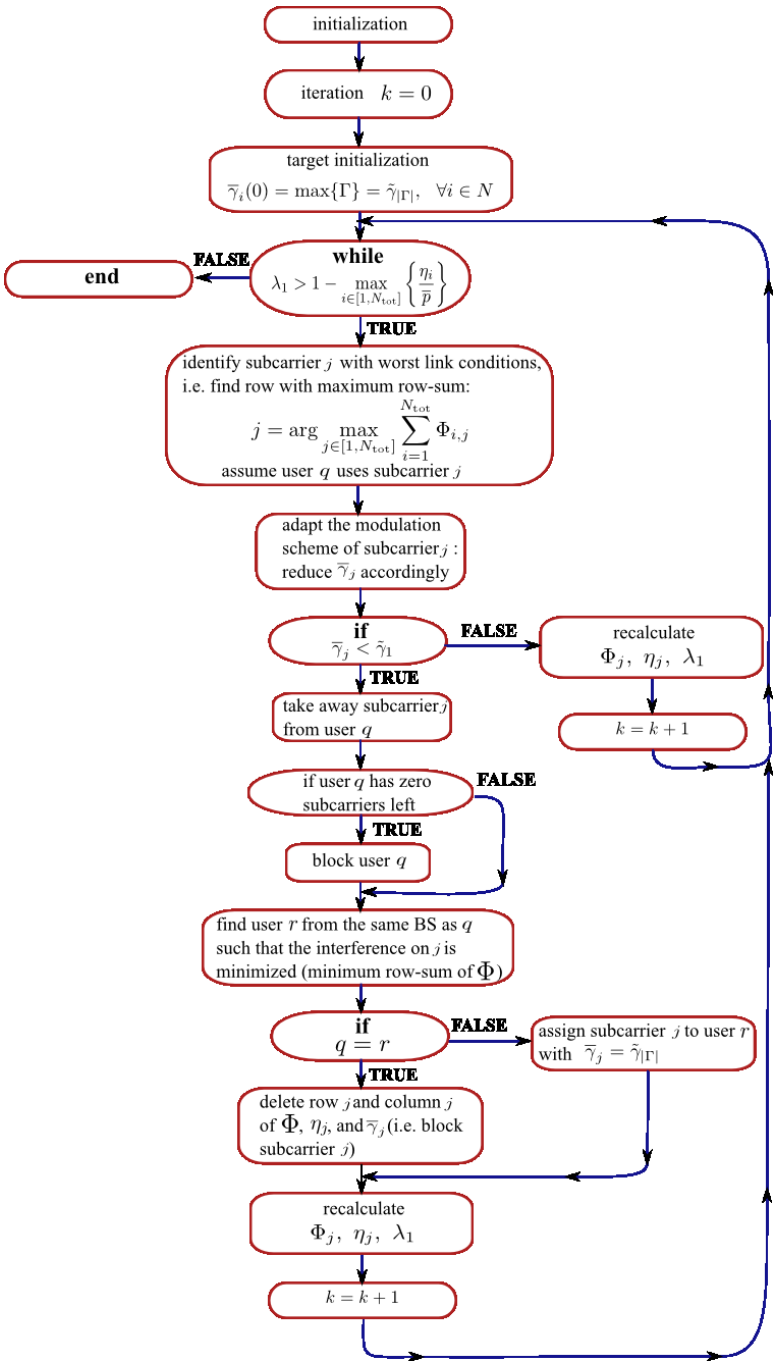

Figure 4.9: *Flowchart of the modified OTA-SRR algorithm*

4.5.3 System validity check results

Due to the complexity of the simulations used in this chapter, it is not possible to verify the underlying model mathematically. This is why Monte Carlo simulations are used in order to

verify the system behaviour against intuition. The results are presented in this section.

In order to validate the system model, the system performance in terms of spectral efficiency is analysed. *Spectral efficiency* is defined as the total system throughput normalised to the product of the total bandwidth and the number of BSs. Note that the total throughput is obtained by summing over the subcarrier data rates and the subcarrier data rate assignment is done according to the adaptive modulation method described in the previous section.

The following systems are employed using UL:DL ratio of 1:1: benchmark, "ideal", FSA, "NLOS", and "LOS". All systems except the benchmark are designed according to the system model outlined in Section 4.5.1. In addition, the characteristics of each of the systems is outlined in Table 4.3. The model of the *benchmark* scenario is as follows. The system considers neither frequency offset errors nor Doppler errors, i.e. it is a purely orthogonal system where the only source of interference is CCI. The resources are allocated randomly at the beginning of each iteration and the SINR per subcarrier is calculated. If the SINR of a particular subcarrier is below the minimum required threshold (Table 4.2), the subcarrier is discarded and not utilised. The SINR of the subcarriers that can maintain a successful link are used to determine their respective data rates and the spectral efficiency of the system. It should be pointed out that the *ideal* system is also a purely orthogonal system but, unlike the benchmark system, has resource allocation and adaptive modulation in place.

Characteristic ↓ ⋱ System →	Benchmark	"Ideal"	FSA	"NLOS"	"LOS"
RTSO, FSA	RTSO		FSA	RTSO	
Resource allocation	No	OTA-SRR			
Adaptive modulation	No	Yes			
LOS/NLOS among BSs	NLOS		N/A	NLOS	LOS
MAI, CCI	CCI		Both		
Frequency offset errors	No		Yes		

Table 4.3: *System characteristics*

It can be expected that the benchmark system performs worst, due to the lack of a resource allocation mechanism and the lack of an adaptive modulation mechanism. In addition, the "ideal" system is expected to perform best, because of the assumption of pure orthogonality among subcarriers and because both resource allocation and adaptive modulation are used,

while NLOS conditions among BSs are assumed. The FSA system and the "NLOS" system should achieve about the same performance, however, the FSA system is expected to perform better in about 50% of the cases, i.e. whenever the FSA system is in DL. This is because in 50% of the cases all cells in the FSA system are in UL simultaneously, hence the performance is worse than the performance of RTSO. The reason stems from the fact that in RTSO there are both UL and DL cells at any given time slot due to the time slot randomisation. Regarding the "LOS" system, it can be safely envisaged that it performs worse than the "NLOS" system. The results are shown in Fig. 4.10 and it can be observed that they support the reasoning outlined above.

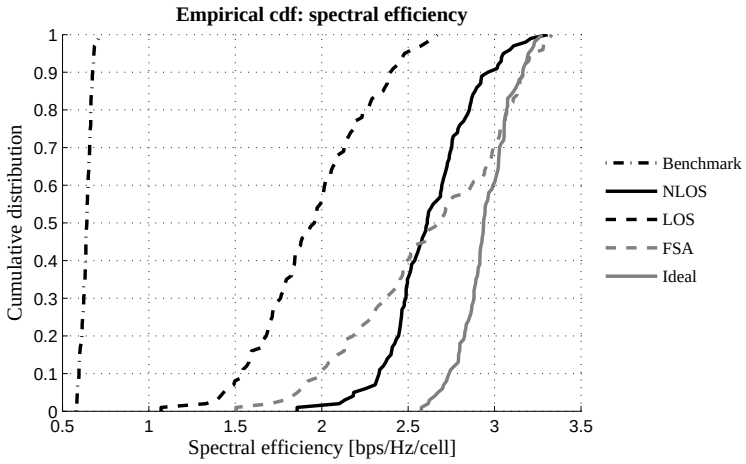

Figure 4.10: *Spectral efficiency attained by the OTA-SRR for UL:DL ratio of 1:1.*

A few comments are in order regarding Fig. 4.10. Firstly, it is interesting to note that the FSA system exhibits better spectral efficiency than the ideal system in about 5% of the cases. The reason for this behaviour lies in the fact that the in the ideal system there are both UL and DL links at the same time, while in the case of FSA the system is either in UL or in DL. Even though the ideal system does not suffer from LOS among BS, the UL still underperforms in comparison to DL due to MAI. Therefore, it is observed that in about 25% of the cases FSA achieves about the same performance as the ideal system and outperforms it in about 5% as mentioned earlier.

It is also worth pointing out that the ideal system exhibits a steeper cdf curve, meaning that there is less variation in the achieved spectral efficiency (only about 0.75 bps/Hz difference between minimum and maximum spectral efficiency). In contrast, FSA shows about 1.75 bps/Hz

difference between the minimum and maximum spectral efficiency achieved, which means that the quality of service varies more. This is the case due to fact that the FSA system is either in UL or in DL, while in the ideal system the UL and DL performance is averaged out as there are both UL and DL links at the same time.

For the reasons outlined above, the 50^{th} percentile comparative trends between the benchmark, "NLOS", "LOS", FSA, and the ideal systems differ slightly from the 10^{th} percentile comparative trends. The basic trends are preserved, except for the fact that at the 10^{th} percentile the FSA system exhibits clearly inferior performance to both the "NLOS" system and the ideal system. Similarly to the ideal system, the "NLOS" system exhibits an averaging out of the spectral efficiency performance of UL and DL, resulting in a steeper cdf curve and more consistent performance in comaprison to the FSA system as discussed above.

4.5.4 FSA vs. RTSO comparison results

The comparison between RTSO and FSA is based on spectral efficiency, subcarrier utilisation, and user outage. *Spectral efficiency* is defined in the previous section. *Subcarrier utilisation* is defined as the ratio of the number of subcarriers used in the system to the total number of subcarriers (number of subcarriers per BS times the number of BSs). *User outage* is defined as the users not served (assigned zero subcarriers) as a fraction of the total number of users in the system. All metrics pertain to the whole system, i.e. UL and DL combined, unless stated otherwise. In addition, as mentioned in Section 4.5.1, a TDD system is simulated assuming a single time slot which is either assigned to UL or DL traffic. This means that for every time slot a different user distribution is analysed. Since TDD can essentially be characterised as a half-duplex system, this is deemed a sensible approach in order to obtain insightful statistical results on essential system metrics.

The spectral efficiency results are shown in Fig. 4.11 for various UL-DL asymmetries for FSA and RTSO. In the case of RTSO, the results demonstrate that shifting more resources to DL results in more than 80% increase in spectral efficiency at the median as compared to the performance of the UL-favoured case. This effect is due to the presence of MAI in UL as well as the fact that LOS conditions among BSs are accounted for, which makes UL the performance limiting factor. In particular, as MAI is only considered in UL, this means that as the number of slots in UL decreases, the overall experienced interference also decreases, resulting in improved system performance. In addition, as the effect of LOS conditions among BSs is

experienced by the cells in UL, a decrease in the number of UL cells means fewer affected BSs and, hence, system performance improvement. In the case of FSA, it can be observed that the spectral efficiency of the DL-favoured scenario is only about 30% better at the median than the spectral efficiency of the UL-favoured scenario. This means that when employing RTSO the improvement in spectral efficiency incurred by allocating more resources to DL is larger than when employing FSA. This stems from the fact that while the UL in RTSO is limited by MAI and LOS conditions among BSs, the UL in FSA is only limited by MAI.

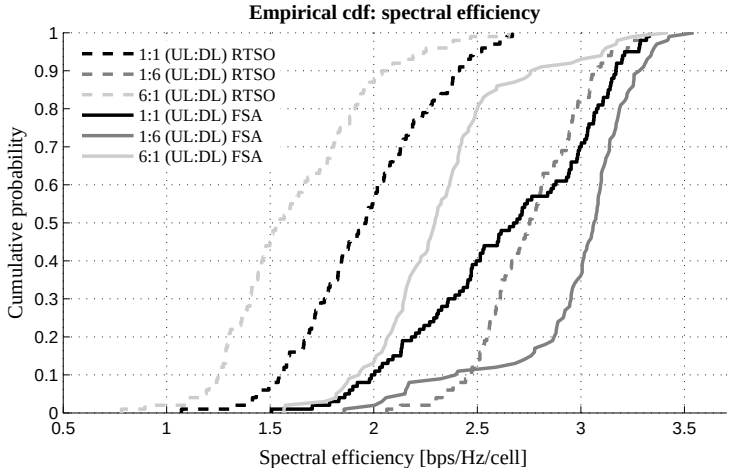

Figure 4.11: *Spectral efficiency [bps/Hz/cell] attained by the OTA-SRR for various UL:DL ratios. Spectral efficiency is the ratio of the total throughput in the system to the product of the bandwidth and the number of cells.*

In this context, a clear trend can be observed: with an increase in the number of time slots allocated to DL, the spectral efficiency increases and reaches about 75% and about 80% of the theoretical maximum in the case of RTSO and FSA, respectively. The theoretical maximum can be calculated as $\frac{216.98}{W_{\mathrm{b}}}$ and equals 4.44 bps/Hz/cell, where W_{b} is the bandwidth per subcarrier, and 216.98 kbps is the maximum data rate per subcarrier (as given in Table 3.1). It is worth noting here that as shown in Section 4.4.1, RTSO results in the highest number of crossed slots in the case of asymmetry of 1:1 (the special case of asymmetry). Hence, it would be expected that the symmetric case would result in worst system performance. However, the results demonstrate that UL-favoured asymmetries perform worse than both the symmetric case and the DL-favoured case. This stems from the effect of MAI and LOS conditions among BSs discussed above.

Fig. 4.11 also shows that for each of the asymmetries considered, the FSA performs better than RTSO. In particular, the difference (at the median) between the spectral efficiency attained with FSA and the spectral efficiency attained with RTSO is about 48%, 36%, and 11% for UL:DL ratios of 6:1, 1:1, and 1:6, respectively. In addition, the symmetric FSA performs better than nearly all considered RTSO scenarios. In particular, considering the case of UL:DL=6:1, it can be observed that the symmetric FSA attains about 80% increase in spectral efficiency at the median as compared to RTSO. In the case of 1:6 (UL:DL), however, while the medians of symmetric FSA and RTSO are almost the same, RTSO performs overall better than FSA in about 60% of the cases. This is because in the case of RTSO about $\frac{6}{7}^{\text{th}}$ of the links are in DL, while in the symmetric FSA half of the links are in DL. The reason why RTSO does not completely outperform symmetric FSA is the fact that LOS conditions among BSs are considered.

The subcarrier utilisation results shown in Fig. 4.12 display similar trends as the spectral efficiency results. In the case of RTSO, the subcarrier utilisation attained by the DL-favoured system is about 33% better at the median in comparison with the subcarrier utilisation attained by the UL-favoured system. In contrast, when the analogous comparison is made for the case of FSA, the difference between the subcarrier utilisation of the DL-favoured system and the UL-favoured system is only 13%. In addition, it can be observed that FSA outperforms RTSO in terms of subcarrier utilisation by about 36%, 35%, and 12% for UL:DL ratios of 6:1, 1:1, and 1:6, respectively. Furthermore, the symmetric FSA performs better in terms of subcarrier utilisation than all considered RTSO scenarios. In particular, the symmetric FSA attains about 38%, 36%, and 6% better subcarrier utilisation (at the median) than RTSO for UL:DL ratios of 6:1, 1:1, and 1:6, respectively.

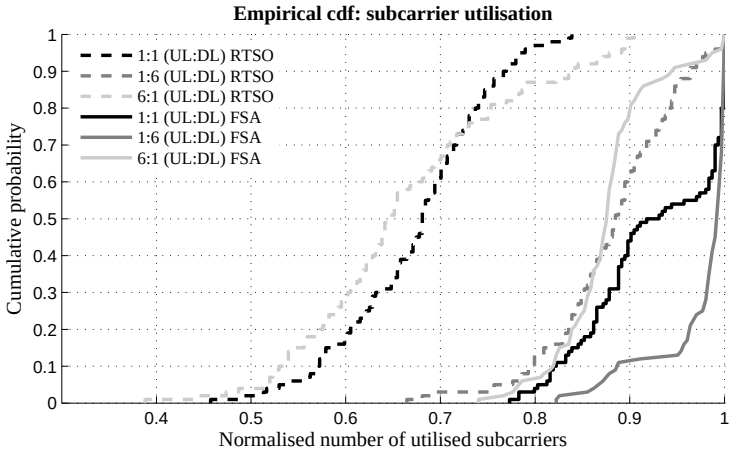

Figure 4.12: *Subcarrier utilisation attained by the OTA-SRR for various UL:DL ratios. Subcarrier utilisation is the ratio of the number of subcarriers in the system which are utilised for transmission (i.e. the assigned data rate is greater than 0) to the total number of subcarriers in the system,* $N_{\mathrm{c}} \times B$.

The user outage results are presented in Fig. 4.13. Unlike the spectral efficiency results and the subcarrier utilisation results, the outage results show that FSA does not always outperform RTSO. In particular, for UL:DL ratio of 1:6 FSA achieves about 9% (at the median) better user outage than RTSO. However, the cdf curve demonstrates that the outage performance of FSA is better than that of RTSO about 87% of the time. It can be noted that 87% corresponds to $\frac{6}{7}^{\mathrm{th}}$ which means that FSA outperforms RTSO when the system is in DL. Similarly, for UL:DL ratio of 1:1, FSA achieves better user outage than RTSO about 50% of the time and the medians of the respective cdf curves coincide. The case of UL:DL ratio of 6:1 is slightly different, and for this particular scenario FSA completely outperforms RTSO while achieving about 3% better user outage at the median. This is due to the fact that when the UL:DL asymmetry is 6:1, RTSO is predominantly in UL and the effect of BS→BS interference is the most significant as compared to the rest of the considered asymmetry ratios. It should be noted the outage metric is a relative metric, used for comparison purposes only. The low percantage of served users is due to the severe interference conditions considered.

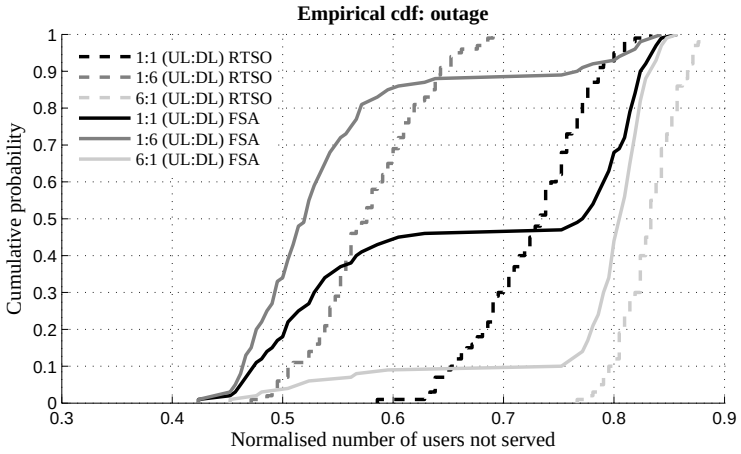

Figure 4.13: *User outage attained by the OTA-SRR for various UL:DL ratios. User outage is the ratio of the number of users which are not served to the total number of users in the system.*

An interesting observation can be made with regard to the spectral efficiency, the subcarrier utilisation, and especially the user outage results – the FSA scheme exhibits a "plateau" behaviour (bi-modal distribution). This can be explained by the presence of MAI in UL, which, as mentioned previously in this section, creates a significant gap between UL and DL performance.

4.6 A comparison between ZD and FSA

This section presents a comparison between ZD and FSA, based on computer simulation results [70] and uses a different approach to analyse the BS→BS interference problem as comapared the approach used in the analysis of RTSO and FSA. In particular, this section studies the impact of BS→BS interference on a single "victim" cell. To this end, also a dissimilar simulation platform is used (as compared to the platform used in the previous section), which is detailed in the following.

4.6.1 Simulation model

A seven-cell OFDMA-TDD system (one cell at the centre and six surrounding cells) is designed and simulated adopting a Monte Carlo approach. Each of the seven cells has a centrally-placed

omnidirectional BS and full frequency reuse is assumed. Twenty users are distributed uniformly in each of the seven cells at the beginning of each iteration and a snap-shot analysis is performed. Similar to the envisaged traffic asymmetry in data-packet services, traffic is on average DL-favoured. The centre cell, however, is UL-overloaded and hence generates UL-favoured traffic in order to expose the effects of BS→BS interference on the centre cell. The holding time is the same for all users and equals one chunk during a time slot (5 OFDM symbols). Each cell is given a mean offered load, which governs the respective user mean inter-arrival times and each user independently generates holding times with exponentially distributed interarrival times. The traffic per user is stored in a buffer and served on a first-in-first-out basis. The maximum waiting time per packet is 20ms [13] and should this time be exceeded, the packet is discarded. Path loss is calculated using the IST-WINNER C1 path loss model (NLOS) for urban environment [87] according to (3.3), where a and b are given in Table 4.4 (log-normal shadowing is not considered). It should be noted that the values of a and b depend on whether MS–MS path loss, BS–MS path loss, or BS–BS path loss is calculated. For the latter line-of-sight conditions are assumed. MSs are associated with serving BSs based on minimum path loss. Perfect synchronisation is assumed and only co-channel interference from all active other-cell transmitters is taken into account. Time-frequency resources are allocated following a score-based approach [88], where the score is evaluated based on buffer-size. In particular, a given resource is allocated to the user with the largest average buffer size, monitored during a time window of eight frames (the size of a superframe [13]). The condition of choosing a user to be allocated a resource can be expressed as:

$$u(r,t) = \arg \max_{i=1,..,U_c} \frac{1}{8} \sum_{l=t-8}^{t-1} \iota_{\mathrm{b},i}(l), \tag{4.7}$$

where $u(r,t)$ is the user allocated resource r at time instant t; U_c is the number of users per cell; and $\iota_{\mathrm{b},i}(l)$ is the buffer length of user i at frame l. The simulation parameters are shown in Table 4.4. For demonstration purposes, 16 OFDM subcarriers are considered.

Carrier frequency	5 GHz
Time slot duration	0.1152 ms
Number of time slots/ frame	6
Number of OFDM symbols/ time slot	5
Transmit power/ link	251 mW (24 dBm)
Shortest BS-BS distance	1 km
BS height	25 m
MS height	1.5 m
Path loss parameter a	MS–BS: 39.61 MS–MS: 32.49 BS–BS: 41.2
Path loss parameter b	MS–BS: 35.74 MS–MS: 43.75 BS–BS: 23.8

Table 4.4: *Fixed simulation parameters [52], [87]*

It should be noted that in the case of ZD, each cell sets its TDD SP according to the ratio of UL-DL user demand. When FSA is employed, the UL↔DL SPs are synchronised across the cells allocating half of the resources to UL and DL each [13], i.e. the SP is set at 1:1 (UL:DL). As the SP is symmetric, both UL and DL are allocated 16 subcarriers/time slot $\times$ 3 time slots/frame = 48 chunks/frame (as one chunk is one subcarrier).

A simplifying assumption is made, where the SINR values are calculated using (3.8), assuming constant channel coefficients and perfect synchronisation (no MAI and offset errors). These assumptions account for an ideal system. This is in contrast to the system model discussed in the previous section, which assumes worst case interference when calculating SINR. Employing an ideal model in this section provides a complementary approach to demonstrating the severity of BS→BS interference.

A simple SINR-based power control is applied to all links with an SINR target of 20 dB (32 cross constellation at BER of 10^{-7} [61]) and thermal noise power per subcarrier of -157.11 dBW [52]. The total power per link is limited by the maximum transmit power given in

Table 4.4. The capacity per chunk is calculated using Shannon's capacity equation as follows:

$$\overline{C}_k = \log_2(1+\gamma_k) \ \text{bps/Hz}, \tag{4.8}$$

where γ_k is the SINR per chunk as defined in (3.8). Power control is applied in order to limit power usage and interference in comparison to a fixed power scenario. The relatively high SINR target aims to provide the well-placed links in terms of link conditions with high data rates. If the SINR target cannot be met on some links even when the power control algorithm has reached convergence[1], the links are still allowed to transmit with their maximum power as per the power budget. The total spectral efficiency in the system, $\overline{C}_\text{s}$, is calculated as shown in (4.9):

$$\overline{C}_\text{s} = \frac{1}{C_\text{tot}} \left(\sum_{k=1}^{M_u} \overline{C}_k \right) \ \text{bps/Hz}, \tag{4.9}$$

where $M_u = \frac{n_\text{UL}}{n_\text{UL}+n_\text{DL}} C_\text{tot}$ is the number of chunks allocated to UL as per the network-wide SP; and C_tot is the total number of resources per frame (and $C_\text{tot} = 48 \times 2 = 96$ as mentioned before). It should be noted that the normalisation factor C_tot is applied in order to account for the resource utilisation in the frame.

The comparison between FSA and ZD is made based on a defined scenario, which allows for a clear demonstration of the effect of LOS among BS on spectral efficiency for the case of ZD. The details of the scenario are as follows: The resource demand at each of the seven cells is shown in Table 4.5 for both UL and DL. Note that for the case of DL at the first-tier cells, 0→40 means that the demand is systematically varied from 0 to 40% (simultaneously for all six first-tier cells). This means that, as the UL demand is 15%, the first-tier cells start off with UL-favoured SP. As the DL demand is increased, the SP is adjusted to accommodate it. When the DL demand reaches 40%, all six first-tier cells have DL-favoured SPs. The centre cell, i.e. the cell of interest (CoI), on the other hand, demands 100% of the frame to be allocated to UL and as a result, the SP is highly UL-favoured. This scenario of increasing DL demand of the first-tier cells, while the CoI has constant high UL demand, makes the BS→BS interference experienced at the CoI vary from non-existent to severe, as will be demonstrated in the next section.

The defined scenario allows for the demand at all six first-tier cells to be accommodated both by

[1]Convergence is reached when for all links it holds that the power value allocated to each link does not change from one iteration to the next within some small value δ_c.

ZD and by FSA. In contrast, neither FSA nor ZD are capable of accommodating the demanded UL traffic at the CoI. Furthermore, FSA allocates only 50% of the frame resources to UL, while ZD allocates up to five out of the six time slots per frame to UL [52]. It is then interesting to see whether FSA can offset the loss incurred by not accommodating the demanded UL traffic by avoiding BS→BS interference at the CoI. The results are presented in the next section.

Cell number → Link direction ↓	1 (CoI)	2	3	4	5	6	7
UL	100	15					
DL	0→40						

Table 4.5: *Resource demand for UL and DL (in %)*

4.6.2 ZD vs. FSA comparison results

The comparison between ZD and FSA is done based on the UL-DL resource allocation at the CoI and the UL spectral efficiency at the CoI. The resource allocation is measured as the ratio of the number of resources allocated to UL per frame to the total number of resources per frame. Spectral efficiency is calculated based on Shannon's capacity equation as defined in the previous section. It should be pointed out that UL spectral efficiency is considered as a metric in order to focus the results on the specific effect of BS→BS interference on spectral efficiency and BS→BS interference is only experienced by links in UL.

Results on UL-DL resource allocation are shown in Fig. 4.14. The allocation by the FSA is shown by the solid horizontal line at 50%. ZD, on the other hand, allocates resources depending on the cell-specific demand. This means that at the CoI as the demand in DL increases, the ratio of the UL-to-DL demand decreases and as a result, the switching point shifts towards the DL to accommodate the change. On the other hand, as expected, when the DL demand at the first-tier cell increases, there is hardly any effect on the resource allocation at the CoI both in the case of ZD and FSA. For the case of ZD, the reason why there is a slight increase in the resources allocated to UL between the points of 0% and 10% DL demand at the CoI (for 20% and 40% DL demand at the first-tier cells) lies in the way ZD functions. In particular, as the DL demand becomes greater than zero, UL crossed slots are introduced. According to ZD, introducing UL crossed slots means that generally not all UL resources can be allocated because only users in the inner cell region are served during crossed slots. As a result, the total UL buffer of users in

the system increases. Consequently, as the SP allocation depends on the size of the UL buffer in relation to the DL buffer, the SP becomes more UL-favoured.

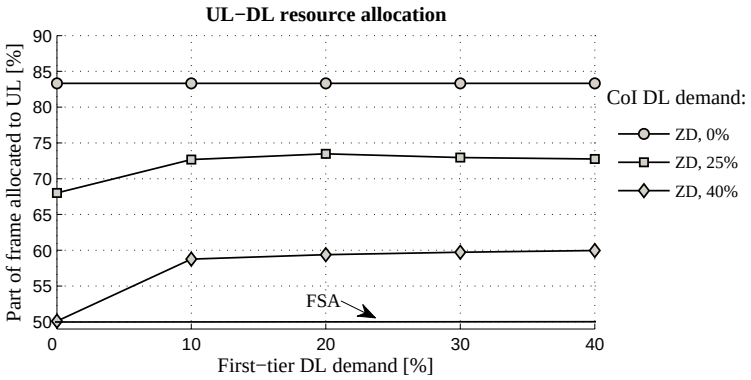

Figure 4.14: *Fraction of the resources per frame allocated to UL at the CoI.*

It should be noted that in ZD the maximum asymmetry which can be supported is 5:1 in favour of either link direction [52] (as seen on Fig. 4.14). This constraint which is necessary for singalling and synchronisation depends purely on the network architecture and the frame structure it employs.

As previously mentioned, ZD and FSA are fundamentally different in that in ZD crossed slots occur. Hence, it is expected that when ZD is employed, increasing the DL load at the first-tier cells will have a negative effect on the CoI UL spectral efficiency. This is because an increase in the number of time slots allocated to DL at the first-tier cells will result in an increase in the BS→BS interference per frame experienced at the CoI (assuming the CoI exhibits an UL-favoured SP). UL spectral efficiency results for the CoI are shown in Fig. 4.15.

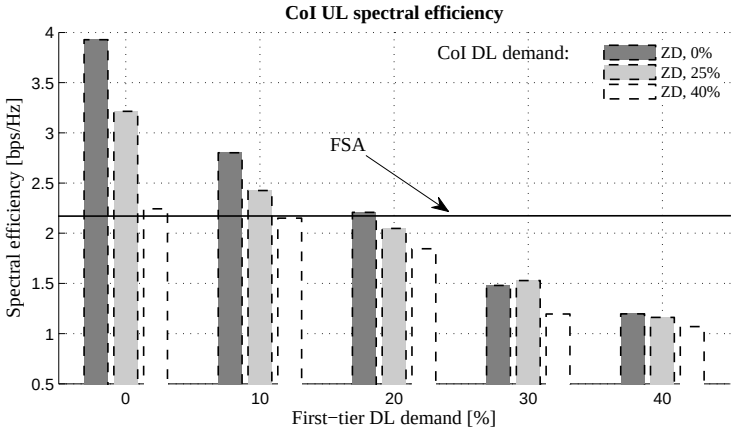

Figure 4.15: *UL spectral efficiency [bps/Hz] attained at the CoI by ZD and FSA for variable DL demand at the CoI and first-tier cells. The spectral efficiency is the ratio of the the total capacity (as defined by Shannon's equation) at the CoI to the total number of chunks (UL and DL) per frame.*

Two main trends can be observed in Fig. 4.15 with respect to the performance of ZD. The first one is observed when noting that the spectral efficiency varies as the DL demand at the CoI is increased. This is as expected because as the DL demand increases fewer resources are allocated to UL within a frame, and the spectral efficiency is normalised to the total number of resources per frame. The second, more important, trend is the variation of UL spectral efficiency at the CoI as the first-tier DL demand increases. Fig. 4.15 shows that as the first-tier DL demand increases, which causes the BS→BS interference experienced at the CoI to increase, the CoI UL spectral efficiency suffers tremendously. For example, for 25% DL load at the CoI when comparing the CoI spectral efficiency at 0% first-tier DL load with the CoI spectral efficiency at 40% first-tier DL load, it can be observed that the decrease in CoI UL spectral efficiency is about 2/3. This clearly demonstrates the severe effect that BS→BS interference has on the UL spectral efficiency.

Regarding the comparative performance of ZD and FSA, note that ZD allocates more resources to UL than FSA (referring to Fig. 4.14). However, Fig. 4.15 shows that ZD significantly outperforms FSA only when the probability for crossed slots is negligible, i.e. in the case of 0% and 10% DL demand at all of the first-tier cells. This means that ZD results in large inefficiency in resource utilisation. Furthermore, in the cases of severe crossed slots (40% first-tier DL demand) FSA consistently attains about two times the spectral efficiency of ZD independent of

the DL demand at the CoI.

4.6.3 System validity check results

The following results will be used as a validity check in order to demonstrate that the system behaves according to intuition and that, therefore, the results presented above are reliable. Results for the DL spectral efficiency attained with ZD and FSA at the CoI are shown in Fig. 4.18 and resource utilisation results are shown in Fig. 4.16 and Fig. 4.17 for DL and UL, respectively. Note that Fig. 4.16 and Fig. 4.17 also show results for resource allocation as displayed on Fig. 4.14. (The graphs for resource allocation in DL are obtained from the graphs for resource allocation in UL by using that the sum of UL and DL resource allocation equals 100.) Considering the DL resource utilisation (Fig. 4.16), it can be observed that, as expected, for both FSA and ZD the resource utilisation and resource allocation at the CoI are independent of the DL demand at the first-tier cells. The only exception to this trend is the case of ZD when the CoI DL demand is 0%. This exception was already discussed in relation to the UL spectral efficiency results.

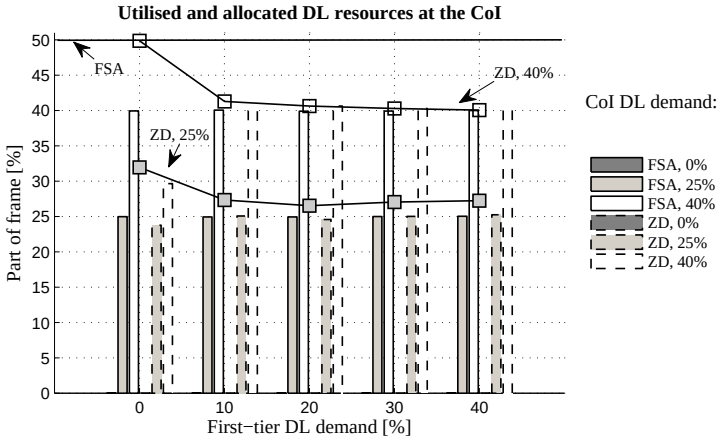

Figure 4.16: *DL resource utilisation [%] attained at the CoI by ZD and FSA for variable DL demand at the CoI and first-tier cells (shown by bar graph). The respective resource allocation is shown by lines with square markers.*

While in the case of FSA the resource utilisation for both UL and DL is independent of the first-tier DL demand, as expected, the trend exhibited by the ZD UL resource utilisation results is different from the trend of the ZD DL utilisation results. It can be seen that as the DL resource

demand at the first-tier cells increases, the UL resource utilisation at the CoI decreases due to the increased BS→BS interference. As ZD only serves MSs from the inner cell region during crossed slots, an increase in the number of crossed slots results in resource underutilisation, as discussed in Section 4.4.2 and confirmed by the results in Fig. 4.17. By resource underutilisation it is meant that there is resource demand and resources are allocated, however, the ratio of non-crossed slots to crossed slots does not correspond to the ratio of the demand generated by the whole cell to the demand generated by the inner cell region only. This means that crossed slots are left unoccupied.

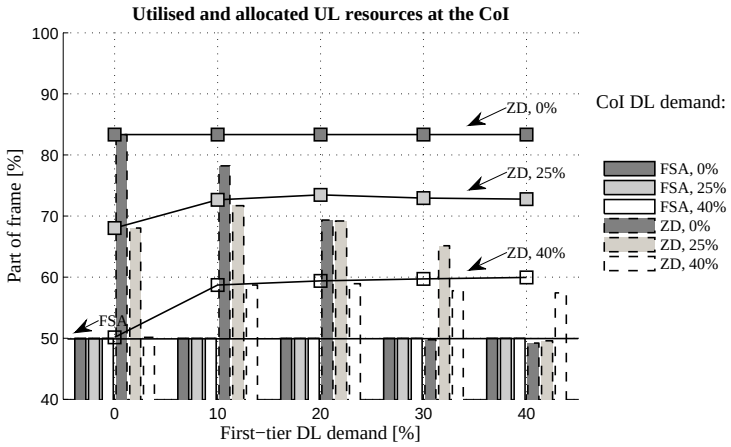

Figure 4.17: *UL resource utilisation [%] attained at the CoI by ZD and FSA for variable DL demand at the CoI and first-tier cells (shown by bar graph). The respective resource allocation is shown by lines with square markers.*

In relation to the DL spectral efficiency at the CoI, it is expected that for a given DL demand at the CoI as the DL demand at the first-tier cells increases, the DL spectral efficiency at the CoI will decrease. This decrease is caused by the increased interference which results from the higher load. Observing Fig. 4.18 this trend is confirmed, and as expected, holds for both ZD and FSA. In addition, it is expected that for low first-tier DL demand, FSA exhibits better DL spectral efficiency than ZD. This is because for the case of ZD for 0% and 10% DL demand at the first-tier cells the SP is generally UL-favoured (because the UL demand is 10%), which means that the DL at the CoI is likely to experience crossed slots, especially for DL demand at the CoI of 40%. Furthermore, as the DL demand at the first-tier cells increases, the DL at the CoI seizes to be exposed to crossed slots, that is why the DL spectral efficiency attained with ZD and FSA tends to be equal. It can be observed that for DL demand at the CoI of 40%

when the DL demand at the first-tier cells is 30% and 40%, ZD achieves slightly better spectral efficiency than FSA. This result is intuitive because 30% and 40% DL demand at the first-tier cells means that the SP is DL-favoured (as the UL demand is only 15%). As a result, more than half of the frame is allocated to DL at the first-tier cells whilst the demand is less than half. This means that, as compared to FSA which allocates half of the resources per frame to DL, in ZD the probability for a DL resource to be occupied at a first-tier cell is smaller. As a result of this and because the SPs at the CoI in the case of ZD and FSA do not significantly differ (refer to Fig. 4.16) the interference experienced at the CoI is smaller as compared to FSA. However, the same effect cannot be observed for 25% DL demand at the CoI. In particular, FSA outperforms ZD for all considered first-tier DL demands (except for 0% as explained previously). This is because as compared to ZD, at the CoI FSA allocates twice as much resources to DL (refer to Fig. 4.16), which increases the degrees of freedom for resource allocation and hence, the overall experienced interference is decreased.

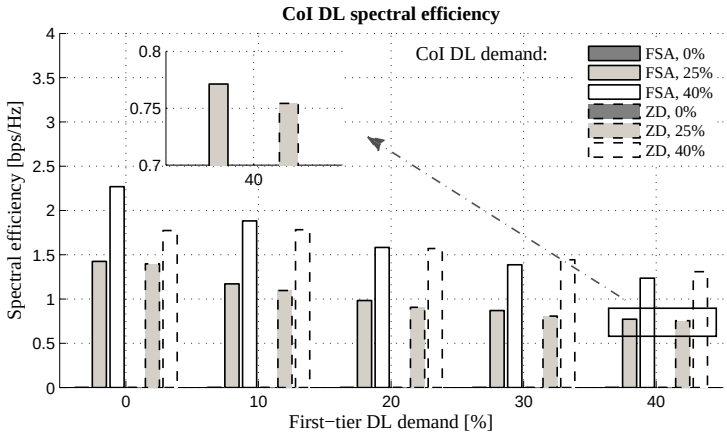

Figure 4.18: *DL spectral efficiency [bps/Hz] attained at the CoI by ZD and FSA for variable DL demand at the CoI and first-tier cells.*

4.7 Summary

This chapter highlighted the importance of interference mitigation techniques in OFDMA-TDD-based cellular networks and demonstrated the severity of BS→BS interference. Interference mitigation techniques targeted towards the CCI problem in OFDMA-based networks were discussed, as well as techniques which specifically address interference resulting from crossed slots in TDD. Pertaining to the first group of methods, variations of the fractional/soft

frequency reuse concept were reviewed. Pertaining to the latter group of methods, RTSO and ZD were discussed and compared to FSA based on simulations.

It was shown that interference mitigation techniques, such as RTSO and ZD, are not able to resolve the BS→BS interference in the case of LOS conditions among BSs. In particular, FSA achieves up to about 80% spectral efficiency improvement with respect to RTSO and up to about 100% spectral efficiency improvement with respect to ZD when severe BS→BS interference is present. The complete avoidance of BS→BS interference is possible, when the TDD switching points across cells are synchronised. However, such an approach limits the flexibility of TDD. This constitutes an important open issue for research, namely, how to retain the flexibility in cell specific UL/DL asymmetry assignment while keeping the SP fixed. This issue is solved in the next chapter through the introduction of a "virtual SP". To the best of the author's knowledge, such a virtual SP is proposed for the first time.

Chapter 5
Interference avoidance for cellular OFDMA-TDD networks

5.1 Introduction

It was demonstrated that avoidance of BS→BS interference is of paramount importance to OFDMA-TDD cellular networks as this type of interference severely degrades the system's performance. This chapter introduces a novel method, termed *asymmetry balancing* [70, 89, 90], which exploits the capabilities of MCNs in order to support cell-specific asymmetry demands while completely avoiding BS→BS interference. A further novelty, introduced in this chapter is the concept of virtual SP. The concept refers to the capability of the asymmetry balancing method to serve cell-specific asymmetry demands even though the network-wide SP is synchronised among cells.

This chapter is organised as follows. First, related work is presented and the asymmetry balancing concept is introduced in detail. The discussion concentrates on UL asymmetry balancing in light of the envisaged dominance of DL-favoured or symmetric traffic (and therefore DL-favoured or symmetric SPs), which may result in occasional significant shortage of UL resources. DL asymmetry balancing, however, can be straightforwardly deduced. Next, the concept of the virtual SP is introduced and a mathematical framework is developed. The framework has two main components, namely: resource availability and availability of relay stations. Based on the available resources in a network, the mathematical framework enables the calculation of the average number of resources which can be utilised for asymmetry balancing and the "position" of the virtual SP in the frame. Finally, simulation results are presented. The performance of asymmetry balancing is compared to the performance of ZD and FSA based on UL resource allocation and UL spectral efficiency.

5.2 Asymmetry balancing

5.2.1 Related work

An effective strategy to ameliorate the spectral efficiency performance without increasing hardware cost is to make use of existing infrastructure and to introduce cooperation among the network entities. As described in Chapter 2, such cooperation leads to MCNs [6]. For example, in [91] Qiao, Wu and Tonguz describe a load balancing method via mobile dedicated transceivers, which can be replaced according to user traffic demand, in order to divert traffic using the unlicensed frequency bands. However, MCNs where the MSs in the network serve as RSs are of special interest. This is because mobile services are becoming increasingly popular which means that the availability of mobile terminals can be exploited. This is especially true at largely populated areas where network capacity becomes a limiting factor. Capacity improvement has been shown in [92–94], where *active* in-cell users cooperatively serve as relays to form virtual antenna arrays. This is achieved by assigning a partner MS to each MS in the network. The partner MS receives the data of another MS (from the same cell) and forwards the data to the respective BS together with its own data. In this way, the BS receives two copies of the same information and these copies are affected by independently fading channels. The principle of this method is analogous to the principle of multiple-input-multiple output (MIMO) and allows for single-antenna MSs to exploits transmit diversity (refer to Fig. 5.1). The method is known as *cooperative communication* and is shown to increase system capacity when applied to CDMA systems [93] and OFDMA systems [94].

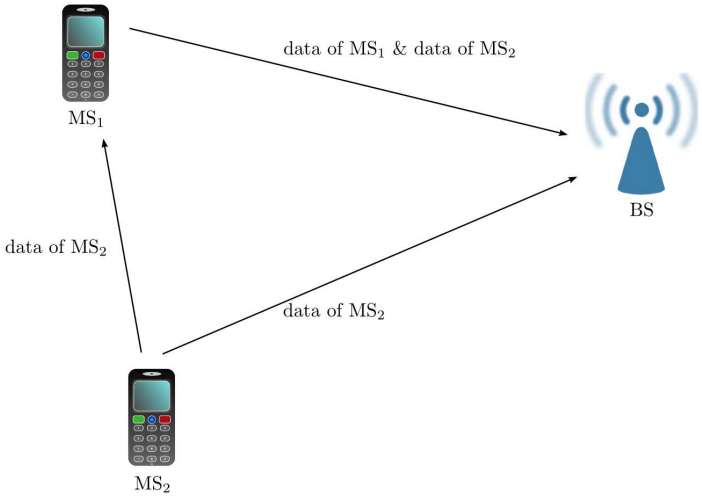

Figure 5.1: *In cooperative transmission, an MS receives the data of another MS from the same cell and along with its own data forwards the received data to the BS, thereby achieving transmit diversity.*

The asymmetry balancing concept introduced here utilises the cooperation capabilities of MCNs, however, asymmetry balancing is a very different type of cooperative communication as is detailed in the next section. The core purpose of the asymmetry balancing method is to *avoid interference*. In Chapter 4, it was demonstrated that interference mitigation mechanisms, such as ZD and RTSO, are not capable of tackling the BS→BS interference problem whenever there are LOS conditions among BSs, due to the significant interference stemming from the direct path between BSs. The proposed asymmetry balancing concept completely avoids BS→BS interference by employing both FSA and load balancing via *ad hoc* communication such that the advantages of TDD are in effect retained.

5.2.2 The asymmetry balancing concept

The essence of the asymmetry balancing concept is, as the name suggests, to balance the asymmetry demand across the cells in a network. To this end, the TDD SP is synchronised across cells, which might result in a shortage of resources in a particular cell, while a neighbouring cell might have spare resources (assuming cell-independent traffic asymmetry demands). In order to resolve any mismatch between resource availability and resource demand, the *ad hoc* capabilities of an MCN are exploited. In particular, assume an MS which cannot be served in either UL or DL by its associated BS due to shortage of resources. Then this MS can be served

by a neighbouring cooperating BS, which has spare resources in both link directions. The established MS↔BS link is a two-hop link where the intermediate node is an MS associated with the cooperating BS. In this way, despite the fact that the network maintains a synchronised SP, cell-specific asymmetries are effectively supported. At this stage it is worth pointing out that *the asymmetry balancing does not suffer from the multi-hop burden*, because asymmetry balancing simply exploits free resources which would otherwise be wasted, therefore increasing spectrum utilisation.

It is assumed that cells are differently loaded at any given time, which is a reasonable assumption for future wireless networks which will mainly support packet-data traffic characterised by a high peak-to-average load ratio. In addition, because traffic is envisaged to be DL-favoured the network-wide SP will be primarily DL-favoured (or occasionally symmetric), it is expected that a cell which requires UL-favoured SP will not be able to support the UL demand. Therefore, this study focuses on UL asymmetry balancing.

As the asymmetry balancing concept relies on cooperation, it is important to identify the cooperating entities and when they can cooperate. If hexagonal cells are considered, each cell can be treated as a CoI, surrounded by six neighbouring cells, which are the potential cooperating cells. Fig. 5.2 illustrates the aforementioned geometry during a DL time slot. Assume that there are only two frequency resources per cell per link direction per frame, which are marked by boxes on Fig. 5.2. A black box signifies an allocated resource, while a white box signifies a free resource. Let the CoI suffer from shortage of UL resources, while it has a DL resource available. The MS at the CoI, which needs UL service and desires to off-load traffic is marked by a solid ellipse. The first-tier cells which are marked with dashed hexagons have spare UL and DL resources and hence are the cooperating cells. Associated with the cooperating cells are the MSs which can serve as RSs (identified by dashed ellipses). The tagged MS at the CoI can relay to any of the available RSs. The MS→RS link uses a DL resource, which is free both at the CoI and the cooperating cell which serves the respective RS. Such resources are referred to as common free resources (CFR). In addition, the off-loading MSs can form *ad hoc* links to either idle MSs in neighbouring cells, or active MSs which are already receiving in DL from their BS. The latter case exploits the fact that a DL transmission usually does not occupy all subchannels, and this is accounted for by the use of TDMA/FDMA in combination with OFDM. It should be noted that in an OFDMA-TDD network the smallest resource unit that can

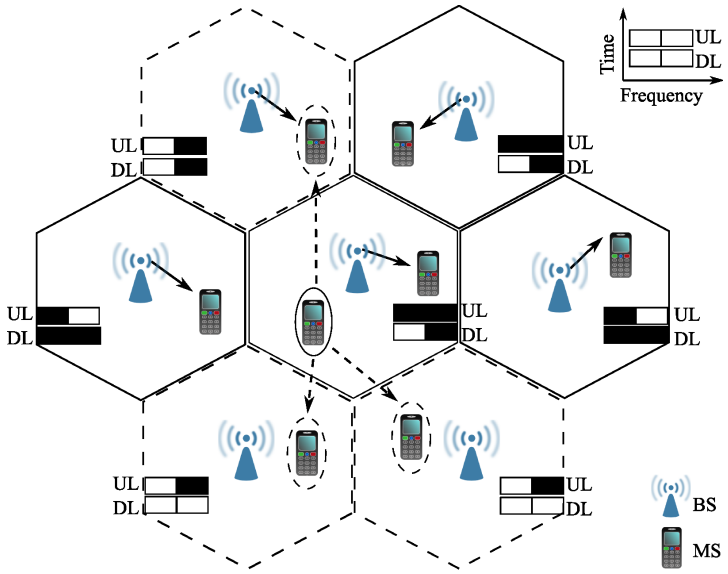

Figure 5.2: *The MSs in the centre cell, i.e. the CoI, can off-load UL traffic to neighbouring cooperating cells (marked by dashed hexagons) using free DL resources (marked by white boxes). As an example, the MS at the CoI which needs UL service (marked by a solid ellipse) can form an ad hoc link with any of the available MSs (marked by dashed ellipses) at the cooperating cells. Active DL links are shown as solid arrows, while possible concurrent ad hoc links are shown as dashed arrows.*

be allocated to a particular user is termed a chunk[1], i.e. a number of subcarriers during one time slot. Based on the above, the main steps of the UL asymmetry balancing technique for multiple cell scenario are summarised as follows:

1. A CoI is overloaded in UL and requires cooperation.
2. The set of first-tier cells surrounding the CoI, which have spare resources both in UL and DL, are the cooperating cells.
3. There are DL CFRs between the CoI and at least one of the cooperating cells.
4. Utilise the CFRs to transfer UL load from the CoI to the cooperating cells. Use *ad hoc* communication to form MS→RS links between MSs associated with the CoI and RSs associated with any of the cooperating cells.

Similarly, if the CoI suffers from DL overload, MSs at the CoI can be served indirectly by the cooperating cells via near-by MSs (operating as RSs). This would involve BS-BS communica-

[1]The terms chunk and resource are used interchangeably throughout this text.

tion which could be done directly or via the backbone, similarly to the communication during a handover.

From the above it can be concluded that the asymmetry balancing requires first, *available resources* and second, *available RSs*. The next two sections will treat these factors in detail. Even though the analysis is performed for the case of UL asymmetry balancing, it is valid for DL asymmetry balancing as well.

5.2.3 Resource availability and the virtual SP concept

When the centre cell uses DL resources to off-load UL traffic to cooperating neighbouring cells, "virtual" UL resources are in effect created, which allow for cell-specific asymmetry demands to be supported. In this way, with cooperation the UL resource capacity of the CoI increases. For example, if the network-wide SP allocates half of the frame to UL and half to DL, and 20% of the DL resources are CFRs, the UL resource capacity of the CoI increases by 20%. Hence, an UL-to-DL traffic ratio of $\frac{0.5+0.5\times0.2}{0.5-0.5\times0.2}$, i.e. $\frac{3}{2}$, can be served at the CoI, even though the actual network-wide SP is set as $\frac{1}{1}$. *This means that a "virtual" cell-specific SP can be established depending on the network-wide SP and the DL CFRs.*

It is of interest to quantify the UL-to-DL ratios that a virtual SP can support, for a given network-wide SP and a given number of free resources at the CoI and its neighbouring cells. Let the number of CFRs be N, where N takes on values $n \in [0, C_{\mathrm{o}}]$, and C_{o} is the total number of resources per cell in DL. Since the SPs are synchronised across the network, C_{o} is the same for all cells. The problem of finding the distribution of N can be readily addressed by the binomial distribution. In particular, consider that having a CFR is a success, which occurs with probability p and not having such is a failure, which occurs with probability $1-p$. A success occurs when a given chunk is free at the centre cell and at the same time, at at least one of the neighbouring cells. A failure, on the other hand, occurs when a chunk is busy at the centre cell, *or* is free at the centre cell and at the same time is busy at all of the neighbouring cells. Thus, the distribution of the number of common free chunks, f_N, is a function of the resource occupancy probabilities at the CoI and at the first-tier cells. Resource occupancy probability is the probability that a chunk is occupied. The distribution of f_N is derived in this work is as follows:

$$f_N(n) = p(L_{\mathrm{c}}, L_{\mathrm{t},1}, \ldots, L_{\mathrm{t},B_{\mathrm{t}}}, B_{\mathrm{t}})^n \cdot [1 - p(L_{\mathrm{c}}, L_{\mathrm{t},1}, \ldots, L_{\mathrm{t},B_{\mathrm{t}}}, B_{\mathrm{t}})]^{C_{\mathrm{o}}-n} \cdot \binom{C_{\mathrm{o}}}{n}, \quad (5.1)$$

where B_t is the number of cooperating cells; $L_{\mathrm{t},i}$ is the probability that a resource is occupied at a first-tier cell i; L_c is the probability that a resource is occupied at the CoI; and $p(L_\mathrm{c}, L_{\mathrm{t},1}, \ldots, L_{\mathrm{t},B_\mathrm{t}}, B_\mathrm{t})$ is the probability of having a CFR and depending on the number of cooperating cells and the resource occupancy. The equation for $p(L_\mathrm{c}, L_{\mathrm{t},1}, \ldots, L_{\mathrm{t},B_\mathrm{t}}, B_\mathrm{t})$ is formulated in this work as follows:

$$p(L_\mathrm{c}, L_{\mathrm{t},1}, \ldots, L_{\mathrm{t},B_\mathrm{t}}, B_\mathrm{t}) = (1 - \prod_{i=1}^{B_\mathrm{t}} L_{\mathrm{t},i}) \cdot (1 - L_\mathrm{c}). \tag{5.2}$$

The expected value of the binomial distribution in (5.1) yields $E[N] = C_\mathrm{o} \cdot p$, hence the expected value of the number of CFRs as a fraction of the total number of DL resources is $\frac{E[N]}{C_\mathrm{o}} = p$.

Then at the CoI, the expected value of the fraction of resources in the frame which can be used for UL traffic including off-loading, R_ul, is:

$$R_\mathrm{ul} = \frac{\frac{n_\mathrm{UL}}{n_\mathrm{DL}+n_\mathrm{UL}} C_\mathrm{tot} + p\,\frac{n_\mathrm{DL}}{n_\mathrm{DL}+n_\mathrm{UL}} C_\mathrm{tot}}{C_\mathrm{tot}} \equiv \underbrace{\frac{n_\mathrm{UL}}{n_\mathrm{DL}+n_\mathrm{UL}}}_{\text{actual SP}} + \underbrace{p\,\frac{n_\mathrm{DL}}{n_\mathrm{UL}+n_\mathrm{DL}}}_{\text{virtual SP}}, \tag{5.3}$$

where n_UL and n_DL are the number of UL time slots per frame and DL time slots per frame, respectively, as per the network-wide SP; and C_tot is the total (UL+DL) chunks per frame. This means that at the CoI the virtual SP divides the frame in an UL-to-DL ratio of $(n_\mathrm{UL} + p\,n_\mathrm{DL}) : (n_\mathrm{DL} - p\,n_\mathrm{DL})$. It can be observed that when $p \to 0$, i.e. when there are no available resources for off-loading, then the resource allocation is according to the actual network-wide SP. When $p \to 1$, i.e. when all DL resources at the CoI can be used to off-load UL traffic, then $R_\mathrm{ul} \to 1$ and the whole frame can be allocated to UL. An illustration of the concept of the virtual SP is shown in Fig. 5.3. Note that, while the network-wide SP allocates resources on the time slot level, the virtual SP allocates resources on the chunk level. Smaller granularity in resource allocation actually means more flexibility and hence helps in more efficient resource utilisation, as will be later seen in this chapter. Fig. 5.4 shows a plot of $R_\mathrm{ul} \times 100\%$ depending on the actual SP, the number of cooperating BSs, and on the resource occupancies at the CoI and at the cooperating BSs.

In order to study the effect of the virtual SP a best-case and a worst-case scenario are considered. The number of cooperating BSs is one for the worst-case scenario and six for the best-case scenario. The resource occupancies in the case when all six cells can cooperate are kept the

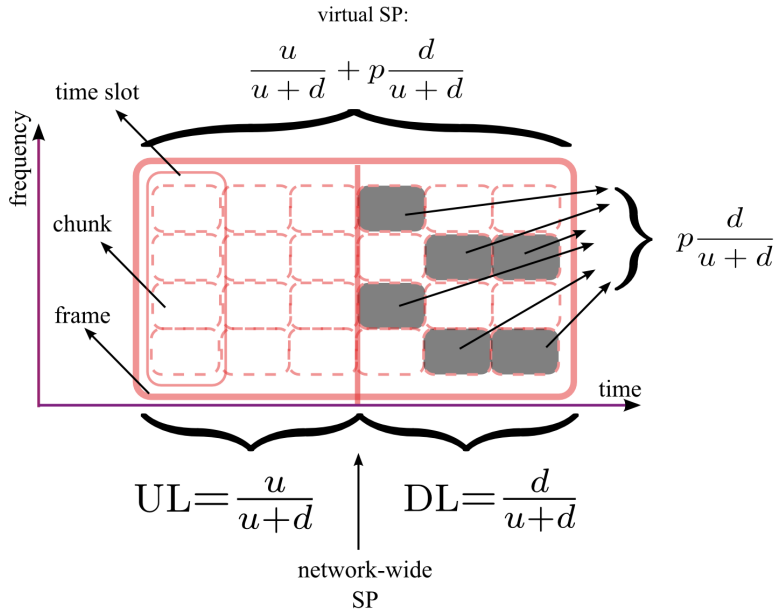

Figure 5.3: *The virtual SP allocates additional resources to UL as compared to the network-wide SP. Furthermore, the virtual SP allocates on the chunk level, unlike the network-wide SP which allocates on the time slot level.*

same ($L_{\mathrm{t},1} = L_{\mathrm{t},2} = \ldots = L_{\mathrm{t}}$), while when only one cell cooperates $L_{\mathrm{t},1} = L_{\mathrm{t},2} = \ldots = L_{\mathrm{t},5} = 1$ and $L_{\mathrm{t},6} = L_{\mathrm{t}}$. The values for L_{t} are varied as shown in Fig. 5.4. Overall, it can be observed that, as expected, when there are no free resources (L_{c} and/or L_{t} are one), the virtual SP is the same as the network-wide SP. Consequently, when there are free DL resources, the virtual SP exploits the resource availability to allocate additional resources to UL. Furthermore, when all DL resources at the CoI are free, the whole frame can be allocated to UL for low to moderate loads at the cooperating cells when six cells cooperate. Even in the case when only one cell cooperates the same effect can be achieved if L_{t}=0. As expected, when overall the DL resource occupancy increases, the number of resources allocated to UL by means of the virtual SP at the CoI decreases. In addition, when comparing the three plots in Fig. 5.4, it can be seen that for low loads at the CoI, the virtual SP is almost the same for different network-wide SPs. Overall, it is seen that asymmetry balancing offers flexibility in resource allocation and can adaptively allocate resources based on availability and potentially can give all the resources in a frame to one link direction.

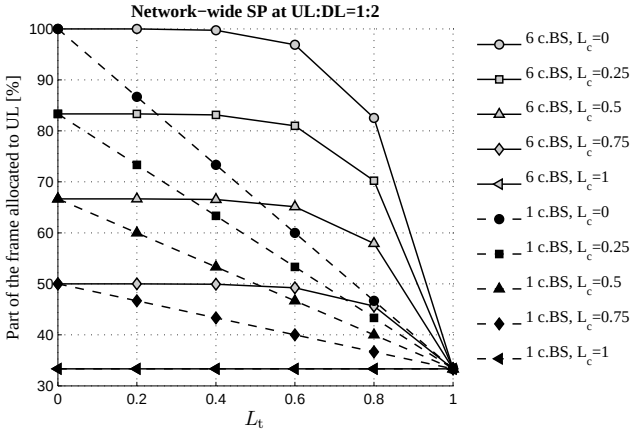

(a) The network-wide SP allocates 33% of the frame to UL (base line).

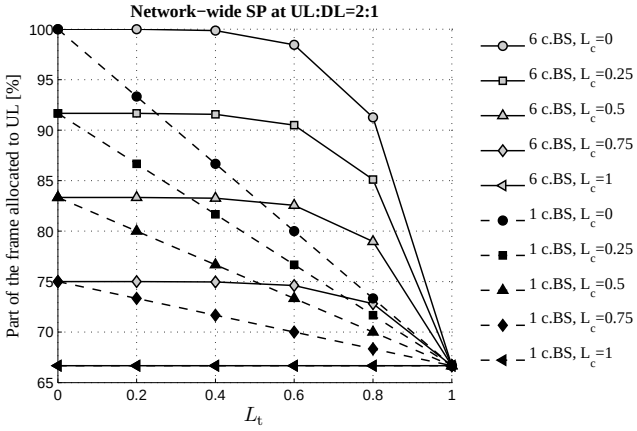

(b) The network-wide SP allocates 66% of the frame to UL (base line).

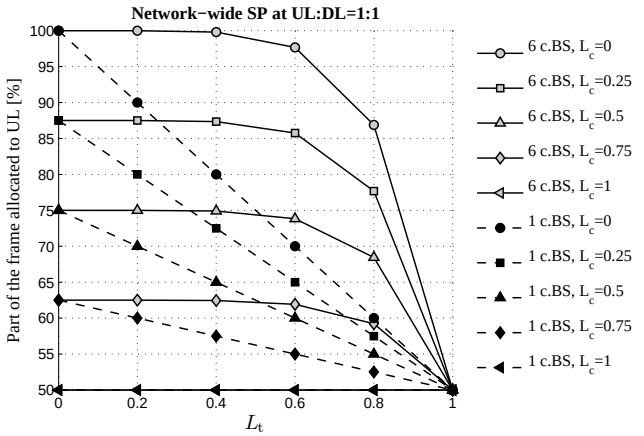

(c) The network-wide SP allocates 50% of the frame to UL (base line).

Figure 5.4: *The virtual SP allocates resources to UL, based on the actual network-wide SP, as well as on the resource demand at the CoI and its neighbouring cells. The number of cooperating BSs (c.BS) takes on values of 1 and 6.*

5.2.4 Relay station availability

The previous section determined the expected number of resources, which are available for off-loading and this section concentrates on the second enabler for asymmetry balancing, i.e. availability of RSs. Given that there is a CFR, the CFR can be utilised if RSs are available such that a two-hop path can be found from the MS, which needs to off-load traffic to the cooperating BS. In other words, the MS→RS *ad hoc* links are "opportunistic" in that they exploit CFRs and available RSs, and also are managed in a decentralised fashion. How to find a two-hop path is a matter of routing, and determining an optimum routing strategy is beyond the scope of this thesis. It is assumed here that future wireless networks will be equipped with multi-hop and relaying functionality in which case no significant additional signalling overhead is required for managing the MS→RS links.

In this study a simple path loss based routing scheme is implemented which is illustrated with the help of Fig. 5.5: $\mathrm{BS_{CoI}}$ faces shortage of UL resources and $\mathrm{MS_{OL}}$ needs to relay to $\mathrm{RS_c}$, which is associated with the cooperating $\mathrm{BS_c}$. Given that there is a CFR, $\mathrm{RS_c}$ is chosen as an RS during this CFR if two conditions, C_1 and C_2, are satisfied (not considering protection of on-going links):

$$\mathrm{C}_1\text{: } L_{\mathrm{p}}^{\mathrm{mb}} > L_{\mathrm{p}}^{\mathrm{mr}} + \Delta_1 \text{ [dB]}$$

$$\mathrm{C}_2\text{: } L_{\mathrm{p}}^{\mathrm{mb}} > L_{\mathrm{p}}^{\mathrm{br}} + \Delta_2 \text{ [dB]}$$

where $L_{\mathrm{p}}^{\mathrm{mb}}$ is the path loss between $\mathrm{BS_{CoI}}$ and $\mathrm{MS_{OL}}$; $L_{\mathrm{p}}^{\mathrm{mr}}$ is the path loss between $\mathrm{MS_{OL}}$ and $\mathrm{RS_c}$; $L_{\mathrm{p}}^{\mathrm{br}}$ is the path loss between $\mathrm{BS_c}$ and $\mathrm{RS_c}$; and Δ_1 and Δ_2 are path loss margins, which are further discussed later in this text. The two conditions above aim to ensure that the two-hop link $\mathrm{MS_{OL}} \rightarrow \mathrm{RS_c} \rightarrow \mathrm{BS_c}$ would be able to achieve better link capacity than the potential single hop $\mathrm{MS_{OL}} \rightarrow \mathrm{BS_{CoI}}$ link. $\mathrm{MS_{OL}}$ and $\mathrm{RS_c}$ attain information about $L_{\mathrm{p}}^{\mathrm{mb}}$ and $L_{\mathrm{p}}^{\mathrm{br}}$, respectively, via the pilot signals that BSs typically send. In addition, $L_{\mathrm{p}}^{\mathrm{mr}}$ can be calculated using the busy burst signalling technique described in [95, 96]. There a receiver transmits a time-multiplexed signal upon successful transmission to reserve a resource. In this study it is assumed that a time-multiplexed signal is transmitted by all receivers, which wish to reserve a particular resource. This busy burst signal can be used by the receiver to "advertise" its availability to serve as an RS by means of piggy-back signalling. In addition, essential information, such as $L_{\mathrm{p}}^{\mathrm{br}}$, can be readily obtained from the received busy burst signal at the $\mathrm{MS_{OL}}$ given that the busy burst

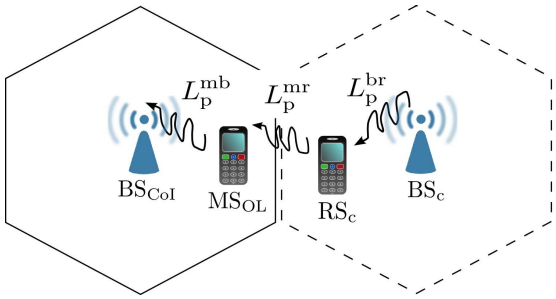

Figure 5.5: *$\mathrm{MS_{OL}}$ decides whether to off-load to $\mathrm{RS_c}$ or not based on a comparison of $L_{\mathrm{p}}^{\mathrm{mb}}$ with $L_{\mathrm{p}}^{\mathrm{mr}}$ and $L_{\mathrm{p}}^{\mathrm{mb}}$ with $L_{\mathrm{p}}^{\mathrm{br}}$.*

power emitted from the RS is constant. As a consequence, $\mathrm{MS_{OL}}$ is equipped to evaluate the routing conditions quoted above in a decentralised fashion and, hence, is enabled to find a suitable RS.

Considering the above, assume that a CFR is shared between the CoI and a number of first-tier cells, K_{t}. Then, the probability that the CFR will be utilised, p_{ucfr}, is the probability that at least one user at the CoI will be able to find at least one two-hop path that satisfies both C_1 and C_2. The probability p_{ucfr} can be expressed as given in:

$$p_{\mathrm{ucfr}} = 1 - (1 - \Pr\{\mathrm{C}_1 \cap \mathrm{C}_2\})^{U_{\mathrm{c}}^2 K_{\mathrm{t}}}, \tag{5.4}$$

where U_{c} is the number of users per cell; and $\Pr\{\mathrm{C}_1 \cap \mathrm{C}_2\}$ is the probability that both C_1 and C_2 are satisfied at the same time and can be determined using conditional probabilities as given in:

$$\Pr\{\mathrm{C}_1 \cap \mathrm{C}_2\} = \Pr\{\mathrm{C}_1 \mid \mathrm{C}_2\}\Pr\{\mathrm{C}_2\}, \tag{5.5}$$

where $\Pr\{\mathrm{C}_1 \mid \mathrm{C}_2\}$ and $\Pr\{\mathrm{C}_2\}$ are defined below:

$$\Pr\{\mathrm{C}_1 \mid \mathrm{C}_2\} = \Pr\{L_{\mathrm{p}}^{\mathrm{mr}} < L_{\mathrm{p}}^{\mathrm{mb}} - \Delta_1 \mid L_{\mathrm{p}}^{\mathrm{br}} < L_{\mathrm{p}}^{\mathrm{mb}} - \Delta_2\}, \tag{5.6}$$

$$\Pr\{\mathrm{C}_2\} = \Pr\{L_{\mathrm{p}}^{\mathrm{br}} < L_{\mathrm{p}}^{\mathrm{mb}} - \Delta_2\}. \tag{5.7}$$

The path losses are random variables and their distributions can be derived by approximating the hexagonal cell structure by a circular cell structure as shown in Appendix C. In particular, both $L_{\mathrm{p}}^{\mathrm{br}}$ and $L_{\mathrm{p}}^{\mathrm{mb}}$ are BS–MS path loss distributions which are identically distributed and their

pdf is approximated as follows (for the derivation please refer to Appendix C):

$$f_q(q) = \frac{2}{R^2 b} 10^{2\frac{q-a}{b}} \ln(10), \;\; q \leq a + b\log_{10}(z), \tag{5.8}$$

where R is the cell radius. Similarly, the MS-RS path loss distribution $L_{\mathrm{p}}^{\mathrm{mr}}$ is approximated by the following pdf (again, for the derivation please refer to Appendix C):

$$f_y(y) = \int_0^R f_y(y|z) f_z(z)\, dz, \tag{5.9}$$

where $f_z(z)$ is the distribution of the distances [96]:

$$f_z(z) = \frac{2\,z}{R^2}, \;\; z \leq R, \tag{5.10}$$

and $f_y(y|z)$ is path loss distribution for a given distance from the centre, z.

Based on the above, (5.6) can be further evaluated as follows:

$$\Pr\{L_{\mathrm{p}}^{\mathrm{mr}} < L_{\mathrm{p}}^{\mathrm{mb}} - \Delta_1 \mid L_{\mathrm{p}}^{\mathrm{br}} < L_{\mathrm{p}}^{\mathrm{mb}} - \Delta_2\} =$$

$$\int_{\forall m} \int_{\forall r}^{m-\Delta_2} F_y(m - \Delta_1) f_q(r) f_q(m) \mathrm{d}m\mathrm{d}r, \tag{5.11}$$

where m and r are dummy variables; $f_q(r)$ is given in (5.8); and $F_y(m)$ is the cumulative distribution function (cdf) according to the pdf in (5.9). The limits of the integration are determined by the cell dimensions and path loss models. In addition, (5.7) can be determined as :

$$\Pr\{L_{\mathrm{p}}^{\mathrm{br}} < L_{\mathrm{p}}^{\mathrm{mb}} - \Delta_2\} = \int_{\forall m} F_q(m - \Delta_2) f_q(m) \mathrm{d}m, \tag{5.12}$$

where $F_q(m)$ is the cdf that corresponds to the pdf in (5.8).

In order to obtain (5.4), (5.11) and (5.12) are numerically evaluated. For ease of computation, five users per cell are used and as an example, $\Delta_1 = \Delta_2 = 3\,\mathrm{dB}$. First of all, the value for $1 - \Pr\{\mathrm{C}_1 \cap \mathrm{C}_2\}$ is obtained. Via Monte Carlo simulation it can be found that $1 - \Pr\{\mathrm{C}_1 \cap \mathrm{C}_2\} \approx 0.99958$, while according to the circular approximation (i.e. numerical evaluation of (5.11) and (5.12)), $1 - \Pr\{\mathrm{C}_1 \cap \mathrm{C}_2\} \approx 0.99765$. Clearly, when using these findings in (5.4) to obtain p_{ucfr}, the discrepancy will increase exponentially with the power of $U_c^2 K_{\mathrm{t}}$. Hence, in order to verify the mathematical model presented, a semi-analytical approach is taken. Namely, the simulation result for $1 - \Pr\{\mathrm{C}_1 \cap \mathrm{C}_2\}$ is used and applied to the formula for p_{ucfr}. The model

# of coop BSs:	1	2	3	4	5	6
S-A:	0.010	0.021	0.031	0.041	0.051	0.061
sim.:	0.009	0.018	0.032	0.043	0.051	0.065

Table 5.1: *Probability p_{ucfr} that at least one two-hop link can be established for five users per cell and $\Delta_1 = \Delta_2 = 3$ dB.*

for p_{ucfr} is successfully verified by simulation and a comparison between semi-analytical and simulation results is shown in Table 5.1, denoted by S-A and sim., respectively. As expected, when the number of cooperating BSs increases, the probability that at least one two-hop link is found which satisfies both C_1 and C_2 increases. At this stage it is interesting to determine how many users per cell are required in order for a two-hop link to be always available, i.e. for p_{ucfr} to become one. It is important to point out here that both idle *and* active users can be RSs. Because the simulation result for $1 - \Pr\{\mathrm{C}_1 \cap \mathrm{C}_2\}$ is closer to one than the theoretical result, p_{ucfr} when obtained via simulation will converge slower. Even then, it can be easily calculated using (5.4) and $1 - \Pr\{\mathrm{C}_1 \cap \mathrm{C}_2\} \approx 0.99958$ that for 110 users per cell and just one cooperating cell, p_{ucfr} is 0.994. Clearly, when more than one cooperating cell is available, convergence to one is reached faster. For example, when six cells cooperate, p_{ucfr} is already 0.982 at $U_c = 40$. In fact, for all practical purposes, for more than 150 users per cell, p_{ucfr} is actually one. For a cell radius of 500 m, the cell area is 0.87 sq. km, which means about 170 users per sq. km. This is a reasonable number, as even suburban areas have at least 100 users per sq. km [97].

It is important to mention that the choice of Δ_1 and Δ_2 has a significant influence on the performance of asymmetry balancing. First of all, Δ_1 and Δ_2 influence how fast p_{ucfr} converges to one. For example, if Δ_1 is kept at 3 dB, but Δ_2 is increased to 5 dB, then according to simulation around 200 users per cell are necessary (240 users per sq. km) for p_{ucfr} to become one. In addition, Δ_1 and Δ_2 control the choice of off-loading MSs and serving RSs. As an example, Fig. 5.6(a) shows the distribution of the off-loading MSs and the serving RSs for $\Delta_1 = \Delta_2 =$3 dB (using the path loss models specified in Section 5.2.5), where the 3 dB value is chosen in analogy to the typical handover margin [18]. It can be seen that as intended, MSs at the cell edges off-load to better-placed MSs in terms of path loss (log-normal shadowing is not considered). Furthermore, as seen when comparing Fig. 5.6(a) with Fig. 5.6(b), increasing Δ_2 for a given Δ_1 will move the "belt" of RSs closer to their associated BSs. In contrast, increasing Δ_1 for a given Δ_2 will shrink both the "belt" of RSs and the "belt" of MSs, as can be seen when comparing Fig. 5.6(a) with Fig. 5.6(c). Multi-hop link optimisation strategies are

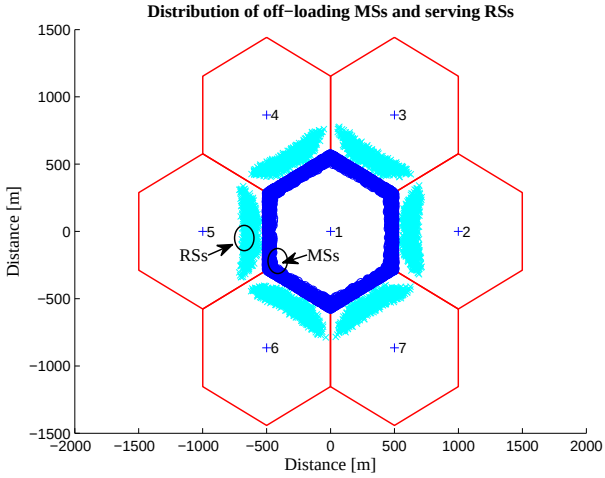

(a) $\Delta_1 = \Delta_2 = 3$ dB

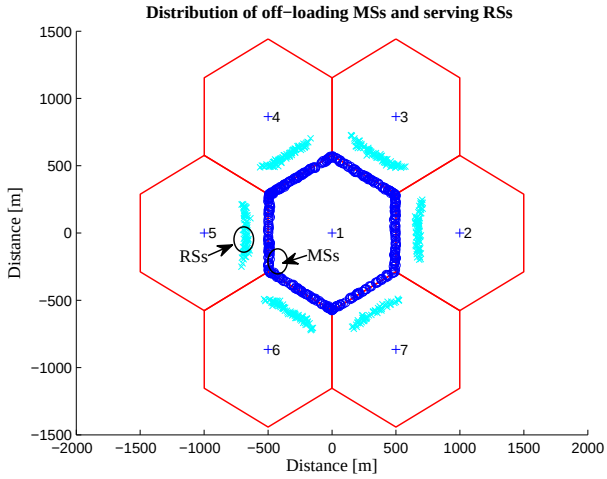

(b) $\Delta_1 = 3$ dB and $\Delta_2 = 6$ dB

presented in [98]. Because optimisation of Δ_1 and Δ_2 pertains to the particular routing strategy in place, it is not considered in this thesis and $\Delta_1 = \Delta_2 = 3$ dB is used.

It can be seen from the above that users at the cell-edges are most likely to use two-hop links. Hence, asymmetry balancing can be combined with "smart" resource allocation such that when a given BS faces overload, it gives priority to users, which are closer to the cell centre, thus encouraging users which are closer to the cell edges to use two-hop communication. "Smart" resource allocation for load balancing is beyond the scope of this thesis.

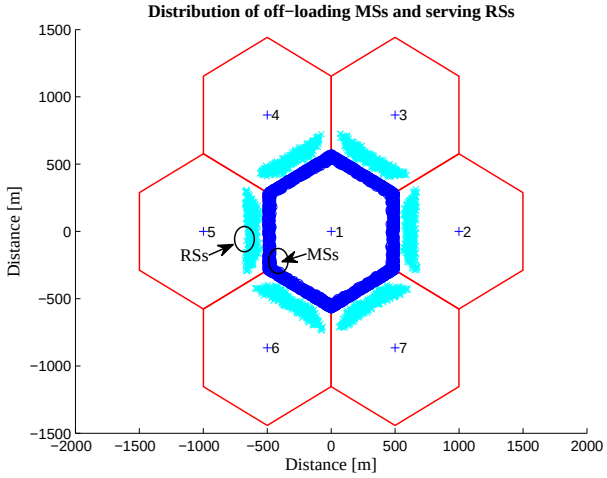

(c) Δ_1 =6 dB and Δ_2 =3 dB

Figure 5.6: *Adjusting Δ_1 and Δ_2 changes the distribution of off-loading MSs and serving RSs.*

5.2.5 Simulation model

A seven-cell OFDMA-TDD system (one cell at the centre and six surrounding cells) is used and simulated adopting a Monte Carlo approach. Note that the simulation platforms of the current study and of the study presented in Section 4.6 are the same. Hence, the simulation model and parameters are presented in Section 4.6.1, and the simulation parameters are repeated in Table 5.2 for convenience. It needs to be added that for the two-hop links utilised by asymmetry balancing, an SNR-based power control is applied at the first hop (MS→RS) as it is assumed that the off-loading links are opportunistic and interference information is not available. The SNR target is 25 dB (128 cross constellation at BER of 10^{-7} [61]). The link capacity is calculated as specified in Section 4.6.1.

It should be noted that in the case of ZD, each cell sets its TDD SP according to the user demand. When FSA and asymmetry balancing are employed, the UL↔DL SPs are synchronised across the cells allocating half of the resources to UL and DL each [13]. However, the model can readily be applied to any asymmetry ratio.

5.2.6 Results

This section presents numerical results comparing asymmetry balancing, ZD and FSA based on UL/DL resource allocation and spectral efficiency. The comparison begins with a discussion

Carrier frequency	5 GHz
Time slot duration	0.1152 ms
Number of time slots/ frame	6
Number of OFDM symbols/ time slot	5
Transmit power/ link	251 mW (24 dBm)
Shortest BS-BS distance	1 km
BS height	25 m
MS height	1.5 m
Path loss parameter a	MS–BS: 39.61 MS–MS: 32.49 BS–BS: 41.2
Path loss parameter b	MS–BS: 35.74 MS–MS: 43.75 BS–BS: 23.8

Table 5.2: *Fixed simulation parameters [52], [87]*

on the way these systems allocate resources to UL and DL and a verification of (5.3).

In Section 5.2.3 it was demonstrated that asymmetry balancing strongly depends on the resource availability both at the CoI and at the neighbouring cells. It is impossible to simulate all scenarios in terms of resource availability, hence two scenarios are defined: (1) a best case 6-cell scenario, where all six first-tier cells cooperate; and (2) a worst-case 1-cell scenario where only one first-tier cell cooperates. Different resource availability conditions are enforced by varying the total *user demand* per frame per cell (in %). In the formulae developed in the previous sections the *probability that a resource is occupied* was used rather than user demand. Considering the case of UL, the mathematical relation between the user demand, $\alpha_{\mathrm{u}}^{\mathrm{UL}}$, and the probability that a resource is occupied, $p_{\mathrm{o}}^{\mathrm{UL}}$, can be expressed as follows:

$$p_{\mathrm{o}}^{\mathrm{UL}} = \alpha_{\mathrm{u}}^{\mathrm{UL}} \cdot \frac{C_{\mathrm{tot}}}{M_{\mathrm{u}}}, \tag{5.13}$$

where M_u is the total number of chunks allocated to UL by the network-wide switching point. Note that for the case of DL, the probability that a resource is occupied can be obtained analogously to (5.13). As already mentioned in this chapter, when asymmetry balancing is employed, the synchronised SP is set to allocate half of the frame resources to UL and DL each. As a result, using (5.13) the probability that a resource is occupied at a particular link direction for a given cell, can be obtained by multiplying the respective user demand by 2. The DL resource occupancy probability both at the CoI and at the cooperating cells is varied from 0 to 0.8, which corresponds to a user demand that varies from 0% to 40%. In order to account for a worst case

scenario in terms of interference experienced by the *ad hoc* links, the non-cooperating cells are assumed to be fully loaded in DL (i.e. the demand is 50%). Because the UL resource demand of the first-tier cells would not influence the results for UL asymmetry balancing, it is kept constant for all considered scenarios. (Clearly, asymmetry balancing only works when the UL at the first-tier cells is not fully loaded.) The UL and DL resource demands are shown in Table 5.3.

The defined scenarios also aim to exhibit different interference conditions for the CoI when ZD is employed. Because each cell sets its SP according to the asymmetry demand at the given cell, the CoI has an UL-favoured SP in all cases. This means that the 6-cell scenario allows for the effect of increase in BS→BS interference (from non-existent to severe) on the performance of the UL at the CoI to be observed as the first-tier DL demand is systematically varied. The 1-cell scenario, on the other hand, exposes the CoI to persistent severe BS→BS interference due to the strongly DL-favoured first-tier traffic demand.

In terms of FSA, the defined resource demand scenarios aim to exhibit the performance of the system when one of the cells (the CoI) is overloaded. Due to the fact that the load per link direction per cell does not exceed 50%, all cells except the CoI are able to support the traffic demand even though the asymmetry per cell might vary.

Cell number → Link direction ↓	1 (CoI)	2	3	4	5	6	7
UL	100	15					
DL (6-cell)	0→40						
DL (1-cell)	0→40	50					

Table 5.3: *Resource demand for UL and DL (in %)*

Results for the UL-DL resource allocation at the CoI achieved with asymmetry balancing and ZD are shown in Fig. 5.7 in terms of the percentage of resources in a frame allocated to UL. For asymmetry balancing the theoretical results for $R_{\mathrm{ul}} \times 100\%$ are also shown and it can be observed that a perfect match between theory and simulation is obtained. Fig. 5.7 shows results for variable CoI DL demand and for variable first-tier DL demand. In the 6-cell scenario the demand is varied together for all six cells, whereas in the 1-cell scenario the demand is varied for only one of the six cells, while the rest have a constant demand of 50%. In the case of asymmetry balancing, as expected, when overall the DL resource occupancy increases, the number of resources allocated to UL by the virtual SP at the CoI decreases. It is interesting to

note that due to the six degrees of freedom, when six cells cooperate, the number of resources allocated to UL by the virtual SP decreases much slower with decrease in resource availability as compared to the case when only one cell cooperates, where the number of UL resources decreases linearly. On Fig. 5.7 it can be seen that asymmetry balancing offers flexibility in resource allocation in that it adaptively allocates resources based on availability. Whenever there is little or no CoI DL demand, the asymmetry balancing can allocate the whole frame to UL, even in the case when only one cell cooperates. In addition, asymmetry balancing actually allocates resources on the chunk level, while ZD is limited to allocating resources to UL and DL on the time slot level according to the network design. A further limitation to ZD is that the maximum asymmetry which can be supported is 5:1 in favour of either link direction [52] (as seen on Fig. 5.7). Note that, as mentioned in the previous chapter, this limitation is a network parameter and if the network permits for the whole frame to be allocated to a single link direction, then the curve of ZD in the 6-cell scenario of 0% DL load at the CoI would be flat at 100%.

Fig. 5.7 also shows that for moderate loads (both at the CoI and at the first-tier cells) the resource allocation achieved with asymmetry balancing (6-cell scenario) and ZD is similar, while for higher loads (1-cell scenario), in most cases ZD allocates more resources to UL than asymmetry balancing. This can be explained by the fact that ZD adapts its SP to the resource demand at the CoI, independently of the first-tier resource demand. In contrast, the virtual SP is limited by the resource availability at the first-tier cells. However, as the subsequent spectral efficiency results demonstrate, the scheme that allocates more resources to UL does not necessarily achieve higher UL spectral efficiency.

The spectral efficiency performance of the UL asymmetry balancing scheme is compared against that of ZD and FSA, based on (5.14), which is obtained by modifying (4.9) to accommodate the contribution of off-loading links:

$$\overline{C}_{\mathrm{b}} = \frac{1}{C_{\mathrm{tot}}} \left(\sum_{k=1}^{M_u} \overline{C}_k + \frac{\overline{M}_{\mathrm{OL}}}{M_{\mathrm{OL}}} \sum_{j=1}^{M_{\mathrm{OL}}} \log_2(1+\gamma_j^{\mathrm{mh}}) \right), \tag{5.14}$$

where $\overline{C}_{\mathrm{b}}$ is the average spectral efficiency per chunk in bps/Hz; $\overline{C}_k$ is the chunk spectral efficiency as defined in (4.8); $\overline{M}_{\mathrm{OL}}$, is the number of DL chunks available for off-loading;

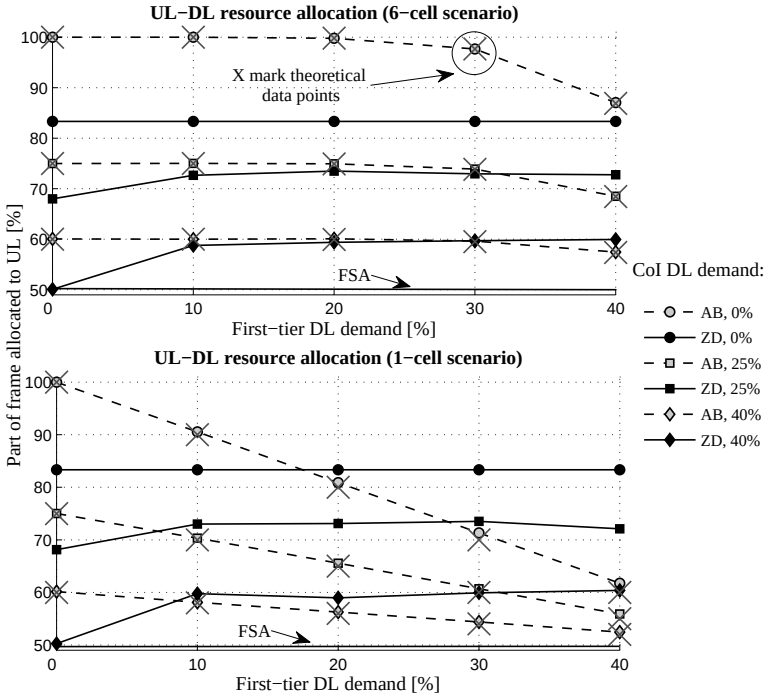

Figure 5.7: *Fraction of the resources per frame allocated to UL at the CoI.*

M_{OL} is the number of chunks actually utilised for off-loading defined in:

$$\overline{M}_{\mathrm{OL}} = p\frac{n_{\mathrm{DL}}}{n_{\mathrm{DL}} + n_{\mathrm{UL}}}C_{\mathrm{tot}}; \tag{5.15}$$

and γ_j^{mh} is the SINR of chunk j for two-hop links. Clearly, for systems which do not employ asymmetry balancing, $p = 0$, which means that the second term of the summation in (5.14) produces a zero. In other words, the second summation accounts for the spectral efficiency contribution of *ad hoc* links and can be non-zero only when *ad hoc* communication is present. In addition, it should be noted that γ_j^{mh} is taken as the minimum of the SINR achieved at the first and second hops for each two-hop link. Furthermore, $\frac{\overline{M}_{\mathrm{OL}}}{M_{\mathrm{OL}}}$ is used as a correction factor. (It should be noted that M_{OL} is obtained via simulation.) The reason is as follows: As previously mentioned, due to simulation complexity, only twenty users per cell are simulated. As a result, not all available CFRs can be utilised for off-loading via a neighbouring RS. The number of available CFRs is only influenced by the actual load, i.e. fraction of available resources, which is independent of the number of users in the system. In contrast, how many of the available CFRs can be utilised for MS→RS links depends on user density (active and non-active users alike) because user density determines if and how often a two-hop path can be found. As a consequence, the spectral efficiency results are also influenced by the number of users in

the system. Because, as was demonstrated in Section 5.2.4, it can be safely assumed that in realistic scenarios all available CFRs can be actually utilised, the correction factor aims to obtain representative spectral efficiency performance. Both $\overline{M}_{\mathrm{OL}}$ and M_{OL} are shown in Fig. 5.8. As expected, $\overline{M}_{\mathrm{OL}}$ is always greater than M_{OL}. Note that the latter is obtained via simulation, whilst the former is obtained according to (5.15).

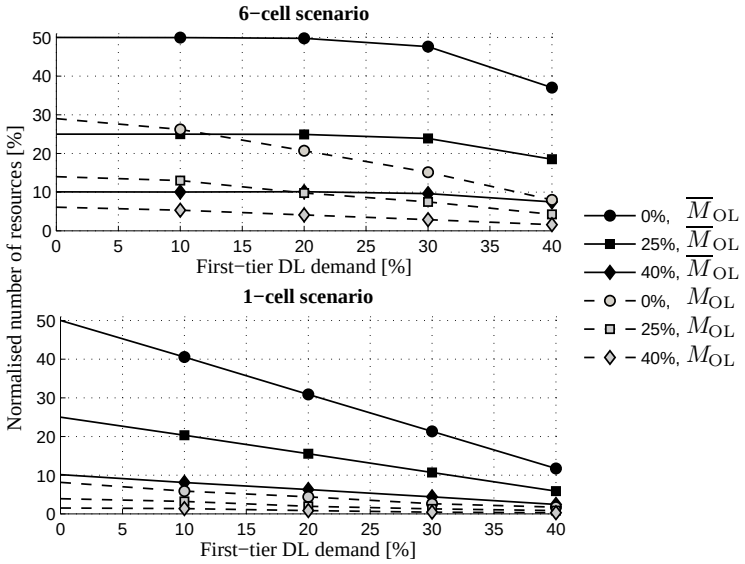

Figure 5.8: *Percentage of the resources per frame available for relaying ($\overline{M}_{\mathrm{OL}}$) and percentage of the resources per frame utilised for relaying (M_{OL}) assuming 20 users per cell.*

The CoI UL spectral efficiency results for different DL resource demands are presented in Fig. 5.9 (top plot and bottom plot for the 6-cell scenario and 1-cell scenario, respectively).

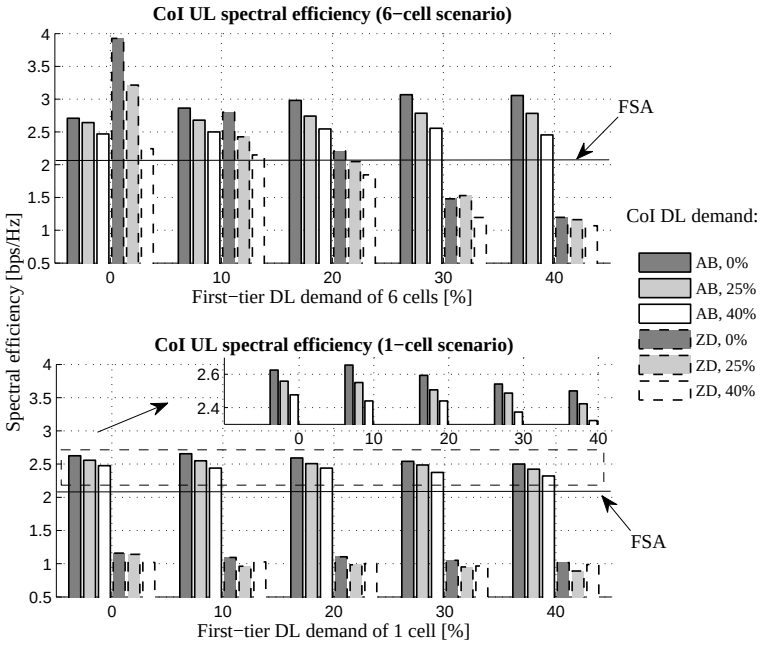

Figure 5.9: *UL spectral efficiency attained at the CoI with asymmetry balancing (AB), ZD, and FSA. The spectral efficiency of asymmetry balancing and ZD is plotted by bars, while the spectral efficiency of the FSA system is denoted by a solid line.*

The solid line at about 2 bps/Hz shows the spectral efficiency achieved by the FSA system. It can generally be observed that when severe BS→BS interference is present (i.e. high first-tier DL demand) such as is the case in the 1-cell scenario and 6-cell scenario for more than 20% DL demand, simply synchronising the TDD SP thereby avoiding the BS→BS results in a significant spectral efficiency improvement. Furthermore, asymmetry balancing attains spectral efficiency amelioration of more than 100% with respect to the spectral efficiency achieved by ZD. ZD outperforms asymmetry balancing only in the case of 0% DL demand in the 6-cell scenario, i.e. when none of the six first-tier cells has DL traffic, which is a highly unlikely situation. In addition, it is noted that in the 1-cell scenario the performance of ZD is relatively constant. This is due to the fact that five cells already cause BS→BS interference, and one additional interfering BS does not produce significant difference in the results. With respect to the asymmetry balancing performance, it can be seen that in the 6-cell scenario, even though there is a slight decrease in the number of resources utilised for asymmetry balancing as the first-tier DL demand increases (Fig. 5.7), the spectral efficiency performance at the CoI actually improves (Fig. 5.9 top plot). This effect can be attributed to the limited transmit power. When

slightly fewer resources are used for transmission, there is more power available per resource and the attained SINR can compensate for the fact that less resources are utilised. A similar trend is observed in the 1-cell scenario (Fig. 5.9 bottom plot, zoomed area), but to a smaller extent because the difference in the number of resources utilised for asymmetry balancing for the varied first-tier DL demand is much greater (Fig. 5.7).

The demonstrated UL spectral efficiency amelioration attained by asymmetry balancing is at a slight loss in spectral efficiency for the first-tier DL transmission as compared to an FSA system. The loss is due to the off-loading *ad hoc* links, which generate MS→MS interference to the concurrent BS→MS links. The results presented in Fig. 5.10 show that overall the loss in spectral efficiency does not surpass 0.6%. It can be observed, that even though the results for the 1-cell scenario and the 6-cell scenario are similar, the loss in the case of six cooperating cells is slightly larger due to the fact that more resources are used for the off-loading *ad hoc* links and, hence, more interference is caused to the first-tier DL transmission. Furthermore, the caused loss decreases with increase in the DL demand (both at the CoI and first-tier cells), as expected, because less resources are used for off-loading. It should be noted that the spectral efficiency loss obtained for twenty users per cell is representative even for larger number of users for the studied scenarios, because the maximum number of active users at a given time slot using a given chunk does not change and is equal to the number of cells under consideration.

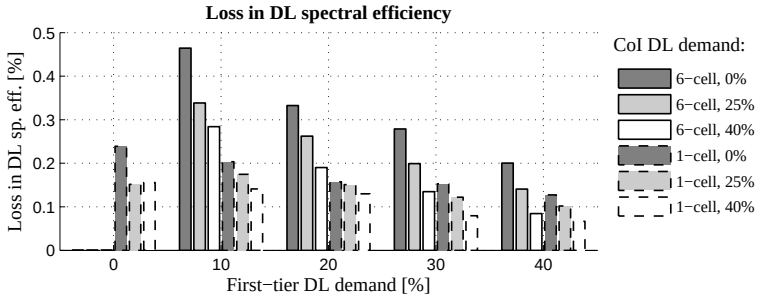

Figure 5.10: *Percentage loss in DL spectral efficiency caused by the off-loading ad hoc links when asymmetry balancing (AB) is employed as compared to an equivalent FSA system.*

The DL spectral efficiency results for asymmetry balancing and ZD are shown in Fig. 5.11. As expected, in the 6-cell scenario asymmetry balancing and ZD attain similar performance, except for in the case of 0% DL demand at the first-tier cells. The results are analogous to

what was discussed in Section 4.6 as asymmetry balancing and the FSA attain almost identical performance (refer to Fig. 5.10). It is interesting to note that in the 1-cell scenario ZD achieves slightly better DL spectral efficiency than asymmetry balancing for DL first-tier demand greater or equal to 10%. This is because the DL at the CoI does not experience any crossed slots and the dynamic SP of ZD is able to accommodate any CoI DL demand greater than 50%, unlike the asymmetry balancing. At first-tier DL demand of 0%, however, asymmetry balancing attains slightly better spectral efficiency than ZD due to the presence of crossed slots caused by the single first-tier cell that has UL-favoured SP.

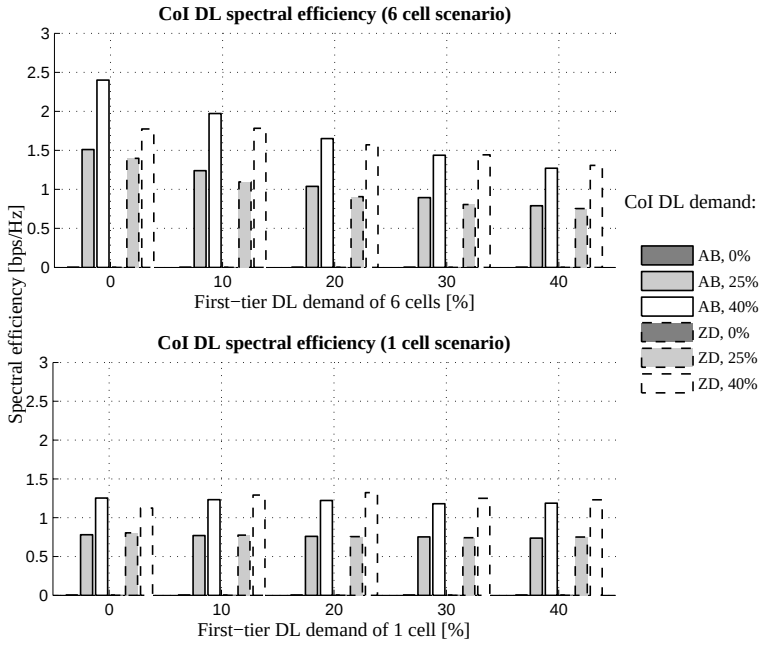

Figure 5.11: *DL spectral efficiency performance comparison between asymmetry balancing (AB) and ZD.*

In order to complete the analysis of the asymmetry balancing scheme, it is important to consider what happens when there are no available resources for off-loading. To this end, a fully loaded system is studied (i.e. the total UL and DL demands add up to 100% for each cell), where each cell has a different traffic asymmetry demand, as shown in Table 5.4. For the CoI two scenarios are defined – UL-favoured and DL-favoured. The first-tier cells all have different asymmetry demands, which range from highly UL-favoured to highly DL-favoured *in order to explore the crossed-slots effects on the CoI*. On average three of the first-tier cells require an UL-favoured SP, while the other three require a DL-favoured SP. Two systems are compared, *viz*: an FSA

Cell number → Link direction ↓	1 (CoI)	2	3	4	5	6	7
UL	15 90	90	75	60	45	30	15
DL	85 10	10	25	40	55	70	85

Table 5.4: *Resource demand for UL and DL (in %)*

system, as the asymmetry balancing system becomes an FSA system in the situation of full network load; and ZD. Results for the UL and DL spectral efficiency at the CoI are presented in Fig. 5.12 (top plot and bottom plot, respectively). When UL spectral efficiency is considered (top plot), it is observed that when the demand at the CoI is UL-favoured and crossed slots are present, by avoiding crossed slots the FSA system actually achieves about 1.6 times better spectral efficiency at the median than the ZD system. As expected, when the demand at the CoI is DL-favoured, the UL spectral efficiency at the CoI is almost the same for a ZD system and an FSA system. This is because the UL demand can be accommodated by both the ZD and the FSA. However, the FSA system performs slightly better due to the fact that the occasional crossed slots which occur in the case of the ZD system result in BS→BS interference for the CoI. When considering the DL spectral efficiency at the CoI (bottom plot), for low DL demand (i.e UL-favoured demand), the ZD system and the FSA system again attain similar performance, with the FSA system exhibiting slightly better results. However, when the DL demand at the CoI is increased (DL-favoured demand), the ZD system manages to provide about 1.2 times better spectral efficiency at the median than the FSA system (referring to the bottom plot of Fig. 5.12).

Overall, the results for the fully-loaded network show that in the case of DL-favoured asymmetries ZD performs better in terms of DL spectral efficiency than the FSA system, while in the case of UL-favoured asymmetries the FSA system exhibits better results for UL spectral efficiency than ZD. The reason for this effect is that DL spectral efficiency suffers less when crossed slots are present as MS→MS interference is not as detrimental in OFDMA-TDD systems with full frequency reuse as BS→BS interference. This is because in order to have high MS→MS interference two MSs need to be using the same chunks at the same time in very close proximity to each other. In contrast, BS positions are fixed and the whole bandwidth is reused in each cell, which means that the total impact of CCI on system performance is much greater. The results demonstrate that FSA does not always work when the system is fully loaded. This

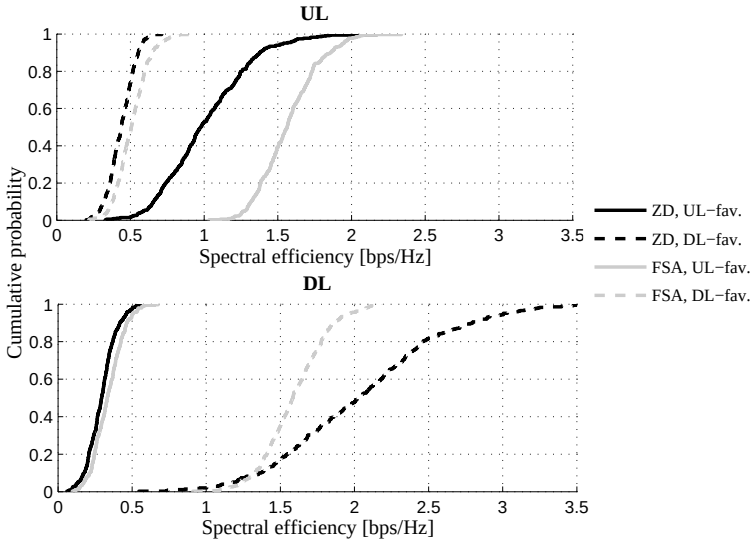

Figure 5.12: *Spectral efficiency performance comparison between FSA and ZD under the assumption of a fully loaded network.*

is expected because if the different cells have different asymmetry demands, a synchronised SP is not able to efficiently meet the demands of individual cells. However, as was demonstrated by Fig. 5.9, when the system is not overloaded, FSA is able to perform much better than ZD and, in addition, asymmetry balancing significantly outperforms both FSA and ZD.

The results presented in this section demonstrate that allowing each cell to set its SP independently leads to suboptimum results in the majority of cases, while synchronising the SP across cells improves spectral efficiency performance significantly. Employing asymmetry balancing, i.e. keeping a network-wide SP and making use of inter-cell relaying, ameliorates the attained spectral efficiency even further. It is expected that optimising the routing strategy will result in even better system performance.

5.3 Summary

In this chapter, a novel method named *asymmetry balancing* has been proposed. It allows the support of cell-independent asymmetries in OFDMA-TDD next generation networks with complete avoidance of the detrimental BS→BS interference. The key to solving this issue is user cooperation in combination with inter-cell relaying. A general mathematical framework for the assessment of the proposed technique has been developed.

It has been demonstrated that in the case of shortage of UL resources a virtual cell-specific SP can be established, depending on the system UL-to-DL asymmetry ratio and the available DL resources at the CoI and its six neighbouring cells. When one or more cells can cooperate, even the whole frame can be virtually allocated for UL traffic. This flexibility in resource allocation comes at a relatively insignificant cost of less than 0.6% loss in DL spectral efficiency incurred due to interference caused by the relaying. Furthermore, it is found that the asymmetry balancing technique significantly outperforms conventional approaches where the TDD SPs are synchronised system-wide as well as ZD. For the UL spectral efficiency of the CoI, the maximum gains with respect to the case of fixed SPs are up to about 50%, whereas the maximum gains with respect to ZD surpass 100%. As expected, BS→BS interference avoidance leads to tremendous spectral efficiency improvement. In addition, it has been demonstrated that when the system is fully loaded, the loss from allowing BS→BS interference can be bigger than the loss which results from not meeting DL demand by synchronising the TDD SP cell-wide.

Chapter 6
Conclusions, limitations, and scope for future research

6.1 Conclusions

The focus of this thesis was the same-entity interference problem (and in particular, BS→BS interference) in OFDMA-TDD-based cellular networks. It was demonstrated that current interference mitigation approaches do not work well when LOS conditions among BSs are present. In particular, it was found that FSA achieves up to about 80% better spectral efficiency than RTSO. Furthermore, FSA achieved up to about 100% improvement in spectral efficiency as compared to ZD. While FSA was demonstrated to perform well in terms of avoiding BS→BS interference, the scheme does not allow for cell-specific asymmetry demands to be supported in the network.

In light of the above findings, this thesis presented a novel *cooperative* resource balancing technique, termed *asymmetry balancing*. Asymmetry balancing completely avoids crossed slots and retains the advantages of TDD in allowing for cell-specific asymmetry demands via the novel *virtual SP* concept. The thesis demonstrated that asymmetry balancing always outperforms FSA and achieves more than 100% higher spectral efficiency with respect to ZD. This gain in performance comes at a relatively insignificant cost of less than 0.6% loss in DL spectral efficiency incurred due to interference caused by the *ad hoc* links. In addition, it was demonstrated that when the system is fully loaded, the loss from allowing BS→BS interference can be bigger than the loss which results from not meeting DL demand by synchronising the TDD SP cell-wide. Hence, the novel interference avoidance approach presented in this thesis is a very promising candidate to solve the crossed slot problem in next-generation OFDMA-TDD-based cellular networks.

6.2 Limitations and scope for future research

The work in this thesis offered insight into the severity of the BS→BS interference problem in OFDMA-TDD-based cellular networks and presented a novel approach to resolving this problem. However, certain assumptions that have been made in this work leave room for further worthwhile investigations.

Firstly, the OTA-SRR algorithm is centralised and requires global channel knowledge to operate. Such channel knowledge is not available in practice. Different, more decentralised algorithms are necessary, especially in light of future trends which focus on distributed networks. In addition, the chosen resource allocation algorithm surely has effect on system performance, therefore, this is another reason to explore different resource allocation schemes. However, it should be pointed out that the study on RTSO seeks to expose trends rather than study a particular resource allocation algorithm. The trends achieved with OTA-SRR have been confirmed in [49, 69] via a comparison with the trends achieved with the resource allocation scheme greedy rate packing (GRP).

Furthermore, the asymmetry balancing method was only investigated based on an UL study. It is important to analogously investigate DL asymmetry balancing as there are key differences between UL asymmetry balancing and DL asymmetry balancing. As an example, DL asymmetry balancing relies on BS→BS communication. Such issues need to considered, as well as their implementation specifics.

Another interesting and important point to consider is extending the asymmetry balancing study to more than seven cells. While it was an adequate choice to study a centre cell and six surrounding cells when noting that each cell can offload traffic to its immediate neighbours only, more cells are needed to test an entire system. To this end it also worth looking into DL asymmetry balancing, which follows directly from the demonstrated UL asymmetry balancing concept.

Furthermore, it is worthwhile to investigate different means for choosing an RS and utilising more than two hops per transmission. This study considered only one possible routing strategy where MSs decide to which RS to transmit based on the respective MS-RS path loss and two parameters, Δ_1 and Δ_2. It is important to investigate the effect of Δ_1 and Δ_2 on the performance of asymmetry balancing. Furthermore, it is interesting to study asymmetry balancing with other routing strategies and find the routing strategy that results in the best system performance. In

addition, this study limited the number of hops per transmission to two. An interesting point is to research the effect of the number of hops and whether it is beneficial to off-load not only to immediate neighbouring cells, but also to second-tier cells. This, however, would require a different system model and mathematical analysis. In regard to the number of utilised hops, it is also important to investigate the delay performance of asymmetry balancing and how it is affected by the number of hops.

Another worthwhile investigation would be to include shadowing in the mathematical formulation and system model for asymmetry balancing to make the model more complete and realistic. It is expected that shadowing will have a positive effect on the results as mobiles which are otherwise far away from their respective RS would be able to benefit from good shadowing conditions and actually achieve better data rates than if shadowing were not considered.

An additional interesting point worth investigating is the resource allocation method when employing asymmetry balancing. The resource allocation method should be considered jointly with the RS selection scheme. This is due to the fact that the choice of a resource for transmission is influenced by the channel, which in turn is influenced by the position of the transmitter relative to the receiver. Clearly, the resource allocation in systems which employ asymmetry balancing will induce some overhead as compared to resource allocation in SCNs. In fact, the overall signalling overhead incurred by the asymmetry balancing method and the implementation specifics have not yet been investigated and both of these issues are important and need to be considered before asymmetry balancing can be applied in practice.

Moreover, it would be worthwile to investigate the “smart” resource allocation concept briefly mentioned at the end of Section 5.2.4. The principle of “smart” resource allocation is to allocate resources to users based on their locations when employing asymmetry balancing. In particular, as users at the cell edges are more likely to find suitable RSs, priority to be served in a single-hop fashion can be given to users closer to the cell centre. In this way cell-edge users are encouraged to use two-hop (or multi-hop) links. It is envisaged that such “smart” resource allocation will further improve the capacity performance of asymmetry balancing.

Finally, it should be pointed out that there are alternatives to the chosen SINR-data rate mapping. For example, instead of using the mapping in [61], Shannon’s capacity multiplied by a factor could be used. Clearly, the chosen mapping has an effect on the achieved capacities, however, the focus in the studies presented in this thesis has been on comparative performances

(FSA against RTSO and ZD) and the comparative performance is not expected to change when the SINR-capacity mapping is changed. However, when the systems are analysed to attain specific independent performance results, then different mapping schemes are worthy of investigation.

Appendix A
Modified Dirichlet function derivation

This Appendix presents a derivation of the modified Dirichlet function used in Section 3.3.1, which accounts for the dependence of the interference contribution from subcarrier k' to subcarrier k on the $|k' - k|$.

Based on the IFFT and FFT operations, the received modulation symbol on subcarrier k (without noise), $\mathcal{R}_k$, can be written as:

$$\mathcal{R}_k = \frac{1}{N_\mathrm{c}} \sum_{i=0}^{N_\mathrm{c}-1} \left[\sum_{k'=0}^{N_\mathrm{c}-1} H_{i,k'} S_{k'} \exp\left(\frac{j2\pi i k'}{N_\mathrm{c}}\right) \right] \exp\left(\frac{-j2\pi i k}{N_\mathrm{c}}\right), \tag{A.1}$$

where N_c is the FFT size; $H_{i,k}$ is the channel transfer function of subcarrier k; S'_k is the transmit symbol on subcarrier k'; and j is the imaginary unit. If one contributing propagation path is assumed, the channel transfer function can be expressed as:

$$\begin{aligned} H_{i,k'} &= \exp(j\phi) \exp\left(\frac{j2\pi i(\varepsilon_\mathrm{D} + \omega)}{N_\mathrm{c}}\right) \exp\left(\frac{-j2\pi k' \varepsilon_\tau}{N_\mathrm{c}}\right) \\ &= H_{k'} \exp\left(\frac{j2\pi i(\varepsilon_\mathrm{D} + \omega)}{N_\mathrm{c}}\right), \end{aligned} \tag{A.2}$$

where ϕ is the phase; ε_D is the normalised Doppler shift; ω is the the normalised frequency offset due to synchronisation errors; and ε_τ is the relative propagation delay. After substituting (A.2) into (A.1) and reordering:

$$\begin{aligned} \mathcal{R}_k &= \frac{1}{N_\mathrm{c}} \sum_{i=0}^{N_\mathrm{c}-1} \sum_{k'=0}^{N_\mathrm{c}-1} H_{k'} \exp\left(\frac{j2\pi i(\varepsilon_\mathrm{D} + \omega)}{N_\mathrm{c}}\right) S_{k'} \exp\left(\frac{j2\pi i(k' - k)}{N_\mathrm{c}}\right) \\ &= \frac{1}{N_\mathrm{c}} \sum_{k'=0}^{N_\mathrm{c}-1} H_{k'} S_{k'} \underbrace{\left[\sum_{i=0}^{N_\mathrm{c}-1} \exp\left(\frac{j2\pi i(k' - k + \varepsilon_\mathrm{D} + \omega)}{N_\mathrm{c}}\right) \right]}_{\text{geometric series}}. \end{aligned} \tag{A.3}$$

The geometric series in (A.3) can be simplified. If $\frac{2\pi(k'-k+\varepsilon_\mathrm{D}+\omega)}{N_\mathrm{c}} = \beta$, the geometric series

representation yields:

$$\begin{aligned}\sum_{k=0}^{N_{\mathrm{c}}-1}\exp(j\beta k) &= \frac{1-\exp(j\beta N_{\mathrm{c}})}{1-\exp(j\beta)} \\ &= \exp\left(\frac{j(N_{\mathrm{c}}-1)\beta}{2}\right)\frac{\sin(\frac{N_{\mathrm{c}}\beta}{2})}{\sin(\frac{\beta}{2})}. \end{aligned} \tag{A.4}$$

Using the result from (A.4), the cyclic-sinc function $C_{k,k'}(k'-k+\varepsilon_{\mathrm{D}}+\omega)$ can be derived as:

$$C_{k,k'}(k'-k+\varepsilon_{\mathrm{D}}+\omega) = \frac{1}{N_{\mathrm{c}}}\frac{\sin(\pi(k'-k+\varepsilon_{\mathrm{D}}+\omega))}{\sin(\frac{\pi(k'-k+\varepsilon_{\mathrm{D}}+\omega)}{N_{\mathrm{c}}})}\exp\left(\frac{j\pi(k'-k+\varepsilon_{\mathrm{D}}+\omega)(N_{\mathrm{c}}-1)}{N_{\mathrm{c}}}\right), \tag{A.5}$$

such that (A.3) becomes:

$$\mathcal{R}_k = \sum_{k'=0}^{N_{\mathrm{c}}-1} H_{k'}S_{k'}C_{k,k'}(k'-k+\varepsilon_{\mathrm{D}}+\omega). \tag{A.6}$$

The received symbol in (A.6) includes both an interference component and a useful component and can be written in terms of desired signal power and interference power as:

$$\begin{aligned}\mathcal{R}_k &= \underbrace{\sum_{k'=0,\ k'\neq k}^{N_{\mathrm{c}}-1}|H_{k,k'}|^2P_{k'}G_{k,k'}|C_{k,k'}(k'-k+\varepsilon_{\mathrm{D}}+\omega)|^2}_{\text{interference}} \\ &\quad + \underbrace{|H_k|^2P_kG_k|C_{k,k}(k-k+\varepsilon_{\mathrm{D}}+\omega)|^2}_{\text{useful signal}}\ [W]. \end{aligned} \tag{A.7}$$

It should be noted that Doppler offset and frequency synchronisation errors in the desired signal are not considered as perfect synchronisation is assumed, hence the argument of $|C_{k,k}(k-k+\varepsilon_{\mathrm{D}}+\omega)|^2$ is 0. Using (A.5) and noting that for small α, $\sin(\alpha)\approx\alpha$, it can be shown that as the argument of $|C_{k,k}(k-k+\varepsilon_{\mathrm{D}}+\omega)|^2$ goes to 0, $|C_{k,k}(k-k+\varepsilon_{\mathrm{D}}+\omega)|^2$ goes to 1. Hence, the useful (desired) signal power per subcarrier R_k is expressed as:

$$R_k = P_kG_k|H_k|^2\ [W]. \tag{A.8}$$

Appendix B
OTA constraints and convergence

This Appendix briefly reviews the OTA constraints and the convergence issues pertaining to the OTA-SRR algorithm [73]. More detailed treatment can be found in [73].

The conditions for convergence of the system equation (4.4) are outlined below:

$$\begin{aligned} (\mathbf{I}-\mathbf{\Phi})^{-1} &= \mathbf{I}+\mathbf{\Phi}+\mathbf{\Phi}^2+\ldots \\ (\mathbf{I}+\mathbf{\Phi}+\mathbf{\Phi}^2+\ldots)\mathbf{x} &= (1+\lambda+\lambda^2+\ldots)\mathbf{x}, \end{aligned} \tag{B.1}$$

where $\mathbf{I}$ is the identity matrix; $\mathbf{\Phi}$ is the normalised link gain matrix; and $\mathbf{x}$ is the eigenvector corresponding to the eigenvalue λ of $\mathbf{\Phi}$. The series in (B.1) converges if and only if $\lambda < 1$ and this holds for any eigenvalue of $\mathbf{\Phi}$. Thus, (4.4) has a solution, when $\lambda_1 < 1$.

In order to determine a feasible set of transmit powers, let $\mathbf{P_1}$ be the eigenvector corresponding to $(1-\lambda_1)$, the eigenvalue of $(\mathbf{I}-\mathbf{\Phi})$. Then the system (4.4) becomes:

$$(1-\lambda_1)\mathbf{P_1} \geq \boldsymbol{\eta},$$

where $\boldsymbol{\eta}$ is the normalised noise vector. Equation (B.2) is equivalent to

$$\mathbf{P_1} \geq \frac{\boldsymbol{\eta}}{1-\lambda_1}. \tag{B.2}$$

If $\mathbf{P}_{\max}$ is the vector of maximum transmit powers, $\mathbf{P_1}$ must satisfy the following:

$$\mathbf{P_1} \leq \mathbf{P}_{\max}. \tag{B.3}$$

Thus, based on (B.2) and (B.3), it follows that:

$$\mathbf{P}_{\max} \geq \frac{\boldsymbol{\eta}}{1-\lambda_1}, \tag{B.4}$$

with $0 \leq \lambda_1 \leq 1$. The system constraint can now be expressed by rearranging (B.4) as:

$$1 - \lambda_1 \geq \max_{i \in N_{\text{tot}}} \left\{ \frac{\eta_i}{\overline{p}} \right\}. \tag{B.5}$$

Appendix C
Derivation of the pdf of MS–RS path losses

This chapter presents the derivation of the path loss distribution between MSs and RSs, used in Chapter 5.

In order to determine the BS–MS and MS–RS path loss distributions the cell geometry is approximated by circular geometry (Fig. C.1). The CoI is a circle with radius R and the RSs are outside this circle and within a circle with radius $3R$ (due to the hexagonal cell geometry).

Referring to the small circle, the BS–MS path loss distribution can be approximated using the distribution of the distances between the centre of the circle and any point inside the circle as shown in [99]. In summary, assuming uniformly distributed points along the horizontal and vertical axes, this distribution of the distances, $f_z(z)$, is given in [96]:

$$f_z(z) = \frac{2z}{R^2}, \;\; z \leq R. \tag{C.1}$$

The respective path loss, Q is of the form: $Q = a + b\log_{10}(Z)$, hence using variable transformation [100], the pdf of Q can be obtained as:

$$f_q(q) = \frac{2}{R^2 b} 10^{2\frac{q-a}{b}} \ln(10), \;\; q \leq a + b\log_{10}(z). \tag{C.2}$$

Next, in order to determine the MS–RS path loss distribution, the problem can be formulated as finding the distribution of the distances between any point in the small circle to any point in the ring. Then, variable transformation can be used to find the distribution of the path losses.

Given that a transmitter is z [m] from the circle centre, the pdf, $f_x(x|z)$, of the MS-RS separa-

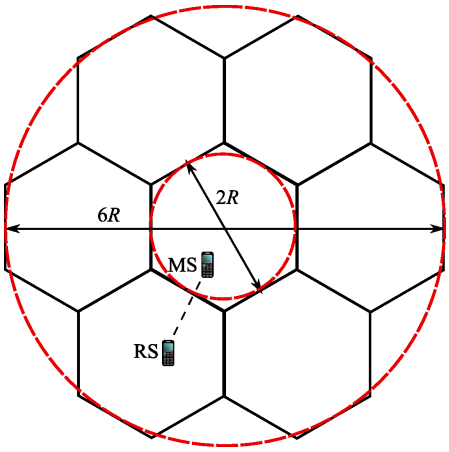

Figure C.1: *Hexagonal cell geometry, approximated by circular geometry.*

tion distances, X, is derived in this thesis as:

$$f_x(x|z) = \begin{cases} \frac{1}{\pi 4R^2}\left(\pi - \arccos(\frac{z^2+x^2-R^2}{2zx})\right)x, & R-z \leq x < R+z \\ \frac{1}{4R^2}x, & R+z \leq x \leq 3R-z \\ \frac{1}{\pi 4R^2}\arccos(\frac{z^2+x^2-(3R)^2}{2zx})x & 3R-z < x \leq 3R+z. \end{cases} \tag{C.3}$$

The next step is to convert the MS–RS distance distribution to path loss distribution. The path loss model used is of the form $Y = a + b\log_{10}(X)$, hence $X = 10^{\frac{Y-a}{b}}$. The path loss distribution for a given distance from the centre, z, is derived as:

$$\begin{aligned} f_y(y|z) &= f_x(x(y)|z)\left|\frac{\mathrm{d}x(y)}{\mathrm{d}y}\right| \\ &= \begin{cases} f_{x,1} = \frac{D}{\pi 4R^2}\left(\pi - \arccos(\frac{z^2+10^{2\frac{y-a}{b}}-R^2}{2z10^{\frac{y-a}{b}}})\right)10^{\frac{y-a}{b}}, & R-z \leq 10^{\frac{y-a}{b}} < R+z \\ f_{x,2} = \frac{D}{4R^2}10^{\frac{y-a}{b}}, & R+z \leq 10^{\frac{y-a}{b}} \leq 3R-z \\ f_{x,3} = \frac{D}{\pi 4R^2}\arccos(\frac{z^2+10^{2\frac{y-a}{b}}-(3R)^2}{2z10^{\frac{y-a}{b}}})10^{\frac{y-a}{b}}, & 3R-z < 10^{\frac{y-a}{b}} \leq 3R+z. \end{cases} \end{aligned} \tag{C.4}$$

where $D = \frac{1}{b}10^{\frac{y-a}{b}}\ln(10)$.

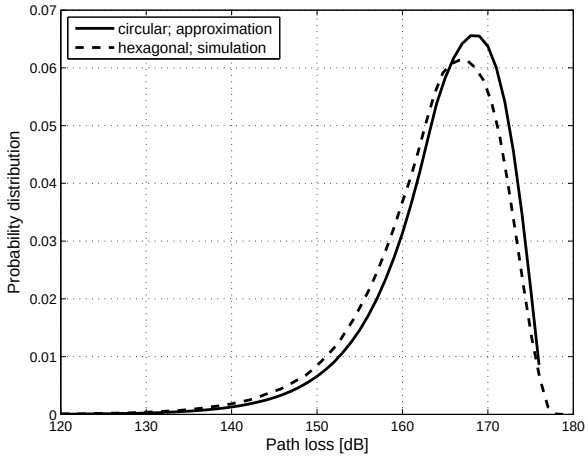

Figure C.2: *Pdf of the MS–RS path losses*

Using (C.1), $f_y(y)$ is derived as (function arguments omitted for clarity):

$$
\begin{aligned}
f_y(y) &= \int_0^R f_y(y|z) f_z(z)\, dz \\
&= \begin{cases}
\displaystyle\int_{R-x}^{R} f_{x,1} f_z\, dz,\ x \in [0,R] + \int_{x-R}^{R} f_{x,1} f_z\, dz,\ x \in [R,2R] \\
\displaystyle\int_{0}^{x-R} f_{x,2} f_z\, dz,\ x \in [R,2R] + \int_{0}^{3R-x} f_{x,2} f_z\, dz,\ x \in [2R,3R] \\
\displaystyle\int_{3R-x}^{R} f_{x,3} f_z\, dz,\ x \in [2R,3R] + \int_{x-3R}^{R} f_{x,3} f_z\, dz,\ x \in [3R,4R].
\end{cases}
\end{aligned}
\tag{C.5}
$$

The above equations are evaluated numerically and compared to a simple Monte Carlo simulation for verification. The results are shown in Fig. C.2. The following simulation parameters (WINNER [87]) are used: R is 500 m, a is 32.49 dB and b is 43.75 dB. In the system model in this study, hexagonal cells are used. Thus, in order to verify that the circular geometry is a good approximation to the hexagonal geometry, simulation results for the path loss distribution in the case of hexagonal geometry are provided for comparison.

Appendix D
Publications

Publications included in this thesis

E. Foutekova, P. Agyapong, and H. Haas, "Channel Asymmetry in Cellular OFDMA-TDD Networks," *EURASIP Journal on Wireless Communications and Networking (JWCN)*, vol. 2008, Article ID 121546, 14 pages, 2008.

E. Foutekova, S. Sinanovic, and H. Haas, "Traffic Asymmetry Balancing in OFDMA-TDD Cellular Networks," *Journal of Communications and Networking (JCN), Special Issue on Wireless Cooperative Transmission and its Applications*, June 2008, Vol. 10, No. 2, pages 137 – 147.

E. Foutekova, S. Sinanovic, and H. Haas, "Asymmetry Balancing in OFDMA-TDD Cellular Networks," *In Proc. of the Symposium on Personal, Indoor and Mobile Radio Communications (PIMRC)*, (Cannes, France), IEEE, Sept. 15-18, 2008.

E. Foutekova, S. Sinanovic, and H. Haas, "Asymmetry Balancing for Channel Asymmetry Support in OFDMA-TDD Cellular Networks," *In Proc. of IEEE International Vehicular Technology Conference (VTC)*, (Calgary, Canada), IEEE, Sept. 21-24, 2008.

A. C. Wook, K. E. Sun, E. Foutekova, H. Haas, and S. McLaughlin, "System and Method for Data Balancing," *European Patent KR20080084455 (A)*, Sept. 19, 2008.

E. Foutekova, P. Agyapong, and H. Haas, "Channel Asymmetry and Random Time Slot Hopping in OFDMA-TDD Cellular Networks," *In Proc. of the International Vehicular Technology Conference (VTC)*, (Marina Bay, Singapore), IEEE, May 11-14, 2008.

E. Foutekova, C. Evers, and H. Haas, "Semi-Analytical Model of Interference in CDMA-TDD Using Random Time Slot Hopping," *In Proc. of the International Vehicular Technology Conference (VTC)*, (Montréal, Canada), IEEE, Sept. 25-28, 2006.

References

[1] H. Haas and S. McLaughlin, eds., *Next Generation Mobile Access Technologies: Implementing TDD*. Cambridge University Press, ISBN: 13:9780521826228, Jan. 2008.

[2] H. Holma, G. J. R. Povey, and A. Toskala, "Evaluation of Interference Between Uplink and Downlink in UTRA/TDD," in *Proc. of the Vehicular Technology Conference (VTC)*, vol. 5, (Amsterdam, The Netherlands), pp. 2616–2620, IEEE, Sept. 19–22, 1999.

[3] ITU-R, "Framework and Overall Objectives of the Future Development of IMT-2000 and Systems Beyond IMT-2000," Tech. Rep. ITU-R M.1645, ITU, Retrieved Jan. 12, 2009 from http://www.itu.int/rec/R-REC-M.1645/e, 2003.

[4] Motorola Inc., "Long Term Evolution (LTE): A Technical Overview," white paper, Motorola Inc., Retrieved Jan. 12, 2009, from business.motorola.com/experiencelte/pdf/LTETechnicalOverview.pdf, 2007.

[5] E. Seidel, "Progress on "LTE Advanced" – the New 4G Standard," newsletter, NOMOR, Münich, Germany, July 24, 2008.

[6] L. Le and E. Hossain, "Multihop Cellular Networks: Potential Gains, Research Challenges, and a Resource Allocation Framework," *IEEE Communications Magazine*, vol. 45, pp. 66–73, Sept. 2007.

[7] IST-4-027756 WINNER II, "D3.5.3 v1.0 Final Assessment of Relaying Concepts for All CGs Scenarios Under Consideration of Related WINNER L1 and L2 Protocol Functions." Retrieved Oct. 12, 2008, from https://www.ist-winner.org/WINNER2-Deliverables/, Sept. 2007.

[8] F. Ali, B. Awoyemi, and T. Brown, "Delivering on the Promise of WiMAX: A White Paper from WireIE's Office of the CTO." Retrieved Oct. 12, 2008, from http://www.wireie.com/pdfs/wimax_white_paper_ver%202%205.pdf, Oct. 12 2007.

[9] WiMAX Forum, "Mobile WiMAX – Part I: A Technical Overview and Performance Evaluation." Retrieved Sept. 30, 2008, from www.wimaxforum.org/news/downloads/, Aug. 2006.

[10] ETSI Special Mobile Group (SMG), "Requirements for the UMTS Terrestrial Radio Access (UTRA) system." TR 101 111 V3.0.1, Nov. 1997.

[11] H. Yin and S. Alamouti, "OFDMA: A Broadband Wireless Access Technology," in *Proc. of the Sarnoff Symposium*, (Princeton, NJ, USA), pp. 1–4, IEEE, Mar. 27–28, 2006.

[12] IST-2003-507581 WINNER, "D2.5 v1.1 Duplex Arrangements for Future Broadband Radio Interfaces." Retrieved Dec. 12, 2007, from http://www.ist-winner.org/deliverables_older.html, Oct. 2004.

[13] IST-4-027756 WINNER II, "D6.13.7, WINNER II Test Scenarios and Calibration Cases Issue 2." Retrieved Mar. 15, 2007, from https://www.ist-winner.org/WINNER2-Deliverables/.

[14] H. Haas, P. K. Jain, and B. Wegmann, "Capacity Improvement Through Random Timeslot Opposing (RTO) Algorithm in Cellular TDD Systems with Asymmetric Channel Utilisation," in *Proc. of the International Symposium on Personal, Indoor and Mobile Radio Communications (PIMRC)*, vol. 2, (Beijing, China), pp. 1790–1794, IEEE, Sept. 7–10 2003.

[15] S.-H. Wie and D.-H. Cho, "Time Slot Allocation Scheme Based on a Region Division in CDMA/TDD Systems," in *Proc. of the Vehicular Technology Conference (VTC)*, (Rhodes, Greece), pp. 2445–2449, May 6–9 2001.

[16] V. Ricquebourg, D. Menga, D. Durand, B. Marhic, L. Delahoche, and C. Loge, "The Smart Home Concept : Our Immediate Future," in *Proc. of the International Conference on E-Learning in Industrial Electronics (ICELIE)*, (Hammamet, Tunisia), pp. 23–28, IEEE, Dec. 18–20, 2006.

[17] K. Feher, *Wireless Digital Communications*. Prentice Hall, ISBN: 8120314727, Seventh Indian Reprint, 2003 ed., 1995.

[18] T. S. Rappaport, *Wireless Communications: Principles and Practice*. Prentice Hall, ISBN: 0130422320, 2 ed., Dec. 2001.

[19] GSM World, "History: Brief History of GSM & the GSMA." Retrieved Mar. 2008, from http://www.gsmworld.com/about-us/history.htm.

[20] V. K. Garg and J. E. Wilkes, *Wireless and Personal Communications Systems*. Prentice Hall, ISBN: 0132346265, 1996.

[21] CDMA Development Group (CDG), "3G CDMA2000," Retrieved June 15, 2008, from http://www.cdg.org/technology/3g.asp.

[22] S. Y. Hui and K. H. Yeung, "Challenges in the Migration to 4G Mobile Systems," vol. 41, pp. 54–59, Dec. 2003.

[23] 3GPP, "LTE-Advanced," Retrieved Jan. 9, 2009, from http://www.3gpp.org/article/lte-advanced.

[24] Motorola Inc., "The Drivers to LTE," solution paper, Motorola Inc., Retrieved Jan. 12, 2009, from http://www.motorola.com, 2007.

[25] P. Laine, C. Boscher, D. Boettle, and L. Feijt, "WiMAX, Making Ubiquitous High-speed Data Services a Reality," white paper, Alcatel, June 2004.

[26] J. Gozalvez, "WiMAX Recognized as an IMT-2000 3G Technology," vol. 2, pp. 53–59, Dec. 2007.

[27] J.-P. Rissen, "Mapping the Wireless Technology Migration Path: The Evolution to 4G Systems," tech. rep., Alcatel-Lucent, Retrieved Aug. 24, 2009, from http://www.alcatel-lucent.com/enrich/v2i12008/article_c4a4.html, 2008.

[28] D. Grace, J. Chen, T. Jiang, and P. Mitchell, "Using Cognitive Radio to Deliver Green Communications," in *Proc. of the 4th International Conference on Cognitive Radio Oriented Wireless Networks and Communications (CROWNCOM)*, (Hannover, Germany), pp. 1 –6, IEEE, June 22-24, 2009.

[29] 3rd Generation Partnership Project (3GPP), Technical Specification Group Radio Access Network, "Evolved Universal Terrestrial Radio Access (E-UTRA); Physical Channels and Modulation (Release 8)." 3GPP TS 36.211 V8.2.0, Mar. 2008.

[30] IST-4-027756 WINNER II, "D6.11.4, Final WINNER II System Requirements." Retrieved Nov. 30, 2007, from https://www.ist-winner.org/WINNER2-Deliverables/, June 2007.

[31] G. J. R. Povey and M. Nakagawa, "A Review of Time Division Duplex-CDMA Techniques," in *Proc. of the International Symposium on Spread Spectrum Techniques and Applications (ISSSTA)*, vol. 2, (Sun City, South Africa), pp. 630–633, IEEE, Sept. 2–4, 1998.

[32] Airspan, "TDD and FDD Wireless Access Systems," tech. rep., 2007. Retrieved Oct. 2008, from http://www.airspan.com/pdfs/whitepaper_AIR0095_WP_2.pdf.

[33] J. Li, S. Farahvash, M. Kavehrad, and R. Valenzuela, "Dynamic TDD and Fixed Cellular Networks," *IEEE Communications Letters*, vol. 4, pp. 218–220, July 2000.

[34] G. J. R. Povey, "Time Division Duplex-Code Division Multiple Access for Mobile Multimedia Services," in *Proc. of the International Symposium on Personal, Indoor and Mobile Radio Communications (PIMRC)*, vol. 3, (Helsinki, Finland), pp. 1034–1037, IEEE, Sept. 1–4, 1997.

[35] 3rd Generation Partnership Project (3GPP), Technical Specification Group Radio Access Network, "Application and Consideration of TDD Mode." 3GPP TSG RAN WG1 R1-051380, Nov. 7 – 11, 2005.

[36] G. J. R. Povey, "Investigation of Multiple Access Interference within UTRA-TDD," in *Proc. of the European Signal Processing Conference (EUSIPCO)*, (Tampere, Finland), EURASIP, Sept. 4–8, 2000.

[37] K. S. Gilhousen, I. M. Jacobs, R. Padovani, A. J. Viterbi, L. A. J. Weaver, and C. E. I. Wheatley, "On The Capacity of a Cellular CDMA System," *IEEE Transactions on Vehicular Technology*, vol. 40, pp. 303–312, May 1991.

[38] A. J. Viterbi, "Wireless Digital Communication: A View Based on Three Lessons Learned," *IEEE Communications Magazine*, vol. 29, pp. 33–36, Sept. 1991.

[39] UMTS World, "3G and UMTS Technology," Retrieved June 15, 2008 from http://www.umtsworld.com/technology/technology.htm.

[40] J. A. C. Bingham, "Multicarrier Modulation for Data Transmission: an Idea Whose Time Has Come," *IEEE Communications Magazine*, vol. 28, pp. 5–14, May 1990.

[41] J. Heiskala and J. Terry, *OFDM Wireless LANs: A Theoretical and Practical Guide*. Sams Publishing, ISBN: 0672321572, 2002.

[42] S. Weinstein and P. Ebert, "Data Transmission by Frequency-Division Multiplexing Using the Discrete Fourier Transform," *IEEE Transactions on Communication Technology*, vol. 19, pp. 628–634, Oct. 1971.

[43] H. Sari, G. Karam, and I. Jeanclaude, "Transmission Techniques for Digital Terrestrial TV Broadcasting," *IEEE Communications Magazine*, vol. 33, pp. 100–109, Feb. 1995.

[44] M. Speth, S. A. Fechtel, G. Fock, and H. Meyr, "Optimum Receiver Design for Wireless Broad-Band Systems Using OFDM– Part I," *IEEE Transactions on Wireless Communications*, vol. 47, no. 11, pp. 1668 – 1677, 1999.

[45] H. Rohling and R. Grünheid, "Performance Comparison of Different Multiple Access Schemes for the Downlink of an OFDM Communication System," in *Proc. of the Vehicular Technology Conference (VTC)*, vol. 3, (Phoenix, AZ), pp. 1365–1369, IEEE, May 4–7, 1997.

[46] K. Doppler, X. He, C. Wijting, and A. Sorri, "Adaptive Soft Reuse for Relay Enhanced Cells," in *Proc. of the Vehicular Technology Conference (VTC)*, (Dublin, Ireland), pp. 758–762, IEEE, Apr. 22 – 25, 2007.

[47] M. Ahmed and S. Mahmoud, "Soft Capacity Analysis of TDMA Systems with Slow-Frequency Hopping and Multiple-Beam Smart Antennas," *IEEE Transactions On Vehicular Technology*, vol. 51, pp. 636–647, July 2002.

[48] R. Kohno, "Spatial and Temporal Filtering for Co-channel Interference in CDMA," in *Proc. of the International Symposium on Spread Spectrum Techniques and Applications (ISSSTA)*, vol. 1, (Oulu, Finland), pp. 51–60, IEEE, July 4–6, 1994.

[49] E. Foutekova, P. Agyapong, and H. Haas, "Channel Asymmetry in Cellular OFDMA-TDD Networks," *EURASIP Journal on Wireless Communications and Networking (JWCN)*, no. Article ID 121546, p. 14 pages, 2008.

[50] G. Li and H. Liu, "Downlink Dynamic Resource Allocation for Multi-cell OFDMA System," in *Proc. of the Vehicular Technology Conference (VTC)*, (Florida, USA), pp. 1698–1702, IEEE, Oct. 4–9, 2003.

[51] C.-H. Yih and E. Geraniotis, "Adaptive Modulation, Power Allocation and Control for OFDM Wireless Networks," in *Proc. of the International Symposium on Personal, Indoor and Mobile Radio Communications (PIMRC)*, vol. 2, (London, UK), pp. 809–813, IEEE, Sept. 18 – 21 2000.

[52] IST-2003-507581 WINNER, "D2.10, Final Report on Identified RI Key Technologies, System Concepts and Their Assessment." Retrieved Mar. 15, 2007, from https://www.ist-winner.org/DeliverableDocuments/, Dec. 2005.

[53] S. Chaudhury, H. Venkataraman, and H. Haas, "Uplink Capacity Comparison of Non-Perfect Frequency Synchronised Cellular OFDM Systems," in *Proc. of International Wireless Communications and Mobile Computing Conference (IWCMC)*, (Vancouver, Canada), July 3–6 2006.

[54] C. Shannon, "A Mathematical Theory of Communication," *Bell System Technical Journal*, vol. 27, pp. 379–423 & 623–656, July – Oct. 1948.

[55] K. Hassan and H. Haas, "User Scheduling for Cellular Multi User Access OFDM System Using Opportunistic Beamforming," in *Proc. of the 10th International OFDM Workshop InOWo'05*, (Hamburg, Germany), pp. 26–30, Aug. 31 – Sept. 1, 2005.

[56] T. Keller and L. Hanzo, "Adaptive Modulation Techniques for Duplex OFDM Transmission," *IEEE Transactions on Vehicular Technology*, vol. 49, pp. 1893–1906, Sept. 2000.

[57] A. Goldsmith, *Wireless Communications*. Cambridge University Press, 2005.

[58] F.-C. Cheng and J. Holtzman, "Wireless Intelligent ATM Network and Protocol Design for Future Personal Communication Systems," *IEEE Journal on Selected Areas in Communications*, vol. 15, no. 7, pp. 1289–1307, 1997.

[59] B. Choi and L. Hanzo, "Optimum Mode-Switching-Assisted Constant-Power Single- and Multicarrier Adaptive Modulation," *IEEE Transactions on Vehicular Technology*, vol. 52, pp. 536–560, May 2003.

[60] T. Hunter and A. Nosratinia, "Cooperation Diversity Through Coding," in *Proc. of the International Symposium on Information Theory (ISIT)*, (Lausanne, Switzerland), p. 220, IEEE, June 30 – July 5, 2002.

[61] K. Hole, H. Holm, and G. Øien, "Adaptive Multidimensional Coded Modulation Over Flat Fading Channels," *IEEE Journal on Selected Areas in Communications*, vol. 18, pp. 1153–1158, July 2000.

[62] W. Webb, L. Hanzo, and R. Steele, "Bandwidth-efficient QAM Schemes for Rayleigh Fading Channels," in *Proc. of the Fifth International Conference on Radio Receivers and Associated Systems*, pp. 139–142, July 23–27, 1990.

[63] J. Forney, G., R. Gallager, G. Lang, F. Longstaff, and S. Qureshi, "Efficient Modulation for Band-Limited Channels," *IEEE Journal on Selected Areas in Communications*, vol. 2, pp. 632–647, Sept. 1984.

[64] J. Zander, "Radio Resource Management – An Overview," in *Proc. of the Vehicular Technology Conference (VTC)*, vol. 1, (Atlanta, GA, USA), pp. 16–20, IEEE, Apr. 28–May 1, 1996.

[65] J. Zander, "Performance of Optimum Transmitter Power Control in Cellular Radio Systems," *IEEE Transactions on Vehicular Technology*, vol. 41, pp. 57–62, Feb. 1992.

[66] L. Yan, Z. Wenan, and S. Junde, "An Adaptive Subcarrier, Bit and Power Allocation Algorithm for Multicell OFDM Systems," in *Proc. of the Canadian Conference on Electrical and Computer Engineering (CCECE)*, vol. 3, (Montreal, Canada), pp. 1531–1534, IEEE, May 4–7, 2003.

[67] A. Behzad and I. Rubin, "On the Performance of Graph-based Scheduling Algorithms for Packet Radio Networks," in *Proc. of Global Communications Conference (GLOBECOM)*, (San Francisco, USA), pp. 3432–3436, IEEE, Dec. 1–5, 2003.

[68] E. Foutekova, P. Agyapong, B. Ghimire, H. Venkataraman, and H. Haas, "Scheduling in Cellular TDD-CDMA Networks," in *Proc. of the Vehicular Technology Conference (VTC)*, (Montréal, Canada), pp. 1–5, IEEE, Sept. 25–28, 2006.

[69] E. Foutekova, P. Agyapong, and H. Haas, "Channel Asymmetry and Random Time Slot Hopping in OFDMA-TDD Cellular Networks," in *Proc. of the Vehicular Technology Conference (VTC)*, (Marina Bay, Singapore), pp. 5 pages on CD–ROM, IEEE, May 11–14, 2008.

[70] E. Foutekova, S. Sinanović, and H. Haas, "Asymmetry Balancing in OFDMA-TDD Cellular Networks," in *Proc. of the International Symposium on Personal, Indoor and Mobile Radio Communications (PIMRC)*, (Cannes, France), IEEE, Sept. 15–18, 2008.

[71] E. Foutekova, C. Evers, and H. Haas, "Semi-Analytical Derivation of Interference in TDD-CDMA Systems Employing Random Time Slot Hopping (RTSH)," in *Proc. of the Vehicular Technology Conference (VTC)*, (Montréal, Canada), pp. 1–5, IEEE, Sept. 25–28, 2006.

[72] J. Zander and S.-L. Kim, *Radio Resource Management for Wireless Networks*. Artech House, ISBN: 1580531466, 2001.

[73] S. Ginde, "A Game-theoretic Analysis of Link Adaptation in Cellular Radio Networks," Master's thesis, Virginica Polytechnic Institute and State University, May 2004.

[74] Ericsson, "Long Term Evolution (LTE): An Introduction," white paper 284 23-3124 Uen, Ericsson, Retrieved Feb. 19, 2009, from www.ericsson.com/technology/whitepapers,Oct. 2007.

[75] Motorola Inc., "Driving 4G: WiMAX & LTE," positioning paper, Motorola Inc., Retrieved Feb. 19, 2009, from http://www.motorola.com, 2007.

[76] 3rd Generation Partnership Project (3GPP), Technical Specification Group Radio Access Network, "Soft Frequency Reuse Scheme for UTRAN LTE." 3GPP TSG RAN WG1 R1-050507, May 9–13, 2005.

[77] 3rd Generation Partnership Project (3GPP), Technical Specification Group Radio Access Network, "Further Analysis of Soft Frequency Reuse Scheme." 3GPP TSG RAN WG1 R1-050841, Aug. 2 – Sept. 29, 2005.

[78] S. Geirhofer and O. Oyman, "Client-centric Fractional Frequency Reuse Based on User Cooperation in OFDMA Networks," in *Proc. of the Annual Conference on Information Sciences and Systems (CISS)*, (Princeton, NJ, USA), pp. 95–100, IEEE, Mar. 19–21, 2008.

[79] H. Lei, L. Zhang, X. Zhang, and D. Yang, "A Novel Multi-Cell OFDMA System Structure Using Fractional Frequency Reuse," in *Proc. of the International Symposium on Personal, Indoor and Mobile Radio Communications (PIMRC)*, (Athens, Greece), pp. 1–5, IEEE, Sept. 3–7, 2007.

[80] B. Fan, Y. Qian, K. Zheng, and W. Wang, "A Dynamic Resource Allocation Scheme Based on Soft Frequency Reuse for OFDMA Systems," in *Proc. of the International*

Symposium on Microwave, Antenna, Propagation and EMC Technologies for Wireless Communications (MAPE), (Hangzhou, China), pp. 1–4, IEEE, Aug. 14–16, 2007.

[81] R. Giuliano, C. Monti, and P. Loreti, "WiMAX Fractional Frequency Reuse for Rural Environments," *IEEE Wireless Communications*, vol. 15, pp. 60–65, June 2008.

[82] S. Kolahi, "Impact of Propagation Parameters on Neighbouring Cells Interference in Power Controlled CDMA Systems," in *Proc. of the International Region 10 Conference (Tencon)*, (Melbourne, Australia), pp. 1–5, IEEE, Nov. 21–24, 2005.

[83] P. Höher, "A Statistical Discrete-Time Model for the WSSUS Multipath Channel," *IEEE Transactions on Vehicular Technology*, vol. 41, pp. 461–468, Nov. 1992.

[84] J. Medbo and P. Schramm, "ETSI/BRAN Document no. 3ERIO85B: Channel Models for HIPERLAN 2." Retrieved Sept. 1, 2006, from http://www.etsi.org/, 1998.

[85] V. Erceg, L. J. Greenstein, S. Y. Tjandra, S. R. Parkoff, A. Gupta, B. Kulic, A. A. Julius, and R. Bianchi, "An Empirically Based Path Loss Model for Wireless Channels in Suburban Environments," *IEEE Journal on Selected Areas in Communications*, vol. 17, pp. 1205–1211, July 1999.

[86] F. R. Gantmacher, *Matrix Theory*, vol. II. New York: Chelsea Publishing Company, 1974.

[87] IST-4-027756 WINNER II, "D1.1.2 v1.2 WINNER II Channel Models." Retrieved Feb. 5, 2008, from https://www.ist-winner.org/WINNER2-Deliverables/.

[88] T. Bonald, "A Score-Based Opportunistic Scheduler for Fading Radio Channels," in *Proc. of the European Wireless Conference (EWC)*, (Barcelona, Spain), Feb. 24–27, 2004.

[89] E. Foutekova, S. Sinanović, and H. Haas, "Asymmetry Balancing for Channel Asymmetry Support in OFDMA-TDD Cellular Networks," in *Proc. of the Vehicular Technology Conference (VTC)*, (Calgary, Canada), IEEE, Sept. 21–24, 2008.

[90] E. Foutekova, S. Sinanović, and H. Haas, "Traffic Asymmetry Balancing in OFDMA-TDD Cellular Networks," *Journal of Communications and Networking (JCN), Special Issue on Wireless Cooperative Transmission and its Applications*, vol. 10, pp. 137 – 147, June 2008. ISSN 1229-2370.

[91] C. Qiao, H. Wu, and O. Tonguz, "Load Balancing via Relay in Next Generation Wireless Systems," in *Workshop on Mobile and Ad Hoc Networking and Computing (MobiHOC)*, (Boston, Massachusetts, USA), pp. 149–150, Aug. 11, 2000.

[92] A. Sendonaris, E. Erkip, and B. Aazhang, "Increasing Uplink Capacity via User Cooperation Diversity," in *Proc. of the IEEE International Symposium on Information Theory*, (Cambridge, MA, USA), p. 156, Aug. 16–21, 1998.

[93] A. Sendonaris, E. Erkip, and B. Aazhang, "User Cooperation Diversity. Part I. System Description," *IEEE Transactions on Communications*, vol. 51, pp. 1927–1938, Nov. 2003.

[94] S. Yatawatta and A. Petropulu, "A Multiuser OFDM System with User Cooperation," in *Conference Record of the Thirty-Eighth Asilomar Conference on Signals, Systems and Computers*, vol. 1, pp. 319–323, Nov. 7–10, 2004.

[95] G. Auer, H. Haas, and P. Omiyi, "Interference Aware Medium Access for Dynamic Spectrum Sharing," in *Proc. of the International Symposium on New Frontiers in Dynamic Spectrum Access Networks (DySPAN)*, (Dublin, Ireland), pp. 399–402, Apr. 17-20 2007.

[96] P. Omiyi, H. Haas, and G. Auer, "Analysis of TDD Cellular Interference Mitigation Using Busy-Bursts," *IEEE Transactions on Wireless Communications*, vol. 6, pp. 2721–2731, July 2007.

[97] F. Gessler, "Developing Technical Standards – Balancing History and Pre-conceptions," in *Proc. of the International Association for Management Technology Conference (IAMOT)*, (Lausanne, Switzerland), Mar. 19–22, 2001.

[98] J. Cho and Z. Haas, "On the Throughput Enhancement of the Downstream Channel in Cellular Radio Networks Through Multihop Relaying," *IEEE Journal on Selected Areas in Communications*, vol. 22, pp. 1206–1219, Sept. 2004.

[99] Z. Bharucha and H. Haas, "The Distribution of Path Losses for Uniformly Distributed Nodes in a Circle," *Research Letters in Communications*, vol. 2008, no. Article ID 376895, p. 4 pages, 2008.

[100] R. F. Riley, M. P. Hobson, and S. J. Bence, *Mathematical Methods for Physics and Engineering*. Cambridge University Press, second ed., 2002.

Traffic Asymmetry Balancing in OFDMA-TDD Cellular Networks

Ellina Foutekova, Sinan Sinanović and Harald Haas

Abstract: **This paper proposes a novel approach to interference avoidance via inter-cell relaying in cellular OFDMA-TDD (orthogonal frequency division multiple access - time division duplex) systems. The proposed scheme, termed asymmetry balancing, is targeted towards next-generation cellular wireless systems which are envisaged to have *ad hoc* and multi-hop capabilities. Asymmetry balancing resolves the detrimental base station (BS)-to-BS interference problem inherent to TDD networks by synchronizing the TDD switching points (SPs) across cells. In order to maintain the flexibility of TDD in serving the asymmetry demands of individual cells, inter-cell relaying is employed. Mobile stations (MSs) in a cell which has a shortage of uplink (UL) resources and spare downlink (DL) resources use free DL resources to off-load UL traffic to cooperating MSs in a neighboring cell using *ad hoc* communication. In an analogous fashion DL traffic can be balanced. The purpose of this paper is to introduce the asymmetry balancing concept by considering a seven-cell cluster and a single overloaded cell in the center. A mathematical model is developed to quantify the envisaged gains in using asymmetry balancing and is verified via Monte Carlo simulations. It is demonstrated that asymmetry balancing offers great flexibility in UL-DL resource allocation. In addition, results show that a spectral efficiency improvement of more than 100% can be obtained with respect to a case where the TDD SPs are adapted to the cell-specific demands.**

Index Terms: **Ad hoc, cellular, multi-hop, OFDMA, TDD.**

I. INTRODUCTION

With varying throughput, delay and traffic asymmetry requirements, the development of new solutions and concepts that allow for a flexible and dynamic radio resource allocation for the support of high peak-to-average transmission rates, and that are able to be more spectrally efficient than conventional cellular systems is a key challenge. An effective strategy which is envisioned for next-generation wireless cellular networks to ameliorate the spectral efficiency performance without increasing hardware cost is to make use of existing infrastructure and to introduce cooperation among the network entities. Naturally, such cooperation leads to multi-hop cellular networks (MCN) [1], i.e., cellular networks which have relaying capabilities. A relay station (RS) is an intermediate node between an MS and the servicing base station (BS) and the relay can be either a dedicated transceiver or an mobile station (MS). For example, in [2], Qiao, Wu, and Tonguz describe a load balancing method via mobile dedicated transceivers, which can be replaced according to user traffic demand, in order to divert traffic using the unlicensed frequency bands. However, MCNs where the relays are MSs are of special interest due the wide availability of mobile terminals, especially in highly populated areas, where network capacity becomes a limiting factor. Capacity improvement has been shown in [3] and [4], where in-cell users act as relays to form virtual antenna arrays and thereby exploit transmit diversity.

The *ad hoc* capabilities in an MCN are actually enabled by TDD. In addition, the support for cell-independent traffic asymmetry offered by time division duplex (TDD) together with the advantages of orthogonal frequency division multiple access (OFDMA) [5], make OFDMA-TDD a promising choice for next generation wireless networks [6]. However, TDD suffers from additional interference as compared to frequency division duplex (FDD). In particular, TDD suffers from same-entity interference, MS→MS and BS→BS, which presents a major problem in actual cellular TDD deployment when cell-independent asymmetry is to be supported. Known solutions to interference avoidance in TDD include the concept of zone/region division [7], which restricts crossed slot operation only within a radius r around the BS. Optimum performance has been found for r=52% of the cell radius [7]. This strategy reduces MS→MS interference, but does not solve the more detrimental BS→BS interference problem. Moreover, it also imposes restrictions on the flexibility of TDD by compromising user demand. Furthermore, a strategy for same-entity interference mitigation, similar to frequency hopping, termed time-slot opposing, has been proposed in [8]. The time multiplexed busy tone approach in [9] also mitigates the problem of same-entity interference.

In this paper a novel idea termed *asymmetry balancing* is proposed to entirely avoid the detrimental BS→BS interference. The essence of the asymmetry balancing concept is, as the name suggests, to balance the asymmetry demand across the cells in a network. To this end, the TDD switching point (SP) is synchronized across cells, which might result in a shortage of resources in a particular cell, while a neighboring cell might have spare resources (assuming cell-independent traffic asymmetry demands). In order to resolve any mismatch between resource availability and resource demand, the *ad hoc* capabilities of an MCN are exploited. In particular, an MS which cannot be served in either uplink (UL) or downlink (DL) by its associated BS due to shortage of resources is served by a neighboring cooperating BS, which has spare resources in both link directions. The established MS↔BS link is a two-hop link where the intermediate node is an MS associated with the cooperating BS. In this way, despite the fact that the network maintains a synchronized SP, cell-specific asymmetries are effectively supported.

It is assumed that cells are differently loaded, which is a reasonable assumption for future wireless networks which will mainly support packet-data traffic characterized by a high peak-

Manuscript received November 20, 2007.

The authors are with the Institute for Digital Communications at the School of Engineering & Electronics, The University of Edinburgh, Edinburgh EH9 3JL, UK, email: {E.Foutekova, S.Sinanovic, H.Haas}@ed.ac.uk.

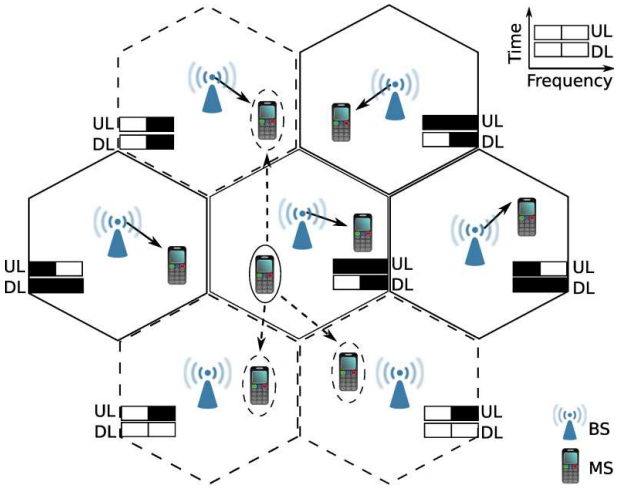

Fig. 1. The MSs in the center cell, i.e., the CoI, can off-load UL traffic to neighboring cooperating cells (marked by dashed hexagons) using free DL resources (marked by white boxes). As an example, the MS at the CoI which needs UL service (marked by a solid ellipse) can form an *ad hoc* link with any of the available MSs (marked by dashed ellipses) at the cooperating cells. Active DL links are shown as solid arrows, while possible concurrent *ad hoc* links are shown as dashed arrows.

to-average load ratio. In addition, because traffic is envisaged to be DL-favored the network-wide SP will be primarily DL-favored (or occasionally symmetric), it is expected that a cell which requires UL-favored SP will not be able to support the UL demand. Therefore, this study focuses on UL asymmetry balancing.

The rest of the paper is organized as follows. Section II introduces the novel asymmetry balancing idea and the simulation model is presented in Section III, while the results are given in Section IV. The paper concludes with Section V.

II. ASYMMETRY BALANCING VIA INTER-CELL RELAYING

As the asymmetry balancing concept relies on cooperation, it is important to identify the cooperating entities and when they can cooperate. If hexagonal cells are considered, each cell can be treated as a cell of interest (CoI), surrounded by six neighboring cells, which are the potential cooperating cells. Fig. 1 illustrates the aforementioned geometry during a DL time slot. Assume that there are only two frequency resources per cell per link direction per frame, which are marked by boxes on Fig. 1. A black box signifies an allocated resource, while a white box signifies a free resource. Let the CoI suffer from shortage of UL resources, while it has a DL resource available. Marked by a solid ellipse is the MS at the CoI, which needs UL service and desires to off-load traffic. The first-tier cells which are marked with dashed hexagons have spare UL and DL resources and hence are the cooperating cells. Associated with the cooperating cells are the MSs which can serve as RSs (identified by dashed ellipses). The tagged MS at the CoI can relay to any of the available RSs.

The MS→RS link uses a DL resource, which is free both at the CoI and the cooperating cell which serves the respective RS. Such resources are referred to as common free resources (CFR). In addition, the off-loading MSs can form *ad hoc* links to either idle MSs in neighboring cells, or active MSs which are already receiving in DL from their BS. The latter case exploits the fact that a DL transmission usually does not occupy all subchannels, and this is accounted for by the use of frequency division multiple access (FDMA) in combination with OFDM. It should be noted that in an OFDMA-TDD network the smallest resource unit allocatable to a particular user is termed a chunk[1], i.e., a number of subcarriers during one time slot.

Based on the above, the main steps of the UL asymmetry balancing technique for multiple cell scenario are summarized below:

1. A CoI is overloaded in UL and requires cooperation.
2. The set of first-tier cells surrounding the CoI, which have spare resources both in UL and DL, are the cooperating cells.
3. There are DL CFRs between the CoI and at least one of the cooperating cells.
4. Utilize the CFRs to transfer UL load from the CoI to the cooperating cells. Use *ad hoc* communication to form MS→RS links between MSs associated with the CoI and RSs associated with any of the cooperating cells.

Similarly, if the CoI suffers from DL overload, MSs at the CoI can be served indirectly by the cooperating cells via nearby MSs (operating as RSs).

From the above it can be concluded that the asymmetry balancing requires first, available resources and second, available RSs. The next two sections will treat these factors in detail. Even though the analysis is performed for the case of UL asymmetry balancing, it is valid for DL asymmetry balancing as well, by replacing UL with DL.

A. Resource Availability

When the center cell uses DL resources to off-load UL traffic to cooperating neighboring cells, UL resources are in effect created, which allow for cell-specific asymmetry demands to be supported. In this way, with cooperation the UL resource capacity of the CoI increases. For example, if the network-wide SP allocates half of the frame to UL and half to DL, and 20% of the DL resources are CFRs, the UL resource capacity of the CoI increases by 20%. Hence, an UL-to-DL traffic ratio of $\frac{0.5+0.5\times0.2}{0.5-0.5\times0.2}$, i.e., $\frac{3}{2}$, can be served at the CoI, even though the actual network-wide SP is set as $\frac{1}{1}$. This means that a "virtual" cell-specific SP can be established depending on the network-wide SP and the DL CFRs.

It is of interest to quantify the UL-to-DL ratios that a virtual SP can support, for a given network-wide SP and a given number of free resources at the CoI and its neighboring cells. Let the number of CFRs be N, where N takes on values $n \in [0, C]$, and C is the total number of resources per cell in DL. Since the SPs are synchronized across the network, C is the same for all cells. The problem of finding the distribution of N can be readily addressed by the binomial distribution, considering that having a CFR is a success, which occurs with probability p and not having such is a failure, which occurs with probability $1-p$. A success occurs when a given chunk is free at the center cell

[1]The terms chunk and resource are used interchangeably throughout this text.

and at the same time, at at least one of the neighboring cells. A failure, on the other hand, occurs when a chunk is busy at the center cell, *or* is free at the center cell and at the same time is busy at all of the neighboring cells. Thus, the distribution of the number of common free chunks, f_N, is a function of the resource occupancy probabilities at the CoI and at the first-tier cells. Resource occupancy probability is the probability that a chunk is occupied. The formulation of f_N is given in (1):

$$f_N(n) = p(L_{\rm c}, L_{{\rm t},1}, \cdots, L_{{\rm t},B_{\rm t}}, B_{\rm t})^n \cdot [1 - p(L_{\rm c}, L_{{\rm t},1}, \cdots, L_{{\rm t},B_{\rm t}}, B_{\rm t})]^{C-n} \binom{C}{n} \quad (1)$$

where $B_{\rm t}$ is the number of cooperating cells; $L_{{\rm t},i}$ is the probability that a resource is occupied at a first-tier cell i; $L_{\rm c}$ is the probability that a resource is occupied at the CoI; and $p(L_{\rm c}, L_{{\rm t},1}, \cdots, L_{{\rm t},B_{\rm t}}, B_{\rm t})$, which is the probability of having a CFR, depending on the number of cooperating cells and the resource occupancy, is given in (2):

$$p(L_{\rm c}, L_{{\rm t},1}, \cdots, L_{{\rm t},B_{\rm t}}, B_{\rm t}) = (1 - \prod_{i=1}^{B_{\rm t}} L_{{\rm t},i}) \cdot (1 - L_{\rm c}). \quad (2)$$

The expected value of the binomial distribution in (1) yields $E[N] = C \cdot p$, hence the expected value of the number of CFRs as a fraction of the total number of DL resources is $\frac{E[N]}{C} = p$.

Let the network-wide SP split the frame into two sub-frames, such that their time durations are in ratio of $u : d$, where $\frac{u}{u+d}$ of the time the frame is in UL and $\frac{d}{u+d}$ of the time the frame is in DL. Furthermore, let the total (UL+DL) number of chunks available per cell be $C_{\rm tot}$. Then at the CoI, the expected value of the fraction of resources in the frame which can be used for UL traffic including off-loading, $R_{\rm ul}$, is:

$$R_{\rm ul} = \frac{\frac{u}{u+d} C_{\rm tot} + p \frac{d}{u+d} C_{\rm tot}}{C_{\rm tot}} \equiv \underbrace{\frac{u}{u+d}}_{\text{actual SP}} + \underbrace{\frac{p\,d}{u+d}}_{\text{virtual SP}}. \quad (3)$$

This means that at the CoI the virtual SP divides the frame in an UL-to-DL ratio of $(u + p\,d) : (d - p\,d)$. It can be observed that when $p \to 0$, i.e., when there are no available resources for off-loading, then the resource allocation is according to the actual network-wide SP. When $p \to 1$, i.e., when all DL resources at the CoI can be used to off-load UL traffic, then $R_{\rm ul} \to 1$ and the whole frame can be allocated to UL.

Fig. 2 shows a plot of $R_{\rm ul} \times 100\%$ depending on the actual SP, the number of cooperating BSs, and on the resource occupancies at the CoI and at the cooperating BSs. In order to study the effect of the virtual SP a best-case and a worst-case scenario are considered. The number of cooperating BSs is one for the worst-case scenario and six for the best-case scenario. The resource occupancies in the case when all six cells can cooperate are kept the same ($L_{{\rm t},1} = L_{{\rm t},2} = \cdots = L_{\rm t}$), while when only one cell cooperates $L_{{\rm t},1} = L_{{\rm t},2} = \cdots = L_{{\rm t},5} = 1$ and $L_{{\rm t},6} = L_{\rm t}$. The values for $L_{\rm t}$ are varied as shown in Fig. 2. Overall, it can be observed that, as expected, when there are no free resources ($L_{\rm c}$ and/or $L_{\rm t}$ are one), the virtual SP is the same as the network-wide SP. Consequently, when there are free DL resources, the virtual SP exploits the resource availability to allocate additional resources to UL. Furthermore, when all DL resources at the CoI are free, the whole frame can be allocated to UL for low to moderate loads at the cooperating cells when six cells cooperate. Even in the case when only one cell cooperates the same effect can be achieved if $L_{\rm t} = 0$. As expected, when overall the DL resource occupancy increases, the number of resources allocated to UL by the virtual SP at the CoI decreases. It is interesting to note that due to the six degrees of freedom, when six cells cooperate, $R_{\rm ul} \times 100\%$ decreases much slower with decrease in resource availability as compared to the case when only one cell cooperates, where $R_{\rm ul} \times 100\%$ decreases linearly. Overall, it is seen that asymmetry balancing offers flexibility in resource allocation and can adaptively allocate resources based on availability and potentially can give all the resources in a frame to one link direction.

B. Relay Station Availability

The previous section determined the expected number of resources, which are available for off-loading and this section concentrates on the second enabler for asymmetry balancing, i.e., availability of RSs. Given that there is a CFR, the CFR can be utilized if RSs are available such that a two-hop path can be found from the MS, which needs to off-load traffic to the cooperating BS. In other words, the MS→RS *ad hoc* links are "opportunistic" in that they exploit CFRs and available RSs, and also are managed in a decentralized fashion. How to find a two-hop path is a matter of routing, and determining an optimum routing strategy is beyond the scope of the current study. It is assumed here that future wireless networks will be equipped with multi-hop and relaying functionality in which case no significant additional signaling overhead is required for managing the MS→RS links.

In this study a simple path loss based routing scheme is implemented which is illustrated with the help of Fig. 3: $\rm BS_{CoI}$ faces shortage of UL resources and $\rm MS_{OL}$ needs to relay to $\rm RS_c$, which is associated with the cooperating $\rm BS_c$. $\rm RS_c$ is chosen as an RS if two conditions, $\rm C_1$ and $\rm C_2$, are satisfied (not considering protection of on-going links):

$$\rm C_1 : L_p^{mb} > L_p^{mr} + \Delta_1[dB]$$
$$\rm C_2 : L_p^{mb} > L_p^{br} + \Delta_2[dB]$$

where $L_{\rm p}^{\rm mb}$ is the path loss between $\rm BS_{CoI}$ and $\rm MS_{OL}$; $L_{\rm p}^{\rm mr}$ is the path loss between $\rm MS_{OL}$ and $\rm RS_c$; $L_{\rm p}^{\rm br}$ is the path loss between $\rm BS_c$ and $\rm RS_c$; and Δ_1 and Δ_2 are path loss margins, which are addressed later in this text. The two conditions above aim to ensure that the two-hop link $\rm MS_{OL} \to RS_c \to BS_c$ would be able to achieve better link capacity than the potential single hop $\rm MS_{OL} \to BS_{CoI}$ link. $\rm MS_{OL}$ and $\rm RS_c$ attain information about $L_{\rm p}^{\rm mb}$ and $L_{\rm p}^{\rm br}$, respectively, via the pilot signals that BSs typically send. In addition, $L_{\rm p}^{\rm mr}$ can be calculated using the busy burst signaling technique described in [9] and [10]. There a receiver transmits a time-multiplexed signal upon successful transmission to reserve a resource. In this study it is assumed that a time-multiplexed signal is transmitted by all receivers, which wish to reserve a particular resource. This busy

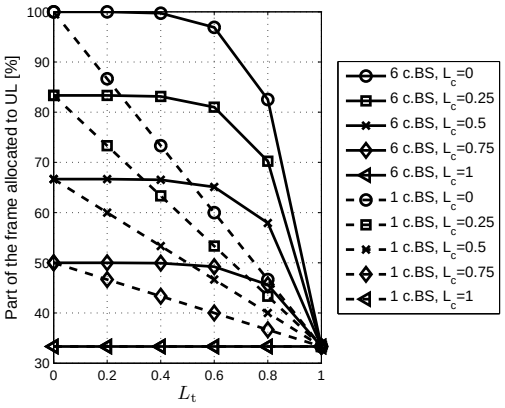

(a)

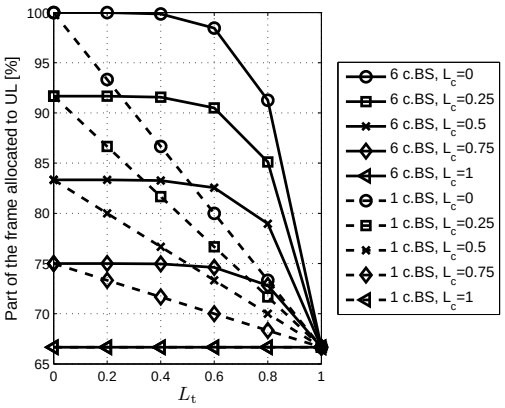

(b)

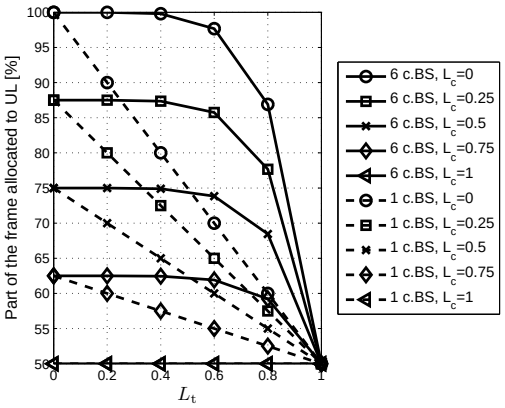

(c)

Fig. 2. The number of cooperating BSs (c.BS) takes on values of 1 and 6: (a) The network-wide SP allocates 33% of the frame to UL (base line), (b) The network-wide SP allocates 66% of the frame to UL (base line), and (c) The network-wide SP allocates 50% of the frame to UL (base line). The virtual SP can allocate additional resources to UL (up to 100% of the frame resources), based on the actual network-wide SP, as well as on the resource occupancies at the CoI and its neighboring cells.

burst signal can be used by the receiver to "advertise" its availability to serve as an RS by means of piggy-back signaling. In addition, essential information, such as $L_{\mathrm{p}}^{\mathrm{br}}$, can be readily obtained from the received busy burst signal at the $\mathrm{MS_{OL}}$ given

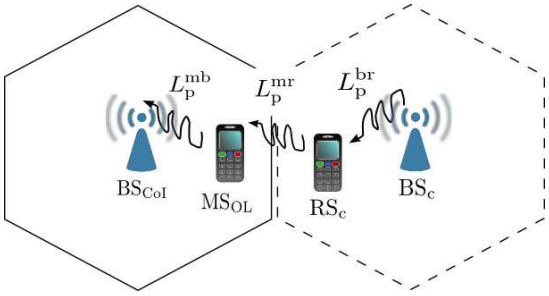

Fig. 3. $\mathrm{MS_{OL}}$ decides whether to off-load to $\mathrm{RS_c}$ or not based on a comparison of $L_{\mathrm{p}}^{\mathrm{mb}}$ with $L_{\mathrm{p}}^{\mathrm{mr}}$ and $L_{\mathrm{p}}^{\mathrm{mb}}$ with $L_{\mathrm{p}}^{\mathrm{br}}$.

that the busy burst power emitted from the RS is constant. As a consequence, $\mathrm{MS_{OL}}$ is equipped to evaluate the routing conditions quoted above in a decentralized fashion and, hence, is enabled to find a suitable RS.

Based on the above, given a CFR is shared between the CoI and a number of first-tier cells, K, the probability, p_{ucfr}, that the CFR will be utilized, is the probability that at least one user at the CoI will be able to find at least one two-hop path, which satisfies both C_1 and C_2. p_{ucfr} can be expressed as given in (4):

$$p_{\mathrm{ucfr}} = 1 - (1 - \Pr\{\mathrm{C}_1 \cap \mathrm{C}_2\})^{U_{\mathrm{c}}^2 K} \tag{4}$$

where U_{c} is the number of users per cell; and $\Pr\{\mathrm{C}_1 \cap \mathrm{C}_2\}$ is the probability that both C_1 and C_2 are satisfied at the same time and can be determined using conditional probabilities as given in (5):

$$\Pr\{\mathrm{C}_1 \cap \mathrm{C}_2\} = \Pr\{\mathrm{C}_1 \mid \mathrm{C}_2\}\Pr\{\mathrm{C}_2\} \tag{5}$$

where $\Pr\{\mathrm{C}_1 \mid \mathrm{C}_2\}$ and $\Pr\{\mathrm{C}_2\}$ are defined below:

$$\Pr\{\mathrm{C}_1 \mid \mathrm{C}_2\} = \Pr\{L_{\mathrm{p}}^{\mathrm{mr}} < L_{\mathrm{p}}^{\mathrm{mb}} - \Delta_1 \mid L_{\mathrm{p}}^{\mathrm{br}} < L_{\mathrm{p}}^{\mathrm{mb}} - \Delta_2\} \tag{6}$$

$$\Pr\{\mathrm{C}_2\} = \Pr\{L_{\mathrm{p}}^{\mathrm{br}} < L_{\mathrm{p}}^{\mathrm{mb}} - \Delta_2\}. \tag{7}$$

The path losses are random variables and their distributions can be derived by approximating the hexagonal cell structure by a circular cell structure as shown in the Appendix. In particular, both $L_{\mathrm{p}}^{\mathrm{br}}$ and $L_{\mathrm{p}}^{\mathrm{mb}}$ are BS–MS path loss distributions which are identically distributed and their probability distribution function (pdf) is approximated as follows (for the derivation please refer to the Appendix):

$$f_q(q) = \frac{2}{R^2 b} 10^{2\frac{q-a}{b}} \ln(10), \quad q \le a + b\log_{10}(z) \tag{8}$$

where R is the cell radius, a is an environment specific constant and $b = 10\,\mu$ with μ being the path loss exponent. Similarly, the MS-RS path loss distribution $L_{\mathrm{p}}^{\mathrm{mr}}$ is approximated by the following pdf (again, for the derivation please refer to the Appendix):

$$f_y(y) = \int_0^R f_y(y|z) f_z(z)\, dz \tag{9}$$

where $f_z(z)$ is the distribution of the distances [9]:

$$f_z(z) = \frac{2\,z}{R^2}, \quad z \le R \tag{10}$$

Table 1. Probability p_{ucfr} that at least one two-hop link can be established for five users per cell and $\Delta_1 = \Delta_2 = 3$ dB.

# of coop BSs:	1	2	3	4	5	6
S-A:	0.010	0.021	0.031	0.041	0.051	0.061
sim.:	0.009	0.018	0.032	0.043	0.051	0.065

and $f_y(y|z)$ is path loss distribution for a given distance from the center, z.

Based on the above, (6) can be further evaluated as follows:

$$\Pr\{L_{\mathrm{p}}^{\mathrm{mr}} < L_{\mathrm{p}}^{\mathrm{mb}} - \Delta_1 \mid L_{\mathrm{p}}^{\mathrm{br}} < L_{\mathrm{p}}^{\mathrm{mb}} - \Delta_2\} = \int_{\forall m} \int_{\forall r}^{m-\Delta_2} F_y(m-\Delta_1) f_q(r) f_q(m) \mathrm{d}m\mathrm{d}r \quad (11)$$

where m and r are dummy variables; $f_q(r)$ is given in (8); and $F_y(m)$ is the cumulative distribution function (cdf) according to the pdf in (9). The limits of the integration are determined by the cell dimensions and path loss models. In addition, (7) can be determined as :

$$\Pr\{L_{\mathrm{p}}^{\mathrm{br}} < L_{\mathrm{p}}^{\mathrm{mb}} - \Delta_2\} = \int_{\forall m} F_q(m-\Delta_2) f_q(m) \mathrm{d}m \quad (12)$$

where $F_q(m)$ is the cdf that corresponds to the pdf in (8).

In order to obtain (4), (11) and (12) are numerically evaluated. Five users per cell are used and as an example, $\Delta_1 = \Delta_2 = 3$ dB. First of all, the value for $1 - \Pr\{\mathrm{C}_1 \cap \mathrm{C}_2\}$ is obtained. According to simulation, $1 - \Pr\{\mathrm{C}_1 \cap \mathrm{C}_2\} \approx 0.99958$, while according to the approximation, $1 - \Pr\{\mathrm{C}_1 \cap \mathrm{C}_2\} \approx 0.99765$. This means that the circular geometry approximation appears to be a lower bound on the probability of not finding a suitable two-hop link. Clearly, when using these findings in the original formula for p_{ucfr} the discrepancy will increase exponentially with the power of $U_{\mathrm{c}}^2 K$. Hence, in order to verify the mathematical model presented, a semi-analytical approach is taken. Namely, the simulation result for $1 - \Pr\{\mathrm{C}_1 \cap \mathrm{C}_2\}$ is used and applied to the formula for p_{ucfr}. The model for p_{ucfr} is successfully verified by simulation and a comparison between semi-analytical and simulation results is shown in Table 1, denoted by S-A and sim., respectively. As expected, when the number of cooperating BSs increases, the probability that at least one two-hop link is found which satisfies both C_1 and C_2 increases. It is interesting to determine how many users per cell are required in order for a two-hop link to be always available, i.e., for p_{ucfr} to become one. Because the simulation result for $1 - \Pr\{\mathrm{C}_1 \cap \mathrm{C}_2\}$ is closer to one than the theoretical result, p_{ucfr} when obtained via simulation will converge slower. It can be calculated that for 110 users per cell and just one cooperating cell, p_{ucfr} is 0.994. Clearly, when more than one cooperating cell is available, convergence to one is reached faster. In fact, for all practical purposes, for more than 150 users per cell, p_{ucfr} is actually one. For a cell radius of 500 m, the cell area is 0.87 km^2, which means about 170 users per km^2. This is a reasonable number, as even suburban areas have at least 100 users per km^2 and typically in the order of thousand (depending on the wireless provider market share) [11], [12].

It is important to mention that the choice of Δ_1 and Δ_2 has a significant influence on the performance of asymmetry balancing. First of all, Δ_1 and Δ_2 influence how fast p_{ucfr} converges to one. For example, if Δ_1 is kept at 3 dB, but Δ_2 is increased to 5 dB, then according to simulation around 200 users per cell are necessary (240 users per km^2) for p_{ucfr} to become one. In addition, Δ_1 and Δ_2 control the choice of off-loading MSs and serving RSs. As an example, Fig. 4(a) shows the distribution of the off-loading MSs and the serving RSs for $\Delta_1 = \Delta_2 = 3$ dB (using the path loss models specified in Section III). It can be seen that as intended, MSs at the cell edges off-load to better-placed MSs in terms of path loss (log-normal shadowing is not considered). Furthermore, as seen when comparing Fig. 4(a) with Fig. 4(b), increasing Δ_2 for a given Δ_1 will move the "belt" of RSs closer to their associated BSs. In contrast, increasing Δ_1 for a given Δ_2 will shrink both the "belt" of RSs and the "belt" of MSs, as can be seen when comparing Fig. 4(a) with Fig. 4(c). Multi-hop link optimization strategies are presented in [13]. Because optimization of Δ_1 and Δ_2 pertains to the particular routing strategy in place, it is not considered in this study and $\Delta_1 = \Delta_2 = 3$ dB is used.

It can be seen from the above that users at the cell-edges are most likely to use two-hop links. Hence, asymmetry balancing can be combined with "smart" scheduling such that when a given BS faces overload, it gives priority to users, which are closer to the cell center, thus encouraging users which are closer to the cell edges to use two-hop communication. "Smart" scheduling for load balancing is beyond the scope of this paper.

III. SIMULATION MODEL

An OFDMA-TDD system, designed according to the UL asymmetry balancing model introduced in Section II, is simulated using a Monte Carlo approach. Each of the seven cells has a centrally-placed omnidirectional BS and full frequency reuse is assumed. Due to complexity issues only twenty users are distributed uniformly in each of the seven cells. The users are distributed at the beginning of each iteration and a snap-shot analysis is performed. For simplicity and demonstration purposes, the UL↔DL SPs are synchronized across the cells at the symmetric state. However, the model can readily be applied to any asymmetry ratio. Similarly to the envisaged traffic asymmetry in data-packet services, traffic is on average DL-favored. The center cell, however, is UL-overloaded and hence generates UL-favored traffic. The holding time is the same for all users and equals one chunk during a time slot (5 OFDM symbols). Each cell is imposed a mean offered load, which governs the respective user mean inter-arrival times and each user independently generates holding times with exponentially distributed interarrival times. The traffic per user is stored in a buffer and served on a first-in-first-out basis. Path loss is calculated using the WINNER C1 path loss model (NLOS) for urban environment [14] as shown below:

$$L_{\mathrm{p}} = a + b \log_{10}(d) \quad (13)$$

where L_{p} is the path loss in dB, a and b are given in Table 2, and d is the transmitter-receiver separation distance in meters. It should be noted that the values of a and b depend on whether MS–RS path loss, BS–MS path loss, or BS–BS path loss is

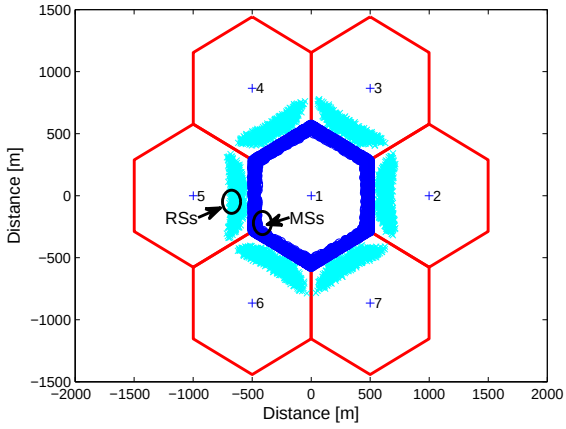

(a)

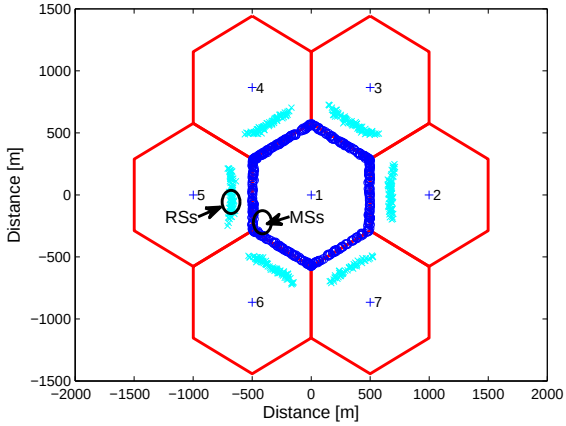

(b)

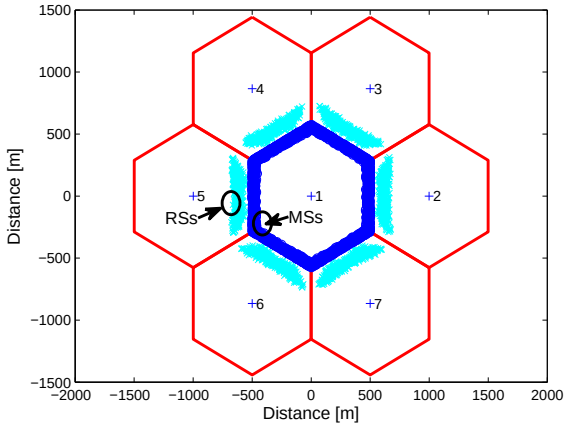

(c)

Fig. 4. Adjusting Δ_1 and Δ_2 changes the distribution of off-loading MSs and serving RSs: (a) $\Delta_1 = \Delta_2 = 3$ dB, (b) $\Delta_1 = 3$ dB and $\Delta_2 = 6$ dB, and (c) $\Delta_1 = 6$ dB and $\Delta_2 = 3$ dB.

calculated. For the latter line-of-sight conditions are assumed. MSs are associated with serving BSs based on minimum path loss. Perfect synchronization is assumed and only co-channel interference from all active other-cell transmitters is taken into account. Time-frequency resources are allocated following a score-based approach [15], where the score is evaluated based on buffer-size. In particular, a given resource is allocated to the user with the largest average buffer size, monitored during a time window of eight frames. The simulation parameters are shown in Table 2. For demonstration purposes, 16 OFDM subcarriers are considered (subject to slow fading effects only). As the SP is symmetric, both UL and DL are allocated 16 subcarriers/time slot $\times$ 3 time slots/frame = 48 chunks/frame (as one chunk is one subcarrier). The transmit power per chunk is fixed to the maximum transmit power divided by the number of chunks per time slot.

Table 2. Simulation parameters [14], [16].

Carrier frequency	5 GHz
Time slot duration	0.1152 ms
Number of time slots/ frame	6
Number of OFDM symbols/ time slot	5
Transmit power/ link	251 mW (24 dBm)
Shortest BS-BS distance	1 km
BS height	25 m
MS height	1.5 m
Path loss parameter a	MS–BS: 39.61 MS–RS: 32.49 BS–BS: 41.2
Path loss parameter b	MS–BS: 35.74 MS–RS: 43.75 BS–BS: 23.8

IV. RESULTS AND DISCUSSION

In this study, the performance of UL asymmetry balancing is investigated. Therefore, it is assumed that the UL in the CoI is overloaded and two particular scenarios in terms of resource availability are defined: (1) A best case 6-cell scenario, where all six first-tier cells cooperate; and (2) a worst-case 1-cell scenario where only one first-tier cell cooperates. (Technically, the worst case is if zero cells cooperate and will be considered later.) Different resource availability conditions are enforced by varying the total *user demand* per frame per cell (in %). In this paper, the synchronized SP is set to allocate half of the frame resources to UL and DL each. As a result, in order to obtain the *probability for resource occupancy* at a particular link direction for a given cell, the respective user demand should be multiplied by 2 (because the user demand is defined on a frame basis). The DL resource occupancy probability both at the CoI and at the cooperating cells is varied from 0 to 0.8, which corresponds to a user demand that varies from 0% to 40%. In order to account for a worst case scenario in terms of interference experienced by the *ad hoc* links, the non-cooperating cells are assumed to be fully loaded in DL (i.e., the demand is 50%). Because the UL resource demand of the first-tier cells would not influence the results for UL asymmetry balancing, it is kept constant for all considered scenarios. The UL and DL resource demands are shown in Table 3. In order to confirm the theoretic model presented in Section II, results displaying the virtual SP at the CoI for the 6-cell scenario and for the 1-cell scenario are shown in Fig. 5 and a perfect match between simulation and theory is ob-

Table 3. Resource demand for UL and DL (in %).

Cell number → Link direction ↓	1 (CoI)	2	3	4	5	6	7
UL	100	15					
DL (6-cell)	0→40						
DL (1-cell)	0→40	50					

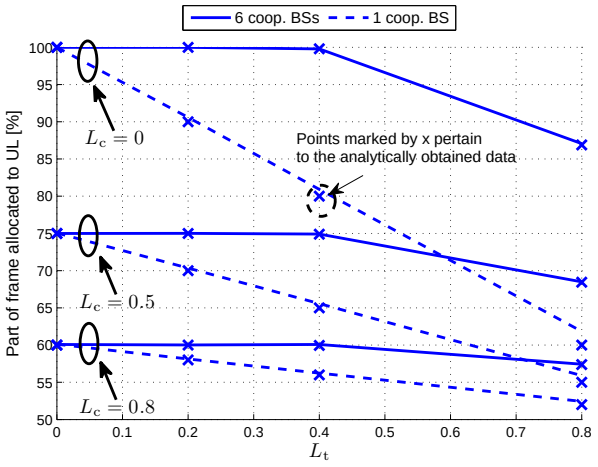

Fig. 5. Frame resources allocated to UL at the CoI by the virtual SP. Solid and dashed lines show simulation results, while analytically obtained data points are marked by "x".

served.

Next, the performance of the UL asymmetry balancing scheme is compared against two systems: 1) An independent SP (ISP) system where each cell independently sets its SP based on the ratio of UL and DL resource demands; and 2) a synchronized SP (SSP) system which is the same as the asymmetry balancing system, but off-loading does not take place. The comparison metric is spectral efficiency as given in (14), because it can capture not only user link conditions, but also how efficiently resources in a frame are utilized:

$$C_{\mathrm{b}} = \frac{1}{C_{\mathrm{tot}}} \left(\sum_{i=1}^{M} \log_2(1+\gamma_i) + \frac{\overline{M}_{\mathrm{OL}}}{M_{\mathrm{OL}}} \sum_{j=1}^{M_{\mathrm{OL}}} \log_2(1+\gamma_j^{\mathrm{mh}}) \right) \tag{14}$$

where C_{b} is the spectral efficiency per chunk in bps/Hz; γ_i is the SINR of chunk i for single hop links; $M = \frac{u}{u+d} C_{\mathrm{tot}}$ is the number of chunks allocated to UL as per the network-wide SP; $\overline{M}_{\mathrm{OL}} = p\frac{d}{u+d} C_{\mathrm{tot}}$, is the number of DL chunks available for off-loading; M_{OL} is the number of chunks actually utilized for off-loading; and γ_j^{mh} is the SINR of chunk j for two-hop links. Clearly, for systems which do not employ asymmetry balancing, $p = 0$, and the second term of the summation in (14) produces a zero. In addition, it should be noted that γ_j^{mh} is taken as the minimum of the SINR achieved at the first and second hops for each two-hop link. Furthermore, $\frac{\overline{M}_{\mathrm{OL}}}{M_{\mathrm{OL}}}$ is used as a correction factor for the following reason. Due to simulation complexity, only twenty users per cell are simulated. As a result, not all available CFRs can be utilized for off-loading via a neighboring RS. The number of available CFRs is only influenced by the

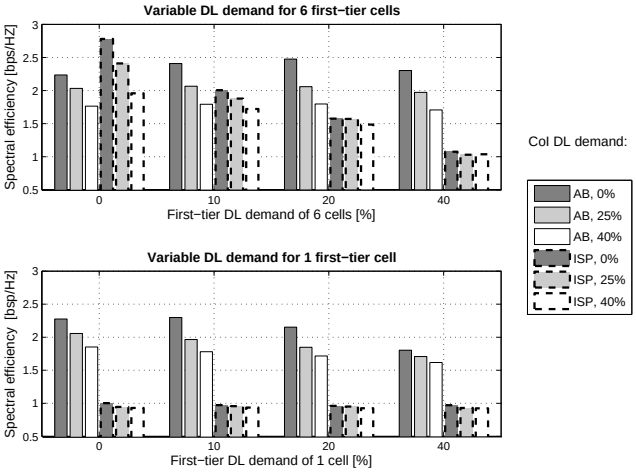

Fig. 6. UL spectral efficiency performance at the CoI achieved with asymmetry balancing (AB) as compared to an ISP system.

actual load, i.e., fraction of available resources, which is independent of the number of users in the system. In contrast, how many of the available CFRs can be utilized for MS→RS links depends on user density (active and non-active users alike) because user density determines if and how often a two-hop path can be found. As a consequence, the spectral efficiency results are also influenced by the number of users in the system. Because, as was demonstrated in Section II, it can be safely assumed that in realistic scenarios all available CFRs can be actually utilized, the correction factor aims to obtain representative spectral efficiency performance.

When the UL spectral efficiency performance of the CoI achieved by the asymmetry balancing scheme is compared to the spectral efficiency performance of an ISP system, the advantages of asymmetry balancing in avoiding BS→BS interference become evident. The results, presented in Fig. 6, show that when the DL demand at the first-tier cells is increased, which in effect increases the number of crossed slots and, hence, the BS→BS interference experienced by the CoI, the spectral efficiency at the CoI attained by the ISP system exhibits very poor performance. Using asymmetry balancing results in a tremendous improvement, and depending on the DL demand at the first-tier cells and at the CoI, a spectral efficiency increase of more than 100% can be achieved (referring to the 1-cell scenario with first-tier DL demand of 0% to 20%). For the considered scenarios, the ISP system results in better UL spectral efficiency for the CoI only when crossed slots are absent. Such is the case in the 6-cell scenario when the DL demand is 0%, i.e., none of the six first-tier cells has DL traffic, which is a highly unlikely situation. For the spectral effiency achieved by the asymmetry balancing system, there is a common trend that as the DL resource demand increases (at the CoI and first-tier cells alike), the spectral efficiency at the CoI decreases. This is as expected, because with an increase in resource demand fewer resources are used for load balancing.

Next, the spectral efficiency attained by asymmetry balancing is compared to that attained by an SSP system, where the SPs are synchronized across cells, which is a common strategy for

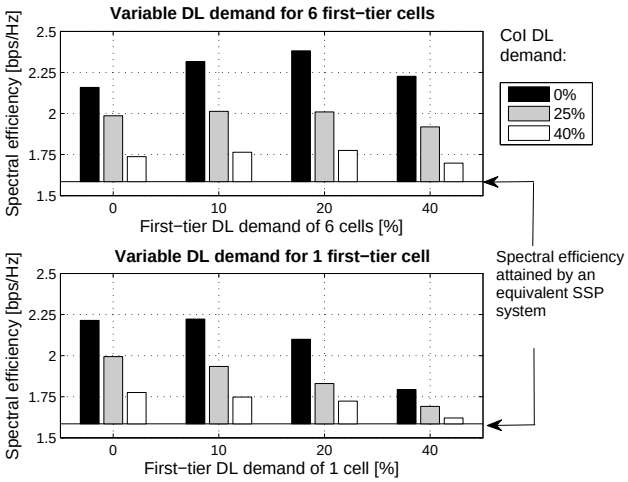

Fig. 7. Spectral efficiency performance of AB as compared to an SSP system. The spectral efficiency attained with asymmetry balancing is plotted by bars, while the spectral efficiency achieved by the SSP system is shown by a constant line as denoted on the plots.

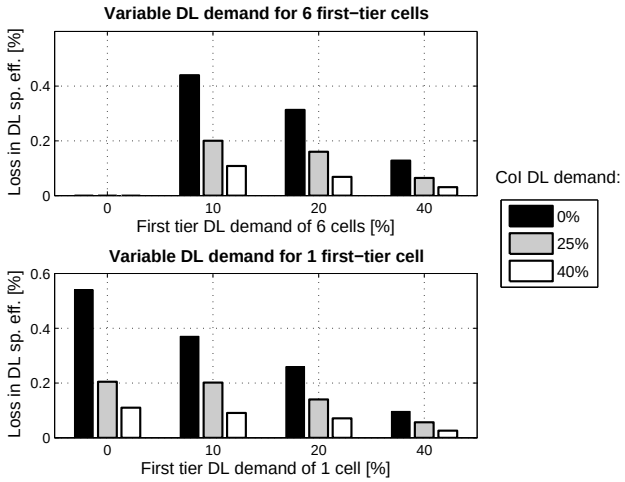

Fig. 8. Percentage loss in DL spectral efficiency caused by the off-loading *ad hoc* links as compared to an equivalent SSP system. As expected, for the 6-cell scenario at 0% DL demand at the first-tier cells, the loss is zero, because there is no DL traffic at the first-tier cells.

avoiding the detrimental BS→BS interference. Results for the UL spectral efficiency attained at the CoI with asymmetry balancing are shown in Fig. 7 for different DL demand scenarios (bar plots) and compared to the performance of an SSP system (solid line). As intuition suggests, when the SPs are synchronized, there is no difference in the CoI UL spectral efficiency performance among the considered scenarios. It is interesting to note that in tackling the poor spectral efficiency attained by the ISP system, simply synchronizing the SPs results in about 50% improvement in spectral efficiency for the cases of severe BS→BS interference (as is the 1-cell scenario), which can be seen by comparing the bottom plot of Fig. 7 and the bottom plot of Fig. 6. Employing asymmetry balancing ameliorates the spectral efficiency even further and from Fig. 7 it can be observed that the system which employs asymmetry balancing always outperforms the SSP system. In the case of 0% DL demand at the CoI, an increase in the spectral efficiency with respect to the SSP system of up to ≈50% is observed for up to 20% DL demand at the first-tier cells. When the DL demand at the CoI is increased to 25%, up to ≈25% increase in spectral efficiency is attained. In general, as expected, the more resources are allocated to UL (referring to Fig. 5), the higher the spectral efficiency achieved by asymmetry balancing. Exception to this trend is the case of 0% DL demand at the CoI (i.e., 100% of the frame resources are allocated to UL) for the 6-cell scenario (and a little less pronounced for the 1-cell scenario), where the achieved spectral efficiency increases slightly with increase in the first-tier DL demand and then decreases again. This effect is caused by using fixed transmit power per chunk. When the transmit power is fixed, the SINR decreases with an increase in the number of simultaneously active users using the same resource.

The demonstrated UL spectral efficiency amelioration attained by asymmetry balancing is at a slight loss in spectral efficiency for the first-tier DL transmission as compared to an SSP system. The loss is due to the off-loading *ad hoc* links, which generate MS→MS interference to the concurrent BS→MS links. The results presented in Fig. 8 show that overall the loss in spectral efficiency does not surpass 0.6%. It can be observed, that even though the results for the 1-cell scenario and the 6-cell scenario are similar, the loss in the case of six cooperating cells is slightly larger due to the fact that more resources are used for the off-loading *ad hoc* links and, hence, more interference is caused to the first-tier DL transmission. Furthermore, the caused loss decreases with increase in the DL demand (both at the CoI and first-tier cells), as expected, because less resources are used for off-loading. It should be noted that the spectral efficiency loss obtained for twenty users per cell is representative even for larger number of users for the studied scenarios, because the number of active users at any given time slot using any given chunk does not change and is equal to the number of cells under consideration.

Table 4. Resource demand for UL and DL (in %).

Cell number → Link direction ↓	1 (CoI)	2	3	4	5	6	7
UL	15 90	90	75	60	45	30	15
DL	85 10	10	25	40	55	70	85

In order to complete the analysis of the asymmetry balancing scheme, it is important to consider what happens when there are no available resources for off-loading. To this end, a fully loaded system is studied (i.e., the total UL and DL demands add up to 100% for each cell), where each cell has a different traffic asymmetry demand, as shown in Table 4. For the CoI two scenarios are defined – UL-favored and DL-favored. The first-tier cells all have different asymmetry demands, which range from highly UL-favored to highly DL-favored in order to explore the crossed-slots effects on the CoI. On average three of the first-tier cells require an UL-favored SP, while the other three require a DL-favored SP. Two systems are compared, *viz*: an SSP sys-

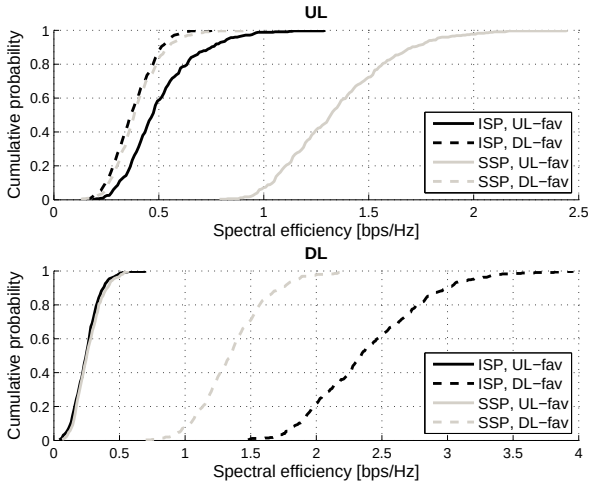

Fig. 9. Spectral efficiency comparison of an ISP system with an SSP system, under the assumption of a fully loaded network.

tem, as the asymmetry balancing system becomes an SSP system in the situation of full network load; and an ISP system. Results for the UL and DL spectral efficiency at the CoI are presented in Fig. 9 (top plot and bottom plot, respectively). When UL spectral efficiency is considered (top plot), it is observed that when the demand at the CoI is UL-favored and crossed slots are present, by avoiding crossed slots the SSP system actually achieves about 2.5 times better spectral efficiency at the 50^{th} percentile than the ISP system. As expected, when the demand at the CoI is DL-favored, the UL spectral efficiency at the CoI is the same for an ISP system and an SSP system. Similarly, when considering the DL spectral efficiency at the CoI (bottom plot), for low DL demand, the ISP system and the SSP system attain similar performance. However, when the DL demand at the CoI is increased, the ISP system manages to provide about 1.7 times better spectral efficiency at the 50^{th} percentile than the SSP system. Here it is important to point out that MS→MS interference is not expected to be a detrimental problem in OFDMA-TDD systems because in order to have high MS→MS interference two MSs need to be using the same chunks at the same time in very close proximity to each other. The situation is different in the case of BS→BS interference, as BS positions are fixed and the whole bandwidth is reused in each cell.

It can be summarized that overall the results demonstrate that allowing each cell to set its SP independently leads to sub-optimum results in the majority of cases, while synchronizing the SP across cells improves spectral efficiency performance significantly. Employing asymmetry balancing, i.e., keeping a network-wide SP and making use of inter-cell relaying, ameliorates the attained spectral efficiency even further. It is expected that optimizing the routing strategy will result in even better system performance.

V. CONCLUSIONS

In this paper, a method named *asymmetry balancing* has been proposed. It allows the support of cell-independent asymmetries in OFDMA-TDD next generation networks with complete avoidance of the detrimental BS→BS interference. The key to solving this issue is user cooperation in combination with inter-cell relaying. A general mathematical framework for the assessment of the proposed technique has been developed, and it has been applied to an UL study. It has been demonstrated that in the case of shortage of UL resources a virtual cell-specific SP can be established, depending on the system UL-to-DL asymmetry ratio and the available DL resources at the CoI and its six neighboring cells. When one or more cells can cooperate, even the whole frame can be virtually allocated for UL traffic. This flexibility in resource allocation comes at a relatively insignificant cost of less than 0.6% loss in DL spectral efficiency incurred due to interference caused by the *ad hoc* links. Furthermore, it is found that the asymmetry balancing technique significantly outperforms conventional approaches where the TDD SPs are synchronized cell-wide and where the TDD SPs are adapted to the cell-specific asymmetry demands. For the UL spectral efficiency of the CoI, the gains with respect to the case of fixed SPs are up to about 50%, whereas the gains with respect to the case of cell-specific SPs surpass 100%. As expected, BS→BS interference avoidance leads to tremendous spectral efficiency improvement. In addition, it has been demonstrated that when the system is fully loaded, the loss from allowing BS→BS interference can be bigger than the loss which results from not meeting DL demand by synchronizing the TDD SP cell-wide. Future work will focus on DL asymmetry balancing and the effect of power control on the *ad hoc* links as well as on the direct links.

APPENDIX

In order to determine the BS–MS and MS–RS path loss distributions the cell geometry is approximated by circular geometry (Fig. 10). The CoI is a circle with radius R and the RSs are outside this circle and within a circle with radius $3R$ (due to the hexagonal cell geometry).

Referring to the small circle, the BS–MS path loss distribution can be approximated using the distribution of the distances between the center of the circle and any point inside the circle as shown in [17]. In summary, assuming uniformly distributed points along the horizontal and vertical axes, this distribution of the distances is given in (15) [9].

$$f_z(z) = \frac{2z}{R^2}, \;\; z \leq R. \tag{15}$$

The respective path loss, Q is of the form: $Q = a + b\log_{10}(Z)$, hence using variable transformation, the pdf of Q can be obtained as:

$$f_q(q) = \frac{2}{R^2 b} 10^{2\frac{q-a}{b}} \ln(10), \;\; q \leq a + b\log_{10}(z). \tag{16}$$

Next, in order to determine the MS–RS path loss distribution, the problem can be formulated as finding the distribution of the distances between any point in the small circle to any point in the ring. Then, variable transformation can be used to find the distribution of the path losses.

Given that a transmitter is z [m] from the circle center, the pdf,

$f_x(x|z)$, of the MS-RS separation distances, X, can be found as:

$$f_x(x|z) = \begin{cases} \frac{1}{\pi 4R^2}\left(\pi - \arccos(\frac{z^2+x^2-R^2}{2zx})\right)x, \\ \qquad\qquad \text{for } R-z \le x < R+z \\ \frac{x}{4R^2} \\ \qquad\qquad \text{for } R+z \le x \le 3R-z \\ \frac{1}{\pi 4R^2}\arccos(\frac{z^2+x^2-(3R)^2}{2zx})x \\ \qquad\qquad \text{for } 3R-z < x \le 3R+z \end{cases}. \tag{17}$$

The next step is to convert the MS–RS distance distribution to path loss distribution. The path loss model used is of the form $Y = a + b\log_{10}(X)$, hence $X = 10^{\frac{Y-a}{b}}$. The path loss distribution for a given distance from the center, z, can be obtained as:

$$\begin{aligned} f_y(y|z) &= f_x(x(y)|z)\left|\frac{\mathrm{d}x(y)}{\mathrm{d}y}\right| \\ &= \begin{cases} f_{x,1} = \frac{D}{\pi 4R^2}\left(\pi - \arccos(\frac{z^2+10^{2\frac{y-a}{b}}-R^2}{2z10^{\frac{y-a}{b}}})\right)10^{\frac{y-a}{b}} \\ \qquad\qquad \text{for } R-z \le 10^{\frac{y-a}{b}} < R+z \\ f_{x,2} = \frac{D\cdot 10^{\frac{y-a}{b}}}{4R^2} \\ \qquad\qquad \text{for } R+z \le 10^{\frac{y-a}{b}} \le 3R-z \\ f_{x,3} = \frac{D}{\pi 4R^2}\arccos(\frac{z^2+10^{2\frac{y-a}{b}}-(3R)^2}{2z10^{\frac{y-a}{b}}})10^{\frac{y-a}{b}} \\ \qquad\qquad \text{for } 3R-z < 10^{\frac{y-a}{b}} \le 3R+z \end{cases} \end{aligned} \tag{18}$$

where $D = \frac{1}{b}10^{\frac{y-a}{b}}\ln(10)$.

Using (15), $f_y(y)$ can be obtained as (function arguments omitted for clarity):

$$\begin{aligned} f_y(y) &= \int_0^R f_y(y|z)f_z(z)\,dz \\ &= \begin{cases} \int_{R-x}^{R} f_{x,1}f_z\,dz,\ x \in [0,R]+ \\ \int_{x-R}^{R} f_{x,1}f_z\,dz,\ x \in [R,2R] \\ \int_{0}^{x-R} f_{x,2}f_z\,dz,\ x \in [R,2R]+ \\ \int_{0}^{3R-x} f_{x,2}f_z\,dz,\ x \in [2R,3R] \\ \int_{3R-x}^{R} f_{x,3}f_z\,dz,\ x \in [2R,3R]+ \\ \int_{x-3R}^{R} f_{x,3}f_z\,dz,\ x \in [3R,4R]. \end{cases} \end{aligned} \tag{19}$$

The above equations are evaluated numerically and compared to a simple Monte Carlo simulation for verification. The results are shown in Fig. 11. The following simulation parameters (WINNER [14]) are used: R is 500 m, a is 32.49 dB and b is 43.75 dB. In the system model in this study, hexagonal cells are used. Thus, in order to verify that the circular geometry is a good approximation to the hexagonal geometry, simulation results for the path loss distribution in the case of hexagonal geometry are provided for comparison.

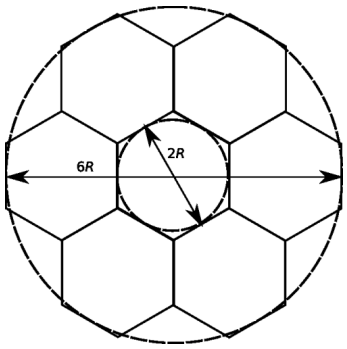

Fig. 10. Hexagonal cell geometry, approximated by circular geometry.

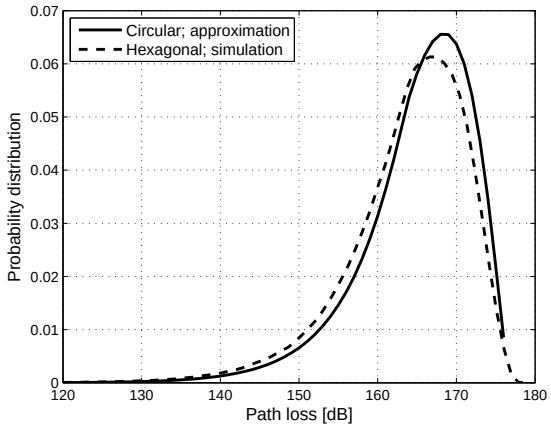

Fig. 11. Pdf of the MS–RS path losses.

ACKNOWLEDGMENT

The authors would like to thank the anonymous reviewers for their constructive and valuable comments and suggestions. The comments clearly helped to improve the manuscript.

REFERENCES

[1] L. Le and E. Hossain, "Multihop cellular networks: Potential gains, research challenges, and a resource allocation framework," *IEEE Commun. Mag.*, vol. 45, no. 9, pp. 66–73, Sept. 2007.

[2] C. Qiao, H. Wu, and O. Tonguz, "Load balancing via relay in next generation wireless systems," in *First Annual Workshop on Mobile and Ad Hoc Networking and Computing (MobiHOC)*, Boston, Massachusetts, USA, Nov. 2000, pp. 149–150.

[3] A. Sendonaris, E. Erkip, and B. Aazhang, "Increasing uplink capacity via user cooperation diversity," in *Proc. of the IEEE ISIT*, Cambridge, MA, USA, 1998, p. 156.

[4] S. Yatawatta and A. Petropulu, "A multiuser OFDM system with user cooperation," in *Conference Record of the Thirty-Eighth Asilomar Conference on Signals, Systems and Computers*, vol. 1, 2004, pp. 319–323.

[5] C. Y. Wong, R. S. Cheng, K. B. Lataief, and R. D. Murch, "Multiuser OFDM with adaptive subcarrier, bit, and power allocation," *IEEE J. Sel. Areas Commun.*, vol. 17, no. 10, pp. 1747–1758, 1999.

[6] H. Haas and S. McLaughlin, Eds., *Next generation mobile access technologies: Implementing TDD*. Cambridge University Press, 2008.

[7] S.-H. Wie and D.-H. Cho, "Time slot allocation scheme based on a region division in CDMA/TDD Systems," in *Proc. IEEE VTC 2001-spring*, 2001, pp. 2445–2449.

[8] H. Haas and S. McLaughlin, "A dynamic channel assignment algorithm for a hybrid TDMA/CDMA-TDD interface using the novel TS-opposing technique," *IEEE J. Sel. Areas Commun.*, vol. 19, no. 10, pp. 1831–1846, 2001.
[9] P. Omiyi, H. Haas, and G. Auer, "Analysis of TDD cellular interference mitigation using busy-bursts," *IEEE Trans. Wireless Commun.*, vol. 6, no. 7, pp. 2721–2731, 2007.
[10] G. Auer, H. Haas, and P. Omiyi, "Interference aware medium access for dynamic spectrum sharing," in *Proc. 2nd IEEE International Symposium on New Frontiers in Dynamic Spectrum Access Networks (DySPAN)*, Dublin, Ireland, 2007, pp. 399–402.
[11] F. Gessler, "Developing technical standards – Balancing history and preconceptions," in *Proc. International Association for Management Technology Conference (IAMOT)*, Lausanne, Switzerland, Mar. 19–22 2001, p. 076FG.
[12] WiMAX Forum, "WiMAX Business Case," [Online]: Available at http://www.hkwtia.org/wtia/ (Date of access: Apr. 8, 2008), 2004.
[13] J. Cho and Z. Haas, "On the throughput enhancement of the downstream channel in cellular radio networks through multihop relaying," *IEEE J. Sel. Areas Commun.*, vol. 22, no. 7, pp. 1206–1219, 2004.
[14] IST-4-027756 WINNER II, "D1.1.2 v1.2 WINNER II channel models," Retrieved Feb. 5, 2008, from https://www.ist-winner.org/WINNER2-Deliverables/.
[15] T. Bonald, "A score-based opportunistic scheduler for fading radio channels," in *Proc. 5th European Wireless Conference (EWC)*, Barcelona, Spain, 2004.
[16] IST-2003-507581 WINNER, "D2.10, Final report on identified RI key technologies, system concept and their assessment," Retrieved Mar. 15, 2007, from https://www.ist-winner.org/DeliverableDocuments/, 2005.
[17] Z. Bharucha and H. Haas, "The distribution of path losses for uniformly distributed nodes in a circle," *Research Lett. in Commun.*, vol. 2008, no. Article ID 376895, 2008.

Ellina Foutekova obtained her B.Sc. degree from Jacobs University Bremen, Bremen, Germany (formerly International University Bremen) in 2005. In the next year she began her Ph.D. studies at the same university and in 2007 transferred to the University of Edinburgh (UoE), Edinburgh, UK. She is currently a Ph.D. student at the Institute for Digital Communications (IDCOM) at UoE, supervised by Dr. Harald Haas. Her main research interests are in the areas of wireless communications, particularly focusing on interference avoidance, load balancing, resource allocation.

Sinan Sinanović obtained his Ph.D. in electrical and computer engineering from Rice University, Houston, Texas in 2006. In the same year, he has joined Jacobs University Bremen in Germany as a post doctoral fellow. In 2007, he has joined the University of Edinburgh in the UK where he currently works as a research fellow in the Institute for Digital Communications. He has previously worked for Texas Instruments in Dallas, Texas on ASIC for the central office modem. While working for Halliburton Energy Services in Houston, Texas, he developed acoustic telemetry receiver for which he was awarded US patent (# 7158446). He is a member of the Tau Beta Pi engineering honor society and a member of Eta Kappa Nu electrical engineering Honor society. He earned his M.S. from Rice University and his B.S.E.E. (summa cum laude) from Lamar University in Texas.

Harald Haas received the Ph.D. degree from the University of Edinburgh in 2001. His main research interests are in the areas of wireless system engineering and digital signal processing, with a particular focus on interference aware MAC protocols, multiuser access, link adaptation, scheduling, dynamic resource allocation, multiple antenna systems and optical wireless communication. From 2001 to 2002, He was project manager at Siemens AG (Information and Communication Mobile Networks) for an international research project on new radio access technologies. He joined International University Bremen (Germany), now Jacobs University Bremen, in September 2002 where he has since been associate professor of Electrical Engineering. In June 2007, He joined the University of Edinburgh (Scotland/UK) where he is Reader in the Institute for Digital Communications (IDCOM). He received a best paper award at the International Symposium on Personal, Indoor and Mobile Radio Communications (PIMRC) in Osaka/Japan in 1999 and holds more than ten patents in the area of wireless communications. He contributed a chapter to the "Handbook of Information Security" entitled "Air Interface Requirements for Mobile Data Services" by John Wiley & Sons, Inc. He co-authors a book entitled "Next Generation Mobile Access Technologies: Implementing TDD" with Cambridge University Press. His work on optical wireless communication was selected for publication in "100 Produkte der Zukunft (100 Products of the Future)" authored by Nobel Laureate T. W. Hänsch.

Hindawi Publishing Corporation
EURASIP Journal on Wireless Communications and Networking
Volume 2008, Article ID 121546, 14 pages
doi:10.1155/2008/121546

Research Article

Channel Asymmetry in Cellular OFDMA-TDD Networks

Ellina Foutekova,[1] Patrick Agyapong,[2,3] and Harald Haas[1]

[1] *Institute for Digital Communications, School of Engineering & Electronics, The University of Edinburgh, Edinburgh, EH9 3JL, UK*
[2] *School of Engineering and Science, Jacobs University Bremen, 28759 Bremen, Germany*
[3] *Department of Engineering and Public Policy, College of Engineering, Carnegie Mellon University, Pittsburgh, PA 15213, USA*

Correspondence should be addressed to Ellina Foutekova, e.foutekova@ed.ac.uk

Received 17 January 2008; Revised 22 July 2008; Accepted 28 October 2008

Recommended by David Gesbert

This paper studies time division duplex- (TDD-) specific interference issues in orthogonal frequency division multiple access- (OFDMA-) TDD cellular networks arising from various uplink (UL)/downlink (DL) traffic asymmetries, considering both line-of-sight (LOS) and non-LOS (NLOS) conditions among base stations (BSs). The study explores aspects both of channel allocation and user scheduling. In particular, a comparison is drawn between the fixed slot allocation (FSA) technique and a dynamic channel allocation (DCA) technique for different UL/DL loads. For the latter, random time slot opposing (RTSO) is assumed due to its simplicity and its low signaling overhead. Both channel allocation techniques do not obviate the need for user scheduling algorithms, therefore, a greedy and a fair scheduling approach are applied to both the RTSO and the FSA. The systems are evaluated based on spectral efficiency, subcarrier utilization, and user outage. The results show that RTSO networks with DL-favored traffic asymmetries outperform FSA networks for all considered metrics and are robust to LOS between BSs. In addition, it is demonstrated that the greedy scheduling algorithm only offers a marginal increase in spectral efficiency as compared to the fair scheduling algorithm, while the latter exhibits up to ≈20% lower outage.

1. INTRODUCTION

In the recent years, orthogonal frequency division multiplexing (OFDM) has been a subject of considerable interest for cellular systems of beyond third generation (3G). Wong et al. [1] show promising results for OFDM as a multiuser technique, focusing particularly on the gains in using adaptive modulation. Results, presented by Keller and Hanzo in [2], also highlight the solid benefits of employing adaptive modulation in OFDM systems. Later, Yan et al. [3] propose an adaptive subcarrier, bit, and power allocation algorithm for a multiuser, multicell OFDM system, which shows significant improvement in throughput when compared to an equal power allocation algorithm. Limiting assumptions include frequency reuse of four, no Doppler effect, no own-cell interference. The gains in combining OFDM with an adequate multiple access scheme have been thoroughly described in [4], specifically emphasizing on the superiority of frequency division multiple access (FDMA).

The combination of OFDMA with time division duplex (TDD), which enables the support of asymmetric services, is of special interest [5]. However, in a system where cell-specific asymmetry demands are to be supported, TDD suffers from additional interference as compared to frequency divisionduplex (FDD), namely same-entity interference (base station (BS) → BS and mobile station (MS) → MS). A possible solution to the same-entity interference problem is fixed slot allocation (FSA). The principle of FSA is that the uplink-downlink (UL-DL) time slot assignment ratio is kept fixed and constant across the cells in a network (and usually allocates half of the resources to UL and DL each). FSA is convenient because, most importantly, same-entity interference is completely avoided, and, in addition, the scheme is simple-to-implement and there is no signaling overhead. The major disadvantage, however, is the lack of flexibility. In other words, one of the primary advantages of TDD, namely, the support for cell-specific asymmetry demands is not exploited.

An interference mitigation technique, which retains the advantages of TDD is random time slot opposing (RTSO) [6]. In RTSO, each cell independently sets the number of UL and DL time slots based on the cell-specific traffic

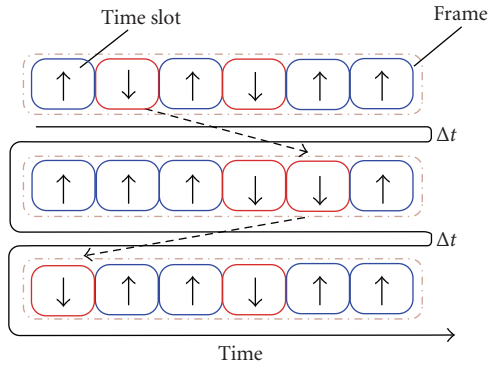

Figure 1: For a given ratio of UL/DL resources, RTSO only permutes the UL and DL time slots once every time interval Δt (greater than the frame duration) [6], keeping the UL/DL ratio fixed. Upward-pointing arrow denotes UL, while DL is denoted by a downward-pointing arrow.

asymmetry demand. In order to mitigate the same-entity interference problem, the time slots are randomly permuted within a frame once every time interval Δt (where Δt is a network parameter) as illustrated in Figure 1. The actual time slot permutation sequence follows a pseudorandom pattern. This pattern can be independently generated at both ends (MS and BS). As a consequence, the signaling effort is almost negligible since only a random code at link setup needs to be conveyed. RTSO avoids persistent severe interference, and in effect achieves interference diversity. Note that an analogy can be made between RTSO and frequency hopping. In the latter, interference diversity is achieved by hopping through different frequency carriers. RTSO has been previously applied to code division multiple access (CDMA) systems [6].

The purpose of this paper is to explore interference aspects arising from cell-specific traffic asymmetry demands in OFDMA-TDD cellular networks, while jointly considering channel allocation and user scheduling. A multiuser, multicell OFDMA-TDD network with full-frequency reuse is studied, assuming both LOS and NLOS conditions among the BSs. RTSO and FSA are the considered channel allocation techniques and the two alternative scheduling algorithms are the fair *optimum target assignment with stepwise rate removals* (OTA-SRRs) [7] and the *greedy rate packing* (GRP) [8].

The rest of the paper is organized as follows. Section 2 presents the system model, while the employed scheduling algorithms are described in Section 3. The simulation model and results are given in Sections 4 and 5, respectively. Concluding remarks are presented in Section 6.

2. SYSTEM MODEL

A wireless cellular network can be modeled mathematically by the signal-to-interference-plus-noise-ratio (SINR) expression in the sense that the SINR expression holds information about the model assumptions on interference sources and power fading alike. In terms of power fading, the system model considered in this study takes on a realistic cross-layer approach to reflect both small-scale fading and large-scale fading in a typical time-variant frequency-selective channel. Small-scale fading pertains to the received signal power variations with frequency, while large-scale fading pertains to the received signal power variations with distance [9]. In previous studies [1–4], one of these impairments is usually neglected. However, for cellular OFDM systems with increasing channel bandwidth (100 MHz for beyond 3G networks [10]), it is important that both fading effects are considered due to the frequency selectivity and frequency granularity, introduced by OFDM. In terms of interference sources, this study considers contributions from own-cell links and other-cell links, termed multiple-access interference (MAI) and cochannel interference (CCI), respectively. Furthermore, impairments such as frequency offset errors due to Doppler and lack of synchronization are also accounted for.

In what follows, expressions for the desired signal power per subcarrier, the received MAI power, and the received CCI power are presented, which are then combined to formulate an SINR expression according to the system model described above.

Let subcarrier $k \in \mathbf{s} = \{a_1, \ldots, a_m\}$, where $a_i \in \{1, \ldots, N_c\}$ and $\mathbf{s}$ is a set of subcarriers belonging to a single user in cell i, and k does not experience interference from the set. The cardinality of $\mathbf{s}$, $|\mathbf{s}|$, is the number of subcarriers per user, which can vary from zero to N_c (total number of subcarriers per BS). The received signal power on subcarrier k in cell i is given by

$$R_k^i = P_k^i G_k^i |H_k^i|^2 \text{ [W]}, \tag{1}$$

where P_k^i is the transmit power on subcarrier k in cell i, G_k^i is the path gain between the MS using subcarrier k and its corresponding BS, and H_k^i is the channel transfer function for subcarrier k in cell i between the MS using subcarrier k and its corresponding BS. Here, it should be noted that the path loss reflects the variation of the received signal power with distance, while the channel transfer function reflects the variation of the received signal power with frequency.

The received MAI power on subcarrier k in UL is given by (2), where it should be noted that MAI in DL is not considered, as perfect synchronization is assumed due to the synchronous nature of point-to-multipoint communication:

$$P_{\text{MAI},k}^i = \sum_{\substack{k'=1 \\ k' \notin \mathbf{s}}}^{N_c} P_{k'}^i G_{k,k'}^i |H_{k,k'}^i|^2 |C_{k,k'}^i(\Delta f + \varepsilon_D + \omega)|^2 \text{ [W]}, \tag{2}$$

where

$$C_{k,k'}^i(x) = \left(\frac{1}{N_c}\right) \frac{\sin(\pi x)}{\sin(\pi x/N_c)} \exp \frac{j\pi x(N_c - 1)}{N_c}, \tag{3}$$

$G_{k,k'}^i$ is the path gain between the transmitter on the link using subcarrier k' and the receiver on the link using subcarrier k, $H_{k,k'}^i$ is the transfer function of the channel between the transmitter on the link using subcarrier k' and

the receiver on the link using subcarrier k, $C^i_{k,k'}(\Delta f + \varepsilon_D + \omega)$, given in (3), is a cyclic sinc function to account for the amount of interference subcarrier k experiences from subcarrier k', j is the imaginary unit, $\Delta f = k' - k$ and $\varepsilon_D = f_{D,max}/\delta_f$ accounts for the Doppler shift (where $f_{D,max}$ is the maximum Doppler frequency and δ_f is the carrier spacing), $\omega = f_c/\delta_f$ is the frequency offset due to synchronization errors between subcarriers k and k', and f_c is the offset in Hz. A derivation of the cyclic sinc function is presented in Appendix C.

The received CCI power per subcarrier is modeled similarly to the received MAI power and is given by (4), where it should be noted that CCI contributions are expected not only from the reused subcarrier but also from neighboring subcarriers, when ε_D and/or ω are non-zero:

$$P^i_{CCI,k} = \sum_{\substack{l=1 \\ l\neq i}}^{B} \sum_{k'=1}^{N_c} P^l_{k'} G^l_{k,k'} |H^l_{k,k'}|^2 |C^l_{k,k'}(\Delta f + \varepsilon_D + \omega)|^2 \text{ [W]}, \tag{4}$$

where B is the number of cells under consideration (cells that contribute nonnegligible interference).

The cyclic sinc function used in modeling MAI and CCI controls the amount of interference subcarrier k' causes to subcarrier k. Given the same transmit power, link gain, and channel, with an increase in $|k' - k + \varepsilon_D + \omega|$, the interference contribution decreases. This behavior is expected as synchronization errors and Doppler effects are significant to neighboring subcarriers and become negligible when the subcarriers are spaced relatively far apart.

Based on (1) through (4), the achieved SINR on subcarrier $k \in \mathbf{s}$ in cell i, γ^i_k, can be written as

$$\gamma^i_k = \frac{P^i_k \widetilde{G}^i_k}{\sum_{l=1}^{B} \sum_{\substack{k'=1 \\ \text{if } l=i, k'\notin \mathbf{s}}}^{N_c} P^l_{k'} \widetilde{G}^l_{k,k'}(\cdot) + n}, \tag{5}$$

where $\widetilde{G}^i_k = G^i_k |H^i_k|^2$ is the weighted gain on the "desired" link for subcarrier $k \in \mathbf{s}$, $\widetilde{G}^l_{k,k'}(\cdot) = G^l_{k,k'} |H^l_{k,k'}|^2 |C^l_{k,k'}(\Delta f + \varepsilon_D + \omega)|^2$ is the weighted gain of the interfering link between the transmitter on the link using subcarrier k' and the receiver on the link using subcarrier k, and n is the thermal noise power per subcarrier. As MAI in DL is not considered, in the case of DL SINR calculation when $i = l$ and $k' \notin \mathbf{s}$, $\widetilde{G}^l_{k,k'}(\cdot) = 0$.

It should be noted that this study assumes that adaptive modulation is in place. For each γ^i_k, $\overline{\gamma}_k$ is assigned, where $\overline{\gamma}_k$ is the target SINR of subcarrier k, such that $\overline{\gamma}_k \leq \gamma^i_k$ and $\overline{\gamma}_k \in \{\widetilde{\gamma}_1 < \widetilde{\gamma}_2 < \cdots < \widetilde{\gamma}_m\}$. Furthermore, suppose that a number of m discrete transmission rates are available, $r_k \in \{r_1 < r_2 < \cdots < r_m\}$ depending on the modulation alphabet, where each SINR target element corresponds to each rate, respectively. Employing adaptive modulation, if a subcarrier has high SINR, high data rate for the same bit error ratio (BER) can be maintained on that subcarrier, simply by using a high-order modulation scheme.

3. SCHEDULING ALGORITHMS

This section treats the GRP and OTA-SRR scheduling algorithms and their adaptation to OFDMA based on the SINR equation formulated in Section 2.

3.1. Modified GRP

GRP is a simple heuristic scheduling algorithm, which formulates the problem of supporting different users with different data rates into a joint power and rate control scheme. GRP allocates high transmission rates to users having high link gains, and hence can be considered a form of water filling. The greedy nature of GRP is exhibited in that the aim is to *maximize throughput* while *minimizing transmit power*. As a result, users with the best link gains are identified and served. Typically, these are the users close to the BS.

An extensive work on GRP for direct sequence CDMA (DS-CDMA) systems is presented in [8], where it was applied to a single cell, using fixed intercell interference. The modified GRP is an iterative algorithm executed by each BS in the network and accounts for both MAI and CCI which are dynamically updated during each iteration. The modified algorithm can be summarized as follows: initially, all subcarriers are assigned maximum available transmit power, then, an iterative procedure begins, where at each iteration step interference is calculated and then the SINR target, power target, and rate target are calculated for all subcarriers and assigned accordingly. Subcarriers which are assigned transmit power higher than the maximum allowed power per subcarrier are blocked. Every single step of the algorithm is first processed by each individual BS before any of the BSs starts processing the subsequent step (pseudoparallel operation). This is repeated until convergence is reached which happens when there are no significant changes (defined as arbitrarily small changes within some interval ϵ) in a feasible SINR target and power target assignment for a series of consecutive iterations. A feasible assignment is an assignment where each assigned SINR target can be achieved while maintaining the maximum power constraint per subcarrier. It should be noted that convergence of the modified GRP algorithm is tested via Monte Carlo simulations, which demonstrate that the algorithm reaches convergence in 50 iterations (not shown). As a safeguard, it is assumed that the algorithm always converges after 100 iterations.

The formulation of the modified GRP utilizes the SINR expression presented in Section 2 and slightly rearranges it to suit the algorithm derivation. Given a vector of powers with elements being the power on each subcarrier, $\mathbf{P} = (P_1, P_2, \ldots, P_{N_c})^T$, the received SINR on subcarrier k, is defined by (6) and (7) for UL and DL, respectively:

$$\gamma_{k,UL} = \frac{P_k G_k |H_k|^2}{\sum_{k'=1,\ k'\notin \mathbf{s}}^{N_c} |S_{k,k'}|^2 |H_{k,k'}|^2 |C_{k,k'}(z)|^2 + P_{CCI,k} + n}, \tag{6}$$

$$\gamma_{k,DL} = \frac{P_k G_k |H_k|^2}{P_{CCI,k} + n}, \tag{7}$$

where $\gamma_{k,\mathrm{UL}}$ and $\gamma_{k,\mathrm{DL}}$ are the SINR on subcarrier k in UL and DL, respectively, $z = \Delta f + \varepsilon_{\mathrm{D}} + \tau$, $|S_{k,k'}|^2 = P_{k'} G_{k,k'}$, and $P_{\mathrm{CCI},k}$ is the received CCI power on subcarrier k. Note that all parameters belong to the same cell, thus superscripts used earlier to indicate cell index are omitted, and further, $G^l_{k,k'}|H^l_{k,k'}|^2|C^l_{k,k'}(z)|^2$ is used instead of $\widetilde{G}^l_{k,k'}(\cdot)$.

Classical water-filling approaches have been intensively studied in literature (e.g., in [11, 12] and the references therein). However, in the light of the recent research initiatives on *green radio*, an interesting question is to find a method of throughput maximization while minimizing total power, for which, to the best knowledge of the authors, no closed-form solution exists. Hence, a heuristic algorithm is employed that finds an SINR target assignment and a power assignment, which results in maximum achievable throughput realized with minimum power.

If it is assumed that subcarriers are allocated discrete SINR targets from the target set $\mathbf{\Gamma}$, many ways exist in which these targets can be assigned, such that the same throughput is maintained; however, it is interesting to obtain an assignment which minimizes the total power. The problem of minimizing the total power for a given sum rate $\widetilde{R}$ can be expressed mathematically as given below, assuming that $\overline{p}$ is the maximum power allowed per subcarrier and using each $\overline{\gamma}_k$ corresponds to an r_k belonging to the set of rates, as defined in Section 2:

$$\min \sum_{k=1}^{N_{\mathrm{c}}} P_k \tag{8}$$

subject to the following constraints:

$$\overline{\gamma}_k \in \mathbf{\Gamma}, \quad \mathbf{\Gamma} = \{0, \widetilde{\gamma}_1, \widetilde{\gamma}_2, \ldots, \widetilde{\gamma}_m\}, \tag{9}$$

$$0 \le P_k \le \overline{p}, \tag{10}$$

$$\sum_{k=1}^{N_{\mathrm{c}}} r_k = \widetilde{R}. \tag{11}$$

Now, assuming that there exists an SINR target assignment which fulfills (9), (10), and (11), an important corollary is used, which is proved for CDMA [8] and can be analogously proved for an OFDMA system (proof not shown), *viz.*

Corollary 1. *If the subcarriers are arranged at each BS according to the weighted link gains, $G_1|H_1|^2 \ge G_2|H_2|^2 \ge \cdots \ge G_{N_{\mathrm{c}}}|H_{N_{\mathrm{c}}}|^2$, the total power in the cell is minimized for a given throughput if the SINR targets are reassigned such that $\overline{\gamma}_1 \ge \overline{\gamma}_2 \ge \cdots \ge \overline{\gamma}_{N_{\mathrm{c}}}$.*

In other words, while maintaining a given sum rate, minimum total power is used if the subcarriers are ordered according to their link gains (best link gain first) and the SINR targets are reassigned in descending order.

An interesting question now is to obtain the maximum possible rate (or throughput) which can be achieved by the system (i.e., taking a best-effort approach), while at the same time ensuring that this is done with minimum power. This problem is solved heuristically by the GRP, which assigns the highest possible SINR target from the target set to each subcarrier in order to maximize throughput, while power is minimized according to Corollary 1. The details of the modified GRP derivation can be found in Appendix A, while the pseudocode of the algorithm is shown in Algorithm 1.

3.2. Modified OTA-SRR

The OTA-SRR is a scheduling algorithm which jointly allocates rate and power. Zander and Kim introduce the stepwise removal algorithm in [13]. Later in [7], Ginde presents the OTA-SRR which is based on the stepwise removal algorithm, and also includes optimization criteria. OTA-SRR aims to maximize the sum of SINR values of the users in a cellular system. The requirements for this maximization are identified by the OTA, which is then the basis for a linear programming problem, solved by the SRR algorithm. The algorithm starts off with assigning all users maximum SINR target out of a predefined set. Then, the users, which experience maximum interference, are identified and their SINR target is decreased in a step-wise manner until the system satisfies the conditions identified by the OTA. Unlike the GRP, which aims to maximize throughput while minimizing power and hence serves the best-placed users in terms of link gain, the OTA-SRR exhibits fairness in that there is no power minimization constraint. As a consequence, all users are initially assigned maximum rate. Rates are then iteratively reduced based on achieved SINR until the system is in a feasible steady state.

In this paper, the aforementioned scheduling scheme is formulated as a subcarrier, rate, and power allocation algorithm for OFDMA systems. An essential part of this new formulation is the SINR equation. This enabled us to directly apply the existing algorithm constraints and derivations. The modified OTA-SRR is summarized as follows: initially, each user gets a number of subcarriers (depending on the number of users in the cell) with maximum SINR targets, out of a predefined set, assigned to all subcarriers. Under the assumption of a moderately loaded or overloaded system, not all users can support the assigned SINR targets. Iteratively, the subcarriers, which experience maximum interference, are identified, and their SINR target is decreased in a step-wise manner, in an effect adapting the modulation scheme. If the SINR target of a subcarrier is downrated below the minimum value from the target set, the subcarrier is given to a different user from the same BS, such that interference on the subcarrier is minimized. If such user is not found, the subchannel is not used. OTA-SRR is executed until the system reaches feasibility according to the constraints presented in this section.

The algorithm takes into account the interference effects among all subcarriers, thus each subcarrier (out of the total considered in the algorithm, i.e., $BN_{\mathrm{c}} = N$) is given a unique identification (ID) in the range $[1, 2, \ldots, N]$ (i.e., subcarrier one used in cell one has ID 1, subcarrier one in cell two has ID $N_{\mathrm{c}} + 1$, subcarrier two used in cell two has ID $N_{\mathrm{c}} + 2$, etc.). Based on this, the SINR equation given in (5) can be rewritten as

$$\gamma_k = \frac{P_k \widetilde{G}_k}{\sum_{k'=1,\ k' \notin \mathbf{s}}^{N} P_{k'} \widetilde{G}_{k,k'} + n}. \tag{12}$$

(1) $\overline{\gamma}_k = 0$ and $P_k = \overline{p}\ \forall k$

(2) Compute $P_{\mathrm{CCI},k}\ \forall k$ and $\underbrace{\sum_{k'=1,\ k' \notin \mathbf{s}}^{N_c} |S_{k,k'}|^2 |H_{k,k'}|^2 |C_{k,k'}(z)|^2}_{\mathrm{MAI}}\ \forall k$ in UL

(3) **for** $k = 1$ **to** N_c **do**

(a) **if** subcarrier k is in UL **then**:

$$\overline{\gamma}_k := \left\{ \max_{\overline{\gamma}_k \in \mathbf{\Gamma}} (\overline{\gamma}_k) : \sum_{k'=1}^{k} \frac{\overline{\gamma}_{k'} |C_{k,k'}(z)|^2}{1 + \overline{\gamma}_{k'} |C_{k,k'}(z)|^2} \le 1 - \frac{\overline{\gamma}_k \sum_{k'=1}^{k} (\overline{\gamma}_{k'} |C_{k,k'}(z)|^2 (P_{\mathrm{CCI},k'} + n)/(1 + \overline{\gamma}_{k'} |C_{k,k'}(z)|^2))}{(1 + \overline{\gamma}_k) \overline{p} G_k |H_k|^2 - \overline{\gamma}_k (P_{\mathrm{CCI},k} + n)} \right\}$$

$$P_k = \frac{\overline{\gamma}_k}{(1 + \overline{\gamma}_k) G_k |H_k|^2} \left(\frac{\sum_{k'=1}^{N_c} (\overline{\gamma}_{k'} |C_{k,k'}(z)|^2 (P_{\mathrm{CCI},k'} + n)/(1 + \overline{\gamma}_{k'} |C_{k,k'}(z)|^2))}{1 - \sum_{k'=1}^{N_c} (\overline{\gamma}_{k'} |C_{k,k'}(z)|^2 / (1 + \overline{\gamma}_{k'} |C_{k,k'}(z)|^2))} + P_{\mathrm{CCI},k} + n \right)$$

(b) **if** subcarrier k is in DL **then**:

$$\overline{\gamma}_k := \left\{ \max_{\overline{\gamma}_k \in \mathbf{\Gamma}} (\overline{\gamma}_k) : \overline{\gamma}_k \le \left\lfloor \frac{\overline{p} G_k |H_k|^2}{P_{\mathrm{CCI},k} + n} \right\rfloor \right\}$$

$$P_k = \frac{\overline{\gamma}_k}{G_k |H_k|^2} (P_{\mathrm{CCI},k} + n)$$

(4) **end**

(5) Update the transmit power, SINR (and respective rate) assignment for all subcarriers

(6) **if** $P_k > \overline{p}\ \forall k$ **then**:
Block subcarrier k

(7) **if** SINR assignment feasible **then**:
Keep power assignment and SINR assignment

(8) **else**
go to 2

Algorithm 1: Modified GRP.

Note that (12) and (5) differ in their representation only. By dividing the numerator and denominator of the right-hand side of (12) by $\widetilde{G}_k$ and transforming it into matrix notation, (12) can be rewritten as

$$(\mathbf{I} - \mathbf{\Phi})\mathbf{P} \ge \boldsymbol{\eta}, \tag{13}$$

where $\mathbf{I}$ is the identity matrix, $\mathbf{\Phi}$ is the normalized link gain matrix (with dimensions $N \times N$), defined as

$$\Phi_{k,k'} = \frac{\overline{\gamma}_k \widetilde{G}_{k,k'}(\cdot)}{\widetilde{G}_k}, \tag{14}$$

and $\boldsymbol{\eta}$ is the normalized noise vector, given as

$$\eta_k = \frac{\overline{\gamma}_k n}{\widetilde{G}_k}, \tag{15}$$

with $\overline{\gamma}_k \in \mathbf{\Gamma}$, for all $k \in N$. The inequality in (13) holds as each subcarrier strives to achieve SINR greater or equal to the target. The OTA constraints on the algorithm are defined based on the properties of $\mathbf{\Phi}$ and its dominant eigenvalue λ_1 (real, positive, and unique, according to the Perron-Frobenius theorem [14]). For $\mathbf{\Phi}$, it holds that it is real, nonnegative, and irreducible, that is, the path gains and the SINR targets are real and nonnegative, and the path gains are assumed to be uncorrelated. A solution for the system inequality given in (13) exists, only if the right-hand side of $\mathbf{P} \ge (\mathbf{I} - \mathbf{\Phi})^{-1}\boldsymbol{\eta}$ converges. The conditions for convergence of the modified OTA-SRR algorithm are presented in Appendix B and the algorithm is shown in Figure 2.

4. SIMULATION MODEL

The simulation model considers an OFDMA-TDD network with a total of 200 uniformly distributed users in a 19-cell region, where each cell has a centrally-located BS. However, a best-effort full-buffer system is in place, which means that all users demand service at all times and the quality of service (QoS) desired by a user corresponds to the maximum data rate it can support. TDD is modeled by assuming a single time slot, where each BS is assigned to either UL or DL, and UL:DL ratios of 1:1, 1:6, and 6:1 are explored. In the case of RTSO, the UL/DL time slot assignment is asynchronous among cells and the assignment of each cell is random with probability depending on the asymmetry ratio studied. When FSA is in place, all cells are synchronously assigned UL or DL with the same probability, thereby modeling symmetric traffic. Here, it should be noted that channel allocation and scheduling are two disjoint processes, so that after each BS has been assigned to either UL or DL, scheduling takes place. A quasistatic model is employed where the link gains between transmitters and receivers remain unchanged for a time slot duration. A BS-MS pair (i.e., a link) is formed based on minimum path loss. The system parameters used in the simulation are shown in Table 1. Note that because of the snapshot nature of the simulation, MSs appear static. However, Doppler frequency offset errors and offset errors due to synchronization are accounted for by using constant offset values. In particular, Doppler frequency offset corresponding to a speed of 30 km/h and 50% synchornization offset are

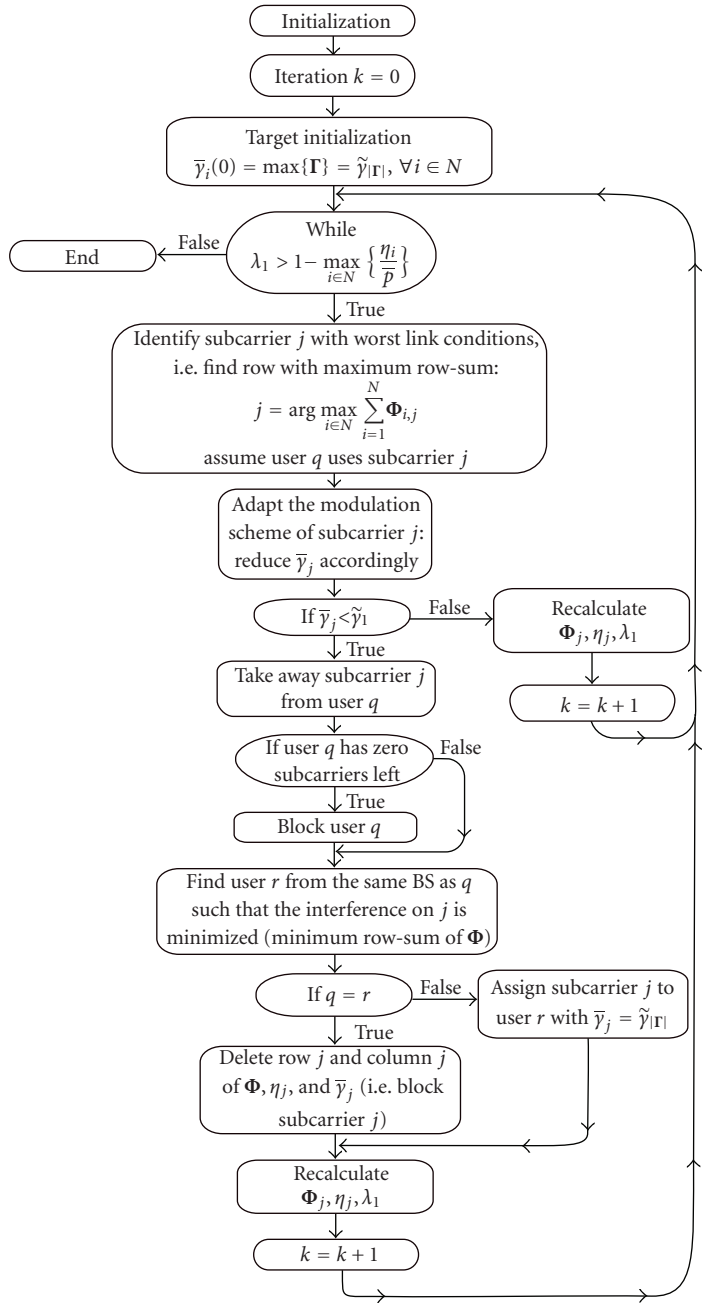

Figure 2: Flowchart of the modified OTA-SRR algorithm.

used. The latter value is chosen to reflect a severe interference scenario (e.g., [15] report ≈30% offset).

The small-scale fading effects are simulated via a Monte Carlo method [16], which takes into consideration the effects of Doppler shift and time delay. A power delay profile is used corresponding to the specified delay spread in Table 1 [17]. It is assumed that a proper cyclic prefix is in place such that intersymbol interference (ISI) is avoided. The path loss model to account for large-scale fading is chosen accordingly, [18]—Terrain Category A (suburban), shown as follows:

$$P_{\mathrm{L}} = 20 \log_{10}\left(\frac{4\pi d_0 f}{c}\right) + 10\xi \log_{10}\left(\frac{d}{d_0}\right) + X_\sigma \ [\mathrm{dB}], \tag{16}$$

where d_0 is the reference distance in meters, f is the carrier frequency, c is the speed of light (3×10^8 m/s), ξ is the path loss exponent, d is the transmitter-receiver

Table 1: Fixed parameters.

Number of BSs	19	Number of MSs	200
Cell radius	500 m	Bandwidth	100 MHz
Number of subcarriers	2048	RMS delay spread	0.27 μs
Carrier frequency	1.9 GHz	Maximum Doppler frequency	190 Hz
Maximum power per link	2 W	Freq. offset due to synchronization	0.5

separation distance in meters, and X_σ is a zero-mean normally distributed random variable. The path loss in (16) is lower-bounded by the free space path loss [9], $\widetilde{P}_{\mathrm{L}}$, given by

$$\widetilde{P}_{\mathrm{L}} = 20\log_{10}\left(\frac{4\pi f}{c}\right) + 20\log_{10}(d)\ [\mathrm{dB}]. \tag{17}$$

Results for a system with NLOS conditions for all TDD interference scenarios (MS → BS, BS → MS, BS → BS, MS → MS) are compared against results for an equivalent system where LOS in the case of BS → BS interference is assumed (and NLOS for the remaining scenarios). The path loss in the case of LOS is calculated using the free space path loss model, given in (17); and the worst-case scenario is assumed with 100% probability of LOS. Adaptive modulation is achieved with seven different modulation schemes [19] given in Table 2, based on the received SINR for a BER of 10^{-7} (necessary for real-time services such as video streaming). The corresponding data rates, Υ, are calculated using $\Upsilon = M\Upsilon_{\mathrm{code}}/T_{\mathrm{s}}$, where M is the number of bits per symbol, Υ_{code} is the code rate (here, 2/3), and T_{s} is the symbol time (including cyclic prefix of 20%). Note that the *cross* and *star* constellations are QAM variations in order to ensure robustness to interference, as described in [20, 21], respectively.

5. RESULTS AND DISCUSSION

The algorithms implemented in this study are evaluated on the basis of three metrics, *viz spectral efficiency*, *subcarrier utilization*, and *user outage*, described below. *Spectral efficiency* is the achieved system throughput divided by the total bandwidth divided by the number of BSs, *subcarrier utilization* is the number of subcarriers used in the system, divided by the total number of subcarriers (number of subcarriers per BS times the number of BSs), and *user outage* is defined as the users not served (assigned zero subcarriers) as a fraction of the total number of users in the system. All metrics pertain to the whole system, that is, UL and DL combined, unless stated otherwise. In addition, as mentioned in Section 4, a TDD system is simulated assuming a single time slot which is either assigned to UL or DL traffic. This means that for every time slot a different user distribution is analyzed. Since TDD can essentially be characterized as a half-duplex system, this is deemed a sensible approach in order to obtain insightful statistical results on essential system metrics.

The variation of spectral efficiency with asymmetry and LOS conditions for the BSs can be seen in Figures 3(a) and 3(b) for the modified OTA-SRR and the modified GRP, respectively. A clear trend can be observed for both scheduling schemes. In particular, with an increase in the number of time slots allocated to DL, the spectral efficiency increases and reaches 90% of the theoretical maximum, which is $(\Upsilon_{\max} \times N_{\mathrm{c}} \times B/W)/B = \Upsilon_{\max}/W_{\mathrm{c}} = 4.44$ bps/Hz/cell, where W is the system bandwidth, W_{c} is the bandwidth per subcarrier, and $\Upsilon_{\max}$ is the maximum data rate per subcarrier (as given in Table 2). Moreover, Figures 3(a) and 3(b) show that LOS conditions among BSs degrade performance significantly. For an asymmetry of 6:1 (UL:DL), the spectral efficiency at the 50th percentile for OTA-SRR and GRP decreases by ≈30% and ≈50%, respectively. In contrast, the systems employing DL-favored asymmetry are more robust to LOS among BSs. The difference between the spectral efficiency achieved by the NLOS system and the LOS system for an asymmetry of 1:6 (UL:DL) amounts to ≈8% and ≈6% at the 50th percentile for OTA-SRR and GRP, respectively. This observation is as expected, due to the fact that in DL-favored asymmetries, the occurrence of BS → BS interference is significantly limited. It is interesting to note, however, that in terms of spectral efficiency, OTA-SRR is considerably more robust to the detrimental BS → BS interference during UL-favored asymmetries than GRP. The algorithms' "robustness" tends to equalize as the asymmetry becomes in favor of DL. The fact that GRP is more sensitive to interference can be explained by its mechanism: GRP identifies the few best-placed users (in terms of path loss) to be served with the highest achievable data rates. With a deterioration in the interference conditions, there is a severe reduction in the number of best-placed users and the data rates that these users can achieve. In contrast, OTA-SRR tries to serve all users, giving each user only the subcarriers that they can utilize. Thus, OTA-SRR adapts to the overall interference and that is why the degradation of performance is not as severe as in the case of GRP.

The outage results shown in Figures 4(a) and 4(b) for OTA-SRR and GRP, respectively, display a similar trend in terms of the comparative performance of the greedy and fair algorithms. Furthermore, the results demonstrate that allocating more resources to DL improves the outage performance and this result is valid for both scheduling algorithms. A comparison between the outage and spectral efficiency results suggests that the relative performance degradation due to LOS is smaller in the case of outage than in the case of spectral efficiency. This is due to employing adaptive modulation, which allows for various SINR levels to be used before discarding a subcarrier. As a consequence, an

Table 2: Adaptive modulation parameters for BER of 10^{-7}.

Modulation scheme	4 QAM	8 star	16 QAM	32 cross	64 QAM	128 cross	256 QAM	
Data rate	54.24	81.37	108.49	135.61	162.73	189.86	216.98	kbps
SINR	9	14	16	19	22.2	25	28.5	dB

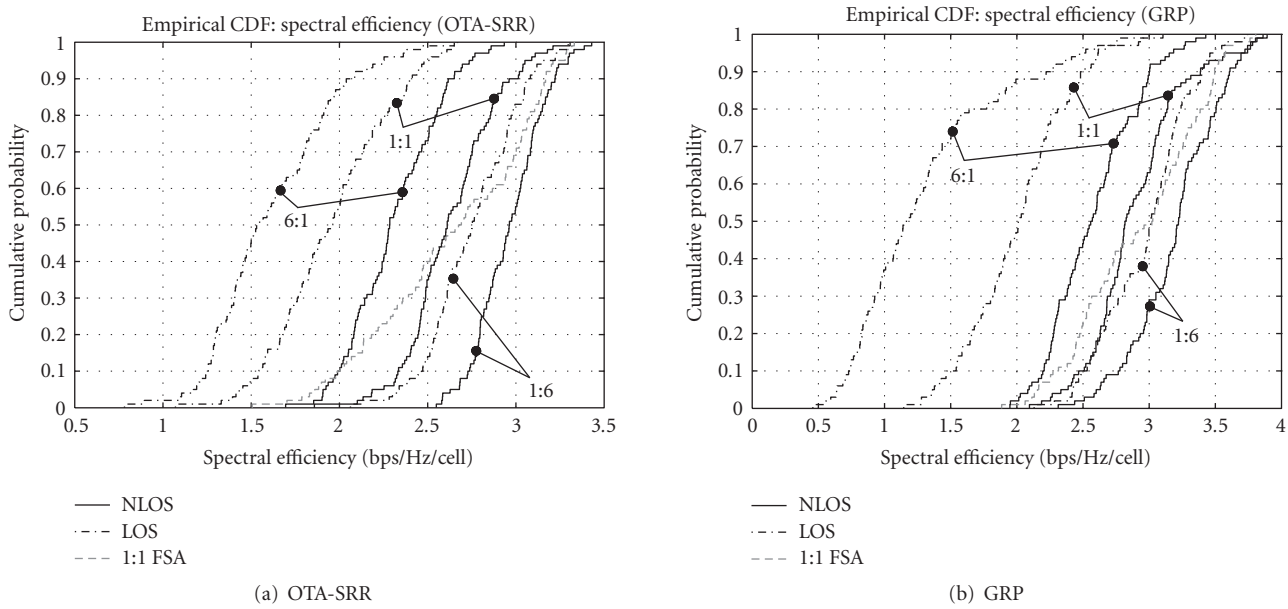

(a) OTA-SRR (b) GRP

Figure 3: *Spectral efficiency* [bps/Hz/cell] attained by the OTA-SRR and GRP for various UL:DL ratios for cases of LOS and NLOS among BSs. The spectral efficiency is the total throughput in the system divided by the total bandwidth divided by the number of cells.

LOS system could serve approximately the same number of users as an NLOS system (given that all other parameters are the same), but with fewer subcarriers and significantly lower data rates, due to the increased interference. Furthermore, the outage results demonstrate that in the case of OTA-SRR (at the 50th percentile), between ≈57% and ≈83% (at the 50th percentile) of the users are not served, whereas GRP puts between ≈80% and ≈92% of the users into outage. As expected, the fair algorithm offers service to a larger population than the greedy algorithm. It should be noted the outage metric is a relative metric, used for comparison purposes only. The low percentage of served users is due to the severe interference conditions considered.

The overall trends discussed above are also seconded by the subcarrier utilization results presented in Figures 5(a) and 5(b). In addition, it is interesting to note that at the 50th percentile, OTA-SRR utilizes between ≈65% and ≈97% of the available subcarriers, while GRP utilizes between ≈40% and ≈90% of the subcarriers. The fact that OTA-SRR utilizes more subcarriers is not surprising due to the algorithm's fair nature. As previously mentioned, OTA-SRR tries to serve as many users as possible, while utilizing as many subcarriers as possible, while GRP chooses only the "best-placed" users with the "best" channels.

So far, the results have demonstrated superiority in the performance of DL as compared to UL for all considered metrics. In order to gain insight into the factors that influence the performance of UL and DL, the spectral efficiency performance of UL and DL is studied separately. Results are presented in Figure 6 assuming an UL:DL asymmetry of 1:1 for the following systems, employing RTSO: an OTA-SRR system with NLOS conditions, an OTA-SRR system with LOS conditions among BSs, an ideal OTA-SRR system, and a benchmark system. The *benchmark system* considers neither frequency offset errors nor Doppler errors, that is, it is a purely orthogonal system where the only source of interference is CCI. The resources are allocated randomly at the beginning of each iteration and the SINR per subcarrier is calculated. If the SINR of a particular subcarrier is below the minimum required threshold (Table 2), the subcarrier is discarded and not utilized. If all subcarriers, allocated to a particular user, are discarded, the user is put into outage. The SINR of the subcarriers that can maintain a successful link is used to determine their respective data rates and the spectral efficiency of the system. The *ideal system* is also a purely orthogonal system but, unlike the benchmark system, has resource allocation and adaptive modulation in place. Figure 6 suggests that the spectral efficiency achieved with the benchmark system is the worst, which is as expected because the absence of a scheduling mechanism does not allow for frequency selectivity to be adequately exploited. Moreover, in all cases, DL performs better than UL.

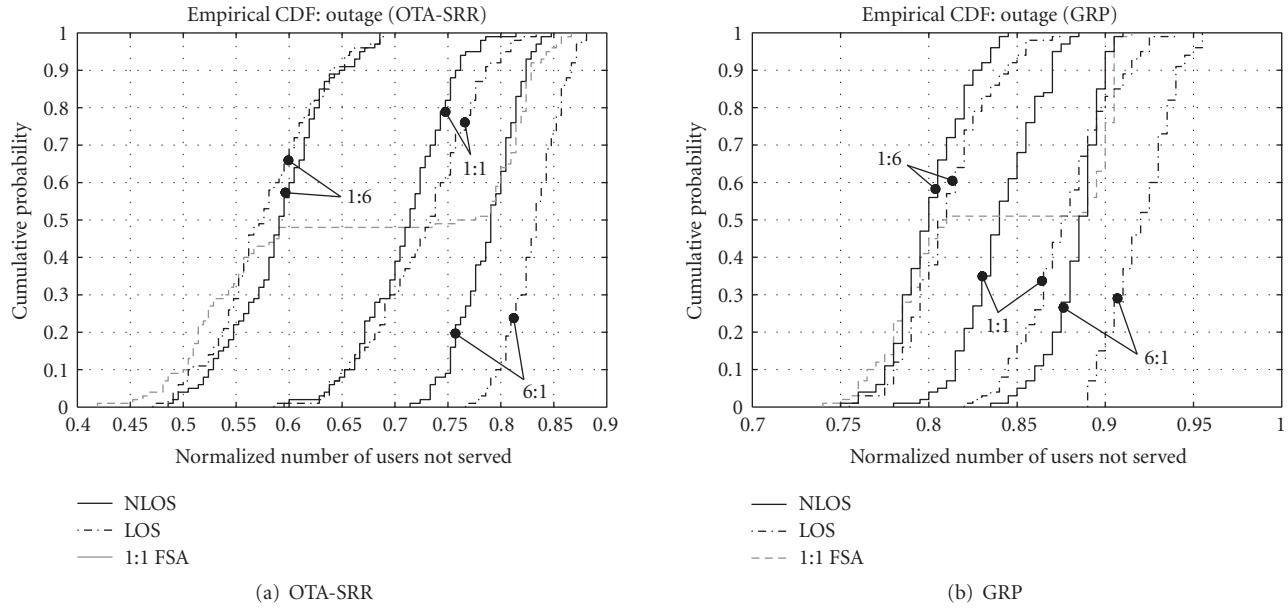

(a) OTA-SRR (b) GRP

Figure 4: *Outage* exhibited by the OTA-SRR and GRP for various UL:DL ratios for cases of LOS and NLOS among BSs. Outage is the ratio of the number of users which are not served to the total number of users in the system.

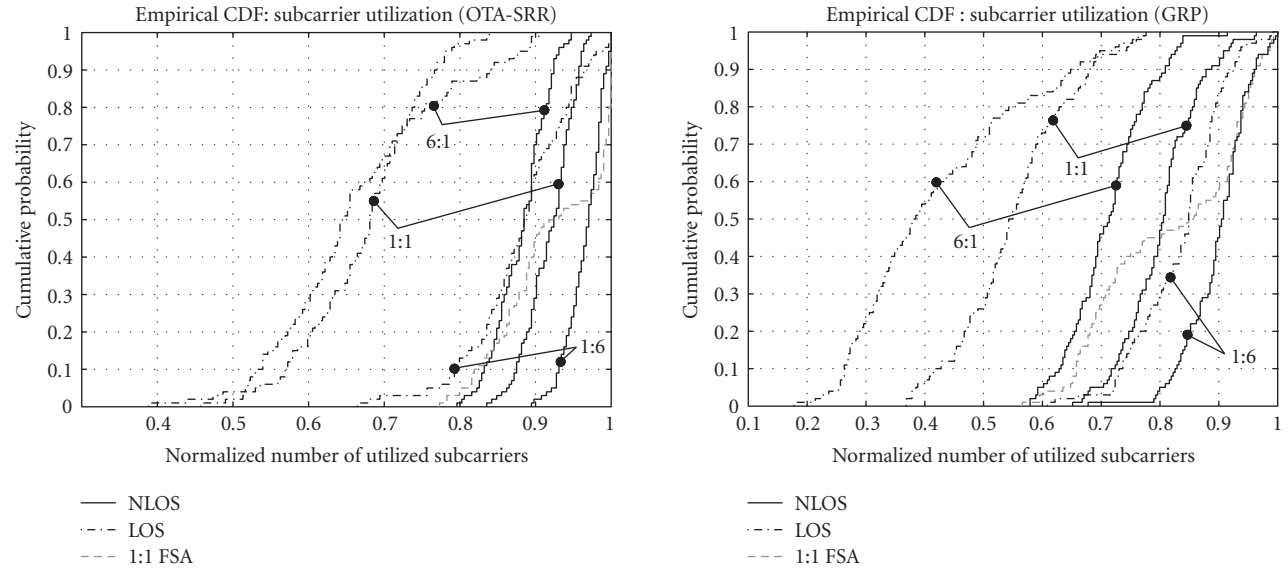

(a) OTA-SRR (b) GRP

Figure 5: *Subcarrier utilization* attained by the OTA-SRR and GRP for various UL:DL ratios for cases of LOS and NLOS among BSs. Subcarrier utilization is the ratio of the number of subcarriers in the system that are used for transmission (i.e., the assigned data rate is greater than (0) to the total number of subcarriers in the system, $N_c \times B$.

This is expected due to the presence of MAI in UL and the lack thereof in DL. In addition, in UL, there is BS → BS and MS → BS interference, while BS → MS and MS → MS interference is characteristic for the DL. For the benchmark system, the difference between UL and DL is about 0.5 bps/Hz/cell at the 50th percentile. In the case of the ideal system, DL only marginally outperforms UL, which is as expected, because frequency selectivity is adequately exploited. However, the difference in UL/DL performance gets more pronounced as LOS conditions for the BSs and offset errors are introduced, that is, in the case of the LOS system and NLOS system, respectively. DL is more favorable in terms of interference, due to the synchronous nature of point-to-multipoint communication and the fact that as the MSs are the receiving units, the detrimental BS → BS LOS effects are not present. Thus, the system

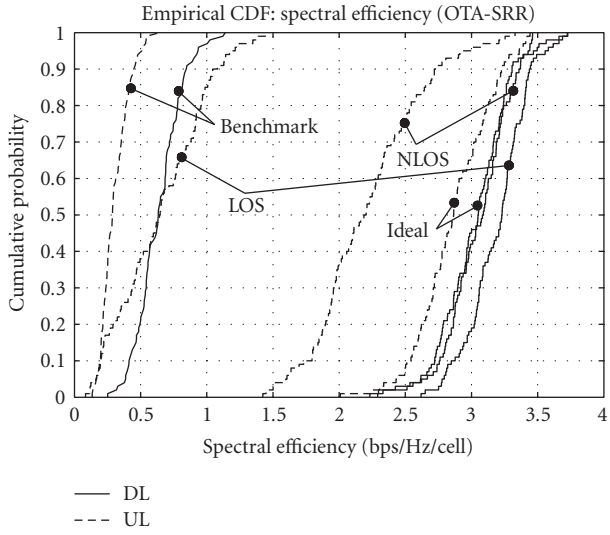

Figure 6: UL and DL spectral efficiency attained by OTA-SRR for UL:DL ratio of 1:1.

performance is expected to improve as the asymmetry is shifted in favor of DL, which is in line with the observed results (Figures 3(a) and 3(b)). It is interesting to note, however, that contrary to intuition, DL LOS performs better than DL NLOS. The reason lies in the mechanism of the OTA-SRR algorithm, which operates on all subcarriers (in the cells under consideration) simultaneously. As already discussed, the UL overall performs worse than DL; and this performance gap is enhanced when LOS conditions are considered. Consequently, in an LOS system, the SINR targets of UL subcarriers generally get down rated before the DL subcarriers. As a result, UL subcarriers are discarded before the DL subcarriers. This means that the dimension of the normalized link gain matrix is decreased, which in turn makes the convergence of the algorithm faster. Fast convergence means fewer iterations of step-wise-rate removal, which in turn means fewer-rate removals. As a result, higher data rate per subcarrier is achieved, and, thus, a system is obtained which achieves better spectral efficiency on the DL than an equivalent NLOS system.

In an FSA network, on the other hand, LOS conditions among BS do not cause interference, due to the synchronized UL/DL switching point across the network. Thus, intuitively, it is expected that a symmetric FSA scheme exhibits better performance than an equivalent RTSO system, since it avoids the detrimental BS → BS interference, as well as the MS → MS interference. However, it can be observed that neither of the schemes is strictly better than the other. For instance, assuming OTA-SRR (Figure 3(a)), it can be found that for RTSO, the probability that the spectral efficiency is greater than 2.25 bps/Hz/cell is about 95%, whereas for FSA, this probability is only about 75%. On the other hand, when assuming a spectral efficiency of 3 bps/Hz/cell, it can be found that the same probability for RTSO is 10%, whereas the probability for FSA is 30%. As expected, their medians generally coincide due to the fact that the rate of asymmetry is the same, and, moreover, the FSA curve spans between the 1:6 (DL-dominated) NLOS and 6:1 (UL-dominated) NLOS RTSO cases. The latter effect is attributed to the shifting of more resources to UL (DL), which creates an interference scenario (MS → BS (BS → MS)) similar to the UL (DL) FSA. Furthermore, it can be observed from all results that the cumulative density function (cdf) graphs for FSA are generally spread out, whereas the cdf graphs for RTSO are comparatively steeper. This means that RTSO offers a more stable and robust QoS, while the QoS offered by the FSA is with larger variation.

An interesting observation can be made with regard to the outage results (Figures 4(a) and 4(b))—the FSA scheme exhibits a "plateau" behavior (bimodal distribution). This can be explained by the presence of MAI in UL, which creates a significant gap between UL and DL performance. Overall, it is observed that the RTSO can successfully exploit interference diversity and thus outperform the FSA scheme in certain scenarios for the same asymmetry. Moreover, shifting more resources in favor of DL achieves better performance than a symmetric FSA system. For example, at a spectral efficiency of 3 bps/Hz/cell, the gain compared to a symmetric UL/DL usage and FSA is about 20% (Figure 3(a)).

With respect to the comparative performance of the two scheduling schemes presented in this paper, the results show a similar trend in the explored metrics. However, GRP, which allocates subcarrier, rate, and power in a greedy manner, achieves only a marginal increase in spectral efficiency at the cost of outage, as compared to the fair OTA-SRR. It is interesting to relate these trends to a similar study done for a CDMA system in [22] with the same cell radius, number of cells, number of users as in the present study. In the case of CDMA, the greedy GRP algorithm as compared to the OTA-SRR scheme displays a twofold increase in terms of total system data rate. At the same time, GRP serves only 30% of the users which are served under the OTA-SRR scheme. Thus, unlike CDMA, in an OFDMA system, the fair OTA-SRR approach is more efficient than the greedy GRP approach.

6. CONCLUSIONS

This paper explored UL/DL asymmetry interference aspects in multicellular multiuser OFDMA-TDD systems considering both LOS and NLOS conditions among BSs, when jointly applying channel allocation and user scheduling. The results demonstrated that under RTSO, UL is the performance limiting factor due to unfavorable interference and the hazardous effect of LOS conditions among BSs. It was, furthermore, shown that shifting more resources in DL provides a system robust to these TDD-inherent problems, which is particularly beneficial as future wireless services are expected to be DL-dominated. Such a DL-favored scenario attained up to 90% of the maximum spectral efficiency achievable by the considered network. In addition, for the same asymmetry, RTSO was found to offer a more stable and robust QoS than FSA. The results also demonstrated that, overall, the fair OTA-SRR scheduling algorithm was more robust to the detrimental TDD-specific BS → BS

interference than the greedy GRP algorithm. Furthermore, the fair OTA-SRR served to up to ≈20% more users, utilizing up to ≈25% more subcarriers, and still achieving spectral efficiencies only marginally lower than those attained by the GRP. Hence, RTSO when combined with OTA-SRR fair scheduling allows the system to retain high spectral efficiency while maintaining fairness in an OFDMA-TDD cellular network with asymmetric traffic.

APPENDICES

A. GRP: TRANSMISSION AND POWER CONSTRAINTS

This section treats the derivation of the transmission and power constraints for the GRP algorithm separately for the cases of DL and UL.

A.1. DL transmission and power constraints

A power minimization problem subject to three constraints was defined in Section 3.1. The first constraint is to choose the SINR targets from the predefined target set $\boldsymbol{\Gamma}$, the second one is to limit the maximum allowed transmit power per subcarrier to $\overline{p}$, and the third one is a constraint on the sum of SINR targets. Given the first two constraints, GRP aims (1) to maximize the achieved throughput by always assigning the maximum possible SINR target from the target set, and (2) to minimize the total power by using Corollary 1. In order to define the DL GRP algorithm, first, the DL problem statement is formulated and then the power constraint and the throughput maximization condition for the case of DL are derived.

The required power, P_k, on a subcarrier k in the DL is given by (A.1), which follows from making P_k the subject of (7). Note that because in DL perfect synchronization is assumed, there is no MAI:

$$P_k = \frac{\overline{\gamma}_k}{G_k|H_k|^2}(P_{\mathrm{CCI},k} + n). \tag{A.1}$$

Hence, the sum of the powers in a cell can be computed as shown below:

$$\sum_{k=1}^{N_c} P_k = \sum_{k=1}^{N_c} \frac{\overline{\gamma}_k}{G_k|H_k|^2}(P_{\mathrm{CCI},k} + n). \tag{A.2}$$

Now the objective function for DL can be expressed as

$$\min\left\{\sum_{k=1}^{N_c} \frac{\overline{\gamma}_k}{G_k|H_k|^2}(P_{\mathrm{CCI},k} + n)\right\}. \tag{A.3}$$

The formulation in (A.3) is subject to a power constraint, which can be expressed mathematically as shown below using (A.1) and limiting the maximum transmit power per subcarrier to $\overline{p}$:

$$\overline{p} \geq \frac{\overline{\gamma}_k}{G_k|H_k|^2}(P_{\mathrm{CCI},k} + n). \tag{A.4}$$

Next, system throughput needs to be maximized. To formulate this for the case of DL, first, the upper bound on $\overline{\gamma}_k$ can be expressed by rearranging (A.4) as follows:

$$\overline{\gamma}_k \leq \frac{\overline{p}G_k|H_k|^2}{P_{\mathrm{CCI},k} + n}. \tag{A.5}$$

This effectively means that for given interference conditions and channel state, the highest SINR target that can be assigned (and achieved) is when the transmit power is maximum. Hence, to maximize throughput, each subcarrier must be assigned the maximum $\overline{\gamma}_k$ from the set $\boldsymbol{\Gamma}$ which satisfies (A.5). Expressed mathematically, the condition for throughput maximization is

$$\max_{\overline{\gamma}_k \in \boldsymbol{\Gamma}}\{\overline{\gamma}_k\} \leq \frac{\overline{p}G_k|H_k|^2}{P_{\mathrm{CCI},k} + n}. \tag{A.6}$$

The modified DL GRP algorithm is developed based on (A.4) and (A.6) and is shown in Section 3.1.

A.2. UL transmission and power constraints

The approach used to formulate the UL GRP algorithm is analogous to the approach used in the case of DL GRP in the previous section.

The required power, P_k, on a subcarrier k in UL is derived using (6), where each side of (6) is multiplied by $|C_{k,k}(z)|^2$. For simplicity, the following notation is used:

$$x_k = P_k G_k |H_k|^2 |C_{k,k}(z)|^2, \qquad y_k = P_{\mathrm{CCI},k} + n, \qquad l_k = \overline{\gamma}_k |C_{k,k}(z)|^2, \tag{A.7}$$

and (6) becomes:

$$l_k = \frac{x_k}{\sum_{k' \notin \mathbf{s}} x_{k'} + y_k}, \tag{A.8}$$

with both y_k and l_k fixed, and x_k to be determined because P_k is of interest. Assuming that $\mathbf{s}$ is composed of only k, the above equation can be rewritten as shown below. Note that this is only a simplifying assumption and does not limit the final result to a particular cardinality of $\mathbf{s}$:

$$l_k = \frac{x_k}{\sum_{k'=1}^{N_c} x_{k'} - x_k + y_k}. \tag{A.9}$$

By rearranging the abovementioned data, x_k can be obtained as

$$x_k = \frac{l_k}{1 + l_k}\left(\sum_{k'=1}^{N_c} x_{k'} + y_k\right). \tag{A.10}$$

Next, (A.10) is summed over k and the result is used to substitute $\sum_{k'=1}^{N_c} x_{k'}$ in (A.10) to obtain

$$x_k = \frac{l_k}{1 + l_k}\left(\frac{\sum_{k'=1}^{N_c}(l_{k'} y_{k'}/(1 + l_{k'}))}{1 - \sum_{k'=1}^{N_c}(l_{k'}/(1 + l_{k'}))} + y_k\right). \tag{A.11}$$

Now substitution for x_k, y_k, and $l_k$and simplification yield

$$P_k = \frac{\overline{\gamma}_k}{(1+\overline{\gamma}_k|C_{k,k}(z)|^2)G_k|H_k|^2} \times \left(\frac{\sum_{k'=1}^{N_c}(\overline{\gamma}_{k'}|C_{k,k'}(z)|^2(P_{\mathrm{CCI},k'}+n)/(1+\overline{\gamma}_{k'}|C_{k,k'}(z)|^2))}{1-\sum_{k'=1}^{N_c}(\overline{\gamma}_{k'}|C_{k,k'}(z)|^2/(1+\overline{\gamma}_{k'}|C_{k,k'}(z)|^2))} + P_{\mathrm{CCI},k} + n\right). \tag{A.12}$$

Note that (A.12) contains $|C_{k,k}(z)|^2$, which is the special case of $|C_{k,k'}(z)|^2$ when k and k' belong to the same user and are the same subcarrier. (Technically, it could also be the case that a subcarrier is reused at a given BS, but this situation is not of interest, as reuse one is assumed here.) Whenever that is the case, there are no errors due to Doppler and no frequency offset errors, and in addition $k-k=0$, hence z is 0. It can be shown that as $z \to 0$, $|C_{k,k'}(z)|^2 \to 1$ (refer to Appendix C). Therefore, using $|C_{k,k}(z)|^2 = 1$, the required power on a subcarrier k can be expressed as

$$P_k = \frac{\overline{\gamma}_k}{(1+\overline{\gamma}_k)G_k|H_k|^2} \times \left(\frac{\sum_{k'=1}^{N_c}(\overline{\gamma}_{k'}|C_{k,k'}(z)|^2(P_{\mathrm{CCI},k'}+n)/(1+\overline{\gamma}_{k'}|C_{k,k'}(z)|^2))}{1-\sum_{k'=1}^{N_c}(\overline{\gamma}_{k'}|C_{k,k'}(z)|^2/(1+\overline{\gamma}_{k'}|C_{k,k'}(z)|^2))} + P_{\mathrm{CCI},k} + n\right). \tag{A.13}$$

Now using (A.13), the objective function for UL is formulated as

$$\min\left\{\sum_{k=1}^{N_c}\frac{\overline{\gamma}_k}{(1+\overline{\gamma}_k)G_k|H_k|^2} \times \left(\frac{\sum_{k'=1}^{N_c}(\overline{\gamma}_{k'}|C_{k,k'}(z)|^2(P_{\mathrm{CCI},k'}+n)/(1+\overline{\gamma}_{k'}|C_{k,k'}(z)|^2))}{1-\sum_{k'=1}^{N_c}(\overline{\gamma}_{k'}|C_{k,k'}(z)|^2/(1+\overline{\gamma}_{k'}|C_{k,k'}(z)|^2))} + P_{\mathrm{CCI},k} + n\right)\right\}. \tag{A.14}$$

As in DL, it is assumed that the maximum transmit power allowed on each subcarrier is $\overline{p}$, however, it should be noted that $\overline{p}$ can be different for UL and DL. Then, the constraint on the UL can be expressed as $P_k \le \overline{p}$ and using the expression for P_k in (A.13) and rearranging it, the UL power constraint can be expressed as

$$\sum_{k'=1}^{N_c}\frac{\overline{\gamma}_{k'}|C_{k,k'}(z)|^2}{1+\overline{\gamma}_{k'}|C_{k,k'}(z)|^2} \le 1-\frac{\overline{\gamma}_k\sum_{k'=1}^{N_c}(\overline{\gamma}_{k'}|C_{k,k'}(z)|^2(P_{\mathrm{CCI},k'}+n)/(1+\overline{\gamma}_{k'}|C_{k,k'}(z)|^2))}{(1+\overline{\gamma}_k)\overline{p}G_k|H_k|^2-\overline{\gamma}_k(P_{\mathrm{CCI},k}+n)}. \tag{A.15}$$

Now, note that for given $\overline{\gamma}_k$, G_k, and $|H_k|^2$, the expression in (A.14) is minimized when $1-\sum_{k'=1}^{N_c}(\overline{\gamma}_{k'}|C_{k,k'}(z)|^2/(1+\overline{\gamma}_{k'}|C_{k,k'}(z)|^2))$ is maximized which is equivalent to minimizing the left-hand side of (A.15), that is, $\sum_{k'=1}^{N_c}(\overline{\gamma}_{k'}|C_{k,k'}(z)|^2/(1+\overline{\gamma}_{k'}|C_{k,k'}(z)|^2))$. This equivalence holds because

$$\sum_{k'=1}^{N_c}\frac{\overline{\gamma}_{k'}|C_{k,k'}(z)|^2}{1+\overline{\gamma}_{k'}|C_{k,k'}(z)|^2} < 1, \tag{A.16}$$

due to the fact that $\overline{\gamma}_{k'}|C_{k,k'}(z)|^2$ is always greater than or equal to 0. Hence, the minimization of the left-hand side of (A.15) can be expressed as

$$\sum_{k'=1}^{N_c}\frac{\overline{\gamma}_{k'}|C_{k,k'}(z)|^2}{1+\overline{\gamma}_{k'}|C_{k,k'}(z)|^2} \le 1-\max\left\{\frac{\overline{\gamma}_k\sum_{k'=1}^{N_c}(Z/(1+\overline{\gamma}_{k'}|C_{k,k'}(z)|^2))}{(1+\overline{\gamma}_k)\overline{p}G_k|H_k|^2-\overline{\gamma}_k(P_{\mathrm{CCI},k}+n)}\right\}, \tag{A.17}$$

where Z denotes $\overline{\gamma}_{k'}|C_{k,k'}(z)|^2(P_{\mathrm{CCI},k'}+n)$.

The fraction on the right-hand side of the above inequality is actually maximized when the largest possible $\overline{\gamma}_k$ is chosen from the set $\boldsymbol{\Gamma}$ such that (A.17) is satisfied. Based on (A.15) and (A.17), a rate packing algorithm is developed for the UL, given in Section 3.1. Note that for the special case where all subcarriers in a cell belong to one user, there is no MAI and the UL GRP algorithm is the same as the DL GRP algorithm.

B. OTA-SRR: CONSTRAINTS AND ALGORITHM CONVERGENCE

This section briefly reviews the OTA constraints and the convergence issues pertaining to the OTA-SRR algorithm [7]. More detailed treatment can be found in [7].

The conditions for convergence of the system equation (13) are outlined below:

$$(\mathbf{I}-\boldsymbol{\Phi})^{-1} = \mathbf{I}+\boldsymbol{\Phi}+\boldsymbol{\Phi}^2+\cdots, \quad (\mathbf{I}+\boldsymbol{\Phi}+\boldsymbol{\Phi}^2+\cdots)\mathbf{x} = (1+\lambda+\lambda^2+\cdots)\mathbf{x}, \tag{B.1}$$

where $\mathbf{x}$ is the eigenvector corresponding to the eigenvalue λ of $\boldsymbol{\Phi}$. The series in (B.1) converges if and only if $\lambda < 1$ and this holds for any eigenvalue of $\boldsymbol{\Phi}$. Thus, (13) has a solution, when $\lambda_1 < 1$.

In order to determine a feasible set of transmit powers, let $\mathbf{P_1}$ be the eigenvector corresponding to $(1-\lambda_1)$, the eigenvalue of $(\mathbf{I}-\boldsymbol{\Phi})$. Then, the system in (13) becomes

$$(1-\lambda_1)\mathbf{P_1} \ge \boldsymbol{\eta},$$

which is equivalent to

$$\mathbf{P_1} \ge \frac{\boldsymbol{\eta}}{1-\lambda_1}. \tag{B.2}$$

If $\mathbf{P}_{\max}$ is the vector of maximum transmit powers, $\mathbf{P_1}$ must satisfy

$$\mathbf{P_1} \le \mathbf{P}_{\max}. \tag{B.3}$$

Thus, based on (B.2) and (B.3), it follows that

$$\mathbf{P}_{\max} \geq \frac{\boldsymbol{\eta}}{1-\lambda_1}, \tag{B.4}$$

with $0 \leq \lambda_1 \leq 1$. The system constraint can now be expressed by rearranging (B.4) as

$$1-\lambda_1 \geq \max_{i\in N}\left\{\frac{\eta_i}{\overline{p}}\right\}. \tag{B.5}$$

The modified OTA-SRR algorithm is illustrated by the flowchart in Figure 2.

C. DERIVATION OF THE CYCLIC SINC FUNCTION

The following is a derivation of the cyclic sinc (or modified Dirichlet) function, which accounts for the dependence of the interference contribution from subcarrier k' to subcarrier k on the $|k'-k|$.

Based on the IFFT and FFT operations, the received modulation symbol on subcarrier k (without noise), $\mathcal{R}_k$, can be written as

$$\mathcal{R}_k = \frac{1}{N_c}\sum_{i=0}^{N_c-1}\left[\sum_{k'=0}^{N_c-1} H_{i,k'}S_{k'}\exp\left(\frac{j2\pi ik'}{N_c}\right)\right]\exp\left(\frac{-j2\pi ik}{N_c}\right), \tag{C.1}$$

where j is the imaginary unit, S_k is the transmit symbol on subcarrier k, and $H_{i,k}$ is the channel transfer function of subcarrier k. If one contributing propagation path is assumed, the channel transfer function can be expressed as

$$\begin{aligned} H_{i,k'} &= \exp(j\phi)\exp\left(\frac{j2\pi i(\varepsilon_D+\omega)}{N_c}\right)\exp\left(\frac{-j2\pi k'\varepsilon_\tau}{N_c}\right) \\ &\equiv H_{k'}\exp\left(\frac{j2\pi i(\varepsilon_D+\omega)}{N_c}\right), \end{aligned} \tag{C.2}$$

where ε_τ is the relative propagation delay, and ϕ is the phase. After substituting (C.2) into (C.1) and reordering result in

$$\begin{aligned} &\mathcal{R}_k \\ &= \frac{1}{N_c}\sum_{i=0}^{N_c-1}\sum_{k'=0}^{N_c-1} H_{k'}\exp\left(\frac{j2\pi i(\varepsilon_D+\omega)}{N_c}\right)S_{k'}\exp\left(\frac{j2\pi i(k'-k)}{N_c}\right) \\ &\equiv \frac{1}{N_c}\sum_{k'=0}^{N_c-1} H_{k'}S_{k'}\underbrace{\left[\sum_{i=0}^{N_c-1}\exp\left(\frac{j2\pi i(k'-k+\varepsilon_D+\omega)}{N_c}\right)\right]}_{\text{geometric series}}. \end{aligned} \tag{C.3}$$

The geometric series in (C.3) can be simplified. If $2\pi(k'-k+\varepsilon_D+\omega)/N_c = \beta$, the geometric series representation yields

$$\begin{aligned} \sum_{k=0}^{N-1}\exp(j\beta k) &= \frac{1-\exp(j\beta N)}{1-\exp(j\beta)} \\ &\equiv \exp\left(\frac{j(N-1)\beta}{2}\right)\frac{\sin(N\beta/2)}{\sin(\beta/2)}. \end{aligned} \tag{C.4}$$

Using the result from (C.4), the cyclic sinc function $C_{k,k'}(k'-k+\varepsilon_D+\omega)$ can be derived as

$$\begin{aligned} C_{k,k'}(k'-k+\varepsilon_D+\omega) &= \frac{1}{N_c}\frac{\sin(\pi(k'-k+\varepsilon_D+\omega))}{\sin(\pi(k'-k+\varepsilon_D+\omega)/N_c)} \\ &\quad\times\exp\left(\frac{j\pi(k'-k+\varepsilon_D+\omega)(N_c-1)}{N_c}\right), \end{aligned} \tag{C.5}$$

such that (C.3) becomes

$$\mathcal{R}_k = \sum_{k'=0}^{N_c-1} H_{k'}S_{k'}C_{k,k'}(k'-k+\varepsilon_D+\omega). \tag{C.6}$$

The received symbol in (C.6) includes both an interference component and a useful component, and can be written in terms of desired signal power and interference power (in Watts) as

$$\begin{aligned} \mathcal{R}_k = &\underbrace{\sum_{k'=0,\ k'\neq k}^{N_c-1}|H_{k,k'}|^2P_{k'}G_{k,k'}|C_{k,k'}(k'-k+\varepsilon_D+\omega)|^2}_{\text{interference}} \\ &+\underbrace{|H_k|^2P_kG_k|C_{k,k}(k-k+\varepsilon_D+\omega)|^2}_{\text{useful signal}}. \end{aligned} \tag{C.7}$$

However, (C.7) models a general case of MAI, which in Section 2 is straightforwardly tailored to account for multiple subcarriers per link and also to account for CCI. It should be noted that Doppler offset and frequency synchronization errors in the desired signal are not considered as perfect synchronization is assumed, hence, the argument of $|C_{k,k}(k-k+\varepsilon_D+\omega)|^2$ is 0. Using (C.5) and noting that for small α, $\sin(\alpha) \approx \alpha$, it can be shown that as the argument of $|C_{k,k}(k-k+\varepsilon_D+\omega)|^2$ goes to 0, $|C_{k,k}(k-k+\varepsilon_D+\omega)|^2$ goes to 1. Hence, the useful (desired) signal power per subcarrier, R_k, is expressed as

$$R_k = P_kG_k|H_k|^2\ [\mathrm{W}]. \tag{C.8}$$

ACKNOWLEDGMENTS

The authors would like to thank the anonymous reviewers for the very useful and constructive comments and suggestions. The reviewers input clearly helped to improve the manuscript. The authors would also like to thank the School of Engineering and Electronics at The University of Edinburgh, Edinburgh, UK, for the financial support of this work.

REFERENCES

[1] C. Y. Wong, R. S. Cheng, K. B. Letaief, and R. D. Murch, "Multiuser OFDM with adaptive subcarrier, bit, and power allocation," *IEEE Journal on Selected Areas in Communications*, vol. 17, no. 10, pp. 1747–1758, 1999.

[2] T. Keller and L. Hanzo, "Adaptive modulation techniques for duplex OFDM transmission," *IEEE Transactions on Vehicular Technology*, vol. 49, no. 5, pp. 1893–1906, 2000.

[3] L. Yan, Z. Wenan, and S. Junde, "An adaptive subcarrier, bit and power allocation algorithm for multicell OFDM systems," in *Proceedings of the Canadian Conference on Electrical and Computer Engineering (CCECE '03)*, vol. 3, pp. 1531–1534, Montreal, Canada, May 2003.

[4] H. Rohling and R. Grünheid, "Performance comparison of different multiple access schemes for the downlink of an OFDM communication system," in *Proceedings of the 47th IEEE Vehicular Technology Conference (VTC '97)*, vol. 3, pp. 1365–1369, Phoenix, Ariz, USA, May 1997.

[5] H. Haas and S. McLaughlin, Eds., *Next Generation Mobile Access Technologies: Implementing TDD*, Cambridge University Press, Cambridge, UK, 2008.

[6] H. Haas, P. K. Jain, and B. Wegmann, "Capacity improvement through random timeslot opposing (RTO) algorithm in cellular TDD systems with asymmetric channel utilisation," in *Proceedings of the 14th International Symposium on Personal, Indoor and Mobile Radio Communications (PIMRC '03)*, vol. 2, pp. 1790–1794, Beijing, China, September 2003.

[7] S. Ginde, *A game-theoretic analysis of link adaptation in cellular radio networks*, M.S. thesis, Virginica Polytechnic Institute and State University, Blacksburg, Va, USA, May 2004.

[8] F. Berggren and S.-L. Kim, "Energy-efficient control of rate and power in DS-CDMA systems," *IEEE Transactions on Wireless Communications*, vol. 3, no. 3, pp. 725–733, 2004.

[9] T. S. Rappaport, *Wireless Communications: Principles and Practice*, Prentice Hall PTR, Upper Saddle River, NJ, USA, 2nd edition, 2001.

[10] IST-2003-507581 WINNER, "D1.3 v1.0 Final Usage Scenarios," June 2005, http://www.ist-winner.org/deliverables_older.html.

[11] W. Yu, G. Ginis, and J. M. Cioffi, "An adaptive multiuser power control algorithm for VDSL," in *Proceedings of the Global Telecommunications Conference (GLOBECOM '01)*, vol. 1, pp. 394–398, San Antonio, Tex, USA, November 2001.

[12] G. Scutari, D. P. Palomar, and S. Barbarossa, "Asynchronous iterative waterfilling for Gaussian frequency-selective interference channels: a unified framework," in *Proceedings of the Information Theory and Applications Workshop (ITA '07)*, pp. 349–358, Lake Tahoe, Calif, USA, September 2007.

[13] J. Zander and S.-L. Kim, *Radio Resource Management for Wireless Networks*, Artech House, Boston, Mass, USA, 2001.

[14] F. R. Gantmacher, *Matrix Theory*, vol. 2, Chelsea, New York, NY, USA, 1974.

[15] M. Speth, S. A. Fechtel, G. Fock, and H. Meyr, "Optimum receiver design for wireless broad-band systems using OFDM. I," *IEEE Transactions on Communications*, vol. 47, no. 11, pp. 1668–1677, 1999.

[16] P. Höher, "A statistical discrete-time model for the WSSUS multipath channel," *IEEE Transactions on Vehicular Technology*, vol. 41, no. 4, pp. 461–468, 1992.

[17] J. Medbo and P. Schramm, "Channel Models for HIPERLAN 2," ETSI/BRAN document no. 3ERIO85B, 1998., September 2006, http://www.etsi.org/.

[18] V. Erceg, L. J. Greenstein, S. Y. Tjandra, et al., "An empirically based path loss model for wireless channels in suburban environments," *IEEE Journal on Selected Areas in Communications*, vol. 17, no. 7, pp. 1205–1211, 1999.

[19] K. J. Hole, H. Holm, and G. E. Øien, "Adaptive multidimensional coded modulation over flat fading channels," *IEEE Journal on Selected Areas in Communications*, vol. 18, no. 7, pp. 1153–1158, 2000.

[20] W. T. Webb, L. Hanzo, and R. Steele, "Bandwidth-efficient QAM schemes for Rayleigh fading channels," in *Proceedings of the 5th International Conference on Radio Receivers and Associated Systems*, pp. 139–142, Cambridge, UK, July 1990.

[21] G. Forney Jr., R. Gallager, G. Lang, F. Longstaff, and S. Qureshi, "Efficient modulation for band-limited channels," *IEEE Journal on Selected Areas in Communications*, vol. 2, no. 5, pp. 632–647, 1984.

[22] E. Foutekova, P. Agyapong, B. Ghimire, H. Venkataraman, and H. Haas, "Scheduling in cellular CDMA-TDD networks," in *proceedings of the 64th IEEE Vehicular Technology Conference (VTC '06)*, pp. 727–731, Montreal, Canada, September 2006.

Asymmetry Balancing for Channel Asymmetry Support in OFDMA-TDD Cellular Networks

Ellina Foutekova, Sinan Sinanović and Harald Haas
Institute for Digital Communications, School of Engineering & Electronics
The University of Edinburgh, Edinburgh EH9 3JL, UK
Email: {E.Foutekova, S.Sinanovic, H.Haas}@ed.ac.uk

***Abstract*—This paper proposes a novel approach to interference avoidance via inter-cell relaying in cellular OFDMA-TDD (orthogonal frequency division multiple access - time division duplex) systems. The proposed scheme, termed asymmetry balancing, is targeted towards next-generation cellular wireless systems which are envisaged to have *ad hoc* and multi-hop capabilities. Asymmetry balancing resolves the detrimental base station (BS)-to-BS interference problem inherent to TDD networks by synchronizing the TDD switching points (SPs) across cells. In order to maintain the flexibility of TDD in serving the asymmetry demands of individual cells, inter-cell relaying is employed. It is demonstrated that asymmetry balancing offers great flexibility in uplink (UL)- downlink (DL) resource allocation. In addition, results show that a spectral efficiency improvement of more than 100% can be obtained with respect to a case where the TDD SPs are adapted to the cell-specific demands.**

I. Introduction

An effective strategy which is envisioned for next-generation wireless cellular networks to ameliorate the spectral efficiency performance without increasing hardware cost is to make use of existing infrastructure and to introduce cooperation among the network entities. Naturally, such cooperation leads to multi-hop cellular networks (MCN) [1], i.e. cellular networks which have relaying capabilities. A relay station (RS) is an intermediate node between a mobile station (MS) and the servicing BS and the relay can be either a dedicated transceiver or an MS. However, MCNs where the relays are MSs are of special interest due the wide availability of mobile terminals, especially in highly populated areas, where network capacity becomes a limiting factor. Capacity improvement has been shown in [2], where in-cell users act as relays to form virtual antenna arrays and thereby exploit transmit diversity.

The *ad hoc* capabilities in an MCN are actually enabled by TDD. In addition, the support for cell-independent traffic asymmetry offered by TDD together with the advantages of OFDMA, make OFDMA-TDD a promising choice for next generation wireless networks [3]. However, TDD suffers from additional interference as compared to frequency division duplex (FDD). In particular, TDD suffers from same-entity interference, MS→MS and BS→BS, which presents a major problem in actual cellular TDD deployment when cell-independent asymmetry is to be supported. Known solutions to interference avoidance in TDD include the concept of zone/region division [4], which restricts crossed slot operation only within a radius r around the BS. Optimum performance has been found for r=52% of the cell radius [4]. This strategy reduces MS→MS interference, but does not solve the more detrimental BS→BS interference problem. Moreover, it also imposes restrictions on the flexibility of TDD by compromising user demand. Furthermore, a strategy for same-entity interference mitigation, similar to frequency hopping, termed time-slot opposing, has been proposed in [5]. The time multiplexed busy tone approach in [6] also mitigates the problem of same-entity interference.

In this paper a novel idea termed *asymmetry balancing* is proposed to entirely avoid the detrimental BS→BS interference. The essence of the asymmetry balancing concept is, as the name suggests, to balance the asymmetry demand across the cells in a network. To this end, the TDD SP is synchronized across cells, which might result in a shortage of resources in a particular cell, while a neighboring cell might have spare resources (assuming cell-independent traffic asymmetry demands). In order to resolve any mismatch between resource availability and resource demand, the *ad hoc* capabilities of an MCN are exploited. In particular, an MS which cannot be served in either UL or DL by its associated BS due to shortage of resources is served by a neighboring cooperating BS, which has spare resources in both link directions. The established MS↔BS link is a two-hop link where the intermediate node is an MS associated with the cooperating BS. In this way, despite the fact that the network maintains a synchronized SP, cell-specific asymmetries are effectively supported.

It is assumed that cells are differently loaded, which is a reasonable assumption for future wireless networks which will mainly support packet-data traffic characterized by a high peak-to-average load ratio. In addition, because traffic is envisaged to be DL-favored the network-wide SP will be primarily DL-favored (or occasionally symmetric), it is expected that a cell which requires UL-favored SP will not be able to support the UL demand. Therefore, this study focuses on UL asymmetry balancing.

The rest of the paper is organized as follows. Section II introduces the novel asymmetry balancing idea and the simulation model is presented in Section III, while the results are given in Section IV. The paper concludes with Section V.

II. Asymmetry Balancing via Inter-Cell Relaying

As the asymmetry balancing concept relies on cooperation, it is important to identify the cooperating entities and when they can cooperate. If hexagonal cells are considered, each cell can be treated as a cell of interest (CoI), surrounded by six

Parts of this manuscript appear in a research article accepted for publication at the Journal of Communications and Networks (JCN), No. 10, vol. 2, Special Issue on Wireless Cooperative Transmission and its Applications (to appear).

978-1-4244-1722-3/08/$25.00 ©2008 IEEE.

neighboring cells, which are the potential cooperating cells. Fig. 1 illustrates the aforementioned geometry during a DL time slot. Assume that there are only two frequency resources per cell per link direction per frame, which are marked by boxes on Fig. 1. A black box signifies an allocated resource, while a white box signifies a free resource. Let the CoI suffer from shortage of UL resources, while it has a DL resource available. Marked by a solid ellipse is the MS at the CoI, which needs UL service and desires to off-load traffic. The first-tier cells which are marked with dashed hexagons have spare UL and DL resources and hence are the cooperating cells. Associated with the cooperating cells are the MSs which can serve as RSs (identified by dashed ellipses). The tagged MS at the CoI can relay to any of the available RSs. The

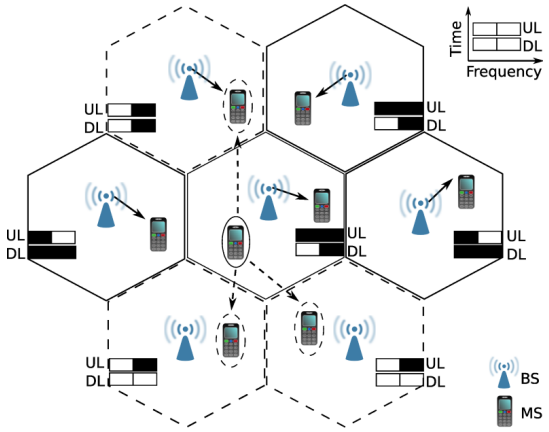

Fig. 1. The MSs in the center cell, i.e. the CoI, can off-load UL traffic to neighboring cooperating cells (marked by dashed hexagons) using free DL resources (marked by white boxes).

MS→RS link uses a DL resource, which is free both at the CoI and the cooperating cell which serves the respective RS. Such resources are referred to as common free resources (CFR). In addition, the off-loading MSs can form *ad hoc* links to either idle MSs in neighboring cells, or active MSs which are already receiving in DL from their BS. The latter case exploits the fact that a DL transmission to a user usually does not occupy all subchannels, and this is accounted for by the use of frequency division multiple access (FDMA). It should be noted that in an OFDMA-TDD network the smallest resource unit allocatable to a particular user is termed a chunk[1], i.e. a number of subcarriers during one time slot.

Based on the above, the main steps of the UL asymmetry balancing technique for multiple cell scenario are summarized below:

1) A CoI is overloaded in UL and requires cooperation.
2) The set of first-tier cells surrounding the CoI, which have spare resources both in UL and DL, are the cooperating cells.
3) There are DL CFRs between the CoI and at least one of the cooperating cells.
4) Utilize the CFRs to transfer UL load from the CoI to the cooperating cells. Use *ad hoc* communication to form MS→RS links between MSs associated with the CoI and RSs associated with any of the cooperating cells.

[1]The terms chunk and resource are used interchangeably throughout this text.

Similarly, if the CoI suffers from DL overload, MSs at the CoI can be served indirectly by the cooperating cells via nearby MSs (operating as RSs).

From the above it can be concluded that the asymmetry balancing requires first, available resources and second, available RSs. The next two sections will treat these factors in detail. Even though the analysis is performed for the case of UL asymmetry balancing, it is valid for DL asymmetry balancing as well, by replacing UL with DL.

A. Resource availability

When the center cell uses DL resources to off-load UL traffic to cooperating neighboring cells, UL resources are in effect created, which allow for cell-specific asymmetry demands to be supported. In this way, with cooperation the UL resource capacity of the CoI increases. This means that a "virtual" cell-specific SP can be established depending on the network-wide SP and the DL CFRs.

It is of interest to quantify the UL-to-DL ratios that a virtual SP can support, for a given network-wide SP and a given number of free resources at the CoI and its neighboring cells. Let the number of CFRs be N, where N takes on values $n \in [0, C]$, and C is the total number of resources per cell in DL. Since the SPs are synchronized across the network, C is the same for all cells. The problem of finding the distribution of N can be readily addressed by the binomial distribution, considering that having a CFR is a success, which occurs with probability p and not having such is a failure, which occurs with probability $1-p$. A success occurs when a given chunk is free at the center cell and at the same time, at at least one of the neighboring cells. A failure, on the other hand, occurs when a chunk is busy at the center cell, *or* is free at the center cell and at the same time is busy at all of the neighboring cells. Thus, the distribution of the number of common free chunks, f_N, is a function of the resource occupancy probabilities at the CoI and at the first-tier cells. Resource occupancy probability is the probability that a chunk is occupied. The formulation of f_N is given in (1):

$$f_N(n) = p^n \cdot [1-p]^{C-n} \cdot \binom{C}{n} \tag{1}$$

where $p = (1 - \prod_{i=1}^{B_\mathrm{t}} L_{\mathrm{t},i}) \cdot (1 - L_\mathrm{c})$; B_t is the number of cooperating cells; $L_{\mathrm{t},i}$ is the probability that a resource is occupied at a first-tier cell i; and L_c is the probability that a resource is occupied at the CoI. The expected value of the binomial distribution in (1) yields $E[N] = C \cdot p$, hence the expected value of the number of CFRs as a fraction of the total number of DL resources is $\frac{E[N]}{C} = p$.

Let the network-wide SP split the frame into two subframes, such that their time durations are in ratio of $u : d$, where $\frac{u}{u+d}$ of the time the frame is in UL and $\frac{d}{u+d}$ of the time the frame is in DL. Furthermore, let the total (UL+DL) number of chunks available per cell be C_tot. Then at the CoI, the expected value of the fraction of resources in the frame which can be used for UL traffic including off-loading, R_ul,

is:

$$R_{\rm ul} = \frac{\frac{u}{u+d}C_{\rm tot} + p\frac{d}{u+d}C_{\rm tot}}{C_{\rm tot}} \equiv \underbrace{\frac{u}{u+d}}_{\text{actual SP}} + \underbrace{\frac{p\,d}{u+d}}_{\text{virtual SP}} \qquad (2)$$

This means that at the CoI the virtual SP divides the frame in an UL-to-DL ratio of $(u + p\,d) : (d - p\,d)$. It can be observed that when $p \to 0$, i.e. when there are no available resources for off-loading, then the resource allocation is according to the actual network-wide SP. When $p \to 1$, i.e. when all DL resources at the CoI can be used to off-load UL traffic, then $R_{\rm ul} \to 1$ and the whole frame can be allocated to UL. In effect, asymmetry balancing offers flexibility in resource allocation and can adaptively allocate resources based on availability and demand on a per-cell basis.

B. Relay station availability

Given that there is a CFR, the CFR can be utilized if RSs are available such that a two-hop path can be found from the MS, which needs to off-load traffic to the cooperating BS. In other words, the MS→RS *ad hoc* links are "opportunistic" in that they exploit CFRs and available RSs, and also are managed in a decentralized fashion. How to find a two-hop path is a matter of routing, and determining an optimum routing strategy is beyond the scope of the current study. It is assumed here that future wireless networks will be equipped with multi-hop and relaying functionality in which case no significant additional signaling overhead is required for managing the MS→RS links.

In this study a simple path loss based routing scheme is implemented, where an MS is chosen as an RS if two conditions are satisfied. Namely, the path loss (minus an offset) between the MS which needs to off-load traffic and its servicing BS is larger than *both*: the path loss between the tagged MS and the intended RS *and* the path loss between the intended RS and its servicing BS. Note that the offset can be different for each condition. As an example, the offsets are fixed to 3 dB in this study. The two conditions above aim to ensure that the two-hop link MS→RS→BS would be able to achieve better link capacity than the potential single hop MS→BS link. The MSs which require to off-load traffic and the intended RSs attain the information on the path losses to their respective BSs via the pilot signals that BSs typically send. In addition, the MS-RS path loss can be calculated using the busy burst signaling technique described in [9]. Using the busy burst technique, MSs needing to off-load are equipped to evaluate the routing conditions quoted above in a decentralized fashion and, hence, are enabled to find a suitable RS. In [10], it has been demonstrated that for all practical purposes, for more than 150 users per cell, the probability of finding a suitable two-hop path, is actually one. For a cell radius of 500 m as assumed in this study, the cell area is 0.87 sq. km, which means about 170 users per sq. km. This is a reasonable number, as even suburban areas have at least 100 users per sq. km and typically in the order of thousand (depending on the wireless provider market share) [11], [12].

TABLE I
SIMULATION PARAMETERS [7], [8]

Carrier frequency	5 GHz	Time slot duration	0.1152 ms
Time slots/ frame	6	OFDM symbols/ time slot	5
Tx power/ link	251 mW	BS↔BS distance	1 km
BS height	25 m	MS height	1.5 m
a, MS–BS	39.61	b, MS–BS	35.74
a, MS–RS	32.49	b, MS–RS	43.75
a, BS–BS	41.2	b, BS–BS	23.8

III. SIMULATION MODEL

An OFDMA-TDD system, designed according the UL asymmetry balancing model introduced in Section II, is simulated using a Monte Carlo approach. Each of the seven cells has a centrally-placed omnidirectional BS and full frequency reuse is assumed. Due to complexity issues only twenty users are distributed uniformly in each of the seven cells (and this limitation will be corrected for later). The users are distributed at the beginning of each iteration and a snapshot analysis is performed. For simplicity and demonstration purposes, the UL↔DL SPs are synchronized across the cells at the symmetric state. However, the model can readily be applied to any asymmetry ratio. Similarly to the envisaged traffic asymmetry in data-packet services, traffic is on average DL-favored. The center cell, however, is UL-overloaded and hence generates UL-favored traffic. The holding time is the same for all users and equals one chunk during a time slot (5 OFDM symbols). Each cell is imposed a mean offered load, which governs the respective user mean inter-arrival times and each user independently generates holding times with exponentially distributed interarrival times. The traffic per user is stored in a buffer and served on a first-in-first-out basis. Path loss is calculated using the WINNER C1 path loss model (NLOS) for urban environment [8] as shown below:

$$L_{\rm p} = a + b\log_{10}(d), \qquad (3)$$

where $L_{\rm p}$ is the path loss in dB, a and b are path loss parameters, given in Table I, and d is the transmitter-receiver separation distance in meters. It should be noted that the values of a and b depend on whether MS–RS path loss, BS–MS path loss, or BS–BS path loss is calculated. For the latter line-of-sight conditions are assumed. MSs are associated with serving BSs based on minimum path loss. Perfect synchronization is assumed and only co-channel interference from all active other-cell transmitters is taken into account. Time-frequency resources are allocated following a score-based approach [13], where the score is evaluated based on buffer-size. In particular, a given resource is allocated to the user with the largest average buffer size, monitored during a time window of eight frames. The simulation parameters are shown in Table I. For demonstration purposes, 16 OFDM subcarriers are considered (subject to slow fading effects only). As the SP is symmetric, both UL and DL are allocated 16 subcarriers/time slot $\times$ 3 time slots/frame = 48 chunks/frame (as one chunk is one subcarrier). A simple signal-to-interference-plus-noise ratio (SINR)-based power control is applied to all single-hop links with an SINR target of 20 dB (32 cross constellation at bit-error-ratio (BER) of 10^{-7} [14]). The thermal noise power per subcarrier is -157.11 dBW [7]. For the two-hop links, a signal-to-noise ratio (SNR)-based power control is applied at the first

hop (MS→RS) as it is assumed that the off-loading links are opportunistic and interference information is not available. The SNR target is 25 dB (128 cross constellation at BER of 10^{-7} [14]). If the SNR/SINR targets cannot be met, transmissions still takes place using maximum available power. The total power per link is limited by the maximum transmit power given in Table I.

IV. Results & Discussion

In this study, the performance of UL asymmetry balancing is investigated. Therefore, it is assumed that the UL in the CoI is overloaded and two particular scenarios in terms of resource availability are defined: (1) a best case 6-cell scenario, where all six first-tier cells cooperate; and (2) a worst-case 1-cell scenario where only one first-tier cell cooperates. Different resource availability conditions are enforced by varying the total *user demand* per frame per cell (in %). In this paper, the synchronized SP is set to allocate half of the frame resources to UL and DL each. As a result, in order to obtain the *probability for resource occupancy* at a particular link direction for a given cell, the respective user demand should be multiplied by 2 (because the user demand is defined on a frame basis). The DL resource occupancy probability both at the CoI and at the cooperating cells is varied from 0 to 0.8, which corresponds to a user demand that varies from 0% to 40%. In order to account for a worst case scenario in terms of interference experienced by the *ad hoc* links, the non-cooperating cells are assumed to be fully loaded in DL (i.e. the demand is 50%). Because the UL resource demand of the first-tier cells would not influence the results for UL asymmetry balancing, it is kept constant for all considered scenarios. The UL and DL resource demands are shown in Table II.

In order to confirm the theoretic model presented in Section II, results displaying the virtual SP at the CoI for the 6-cell scenario and for the 1-cell scenario are shown in Fig. 2 and a perfect match between simulation and theory is observed.

Next, the performance of the UL asymmetry balancing scheme is compared against that of two systems: 1) an independent SP (ISP) system where each cell independently sets its SP based on the ratio of UL and DL resource demands; and 2) a synchronized SP (SSP) system which is the same as the asymmetry balancing system, but off-loading does not take place. The comparison metric is spectral efficiency as given in

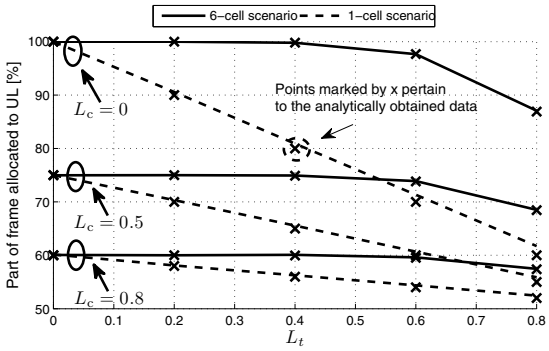

Fig. 2. Frame resources allocated to UL at the CoI by the virtual SP. Solid and dashed lines show simulation results, while analytically obtained data points are marked by "x".

TABLE II
Resource demand for UL and DL (in %)

Cell number → Link direction ↓	1 (CoI)	2	3	4	5	6	7
UL	100	15					
DL (6-cell)	0→40						
DL (1-cell)	0→40	50					

(4), because it can capture not only user link conditions, but also how efficiently resources in a frame are utilized:

$$C_{\mathrm{b}} = \frac{1}{C_{\mathrm{tot}}} \left(\sum_{i=1}^{M} \log_2(1+\gamma_i) + \frac{\overline{M}_{\mathrm{OL}}}{M_{\mathrm{OL}}} \sum_{j=1}^{M_{\mathrm{OL}}} \log_2(1+\gamma_j^{\mathrm{mh}}) \right) \tag{4}$$

where C_{b} is the spectral efficiency per chunk in bps/Hz; γ_i is the SINR of chunk i for single hop links; $M = \frac{u}{u+d} C_{\mathrm{tot}}$ is the number of chunks allocated to UL as per the network-wide SP; $\overline{M}_{\mathrm{OL}} = p\frac{d}{u+d} C_{\mathrm{tot}}$, is the number of DL chunks available for off-loading; M_{OL} is the number of chunks actually utilized for off-loading; and γ_j^{mh} is the SINR of chunk j for two-hop links. Clearly, for systems which do not employ asymmetry balancing, $p = 0$, and the second term of the summation in (4) produces a zero. In addition, it should be noted that γ_j^{mh} is taken as the minimum of the SINR achieved at the first and second hops for each two-hop link. Furthermore, $\frac{\overline{M}_{\mathrm{OL}}}{M_{\mathrm{OL}}}$ is used as a correction factor for the following reason. Due to simulation complexity, only twenty users per cell are simulated. As a result, not all available CFRs can be utilized for off-loading via a neighboring RS. The number of available CFRs is only influenced by the actual load, i.e. fraction of available resources, which is independent of the number of users in the system. In contrast, how many of the available CFRs can be utilized for MS→RS links depends on user density (active and non-active users alike) because user density determines if and how often a two-hop path can be found. As a consequence, the spectral efficiency results are also influenced by the number of users in the system. Because, as was mention in Section II and demonstrated in [10], it can be safely assumed that in realistic scenarios all available CFRs can be actually utilized, the correction factor aims to obtain representative spectral efficiency performance.

The CoI UL spectral efficiency results for different DL resource demands are presented in Fig. 3 (top plot and bottom plot for the 6-cell scenario and 1-cell scenario, respectively). The performance of the system employing asymmetry balancing as well as the performance of the ISP system are denoted by bar plots, while the performance of the SSP system is denoted by a solid line. It can be observed that the asymmetry balancing system always outperforms the SSP system and achieves up to about 50% improvement (6-cell scenario). Furthermore, generally, the asymmetry balancing system exhibits better performance than the ISP system. In particular, when severe BS→BS interference is present (i.e. high DL demand at the first-tier cells) asymmetry balancing attains an amelioration of more than 100% (in all cases in the 1-cell scenario and for 30% and 40% first-tier DL demand in the 6-cell scenario). Exception to this trend is the case in the

6-cell scenario when the DL demand is 0%, i.e. none of the six first-tier cells has DL traffic, which is a highly unlikely situation. It can be seen that, in the 6-cell scenario, even though slightly fewer resources are utilized for asymmetry balancing when the DL demand at the first-tier cells is higher as compared to when the demand is lower (ref. to Fig. 2), the spectral efficiency performance at the CoI is better when the utilized resources are fewer. This effect is achieved, due to the limit on the total transmit power. When slightly fewer resources are used for transmission, there is more power available per resource and the attained SINR can compensate for the fact that less resources are utilized. This trend is not observed in the 1-cell scenario, because the difference in the number of resources utilized for asymmetry balancing for the varied first-tier DL demand is much greater (ref. to Fig. 2).

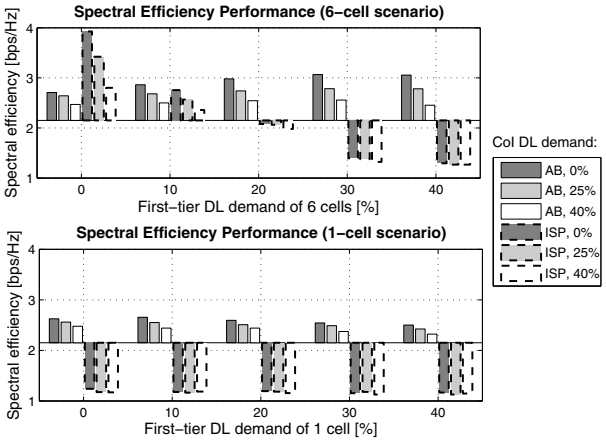

Fig. 3. Bar plots of the UL spectral efficiency performance at the CoI achieved with asymmetry balancing (AB) as compared to an ISP system. The solid line shows the respective performance of an SSP system.

The demonstrated UL spectral efficiency amelioration attained by asymmetry balancing is at a slight loss in spectral efficiency for the first-tier DL transmission as compared to an SSP system. The loss is due to the off-loading *ad hoc* links, which generate MS→MS interference to the concurrent BS→MS links. The results presented in Fig. 4 show that overall the loss in spectral efficiency does not surpass 0.5%. It can be observed, that even though the results for the 1-cell scenario and the 6-cell scenario are similar, the loss in the case of six cooperating cells is slightly larger due to the fact that more resources are used for the off-loading *ad hoc* links and, hence, more interference is caused to the first-tier DL transmission.

V. Conclusions

In this paper, a method named *asymmetry balancing* has been proposed. It allows the support of cell-independent asymmetries in OFDMA-TDD next generation networks with complete avoidance of the detrimental BS→BS interference. The key to solving this issue is user cooperation in combination with inter-cell relaying. It has been demonstrated that in the case of shortage of UL resources a virtual cell-specific SP can be established, depending on the system UL-to-DL asymmetry ratio and the available DL resources at the CoI and its six neighboring cells. When one or more cells can

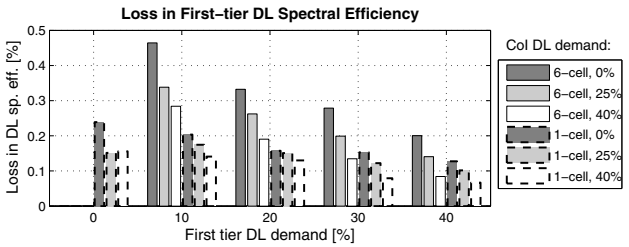

Fig. 4. Percentage loss in DL spectral efficiency caused by the off-loading *ad hoc* links as compared to an equivalent SSP system. As expected, for the 6-cell scenario at 0% DL demand at the first-tier cells, the loss is zero, because there is no DL traffic at the first-tier cells.

cooperate, even the whole frame can be virtually allocated for UL traffic. This flexibility in resource allocation comes at a relatively insignificant cost of less than 0.5% loss in DL spectral efficiency incurred due to interference caused by the *ad hoc* links. For the UL spectral efficiency of the CoI, the gains with respect to the case of fixed SPs are up to about 50%, whereas the gains with respect to the case of cell-specific SPs surpass 100%.

References

[1] L. Le and E. Hossain, "Multihop Cellular Networks: Potential Gains, Research Challenges, and a Resource Allocation Framework," *IEEE Communications Magazine*, vol. 45, no. 9, pp. 66–73, Sep. 2007.

[2] A. Sendonaris, E. Erkip, and B. Aazhang, "Increasing Uplink Capacity via User Cooperation Diversity," in *Proceedings of the IEEE International Symposium on Information Theory*, Cambridge, MA, USA, Aug. 16–21 1998, p. 156.

[3] H. Haas and S. McLaughlin, Eds., *Next Generation Mobile Access Technologies: Implementing TDD*. Cambridge University Press, ISBN: 13:9780521826228, Jan. 2008, 420 pages.

[4] S.-H. Wie and D.-H. Cho, "Time Slot Allocation Scheme Based on a Region Division in CDMA/TDD Systems," in *Proceedings of the 53rd IEEE Vehicular Technology Conference (VTC)*, Rhodes, Greece, May 6–9 2001, pp. 2445–2449.

[5] H. Haas and S. McLaughlin, "A Dynamic Channel Assignment Algorithm for a Hybrid TDMA/CDMA-TDD Interface Using the Novel TS-Opposing Technique," *IEEE Journal on Selected Areas in Communications*, vol. 19, no. 10, pp. 1831–1846, Oct. 2001.

[6] P. Omiyi, H. Haas, and G. Auer, "Analysis of TDD Cellular Interference Mitigation Using Busy-Bursts," *IEEE Transactions on Wireless Communications*, vol. 6, no. 7, pp. 2721–2731, Jul. 2007.

[7] IST-2003-507581 WINNER, "D2.10, Final report on identified RI key technologies, system concept and their assessment," Retrieved Mar. 15, 2007, from https://www.ist-winner.org/DeliverableDocuments/, Dec. 2005.

[8] IST-4-027756 WINNER II, "D1.1.2 v1.2 WINNER II Channel Models," Retrieved Feb. 5, 2008, from https://www.ist-winner.org/WINNER2-Deliverables/.

[9] G. Auer, H. Haas, and P. Omiyi, "Interference Aware Medium Access for Dynamic Spectrum Sharing," in *Proceedings of the 2nd IEEE International Symposium on New Frontiers in Dynamic Spectrum Access Networks (DySPAN)*, Dublin, Ireland, Apr. 17–20 2007, pp. 399–402.

[10] E. Foutekova, S. Sinanović, and H. Haas, "Traffic Asymmetry Balancing in OFDMA-TDD Cellular Networks," *Journal of Communications and Networking (JCN), Special Issue on Wireless Cooperative Transmission and its Applications*, vol. 10, no. 2, p. (to appear), 2008.

[11] F. Gessler, "Developing Technical Standards – Balancing History and Pre-conceptions," in *Proceedings of the International Association for Management Technology Conference (IAMOT)*, Lausanne, Switzerland, Mar. 19–22 2001, p. 076FG.

[12] WiMAX Forum, "WiMAX Business Case," Available at http://www.hkwtia.org/wtia/ (Date of access: Apr. 8, 2008), Sep. 2004.

[13] T. Bonald, "A Score-Based Opportunistic Scheduler for Fading Radio Channels," in *Proceedings of the 5th European Wireless Conference (EWC)*, Barcelona, Spain, Feb. 24–27, 2004.

[14] K. Hole, H. Holm, and G. Øien, "Adaptive Multidimensional Coded Modulation Over Flat Fading Channels," *IEEE Journal on Selected Areas in Communications*, vol. 18, no. 7, pp. 1153–1158, Jul. 2000.

Asymmetry Balancing in OFDMA-TDD Cellular Networks

Ellina Foutekova, Sinan Sinanović and Harald Haas
Institute for Digital Communications, School of Engineering & Electronics
The University of Edinburgh, Edinburgh EH9 3JL, UK
Email: {E.Foutekova, S.Sinanovic, H.Haas}@ed.ac.uk

***Abstract*—The purpose of this paper is to compare two interference avoidance techniques for time division duplex (TDD) wireless networks, viz.: a novel technique termed asymmetry balancing and the known zone division (ZD) principle. Both asymmetry balancing and ZD strive to reduce the same-entity interference (mobile station (MS)-to-MS and base station (BS)-to-BS) that occurs during crossed slots, i.e. slots which are simultaneously used for uplink (UL) in one cell and for downlink (DL) in a neighbouring cell. Asymmetry balancing eliminates crossed slots by synchronising the TDD switching point (SP) among cells. Cell-specific asymmetry demands are still maintained through cooperation among the entities in the network. ZD, on the other hand, reduces same-entity interference by decreasing transmission range. This study demonstrates that asymmetry balancing achieves more than 100% higher spectral efficiencies than ZD for the considered scenarios.**

I. Introduction

An effective strategy which is envisioned for next-generation wireless cellular networks to ameliorate the spectral efficiency performance without increasing hardware cost is to make use of existing infrastructure and to introduce cooperation among the network entities. Naturally, such cooperation leads to multi-hop cellular networks (MCN) [1], i.e. cellular networks which have relaying capabilities. A relay station (RS) is an intermediate node between an MS and the servicing BS and the relay can be either a dedicated transceiver or an MS. For example, in [2] Qiao, Wu and Tonguz describe a load balancing method via mobile dedicated transceivers, which can be replaced according to user traffic demand, in order to divert traffic using the unlicensed frequency bands. However, MCNs where the relays are MSs are of special interest due the wide availability of mobile terminals, especially in highly populated areas, where network capacity becomes a limiting factor.

The *ad hoc* capabilities in MCNs are actually enabled by TDD, which is the envisioned duplex scheme for next-generation networks, due to the offered efficient support for cell-independent traffic asymmetry [3]. However, in TDD, when neighbouring cells have different asymmetry demands, crossed slots cause BS→BS interference, which is a particularly detrimental problem due to the exposed locations of BSs and the high probability of line-of-sight (LOS) conditions among BSs. Hence, the issue of crossed slots is the major hurdle to be overcome before the advantages of TDD in supporting cell-independent traffic asymmetries can be fully exploited. To this end, making use of the capabilities of MCNs to balance traffic across the network can be particularly useful.

A novel concept, termed asymmetry balancing, is targeted towards MCNs and utilises load balancing to completely avoid BS→BS interference by synchronising the TDD SP among the cells in a network. Entities which face overload as a result of the synchronised SP can off-load to other-cell entities, which have available resources. In this manner, the traffic within a network can be balanced across cells, ultimately balancing the asymmetry demand across cells. The asymmetry balancing concept has been introduced in detail in [4, 5], where it has been demonstrated that asymmetry balancing offers great flexibility in UL-DL resource allocation and can efficiently support cell-independent asymmetry demands while completely avoiding BS→BS interference.

The purpose of the current study is to compare the performance of asymmetry balancing to another interference avoidance approach, namely ZD (also known as region division, or fractional reuse) [6], in the context of orthogonal frequency division multiple access (OFDMA)-TDD. ZD is a centralised interference mitigation technique considered by the Wireless World Initiative New Radio (WINNER) project [7] for next generation TDD networks.

The rest of the paper is organised as follows. Section II briefly outlines the principles of asymmetry balancing and ZD. Section III provides the simulation setup, while results are presented in Section IV. The paper concludes with Section V.

II. Asymmetry Balancing & Zone Division

In this study it is assumed that cells are differently loaded, which is a reasonable assumption for future wireless networks which will mainly support packet-data traffic characterised by a high peak-to-average load ratio. In addition, traffic is generally DL-favoured, in accordance with what is envisaged for next-generation networks. It is expected that occasionally a cell would have UL-favoured demand. This will result in strong BS→BS interference experienced at the UL-favoured cell. To study how efficiently ZD and asymmetry balancing mitigate BS→BS interference, the following scenario is defined. A hexagonal cell of interest (CoI) is considered, surrounded by six neighbouring cells, where the CoI has UL-favoured traffic demand, while its neighbouring cells have DL-favoured traffic demands. The paper compares UL asymmetry balancing to ZD in terms of the UL spectral efficiency attained at the CoI and the UL-DL resource allocation at the CoI.

Parts of this manuscript appear in a paper accepted for publication in the Journal of Communications and Networks (JCN), No. 10, vol. 2, Special Issue on Wireless Cooperative Transmission and its Applications (to appear).

978-1-4244-2644-7/08/$25.00 ©2008 IEEE

Before the comparison is carried out, asymmetry balancing and ZD are briefly summarised in the next two sections.

A. Asymmetry Balancing

The asymmetry balancing concept exploits cooperation among entities in the MCN and utilises free resources. Hence, there are two enablers for asymmetry balancing, *viz*: availability of resources and cooperating entities.

If hexagonal cells are considered, each cell can be treated as a cell of interest (CoI), surrounded by six neighboring cells, which are the potential cooperating cells. Fig. 1 illustrates the aforementioned geometry during a DL time slot. Assume that there are only two frequency resources per cell per link direction per frame, which are marked by boxes on Fig. 1. A black box signifies an allocated resource, while a white box signifies a free resource. Let the CoI suffer from shortage of UL resources, while it has a DL resource available. Marked by a solid ellipse is the MS at the CoI, which needs UL service and desires to off-load traffic. The first-tier cells which are marked with dashed hexagons have spare UL and DL resources and hence are the cooperating cells. Associated with the cooperating cells are the MSs which can serve as RSs (identified by dashed ellipses). The tagged MS at the CoI can relay to any of the available RSs, which are potentially both idle MSs and active MSs already receiving in DL from their BS. The latter case exploits the fact that a DL transmission to a user usually does not occupy all subchannels, and this is accounted for by the use of frequency division multiple access (FDMA). The MS→RS link uses DL resources, which are

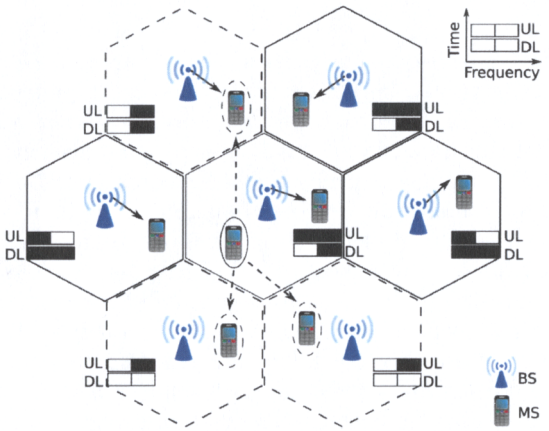

Fig. 1. The MSs in the centre cell, i.e. the CoI, can off-load UL traffic to neighboring cooperating cells (marked by dashed hexagons) using free DL resources (marked by white boxes).

free both at the CoI and the cooperating cell which serves the respective RS. Such resources are referred to as common free resources (CFR) and in the case of OFDMA-TDD a resource is equivalent to a chunk, i.e. a number of subcarriers per time slot. When the centre cell uses CFRs to off-load UL traffic to cooperating neighbouring cells, UL resources are effectively created. As a consequence, cell-specific asymmetry demands are supported while the SP is synchronised throughout the network. This means that a "virtual" cell-specific SP can be established depending on the network-wide SP and the DL CFRs.

The cell-specific virtual SP can be quantified as follows. Let the network-wide SP split the frame into two sub-frames, such that their time durations are in ratio of $u : d$, where $\frac{u}{u+d}$ of the time the frame is in UL and $\frac{d}{u+d}$ of the time the frame is in DL. Furthermore, let the total (UL+DL) number of chunks available per cell be C_{tot}. It should be noted here that there is no fixed resource reuse in place, rather full frequency reuse is assumed and all cells have all resources available. Hence, according to the network-wide SP, the resources per frame allocated to UL are expressed as $\frac{u}{u+d}C_{\text{tot}}$. The virtual SP at the CoI allocates an additional of at most $\frac{d}{u+d}C_{\text{tot}}$ resources. The expected value of the normalised number of resources allocated to UL by the virtual SP, R_{ul}, is given in (1):

$$R_{\text{ul}} = \frac{\frac{u}{u+d}C_{\text{tot}} + p\frac{d}{u+d}C_{\text{tot}}}{C_{\text{tot}}} \equiv \underbrace{\frac{u}{u+d}}_{\text{actual SP}} + \underbrace{\frac{p\,d}{u+d}}_{\text{virtual SP}} \qquad (1)$$

where $p = (1 - \prod_{i=1}^{B_{\text{t}}} L_{\text{t},i}) \cdot (1 - L_{\text{c}})$ is the probability that a given DL resource is a CFR; B_{t} is the number of cooperating cells; $L_{\text{t},i}$ is the probability that a resource is occupied at a first-tier cell i; and L_{c} is the probability that a resource is occupied at the CoI.

Given that there is a CFR, the CFR can be utilised if RSs are available such that a two-hop path can be found from the MS, which needs to off-load traffic to the cooperating BS. In other words, the MS→RS *ad hoc* links are "opportunistic" in that they exploit CFRs and available RSs, and also are managed in a decentralised fashion. How to find a two-hop path is a matter of routing, and determining an optimum routing strategy is beyond the scope of this paper. It is assumed here that future wireless networks will be equipped with multi-hop and relaying functionality in which case no significant additional signalling overhead is required for managing the MS→RS links. In this study a simple path loss based routing scheme is implemented according to [4]. Furthermore, in [4], it has been demonstrated that for all practical purposes, for more than 150 users per cell, it is fair to assume that the probability of finding a suitable two-hop path is actually one (>0.994). For a cell radius of 500 m as assumed here, the cell area is 0.87 sq. km, which means about 170 users per sq. km. This is a reasonable number, as even suburban areas have at least 100 users per sq. km and typically in the order of thousand (depending on the wireless provider market share) [8, 9].

B. Zone Division

As opposed to the asymmetry balancing technique, ZD is a centralised scheme, which heavily relies on coordination among BSs. The principle is proposed in [6] as a time slot allocation based on region division for CDMA networks. ZD is a fractional reuse concept which aims to mitigate interference by reducing the transmission range during crossed slots. The reduced transmission range in effect increases the separation distance between transmitters and vulnerable receivers and hence reduces interference. BSs share information about their TDD SP and thereby have knowledge which time slots are crossed slots. Each BS divides its coverage area to an inner region and an outer region. During crossed slots, resources are allocated only to MSs which are located in the inner region.

The authors of [6] found the radius of the inner region to be 52% of the cell radius. Assuming uniform user distribution and cell radius R, it can be calculated that only $\frac{\pi(0.52R)^2}{\pi R^2} \approx \frac{1}{4}$ of the users are in the inner region. This means that whenever a large number of crossed slots is present in comparison to non-crossed slots, the resources could be ineffciently utilised.

It should be noted that ZD does not result in interference avoidance, but rather in interference reduction. To achieve this, in practice ZD requires significant overhead. The division of a cell to regions needs MSs to report to their respective BSs the received power of a reference signal (for example, the pilot signal BSs usually send). Based on the reported values, BSs tag MSs as being in the inner/outer region. In addition, ZD does not work unless tight DL power control is in place. Tight power control, however, is not desirable in OFDMA systems, because it limits the use of higher order modulation, which is especially important for users with good channel conditions (such as the users close to the BS).

III. Simulation Setup

An OFDMA-TDD system is designed according to the model introduced in Section II and simulated using a Monte Carlo approach. Users are uniformly distributed at the beginning of each iteration and a snap-shot analysis is performed. Each of the seven cells has a centrally-placed omnidirectional BS. In the case of asymmetry balancing, for simplicity and demonstration purposes, the synchronised TDD SP allocates half of the frame resource to UL and DL each. However, the model can readily be applied to any asymmetry ratio. In the case of ZD, the SP is set according to the ratio of the demanded UL and DL resources. Each user independently generates exponentially distributed interarrival times with mean, governed by the offered load imposed on each cell. The holding time is the same for all users and equals one chunk during a time slot (5 OFDM symbols). The traffic per user is stored in a buffer and served on a first-in-first-out basis. The maximum waiting time per generated holding time is 20 ms [7]. Path loss is calculated using the WINNER C1 path loss model (NLOS) for urban environment [10] as shown below:

$$L_{\mathrm{p}} = a + b\log_{10}(d), \tag{2}$$

where L_{p} is the path loss in dB, a is an environment specific constant, $b = 10\,\mu$ with μ being the path loss exponent, and d is the transmitter-receiver separation distance in metres. It should be noted that the values of a and b (given in Table I) depend on whether MS–RS path loss, BS–MS path loss, or BS–BS path loss is calculated. For the latter LOS conditions are assumed. MSs are associated with serving BSs based on minimum path loss. Perfect synchronisation is assumed and only co-channel interference from all active other-cell transmitters is taken into account. Time-frequency resources are allocated following a score-based approach [11], where the score is evaluated based on buffer-size. In particular, a given resource is allocated to the user with the largest average buffer size, monitored during a time window of eight frames. The simulation parameters are shown in Table I. For demonstration purposes, 16 OFDM subcarriers per cell are considered (subject to slow fading effects only). As the SP is symmetric, both UL and DL are allocated 16 subcarriers/time slot $\times$ 3 time slots/frame = 48 chunks/frame (as one chunk is one subcarrier). In addition, only 20 users per cell are considered due to the fact that introducing more users in the system results in cumbersome simulations. However, because this number of users does not reflect a realistic deployment scenario (ref. to Section II), a correction factor will be introduced in the next section. The number of users is not expected to influence the trends of the performance of the ZD system.

A simple signal-to-interference-plus-noise ratio (SINR)-based power control is applied to all single-hop links with an SINR target of 20 dB (32 cross constellation at bit-error-ratio (BER) of 10^{-7} [12]). The thermal noise power per subcarrier is -157.11 dBW [7]. For the two-hop links, a signal-to-noise ratio (SNR)-based power control is applied at the first hop (MS$\rightarrow$RS) as it is assumed that the off-loading links are opportunistic and interference information is not available. The SNR target is 25 dB (128 cross constellation at BER of 10^{-7} [12]). If the SNR/SINR targets cannot be met, transmissions still takes place. The total power per link is limited by the maximum transmit power given in Table I.

TABLE I
Simulation Parameters [7, 10]

Carrier frequency	5 GHz	Time slot duration	0.1152 ms
Time slots/ frame	6	OFDM symbols/ time slot	5
Tx power/ link	251 mW	BS$\leftrightarrow$BS distance	1 km
BS height	25 m	MS height	1.5 m
a, MS–BS	39.61	b, MS–BS	35.74
a, MS–RS	32.49	b, MS–RS	43.75
a, BS–BS	41.2	b, BS–BS	23.8

IV. Results

The comparison of asymmetry balancing and ZD begins with a discussion on the difference between asymmetry balancing and ZD in terms of the way resources are allocated to UL and DL. In Section II it was demonstrated that asymmetry balancing strongly depends on the resource availability both at the CoI and at the neighbouring cells. It is impossible to simulate all possible scenarios in terms of resource availability, hence two scenarios are defined: (1) a best case 6-cell scenario, where all six first-tier cells cooperate; and (2) a worst-case 1-cell scenario where only one first-tier cell cooperates. Different resource availability conditions are enforced by varying the total *user demand* per frame per cell (in %). As already mentioned, in this paper, when asymmetry balancing is employed, the synchronised SP is set to allocate half of the frame resources to UL and DL each. As a result, in order to obtain the *probability that a resource is occupied* at a particular link direction for a given cell, the respective user demand should be multiplied by 2 (because half of the resources per frame are allocated to the given link direction and the user demand is defined on a frame basis). The DL resource occupancy probability both at the CoI and at the cooperating cells is varied from 0 to 0.8, which corresponds to a user demand that varies from 0% to 40%. In order to account for a worst case scenario in terms of interference experienced by the *ad hoc* links, the non-cooperating cells are assumed to be fully loaded in DL (i.e. the demand is 50%). Because the UL resource demand of the first-tier cells would not influence the results for UL asymmetry balancing, it is kept constant for all considered

scenarios. The UL and DL resource demands are shown in Table II.

The defined scenarios also aim to exhibit different interference conditions for the CoI when ZD is employed. Because each cell sets its SP according to the asymmetry demand at the given cell, the CoI will have an UL-favoured SP in all cases. This means that the 6-cell scenario puts the CoI in the situation of relatively mild BS→BS interference due to the low first-tier DL load, while the 1-cell scenario will cause severe BS→BS interference for the CoI due to the higher first-tier DL load.

TABLE II
RESOURCE DEMAND FOR UL AND DL (IN %)

Cell number → Link direction ↓	1 (CoI)	2	3	4	5	6	7
UL	100	15					
DL (6-cell)	0→40						
DL (1-cell)	0→40	50					

Results for the UL-DL resource allocation at the CoI achieved with asymmetry balancing and with ZD are shown in Fig. 2 in terms of the percentage of resources in a frame allocated to UL. The graph shows results for variable CoI DL demand and for variable first-tier DL demand. In the 6-cell scenario the demand is varied together for all six cells, whereas in the 1-cell scenario the demand is varied for only one of the six cells, while the rest have a constant demand of 50%. For asymmetry balancing the theoretical results for $R_{\mathrm{ul}} \times 100\%$ are omitted due to space constraints, however, a perfect match between theory and simulation is shown in [4, 5]. In the case of asymmetry balancing, as expected, when overall the DL resource occupancy increases, the number of resources allocated to UL by the virtual SP at the CoI decreases. It is interesting to note that due to the six degrees of freedom, when six cells cooperate, the number of resources allocated to UL by the virtual SP decreases much slower with decrease in resource availability as compared to the case when only one cell cooperates, where the number of UL resources decreases linearly. On Fig. 2 it can be seen that asymmetry balancing offers flexibility in resource allocation in that it adaptively allocates resources based on availability. Whenever there is little or no CoI DL demand, the asymmetry balancing can allocate the whole frame to UL, even in the case when only one cell cooperates. In addition, asymmetry balancing actually allocates resources on the chunk level, while ZD is limited to allocating resources to UL and DL on the time slot level according to the network design. Further limitation to ZD is that the maximum asymmetry which can be supported is 5:1 in favour of either link direction [7] (as seen on Fig. 2).

As was previously mentioned, when ZD is employed each cell sets its SP according to the ratio of UL and DL buffer size. This feature has an effect on the SP allocation as follows. The number of crossed slots influences the overall buffer size because as was explained in Section II only about a quarter of the users belonging to a given cell can be allocated during crossed slots. Hence, in general, the presence of crossed slots in a given link direction would result in more resources allocated to that link direction as compared to when there are no crossed slots. This effect is clearly seen on Fig. 2 for both the 1-cell scenario and the 6-cell scenario, where for 25% and 40% CoI DL demand there is an increase in the resources allocated to UL between 0% and 10% first-tier DL demand. When the first-tier DL demand is 0% the CoI UL does not experience any crossed slots, while the CoI DL experiences crossed slots (ref. to Table II). In constrast, when the first-tier DL demand is increased, the effect is reversed and the probability for crossed slots in UL increases while in DL the crossed slots probability decreases. The number of resources allocated to UL does not increase further (beyond 10% first-tier DL demand) because there is a limit on the maximum waiting time a packet can tolerate before being discarded (ref. to Section III), hence the UL buffer cannot grow infinitely.

Fig. 2 also shows that for moderate loads (both at the CoI and at the first-tier cells) the resource allocation achieved with asymmetry balancing (6-cell scenario) and ZD is similar, while for higher loads (1-cell scenario), in most cases ZD allocates more resources to UL than asymmetry balancing. However, as the spectral efficiency results demonstrate in the following, the scheme that allocates more resources to UL does not necessarily achieve higher UL spectral efficiency.

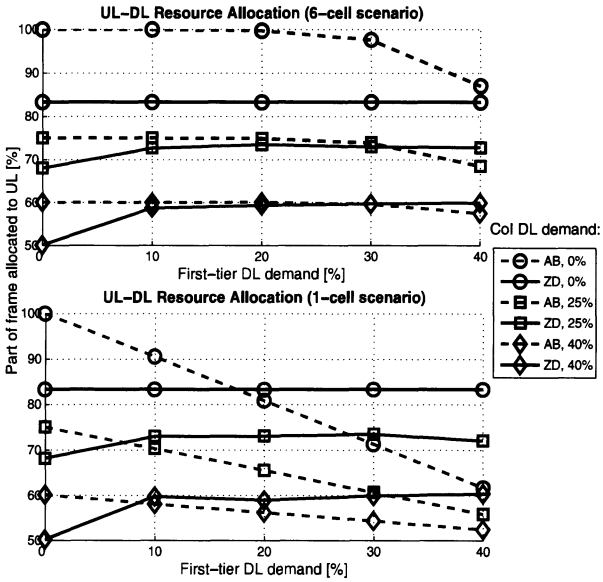

Fig. 2. Resources allocated to UL at the CoI by asymmetry balancing (AB) and ZD for various CoI DL demand: 6-cell scenario (top plot) and 1-cell scenario (bottom plot).

The spectral efficiency performance of the UL asymmetry balancing scheme is compared against that of ZD, based on (3), because it can capture not only SINR, but also resource utilisation:

$$C_{\mathrm{b}} = \frac{1}{C_{\mathrm{tot}}} \left(\sum_{i=1}^{M} \log_2(1+\gamma_i) + \frac{\overline{M}_{\mathrm{OL}}}{M_{\mathrm{OL}}} \sum_{j=1}^{M_{\mathrm{OL}}} \log_2(1+\gamma_j^{\mathrm{mh}}) \right) \quad (3)$$

where C_{b} is the spectral efficiency per chunk in bps/Hz; γ_i is the SINR of chunk i for single hop links; $M = \frac{u}{u+d} C_{\mathrm{tot}}$ is the number of chunks allocated to UL as per the network-wide SP; $\overline{M}_{\mathrm{OL}} = p\frac{d}{u+d} C_{\mathrm{tot}}$, is the number of DL chunks available for off-loading; M_{OL} is the number of chunks actually utilised for off-loading; and γ_j^{mh} is the SINR of chunk j for two-hop links. Clearly, for systems which do not employ asymmetry

balancing, $p = 0$, and the second term of the summation in (3) produces a zero. In addition, it should be noted that γ_j^{mh} is taken as the minimum of the SINR achieved at the first and second hops for each two-hop link. Furthermore, $\frac{M_{\mathrm{OL}}}{M_{\mathrm{OL}}}$ is used as a correction factor. The reason is as follows: As previously mentioned, due to simulation complexity, only twenty users per cell are simulated. As a result, not all available CFRs can be utilised for off-loading via a neighbouring RS. The number of available CFRs is only influenced by the actual load, i.e. fraction of available resources, which is independent of the number of users in the system. In contrast, how many of the available CFRs can be utilised for MS→RS links depends on user density (active and non-active users alike) because user density determines if and how often a two-hop path can be found. As a consequence, the spectral efficiency results are also influenced by the number of users in the system. Because, as was mentioned in Section II and demonstrated in [4], it can be safely assumed that in realistic scenarios all available CFRs can be actually utilised, the correction factor aims to obtain representative spectral efficiency performance.

The CoI UL spectral efficiency results for different DL resource demands are presented in Fig. 3 (top plot and bottom plot for the 6-cell scenario and 1-cell scenario, respectively). The solid line at about 2 bps/Hz shows the spectral efficiency

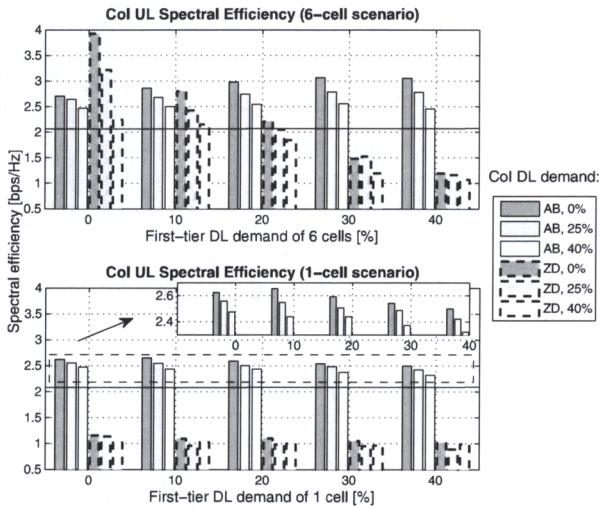

Fig. 3. Bar plots of the UL spectral efficiency performance at the CoI achieved with asymmetry balancing (AB) as compared to a ZD system.

achieved by a system where the TDD SP is synchronised. It can generally be observed that when severe BS→BS interference is present (i.e. high first-tier DL demand) such as is the case in the 1-cell scenario and 6-cell scenario for more than 20% DL demand, simply synchronising the TDD SP thereby avoiding the BS→BS results in a significant spectral efficiency improvement. Furthermore, asymmetry balancing attains spectral efficiency amelioration of more than 100% with respect to the spectral efficiency achieved by ZD. ZD outperforms asymmetry balancing only in the case of 0% DL demand in the 6-cell scenario, i.e. when none of the six first-tier cells has DL traffic, which is a highly unlikely situation. In addition, it is noted that in the 1-cell scenario the performance of ZD is relatively constant. This is due to the fact that five cells already cause BS→BS interference, and one additional interfering BS does not produce significant difference in the results. With respect to the asymmetry balancing performance, it can be seen that in the 6-cell scenario, even though there is a slight decrease in the number of resources utilised for asymmetry balancing as the first-tier DL demand increases (Fig. 2), the spectral efficiency performance at the CoI actually improves (Fig. 3 top plot). This effect can be attributed to the limited transmit power. When slightly fewer resources are used for transmission, there is more power available per resource and the attained SINR can compensate for the fact that less resources are utilised. A similar trend is observed in the 1-cell scenario (Fig. 3 bottom plot, zoomed area), but to a smaller extend because the difference in the number of resources utilised for asymmetry balancing for the varied first-tier DL demand is much greater (Fig. 2).

V. Conclusions

This study focused on the comparison of UL asymmetry balancing to the ZD interference avoidance approach. It was demonstrated that ZD compromises user demand by serving only about a quarter of the users during crossed slots, while BS→BS interference is not avoided. Asymmetry balancing, on the other hand, completely avoids BS→BS interference and achieves more than 100% higher UL spectral efficiency in comparison to the spectral efficiency attained with ZD for the considered scenarios.

References

[1] L. Le and E. Hossain, "Multihop Cellular Networks: Potential Gains, Research Challenges, and a Resource Allocation Framework," *IEEE Communications Magazine*, vol. 45, no. 9, pp. 66–73, Sep. 2007.

[2] C. Qiao, H. Wu, and O. Tonguz, "Load Balancing via Relay in Next Generation Wireless Systems," in *Workshop on Mobile and Ad Hoc Networking and Computing (MobiHOC)*, Boston, Massachusetts, USA, Aug. 11 2000, pp. 149–150.

[3] H. Haas and S. McLaughlin, Eds., *Next Generation Mobile Access Technologies: Implementing TDD*. Cambridge University Press, ISBN: 13:9780521826228, Jan. 2008, 420 pages.

[4] E. Foutekova, S. Sinanović, and H. Haas, "Traffic Asymmetry Balancing in OFDMA-TDD Cellular Networks," *Journal of Communications and Networking (JCN), Special Issue on Wireless Cooperative Transmission and its Applications*, vol. 10, no. 2, p. (to appear), 2008.

[5] ——, "Asymmetry Balancing for Channel Asymmetry Support in OFDMA-TDD Cellular Networks," in *Proc. of the 68th IEEE Vehicular Technology Conference (VTC)*, Calgary, Canada, Sep. 21–24 2008.

[6] S.-H. Wie and D.-H. Cho, "Time Slot Allocation Scheme Based on a Region Division in CDMA/TDD Systems," in *Proc. of the Vehicular Technology Conference (VTC)*, Rhodes, Greece, May 6–9 2001, pp. 2445–2449.

[7] IST-2003-507581 WINNER, "D2.10, Final report on identified RI key technologies, system concept and their assessment," Retrieved Mar. 15, 2007, from https://www.ist-winner.org/DeliverableDocuments/, Dec. 2005.

[8] F. Gessler, "Developing Technical Standards – Balancing History and Pre-conceptions," in *Proc. of the International Association for Management Technology Conference (IAMOT)*, Lausanne, Switzerland, Mar. 19–22 2001.

[9] WiMAX Forum, "WiMAX Business Case," Retrieved Apr. 8, 2008 from http://www.hkwtia.org/wtia/, Sep. 2004.

[10] IST-4-027756 WINNER II, "D1.1.2 v1.2 WINNER II Channel Models," Retrieved Feb. 5, 2008, from https://www.ist-winner.org/WINNER2-Deliverables/.

[11] T. Bonald, "A Score-Based Opportunistic Scheduler for Fading Radio Channels," in *Proc. of the European Wireless Conference (EWC)*, Barcelona, Spain, Feb. 24–27, 2004.

[12] K. Hole, H. Holm, and G. Øien, "Adaptive Multidimensional Coded Modulation Over Flat Fading Channels," *IEEE Journal on Selected Areas in Communications*, vol. 18, no. 7, pp. 1153–1158, Jul. 2000.

Channel Asymmetry and Random Time Slot Hopping in OFDMA-TDD Cellular Networks

Ellina Foutekova*, Patrick Agyapong†, and Harald Haas*
*Institute for Digital Communications, The University of Edinburgh, Edinburgh EH9 3JL, UK
E-mail: {E.Foutekova, H.Haas}@ed.ac.uk
† E-mail: pagyapong@jacobs-alumni.de

***Abstract*—This paper studies the performance of orthogonal frequency division multiple access – time division duplex (OFDMA-TDD) cellular networks when jointly applying dynamic channel allocation (DCA) and user scheduling under the assumption of asymmetric uplink (UL)/downlink (DL) loads. Specifically, a comparison between a fixed slot allocation (FSA) scheme, where the uplink UL/DL switching is synchronised across the network, and the random time slot opposing (RTSO) technique is made. The RTSO resembles an opportunistic interference mitigation technique. RTSO, however, does not obviate the need for user scheduling algorithms, but the combined use of RTSO and scheduling has not been studied. Therefore, two different scheduling algorithms, greedy and fair, are adapted to suit the OFDMA-TDD architecture. Their performance for various channel asymmetries under RTSO and symmetric FSA is evaluated, based on spectral efficiency and user outage. In order to account for the exposed location of base station (BS) antennas in a cellular environment, the effect of line-of-sight (LOS) propagation among BSs is considered. The results show that LOS among BSs in a system with unsynchronised switching points strongly hampers the network's performance. This effect, however, is demonstrated to be substantially offset by DL-favoured asymmetries (dominant in data-centric networks) in combination with RTSO. Furthermore, it is shown that the greedy algorithm only offers a marginal increase in spectral efficiency as compared to the fair algorithm, while the fair algorithm exhibits up to ≈20% lower outage.**

I. Introduction

Orthogonal frequency division multiplexing (OFDM) has been a subject of considerable interest in the recent years for cellular systems of 3G evolution and beyond. Wong *et al*. [1] show promising results for OFDM as a multi-user technique, particularly focusing on the gains in using adaptive modulation. The gains in combining OFDM with an adequate multiple access scheme have been thoroughly described in [2], specifically emphasising on the superiority of frequency division multiple access (FDMA).

The combination of OFDM with TDD, which enables the support of asymmetric services, is of especial interest. However, in an unsynchronised system, TDD suffers from additional interference as compared to frequency division duplex (FDD). One approach to overcome this drawback is to synchronise the transmission states of all cells (synchronised UL/DL switching points), as is the case in an FSA scheme. The FSA, however, significantly hampers the key advantage of TDD, namely to dynamically adapt to cell specific channel asymmetry demands.

A technique, which exploits the inherent interference diversity in cellular TDD networks in order to decrease the detrimental BS-BS interference, while retaining the channel asymmetry support, has been previously reported as RTSO and tested on code division multiple access (CDMA) systems [3]. RTSO, i.e. the random assignment of UL/DL time slots, when used in cellular systems, has been shown to result in occasionally lower interference than that of an equivalent FDD network.

This study is in the framework of a multi-user, multi-cell OFDMA-TDD network with full frequency reuse. The performance of a system employing RTSO under various channel asymmetries is compared to the performance of a symmetric FSA system. A fair and a greedy approach to scheduling are studied and scenarios with LOS and non-line-of-sight (NLOS) conditions among the BSs are considered. The purpose of this paper is to get insight into the severity of interference during various UL/DL channel asymmetries and explore the extent to which RTSO mitigates this interference. Furthermore, in the above context, we draw conclusions with respect to the comparative performance of a greedy and a fair approach to scheduling in an OFDMA-TDD system. The two considered algorithms are the fair *optimum target assignment with stepwise rate removals* (OTA-SRR) [4] and the greedy *greedy rate packing* (GRP) [5].

II. System Model

This section introduces the model of the signal-to-interference-plus-noise ratio (SINR) and its interference components: multiple access interference (MAI) and co-channel interference (CCI). MAI is the interference experienced from own-cell links, whilst CCI is the interference experienced from other-cell links.

Let $\overline{\gamma}_k$ be the target SINR of subcarrier k, such that $\overline{\gamma}_k \in \{\tilde{\gamma}_1 < \tilde{\gamma}_2 < \cdots < \tilde{\gamma}_m\}$ and suppose a number of m discrete transmission rates are available, $r_k \in \{r_1 < r_2 < \cdots < r_m\}$ depending on the modulation alphabet, where each SINR target element corresponds to each rate respectively. Employing adaptive modulation, if a subcarrier can support a high SINR, high data rate transmission for the same BER (bit error ratio) can be maintained on that subcarrier, simply by using a high order modulation scheme.

In determining a subcarrier's SINR both small-scale fading and large-scale fading are taken into consideration. Let subcarrier $k \in \boldsymbol{s} = \{a_1, \ldots, a_m\}$, where $a_i \in \{1, \ldots, N_c\}$ and $\boldsymbol{s}$ is a set of subcarriers belonging to a single user in cell i and k does not experience interference from the set. The cardinality of $\boldsymbol{s}$, $|\boldsymbol{s}|$, is the number of subcarriers per user, which can vary from zero to N_c (total number of subcarriers per BS). The received signal power (in Watts) on subcarrier k in cell i

978-1-4244-1645-5/08/$25.00 ©2008 IEEE

is given by:

$$R_k^i = P_k^i G_k^i |H_k^i|^2 \quad (1)$$

where P_k^i is the transmit power on subcarrier k in cell i, G_k^i is the path gain between the MS using subcarrier k and its corresponding BS, and H_k^i is the channel transfer function for subcarrier k in cell i between the MS using subcarrier k and its corresponding BS.

The multiple access interference power (in Watts) on subcarrier k in UL is given by (2). It should be noted that MAI in DL is not considered, as perfect synchronisation is assumed.

$$P_{\mathrm{MAI},k}^i = \sum_{\substack{k'=1 \\ k' \notin \boldsymbol{s}}}^{N_c} P_{k'}^i G_{k,k'}^i |H_{k,k'}^i|^2 |C_{k,k'}^i(\Delta f + \varepsilon_D + \omega)|^2 \quad (2)$$

where

$$C_{k,k'}^i(x) = \left(\frac{1}{N_c}\right) \frac{\sin(\pi x)}{\sin(\pi x/N_c)} \exp \frac{j\pi x(N_c-1)}{N_c} \quad (3)$$

and $G_{k,k'}^i$ is the path gain between the transmitter on the link using subcarrier k' and the receiver on the link using subcarrier k, $H_{k,k'}^i$ is the transfer function of the channel between the transmitter on the link using subcarrier k' and the receiver on the link using subcarrier k, $C_{k,k'}^i(\Delta f + \varepsilon_D + \omega)$, given in (3), is a cyclic sinc function[1] to account for the amount of interference subcarrier k experiences from subcarrier k', j is the imaginary unit, $\Delta f = k' - k$ and $\varepsilon_D = \frac{f_{D,\max}}{\delta_f}$ accounts for the Doppler shift; where $f_{D,\max}$ is the maximum Doppler frequency and δ_f is the subcarrier spacing, $\omega = \frac{f_c}{\delta_f}$ is the normalised frequency offset due to synchronisation errors between subcarriers k and k', with f_c is the offset in Hz.

The co-channel interference power is modeled similarly to the MAI power on a subcarrier and is given by (4). Co-channel interference contributions are expected not only from the reused subcarrier, but also from neighboring subcarriers, since synchronisation errors and Doppler are considered.

$$P_{\mathrm{CCI},k}^i = \sum_{\substack{l=1 \\ l \neq i}}^{B} \sum_{k'=1}^{N_c} P_{k'}^l G_{k,k'}^l |H_{k,k'}^l|^2 |C_{k,k'}^l(\Delta f + \varepsilon_D + \omega)|^2 \quad (4)$$

where B is the number of cells under consideration (cells that contribute non-negligible interference).

Based on (1) through (4), the SINR for subcarrier $k \in \boldsymbol{s}$ in cell i can be written as:

$$\gamma_k^i = \frac{P_k^i \tilde{G}_k^i}{\sum_{l=1}^{B} \sum_{\substack{k'=1 \\ \text{if } l=i, k' \notin \boldsymbol{s}}}^{N_c} P_{k'}^l \tilde{G}_{k,k'}^l(\cdot) + n} \quad (5)$$

where $\tilde{G}_k^i = G_k^i |H_k^i|^2$ is the weighted gain on the "desired" link for subcarrier $k \in \boldsymbol{s}$, $\tilde{G}_{k,k'}^l(\cdot) = G_{k,k'}^l |H_{k,k'}^l|^2 |C_{k,k'}^l(\Delta f + \varepsilon_D + \omega)|^2$ is the weighted gain of the interfering link between the transmitter on the link using subcarrier k' and the receiver on the link using subcarrier k, and n is the thermal noise power per subcarrier.

[1]Due to space constraints the derivation of the cyclic sinc function is omitted.

III. Scheduling Algorithms

The two alternative scheduling approaches, a greedy and a fair one, are presented in this section, along with the modifications introduced by the authors to adapt the scheduling schemes to the OFDMA architecture.

A. Modified GRP

GRP is a simple heuristic rate allocation scheme, which formulates the problem of supporting different users with different data rates into a joint power and rate control. It can be interpreted as a practical form of water-filling, in the sense that high transmission rates and low power are allocated to users having high link gains and low interference.

An extensive work on GRP for direct sequence code division multiple access (DS-CDMA) systems is presented in [5] where it was applied to a single cell, using a fixed intercell interference. In this paper, the GRP algorithm is formulated for a multi-cellular TDD-based OFDMA system, where it is shown that a similar water-filling mechanism can be employed.

Given a vector of powers with elements being the power on each subcarrier, $\boldsymbol{P} = (P_1, P_2, \ldots, P_{N_c})^T$, the received SINR of subcarrier k , is defined by (6) and (7), here slightly rearranged to suit the purpose of the algorithm (all parameters belong to the same cell, thus superscripts used earlier to indicate cell index are omitted).

$$\gamma_{k,UL} = \frac{P_k G_k |H_k|^2}{\sum_{\substack{k'=1 \\ k' \notin \boldsymbol{s}}}^{N_c} |S_{k,k'}|^2 |H_{k,k'}|^2 |C_{k,k'}(z)|^2 + P_{\mathrm{CCI},k} + n} \quad (6)$$

$$\gamma_{k,DL} = \frac{P_k G_k |H_k|^2}{P_{\mathrm{CCI},k} + n} \quad (7)$$

where $\gamma_{k,UL}$ and $\gamma_{k,DL}$ are the SINR on subcarrier k in UL and DL respectively, $z = \Delta f + \varepsilon_D + \omega$, $|S_{k,k'}|^2 = P_{k'} G_{k,k'}$, and $P_{\mathrm{CCI},k}$ is the co-channel interference on subcarrier k.

An interesting question is to find an SINR assignment which maximises the throughput while utilising the minimum power. If $\overline{p}$ is the maximum power allowed per subcarrier and $\boldsymbol{\Gamma}$ is the set of discrete-valued SINR targets in ascending order, the problem of maximising throughput using the optimum power can be expressed mathematically as:

$$\min \textstyle\sum_{k=1}^{N_c} P_k, \quad (8)$$

such that

$$\overline{\gamma}_k \in \boldsymbol{\Gamma}, \ \boldsymbol{\Gamma} = \{0, \tilde{\gamma}_1, \tilde{\gamma}_2, \ldots, \tilde{\gamma}_{|\boldsymbol{\Gamma}|}\}$$

$$0 \leq P_k \leq \overline{p} \quad (9)$$

This problem is solved separately for DL and UL. An important corollary from [5] is used here: *if the subcarriers are arranged according to* $G_1|H_1|^2 \geq G_2|H_2|^2 \geq \cdots \geq G_{N_c}|H_{N_c}|^2$*, the total power in the cell is minimised if the SINR targets are assigned such that* $\overline{\gamma}_1 \geq \overline{\gamma}_2 \geq \cdots \geq \overline{\gamma}_{N_c}$.

1) DL Transmission and Power Constraints: The required power, P_k, on a subcarrier k in the DL is given by:

$$P_k = \frac{\overline{\gamma}_k}{G_k |H_k|^2} \left(P_{\mathrm{CCI},k} + n\right) \quad (10)$$

This follows by rearranging (7). Using (10), the problem statement for DL can be expressed as:

$$\min \textstyle\sum_{k=1}^{N_c} \frac{\overline{\gamma}_k}{G_k |H_k|^2} \left(P_{\mathrm{CCI},k} + n\right),$$

such that (9) becomes

$$\max(\overline{\gamma}_k) \leq \frac{\overline{p}\ G_k |H_k|^2}{P_{\mathrm{CCI},k} + n}$$

2) UL Transmission and Power Constraints: By expanding and rearranging (6), the required power, P_k, on a subcarrier k in UL is given by:

$$P_k = \frac{\overline{\gamma}_k \left(\frac{\sum_{k'=1}^{N_c} \frac{\overline{\gamma}_{k'} |C_{k,k'}(z)|^2 (P_{CCI,k'} + n)}{1 + \overline{\gamma}_{k'} |C_{k,k'}(z)|^2}}{1 - \sum_{k'=1}^{N_c} \frac{\overline{\gamma}_{k'} |C_{k,k'}(z)|^2}{1 + \overline{\gamma}_{k'} |C_{k,k'}(z)|^2}} + P_{\mathrm{CCI},k} + n \right)}{G_k |H_k|^2} \quad (11)$$

where

$$\sum_{k'=1}^{N_c} \frac{\overline{\gamma}_{k'} |C_{k,k'}(z)|^2}{1 + \overline{\gamma}_{k'} |C_{k,k'}(z)|^2} < 1$$

If k and k' belong to the same user, then $|C_{k,k'}(z)|^2 = 0$. For the special case where all subcarriers in a cell belong to one user, the required power is the same as the case for DL.

The equivalent problem statement for UL can be expressed using (11) as:

$$\min \sum_{k=1}^{N_c} \frac{\overline{\gamma}_k \left(\frac{\sum_{k'=1}^{N_c} \frac{\overline{\gamma}_{k'} |C_{k,k'}(z)|^2 (P_{CCI,k'} + n)}{1 + \overline{\gamma}_{k'} |C_{k,k'}(z)|^2}}{1 - \sum_{k'=1}^{N_c} \frac{\overline{\gamma}_{k'} |C_{k,k'}(z)|^2}{1 + \overline{\gamma}_{k'} |C_{k,k'}(z)|^2}} + P_{\mathrm{CCI},k} + n \right)}{G_k |H_k|^2},$$

such that (9) becomes

$$\sum_{k'=1}^{N_c} \frac{\overline{\gamma}_{k'} |C_{k,k'}(z)|^2}{1 + \overline{\gamma}_{k'} |C_{k,k'}(z)|^2} \leq 1 - \max \left(\frac{\overline{\gamma}_k \sum_{k'=1}^{N_c} \frac{\overline{\gamma}_{k'} |C_{k,k'}(z)|^2 (P_{CCI,k'} + n)}{1 + \overline{\gamma}_{k'} |C_{k,k'}(z)|^2}}{\overline{p} G_k |H_k|^2 - \overline{\gamma}_k (P_{\mathrm{CCI},k} + n)} \right) \quad (12)$$

3) GRP Algorithm: Based on the DL and UL power constraints, a rate packing algorithm is developed, which aims to achieve the maximum rate possible while using the minimum power. A main underlying assumption is $G_1|H_1|^2 \geq G_2|H_2|^2 \geq \cdots \geq G_{N_c}|H_{N_c}|^2$. The modified GRP algorithm is shown below:

1) $\overline{\gamma}_k = 0 \; \forall k$

2) **for** $k = 1$ **to** N_c **do**

   a) **if** UL

$$\overline{\gamma}_k = \left\{ \max(\gamma) \in \mathbf{\Gamma} : \sum_{k'=1}^{k} \frac{\overline{\gamma}_{k'} |C_{k,k'}(z)|^2}{1 + \overline{\gamma}_{k'} |C_{k,k'}(z)|^2} \leq 1 - \frac{\gamma \sum_{k'=1}^{k} \frac{\overline{\gamma}_{k'} |C_{k,k'}(z)|^2 (P_{CCI,k'} + n)}{1 + \overline{\gamma}_{k'} |C_{k,k'}(z)|^2}}{\overline{p} G_k |H_k|^2 - \gamma (P_{\mathrm{CCI},k} + n)} \right\}$$

   b) **if** DL

$$\overline{\gamma}_k = \left\{ \max(\gamma) \in \mathbf{\Gamma} : \gamma \leq \left[\frac{\frac{\overline{p}}{\overline{P_{\mathrm{CCI},k} + n}}}{G_k |H_k|^2} \right] \right\}$$

3) **end**

B. Modified OTA-SRR

The OTA-SRR algorithm is a rate and power allocation scheme for UL and DL. Results have been reported for a 2G system with seven-cell reuse and one user per cell [4]. In the current study the OTA-SRR scheduling scheme is formulated as a subcarrier, rate and power allocation algorithm for an OFDMA system architecture. The new algorithm operates at the most basic level, i.e. at the subcarrier level, as generalisation to a more efficient chunk-level operation is straightforward. The mechanism of the modified OTA-SRR is briefly introduced. First, all subcarriers are distributed equally among the users and assigned maximum SINR targets chosen out of a predefined target set. Iteratively the subcarriers, subject to worst link conditions, are identified. Their SINR target is decreased in a step-wise manner, in effect adapting the modulation scheme. If the SINR target of a subcarrier is downrated below the minimum value from the target set, this subcarrier is given to a different user from the same BS, which can make use of it with minimum interference. If no such user is found, the subchannel is not used. OTA-SRR is executed until the number of subcarriers in use and their respective data rates can be supported. The criterion for convergence is subordinated to the basic mathematical framework, outlined in [4].

The algorithm takes into account the interference effects among all subcarriers, thus each subcarrier (out of the total considered in the algorithm, i.e. $BN_c = N$) is given a unique identification (ID) number in the range $[1, 2, \ldots, N]$ (i.e. subcarrier one used in cell one has ID 1, subcarrier one in cell two has ID $N_c + 1$, subcarrier two used in cell two has ID $N_c + 2$, and so on). Based on this, the SINR equation given in (5) can be rewritten as:

$$\gamma_k = \frac{P_k \tilde{G}_k}{\sum_{\substack{k'=1 \\ k' \notin s}}^{N} P_{k'} \tilde{G}_{k,k'} + n} \quad (13)$$

Each subcarrier strives to achieve SINR greater or equal to the target, thus (13) can be straightforwardly written as an inequality. Further, by dividing the numerator and denominator of the right hand side by $\tilde{G}_k$ and transforming it into matrix notation, (13) can be rewritten as $(\mathbf{I} - \mathbf{\Phi})\mathbf{P} \geq \boldsymbol{\eta}$, where $\mathbf{I}$ is the identity matrix, $\mathbf{\Phi}$, defined in (14), is the normalised link gain matrix (with dimensions $N \times N$), and $\boldsymbol{\eta}$ is the normalised noise vector, also defined in (14).

$$\Phi_{k,k'} = \frac{\overline{\gamma}_k \tilde{G}_{k,k'}(\cdot)}{\tilde{G}_k} \qquad \eta_k = \frac{\overline{\gamma}_k n}{\tilde{G}_k} \quad (14)$$

with $\overline{\gamma}_k \in \mathbf{\Gamma}$, $\forall k \in N$. The algorithm is defined based on the properties of $\mathbf{\Phi}$ and its dominant eigenvalue λ_1. For $\mathbf{\Phi}$ it holds that it is real, nonnegative and irreducible, based on (14), i.e. the path gains and the SINR targets are real and nonnegative, and the path gains are assumed to be uncorrelated. The modified OTA-SRR algorithm is outlined below:

1) initialisation: iteration $k = 0$; target

$$\overline{\gamma}_i(0) = \max\{\mathbf{\Gamma}\} = \tilde{\gamma}_{|\mathbf{\Gamma}|}, \forall i \in N$$

2) **while** $\lambda_1 > 1 - \max_{i \in N} \left\{ \frac{\eta_i}{\overline{p}} \right\}$

   a. find row j with maximum row-sum

$$j = \arg \max_{i \in N} \sum_{i=1}^{N} \Phi_{i,j}$$

   used by user q

   b. adapt the modulation scheme of subcarrier j: reduce $\overline{\gamma}_j$ accordingly

   c. **if** $\overline{\gamma}_j < \tilde{\gamma}_1$

      i. take away subcarrier i from user q

      ii. **if** user q has zero subcarriers left

         i. block user q

iii. find user r from the same BS as q such that the interference on j is minimised (minimum row sum of $\mathbf{\Phi}$)
iv. **if** $q = r$
i. delete row j and column j of $\mathbf{\Phi}$, η_j, and $\overline{\gamma}_j$ (i.e. block subcarrier j)
v. **else** assign subcarrier j to user r with $\overline{\gamma}_j = \tilde{\gamma}_{|\mathbf{\Gamma}|}$

d. recalculate Φ_j, η_j, and λ_1
g. $k = k + 1$

IV. Simulation Model

A 19-cell system (Table I) with 200 uniformly distributed users is considered in this paper. Each cell has a centrally-located BS, which can be either transmitting or receiving, with a probability depending on the asymmetry scenario (modeling a TDD system). UL:DL ratios of 1:1, 1:6, and 6:1 are explored. The UL/DL time slots are randomly assigned and can be either synchronised (FSA) or non-synchronised (RTSH) among all cells. A quasi-static model is employed where the link gains between transmitters and receivers remain unchanged for a time slot duration. A BS-MS pair (i.e. a link) is formed based on minimum path loss. It is assumed that the QoS desired by a user corresponds to the maximum data rate it can support. Furthermore, each receiving unit has full channel information, enabling it to calculate the SINR. The signalling overhead introduced is not a subject of this paper, however it is envisaged that this overhead could be offset by the gains in performance. Interference is calculated assuming constant frequency offset and maximum Doppler frequency leading to a worst case scenario. Moreover, it is assumed that proper cyclic prefix is in place such that inter-symbol interference (ISI) is avoided. A cross-layer approach is used to reflect

TABLE I
Fixed parameters

Number of BSs	19		Number of MSs	200
Cell radius	500 m		Bandwidth	100 MHz
Number of subcarriers	2048		RMS delay spread	0.27 μs
Carrier freq.	1.9 GHz		$f_{D,\max}$	190 Hz
Max. power/link	2 W		ω	0.5

small-scale and large-scale fading in a typical time-variant frequency selective channel. The small-scale fading effects for a typical outdoor scenario which includes the effects of Doppler shift and time delay is simulated using a power delay profile corresponding to the specified delay spread in Table I. The path loss model to account for large-scale fading is chosen accordingly, [6] - Terrain Category A (suburban).

Results for NLOS conditions for all TDD interference scenarios (MS-BS, BS-MS, BS-BS, MS-MS) are compared to LOS for BS-BS interference (and NLOS for the remaining scenarios). The path loss in the case of LOS is calculated using the free space path loss model and worst case scenario is assumed with 100% probability of LOS. Adaptive modulation is achieved with seven different modulation schemes [7] given in Table II, based on the received SINR for a BER of 10^{-7} (necessary for real-time services such as video streaming). The corresponding data rates, Υ, are calculated using $\Upsilon = \frac{M\Upsilon_{\text{code}}}{T_{\text{s}}}$, where M is the number of bits per symbol, Υ_{code} is the code rate (here, 2/3), and T_{s} is the symbol time (including cyclic prefix of 20%). It should be noted that the CROSS and STAR constellations are QAM-variations in order to ensure robustness to interference, as described in [8] and [9], respectively.

TABLE II
From top to bottom: modulation schemes (row one) with the respective data rates (row two), and the respective required SINR values (row three) at BER of 10^{-7}

4 QAM	8 STAR	16 QAM	32 CROSS	64 QAM	128 CROSS	256 QAM	units
54.2	81.4	108.5	135.6	162.7	189.9	217.0	kbps
9	14	16	19	22.2	25	28.5	dB

V. Results and Discussion

The algorithms implemented in this study are evaluated on the basis of *spectral efficiency*, and *outage*. Spectral efficiency is the achieved system throughput divided by the total bandwidth divided by the number of base stations and outage is defined as the users not served (due to low SINR) as a fraction of the total number of users in the system.

The variation of spectral efficiency with asymmetry and LOS conditions for the BSs can be seen in Fig. 1. A clear trend can be observed for both scheduling schemes – with an increase in the number of time slots allocated to DL, the spectral efficiency increases and reaches 90% of the theoretical maximum, which is $\frac{\Upsilon_{\max} \times N_c \times B}{W} / B = \frac{\Upsilon_{\max}}{W_c} = 4.44$ bps/Hz/cell, where W is the bandwidth, W_c is the bandwidth per subcarrier, and $\Upsilon_{\max}$ is the maximum data rate per subcarrier (as given in Table II). Moreover, LOS conditions among BSs degrade performance significantly; for an asymmetry of 6:1 (UL:DL), the spectral efficiency (at the 50^{th} percentile) for OTA-SRR and GRP decreases by ≈30% and ≈50%, respectively. The systems employing DL-favoured asymmetry are more robust to LOS. Only a slight decrease in the spectral efficiency is observed when LOS condition among the BSs is introduced: ≈8% and ≈6% at the 50^{th} percentile for OTA-SRR and GRP, respectively. This observation is as expected, due to the fact that in DL-favoured asymmetries, the occurrence of BS-BS interference is significantly limited. The outage results shown in Fig. 2, display a similar trend to the spectral efficiency results.

Intuitively it is expected that a symmetric FSA scheme exhibits better performance than an equivalent RTSO system, since it avoids the detrimental BS-BS, as well as MS-MS interference. However, it can be observed that neither of the schemes is strictly better than the other. For instance, assuming OTA-SRR it can be found that for RTSO the probability that the spectral efficiency is greater than 2.25 bps/Hz/cell is about 95%, whereas for FSA this probability is only about 75%. On the other hand, when assuming a spectral efficiency of 3 bps/Hz/cell, it can be found that the same probability for RTSO is 10% whereas the probability for FSA is 30%. As expected their medians generally coincide (due to the fact that the rate of asymmetry is the same) and moreover, the FSA curve spans between the 1:6 (DL-dominated) NLOS and 6:1 (UL-dominated) NLOS RTSO cases. The latter effect is attributed to the shifting of more resources to UL (DL), which creates an interference scenario (MS-BS (BS-MS)) similar to the UL (DL) FSA. Furthermore, it can be observed that the cumulative density function (cdf) graphs for FSA are

generally spread out, whereas the cdf graphs for RTSO are comparatively steeper. This means that RTSO offers a more stable and robust QoS, whilst the QoS offered by the FSA is with larger variation.

With respect to the comparative performance of the two scheduling schemes presented in this paper, the results show a similar trend in the explored metrics. However, GRP, which allocates subcarrier, rate and power in a greedy manner, fails to fully exploit the frequency selectivity of the channel by allocating resources to the best placed user (in terms of link gain). Thus, only a marginal increase in spectral efficiency is achieved at the cost of outage. It is interesting to draw a comparison of these trends to a similar study done for a CDMA system in [10] with the same cell radius, number of cells, number of users as in the present study. For the case of CDMA, the greedy GRP algorithm as compared to the OTA-SRR scheme displays two-fold increase in terms of total system data rate but serves only 30% of the users, which are served under the OTA-SRR scheme. Thus, unlike CDMA, in an OFDMA system it is not efficient to allocate all resources to one (few) user(s), due to the large bandwidth and thus pronounced frequency selectivity, which can otherwise be successfully exploited by user diversity.

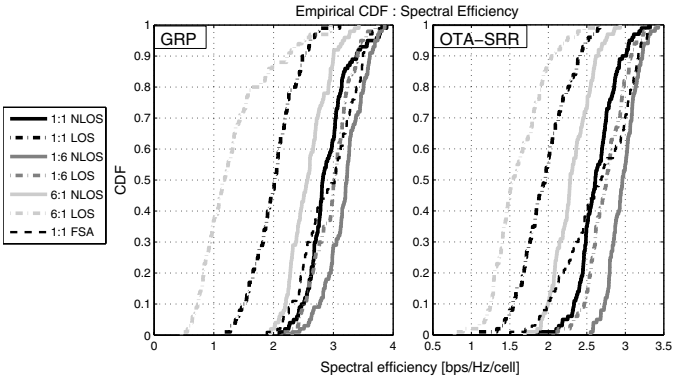

Fig. 1. Spectral efficiency results for various UL:DL asymmetries: GRP (left) and OTA-SRR (right)

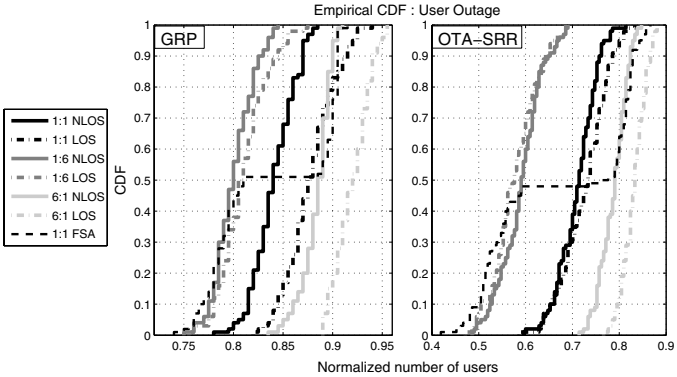

Fig. 2. User outage results for various UL:DL asymmetries: GRP (left) and OTA-SRR (right)

VI. Summary and Conclusions

In this paper, the effects of channel asymmetry on a multi-user OFDMA-TDD system employing RTSO are studied and compared to a symmetric FSA system. The analysis is done based on two scheduling algorithms, following different approaches to resource allocation: greedy and fair. The results demonstrate that UL is the performance limiting factor due to unfavourable interference and the hazardous effect of LOS conditions among BSs. Shifting more resources in DL provides a system which is robust to these TDD-inherent problems, irrespective of whether FSA or RTSO is employed. Such a DL-favoured scenario attains up to 90% of the maximum spectral efficiency achievable by the network. Furthermore, the RTSO can successfully exploit interference diversity and thus outperform the FSA scheme. In particular, for the same asymmetry RTSO performs better than FSA in around 50% of all the cases. The results further show that overall the fair OTA-SRR scheduling algorithm is more robust to the detrimental TDD-specific BS-BS interference than the greedy GRP algorithm. Moreover, the greedy nature of GRP does not allow for the frequency diversity, offered by the large bandwidth, to be effectively exploited. In contrast, the fair OTA-SRR makes use of the frequency diversity by offering service to up to 20% more users and still achieving spectral efficiencies only marginally lower than those attained by the GRP. Hence, RTSO when combined with (OTA-SRR) fair scheduling allows the system to retain high spectral efficiency while maintaining fairness in an OFDM-TDD cellular network with asymmetric traffic.

References

[1] C. Y. Wong, R. S. Cheng, K. B. Lataief, and R. D. Murch, "Multiuser OFDM with adaptive subcarrier, bit, and power allocation," *IEEE Journal on Selected Areas in Communications*, vol. 17, no. 10, pp. 1747–1758, October 1999.

[2] H. Rohling and R. Grüneid, "Performance Comparison of Different Multiple Access Schemes for the Downlink of an OFDM Communication System," in *Proceedings of the 47th IEEE Vehicular Technology Conference (VTC)*, vol. 3, Phoenix, AZ, May 4–7, 1997, pp. 1365–1369.

[3] H. Haas, P. K. Jain, and B. Wegmann, "Capacity Improvement Through Random Timeslot Opposing (RTO) Algorithm in Cellular TDD Systems with Asymmetric Channel Utilisation," in *Proceedings of the 14th IEEE International Symposium on Personal, Indoor and Mobile Radio Communications (PIMRC)*, vol. 2, Beijing, China, September 2003, pp. 1790–1794.

[4] S. Ginde, "A Game-theoretic Analysis of Link Adaptation in Cellular Radio Networks," Master's thesis, Virginica Polytechnic Institute and State University, May 2004.

[5] F. Berggren and S.-L. Kim, "Energy-efficient Control of Rate and Power in DS-CDMA Systems," *IEEE Transactions on Wireless Communications*, vol. 3, no. 3, pp. 725–733, May 2004.

[6] V. Erceg, L. J. Greenstein, S. Y. Tjandra, S. R. Parkoff, A. Gupta, B. Kulic, A. A. Julius, and R. Bianchi, "An Empirically Based Path Loss Model for Wireless Channels in Suburban Environments," *IEEE Journal on Selected Areas in Communications*, vol. 17, no. 7, pp. 1205–1211, July 1999.

[7] K. Hole, H. Holm, and G. Øien, "Adaptive Multidimensional Coded Modulation Over Flat Fading Channels," *IEEE Journal on Selected Areas in Communications*, vol. 18, no. 7, pp. 1153–1158, July 2000.

[8] W. Webb, L. Hanzo, and R. Steele, "Bandwidth-efficient QAM Schemes for Rayleigh Fading Channels," in *Proceedings of the Fifth International Conference on Radio Receivers and Associated Systems*, July 23–27 1990, pp. 139–142.

[9] J. Forney, G., R. Gallager, G. Lang, F. Longstaff, and S. Qureshi, "Efficient Modulation for Band-Limited Channels," *IEEE Journal on Selected Areas in Communications*, vol. 2, no. 5, pp. 632–647, September 1984.

[10] E. Foutekova, P. Agyapong, B. Ghimire, H. Venkataraman, and H. Haas, "Scheduling in Cellular TDD-CDMA Networks," in *Proceedings of the 64th IEEE Vehicular Technology Conference (VTC)*, Montreal, Canada, September 25–28 2006, pp. 1–5.

Semi-Analytical Model of Interference in CDMA-TDD Using Random Time Slot Hopping

Ellina Foutekova, Christine Evers and Harald Haas
School of Engineering and Science
International University Bremen
28759 Bremen, Germany
E-mail: e.foutekova@iu-bremen.de, cevers@world.iu-bremen.de, h.haas@iu-bremen.de

***Abstract*— In this paper, a semi-analytical approach for the performance analysis of the random time slot (TS) hopping (RTSH) algorithm applied to code division multiple access - time division duplex (CDMA-TDD) systems will be given. TDD systems are subject to two independent interference scenarios, giving rise to interference diversity, which is exploited by the RTSH algorithm. Depending on the actual slot assignment, the system either experiences same-entity interference (MS (mobile station)-to-MS and BS (base station)-to-BS interference) or other-entity interference (MS-to-BS and BS-to-MS interference). The RTSH algorithm results in a random switching between these two scenarios, each of which will result in a different level of interference. Thereby, constant severe interference is avoided. It has been shown that the RTSH algorithm results in lowest interference for channel asymmetries in favor of the downlink (DL).**

I. Introduction

The increase in demand for ubiquitous wireless services necessitates improved wireless communication systems with efficient utilization of the limited spectrum. Code division multiple access-time division duplex (CDMA-TDD) efficiently supports both real-time and non-real time traffic [1], by multiplexing uplink (UL) and downlink (DL) into time slots (TS) on the same frequency band [2]. As each user is assigned a unique pseudo noise (PN) code in CDMA, multiple users can occupy the same TS, which is especially beneficial for packet data traffic, as it requires efficient support for a high peak-to-average data rate ratio. Through TDD transmission, asymmetric resource allocation between UL and DL can be flexibly adjusted. This is advantageous, as multimedia services have different and time-varying transmission volume demands in each link. Trading the capacities in both links against each other therefore maximizes resource utilization and the channel reciprocity, characteristic of TDD, allows for accurate and open-loop power control in transmission. Furthermore, in contrast to frequency division duplex (FDD) systems, TDD facilitates ad-hoc and multihop operation.

Interference, as a limiting factor in CDMA, is of particular concern to TDD-based systems. The latter are subject to additional same-entity interference in contrast to FDD systems. This is illustrated in Fig. 1 - in the uplink transmitting MSs interfere with receiving MSs and in the downlink transmitting BSs interfere with receiving BSs if TSs are opposed.

The RTSH algorithm [3], [4] exploits the interference diversity, resulting of two independent and disjoint interference scenarios, of which the effective one is determined by the actual slot assignment. The key principle of RTSH is that after every time interval Δt, the order of the TS within one frame is permuted randomly (Fig. 2). Note that, an analogy can be drawn between RTSH and frequency hopping systems. In the latter frequency diversity is achieved by hopping through different frequency carriers.

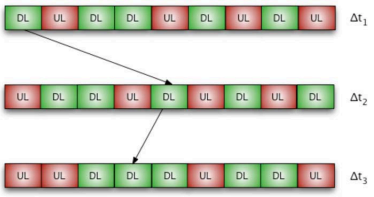

Fig. 2. Permutation of time frames after every period Δt [4]

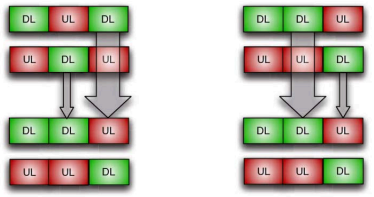

Fig. 3. Interference scenario before (left) and after (right) TS-opposing; Size of arrows indicates potential severity of interference [4]

In a TDD system, in order to produce high same-entity interference, entities have to be of opposite slot assignment, have to be experiencing high link gains between each other, have high transmit power, and be active at the same time. As shown in Fig. 3, the RTSH algorithm aims at reducing the time that a particular entity stays in such a state of high interference. As a consequence the expected value of interference decreases. Moreover, further improvements are anticipated by combining the RTSH algorithm with techniques that exploit time diversity such as interleaving and channel coding. It is thus considered an effective method to improve system performance and to facilitate the possibility of different UL / DL ratios in different cells to meet the varying user traffic profiles.

Performance evaluations via dynamic system level simulation of the RTSH are published in [4] and [3]. This paper will treat the question of how to model the RTSH analytically, assuming equal asymmetries in all cells and activity of all users that can be accommodated per TS. Such a model is

1-4244-0063-5/06/$20.00 ©2006 IEEE

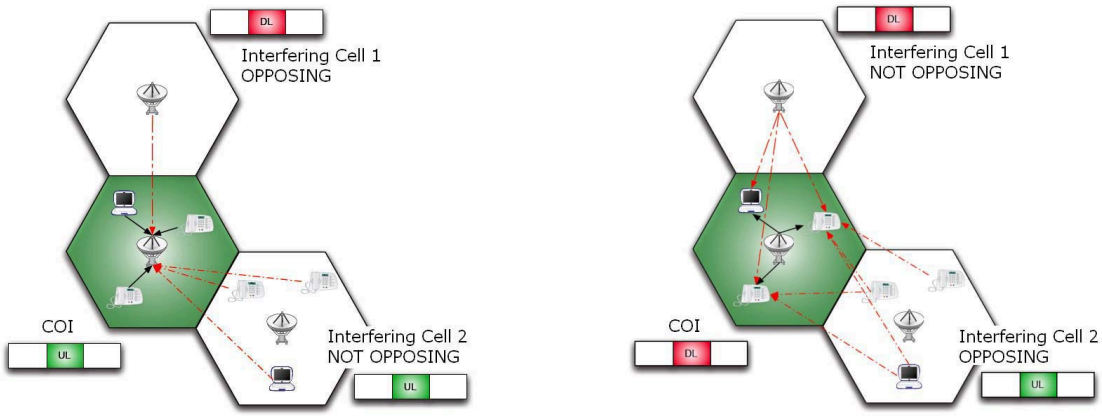

(a) Uplink

(b) Downlink

Fig. 1. Interference caused in uplink and downlink

of practical interest, as it facilitates the rapid performance evaluation of a given system without the need of complex simulations and could serve as a basic framework, which could be further extended to, for example, various distributions of channel asymmetries.

II. Analysis of Interference Components

Three main components determine UL and DL interference, namely the probability that one cell is in DL and an adjacent cell in UL in the same time instant, or vice versa; the probability of a TS being active; and the interference received from same entities and other entities. These three components will be modeled in section II-A, section II-B, and section II-C respectively. As already mentioned in the introduction, this study is within the framework of equal channel asymmetries for all cells.

A. Probability of Time Slot Opposing

In this section, the probability of users being of opposite link assignment (in the following referred to as TS opposing), will be derived. TS opposing introduces same-entity interference to the system and is characteristic for TDD networks. The probability of opposite link assignment is dependent on the asymmetry rate per frame, R_{asym}, defined as the ratio of the number of UL (n_{UL}) and DL (n_{DL}) slots. If the probability of a cell being in an UL TS is $\frac{n_{\text{UL}}}{n_{\text{TOT}}} = P_{\text{UL}}$, where n_{TOT} is the total number of slots per frame, then the probability of two cells being in UL at the same time is $(P_{\text{UL}})^2$. By the same token, the probability of a cell being in a DL TS is $\frac{n_{\text{DL}}}{n_{\text{TOT}}} = 1 - P_{\text{UL}}$, and that of two cells being in DL at the same time is $(1-P_{\text{UL}})^2$. Thus, the probability of TS opposing for two cells, $P_{\text{opp}}(2)$, is given by (1).

$$\begin{aligned} P_{\text{opp}}(2) &= 1 - (P_{\text{UL}}^2 + (1 - P_{\text{UL}})^2) \\ &= 2\frac{n_{\text{UL}} n_{\text{DL}}}{(n_{\text{TOT}})^2} \end{aligned} \tag{1}$$

For n cells the probability of TS opposing is given by (2) and is derived by expanding (1).

$$\begin{aligned} P_{\text{opp}}(n) &= 1 - (P_{\text{UL}}^n + (1 - P_{\text{UL}})^n) \\ &= 1 - \frac{(n_{\text{UL}})^n + (n_{\text{DL}})^n}{(n_{\text{TOT}})^n} \end{aligned} \tag{2}$$

A 16-slot frame (i.e. $n_{\text{TOT}} = 16$) and asymmetry rates (UL:DL) of $2:14$, $4:12$, $6:10$, $8:8$, $10:6$, and $12:4$ are considered. The results, displayed in Fig. 4, are symmetric with respect to $R_{\text{asym}} = 8:8$. Moreover, the symmetric case exhibits the highest probability of TS opposing and as the asymmetry is shifted to favor either UL or DL, the probability of TS opposing decreases.

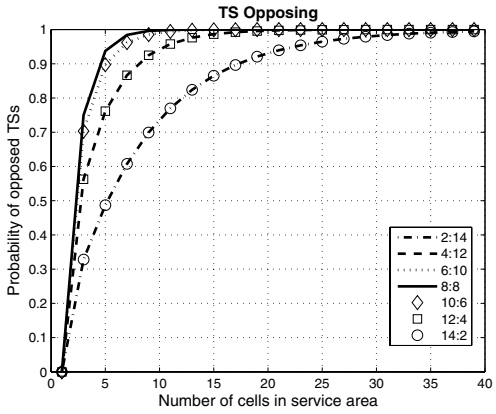

Fig. 4. Probability of TS opposing as a function of the number of cells in service area for different UL:DL ratios.

B. Code Distribution

In this section the number of codes occupied per active TS and the probability of a slot being active, i.e. used for transmission, are analyzed. In order to determine the slot and code activities, the number of users served needs to be known

first. For different asymmetry rates, the number of voice and data users that can be served can be calculated using the equations and dependencies developed in [4]. In summary, the total (UL and DL) number of resource units (RUs) (number of codes per TS $\times$ number of TSs) for the favored link direction,n_a, can be calculated using (3).

$$n_a = n_{\mathrm{ru}} \cdot \frac{K}{K+1} \tag{3}$$

where n_{ru} is the total number of RUs available, and K depends on the ratio of voice users to the total number of users (η) and on the number of RUs required for a data link in the favored link direction (μ), as given by (4)

$$K = \mu + \eta \cdot (1 - \mu) \tag{4}$$

Both η and μ vary with the asymmetry and have been calculated in [4] for a system with 12 codes/TS and 16 TSs. Moreover, (3) is valid under the assumption that the total number of RUs required is exactly one for a data channel in the less favored link direction and exactly two (one for UL and one for DL) for a voice channel. Equation (5) shows the total (UL and DL) number of RUs in the less favored link direction, n_b.

$$n_b = n_{\mathrm{ru}} \cdot \left(1 - \frac{K}{K+1}\right) \tag{5}$$

Given μ and η and using (3) and (5), the total number of voice channels, $n_{\mathrm{ch}}^{\mathrm{v}}$, and data channels, $n_{\mathrm{ch}}^{\mathrm{d}}$, can be found by (6) and (7), respectively.

$$n_{\mathrm{ch}}^{\mathrm{v}} = \eta \cdot n_{\mathrm{ch}} \tag{6}$$

$$n_{\mathrm{ch}}^{\mathrm{d}} = (1-\eta) \cdot n_{\mathrm{ch}} \tag{7}$$

where n_{ch} is the total number of channels available and its value is the same as the total number of RUs available in the less favored link direction (due to the aforementioned assumption that in the less favored link direction both voice and data channels require exactly one RU each). The number of data channels is the total number of channels minus the voice channels. Moreover, the number of active voice ($n_{\mathrm{u}}^{\mathrm{v}}$) and data ($n_{\mathrm{u}}^{\mathrm{d}}$) users in the system depends on the load factor ν as given by (8) and (9), respectively.

$$n_{\mathrm{u}}^{\mathrm{v}} = \nu \cdot n_{\mathrm{ch}}^{\mathrm{v}} \tag{8}$$

$$n_{\mathrm{u}}^{\mathrm{d}} = \nu \cdot n_{\mathrm{ch}}^{\mathrm{d}} \tag{9}$$

The distribution of active codes and active TSs for different asymmetries and load factors can thus be simulated, assuming that the TS with least number of unoccupied codes is occupied first and a user can use at most one TS. Fig. 5 illustrates the results for code activity and shows that an asymmetry, which favors the DL exhibits the same behavior as an asymmetry, which favors the UL, provided that the same rate of asymmetry applies. This characteristic behavior is as expected and has been reported in [4]. A similar trend is valid for the slot activity, thus results are provided only for the downlink (Fig. 6).

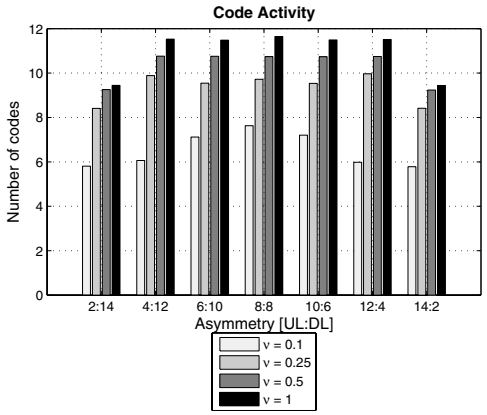

Fig. 5. Code activity: expected number of used codes per active TS depending on ν and $\mathrm{R_{asym}}$

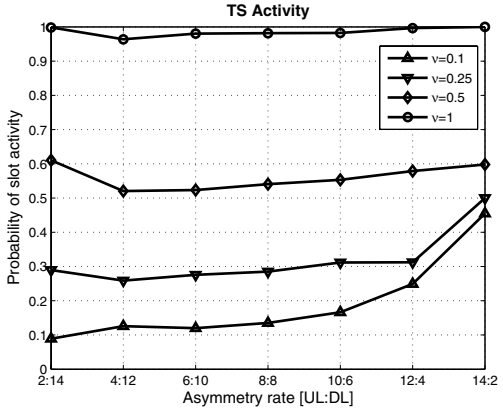

Fig. 6. DL slot activity: probability that a DL TS is used for transmission, depending on the asymmetry and load parameter

C. Same- & Other-Entity Interference

So far it has been shown that for a given asymmetry and load factor, the expected number of codes occupying a TS (Fig. 5), the probability of a TS being active (Fig. 6), and the number of users (given by (8) and (9)) can be determined. These trends are cell-specific in the sense that the results depend on the asymmetry and load in the particular cell, and are independent of the neighboring cells. However, the final interference component, namely the distribution of same- (MS-to-MS, BS-to-BS) and other-entity (MS-to-BS, BS-to-MS) interference, is not cell-specific, but rather is influenced by the intercell interaction. In order to resolve this interference component, a system with specifications given in Table I is realized via a snapshot simulation, assuming an equal asymmetry for all cells. For BS-to-BS interference, a worst case scenario is in place, namely line of sight conditions (LOS) without shadowing, as it is known that in TDD systems the BS-to-BS interference is most detrimental. Further, one interfering tier (six cells) is considered with a cell of interest (COI) in the center and users in each cell are distributed depending on a system-wide varied load and asymmetry. Equations (10) - (13), give the expected values of MS-to-BS, MS-to-MS, BS-to-

TS per frame	16
PN codes per TS	12
Frame length	10 ms
Cell radius	50 m
Chips per slot	2560
Bandwidth	4096 kHz
Path loss model	UMTS indoor [5]
Shadowing constant	8 dB

TABLE I
SIMULATION PARAMETERS

BS, BS-to-MS interference respectively, coming from a single interfering cell in any TS. It should be noted that the indices i and j correspond to the according receiver-transmitter pairs in the equations, such that for (10) G_{ij} is the link gain between BS_i and MS_j, for (11) - between MS_i and MS_j, for (12) - between BS_i and BS_j, and for (13) - between MS_i and BS_j.

$$E[I_{\mathrm{MS-BS}}] = P_{\mathrm{code}} \cdot E[\underbrace{(\sum_{j\in V}^{n_V} G_{ij} + \mu_x \cdot \sum_{j\in D}^{n_D} G_{ij})}_{G'_{\mathrm{MS-BS}}}] \quad (10)$$

$$E[I_{\mathrm{MS-MS}}] = P_{\mathrm{code}} \cdot E[\underbrace{(\sum_{j\in V}^{n_V} G_{ij} + \mu_x \cdot \sum_{j\in D}^{n_D} G_{ij})}_{G'_{\mathrm{MS-MS}}}] \quad (11)$$

$$E[I_{\mathrm{BS-BS}}] = P_{\mathrm{code}} \cdot \tilde{N}_{\mathrm{c}} \cdot E[\underbrace{G_{ij}}_{G_{\mathrm{BS-BS}}}] \quad (12)$$

$$E[I_{\mathrm{BS-MS}}] = P_{\mathrm{code}} \cdot \tilde{N}_{\mathrm{c}} \cdot E[\underbrace{G_{ij}}_{G_{\mathrm{BS-MS}}}] \quad (13)$$

where P_{code} is the maximum code power of 1.7 mW; V and D are the sets of active voice and data users, respectively, in the interfering cell, with according cardinalities n_V and n_D; G_{ij} is the link gain between the transmitter in the interfering cell and the receiver in the COI; $\tilde{N}_{\mathrm{c}}$ is the mean number of active codes per TS (as illustrated in Fig. 5); μ_x is the number of codes required by the data user for a link direction: μ_x = 1 in the less favored link direction, and $\mu_x = \mu$ in the favored link direction. For example, if MS-to-MS interference is to be determined, the COI is in DL, while all other cells are in UL and the total interference coming from each cell is considered in order to resolve the MS-to-MS link gain statistics (over a significant number of simulation events). Similarly, the statistics for the rest of the interference scenarios are determined and results are illustrated for an asymmetry of 8 : 8 and 50% load in Fig. 7. Fig. 8 displays graphically (10) - (13) for a load factor of 0.5.

III. RESULTS

In section II, the three components used in this paper to determine the system interference power, were modeled. To obtain the final analytical model of interference power in a TDD-RTSH system, these components need to be combined. This section will unite the models of the interference components, with the assumption that the different interference

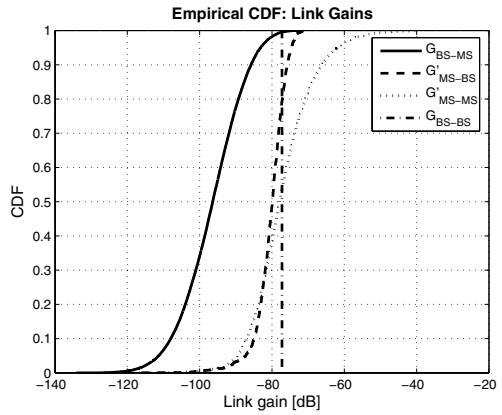

Fig. 7. Distribution of link gains for $\nu = 0.5$ and $\mathrm{R_{asym}} = 8 : 8$

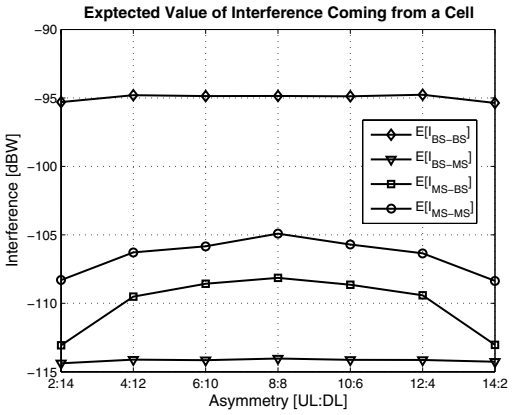

Fig. 8. Expected value of interference power [dBW] depending on $\mathrm{R_{asym}}$ for $\nu = 0.5$

contributions can be approximated by a Gaussian distribution. This assumption appears justified because the central limit theorem can be applied.

If two cells are considered, the COI X in UL and an interfering cell Y, there are two possible scenarios, i.e. either Y is in DL (TS opposing) and thus there is BS-to-BS interference, or Y is in UL and there is MS-to-BS interference (all MSs in Y are interfering). Hence, when considering the whole first tier of cells, the expected value of interference for a COI X in UL, given that X is active, $E\{\mathrm{I_{UL}}|X = \text{active}\}$, is given by

$$E\{\mathrm{I_{UL}}|X = \text{active}\} =$$

$$\Pr\{X = \mathrm{UL}\} \cdot \sum_{i=0}^{n} \binom{n}{i} \Pr\{Y = \mathrm{DL}\}^i \cdot \Pr\{Y = \mathrm{UL}\}^{n-i} \cdot (\Pr\{Y = \text{active}|Y = \mathrm{DL}\} \cdot i \cdot E[I_{\mathrm{BS-BS}}] + \Pr\{Y = \text{active}|Y = \mathrm{UL}\} \cdot (n - i) \cdot E[I_{\mathrm{MS-BS}}]) \quad (14)$$

where n is the total number of interfering cells; $\Pr\{X = \mathrm{UL}\}$ is the probability of the COI being in UL (depending on the asymmetry); $\binom{n}{i} \Pr\{Y = \mathrm{DL}\}^i \cdot \Pr\{Y = \mathrm{UL}\}^{n-i}$ is the

probability of having i out of n interfering cells in DL (TS opposing) and $n-i$ out of n interfering cells in UL (in any combination); $\Pr\{Y = \text{active}|Y = \text{DL}\}$ is the probability of at least one active transmission in a TS, given that the respective TS is used for DL traffic (depending on the load and asymmetry).

In analogy to (14), for the COI X in DL and an interfering cell Y, there are two possible scenarios, i.e. either Y is in UL (TS opposing) and experiences MS-to-MS interference (all MSs in Y are interfering), or Y is in DL and experiences BS-to-MS interference. Hence, when considering the whole first tier of cells, the expected value of interference for a COI X in DL, given that X is active, $E\{\mathrm{I_{DL}}|X = \text{active}\}$, is given by

$$E\{\mathrm{I_{DL}}|X = \text{active}\} \quad =$$

$$\Pr\{X = \text{DL}\} \cdot \sum_{i=0}^{n} \binom{n}{i} \Pr\{Y = \text{UL}\}^{i} \cdot \Pr\{Y = \text{DL}\}^{n-i} \cdot$$
$$(\Pr\{Y = \text{active}|Y = \text{UL}\} \cdot i \cdot E[I_{\mathrm{MS-MS}}] +$$
$$\Pr\{Y = \text{active}|Y = \text{DL}\} \cdot (n-i) \cdot E[I_{\mathrm{BS-MS}}]) \tag{15}$$

Fig. 9 and 10 illustrate the graphical representation of (14) and (15), respectively, and show that with regard to both DL interference (at the MS) and UL interference (at the BS) for a given load factor the interference is generally highest when the UL:DL ratio is symmetric. In other words, channel asymmetry, regardless of whether it is in favor of the DL or in favor of the UL, leads to lower interference both at the MS and at the BS and thus to better performance. This can be attributed to three main effects, the code and TS activity (Fig. 5 and 6 respectively), as well as TS opposing (Fig. 4), which have been incorporated in (14) and (15). This is an important result as it is generally assumed that channel asymmetry in cellular CDMA-TDD systems degrades system DL performance due to high BS-to-BS interference. A further important result is that DL-favored asymmetries generally produce lower interference in the UL (at the BS) than UL-favored asymmetries. In contrast, asymmetry ratios in favor of the UL, e.g. 14:2, result in lower interference in the DL (at the MS), compared to DL-favored asymmetries. It is further worth noting that for a DL-favored scenario, e.g. 2:14, interference in the DL is in general several dB *less* than interference in the uplink. This trend is different in the case of an UL-favored scenario, where interference in the UL is always at least 10 dB higher than interference in the DL.

IV. Conclusion

In this paper, a semi-analytical model of the interference in a TDD-CDMA system employing RTSH was developed. Using the model, the expected value of interference in UL and DL can be computed. Equal asymmetries in all cells and a worst-case interference scenario (e.g., line-of-sight between BSs) has been assumed, where all possibly accommodated users are active and interfering. First, it has been shown that for all system loads, the RTSH algorithm effectively supports channel asymmetry in a cellular CDMA-TDD system, i.e., the special case of assigning UL and DL equal number of TSs, has resulted in highest interference. Second, lowest interference is observed for channel asymmetries in favor of the DL. This means that the use of the RTSH algorithm is very well suited for future data-centric services which impose higher loads onto the DL channel.

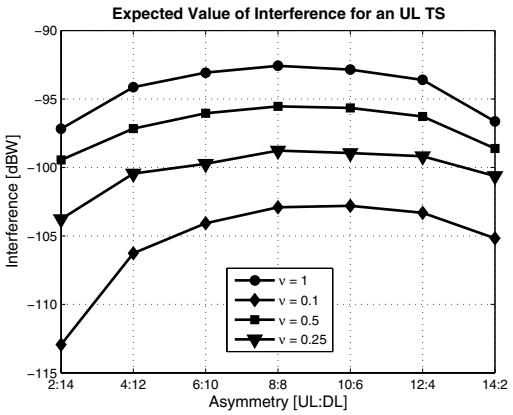

Fig. 9. Expected value of interference power [dBW] for an UL TS depending on ν and $\mathrm{R_{asym}}$

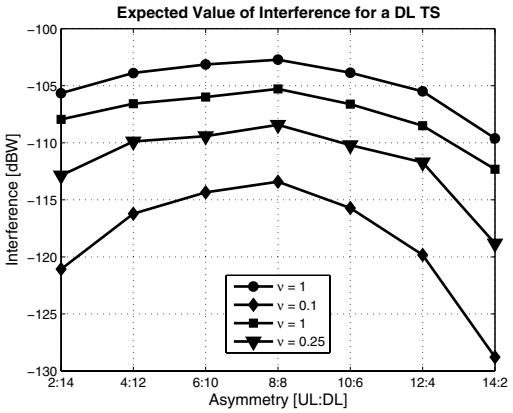

Fig. 10. Expected value of interference power [dBW] for a DL TS depending on ν and $\mathrm{R_{asym}}$

References

[1] V. Huang and W. Zhuang, "Optimal Resource Management in Packet-Switching TDD CDMA Systems," in *IEEE Pers. Commun.*, vol. 6, December 2000, pp. 26–31.

[2] L.-C. Wang, S.-Y. Huang, and Y.-C. Tseng, "Interference Analysis of TDD-CDMA Systems with Directional Antennas," *IEEE Proc. on the* 58^{th} *Vehicular Technology Conference (VTC)*, vol. 2, pp. 1369–1373, October 2003.

[3] H. Haas and S. McLaughlin, "A Dynamic Channel Assignment Algorithm for a Hybrid TDMA/CDMA-TDD Interface using the Novel TS-opposing Technique," in *IEEE Journal on Selec. Areas in Commun.*, vol. 19, 2001, pp. 1831–1846.

[4] H. Haas, P. Jain, and B. Wegmann, "Capacity improvement through random timeslot opposing (RTO) algorithm in cellular TDD systems with asymmetric channel utilization," in *IEEE Proc. on the* 14^{th} *Int. Symp. on Pers., Indoor, and Mobile Radio Commun. (PIMRC), Beijing, China*, September, 7 -10 2003, pp. 1790–1794.

[5] ETSI, "Universal mobile telecommunications system (UMTS); Selection procedures for the choice of radio transmission technologies of the UMTS (UMTS 30.03 version 3.2.0)," ETSI, Tech. Rep. TR 101 112 v3.2.0, April 1998.